

AD-A088 510

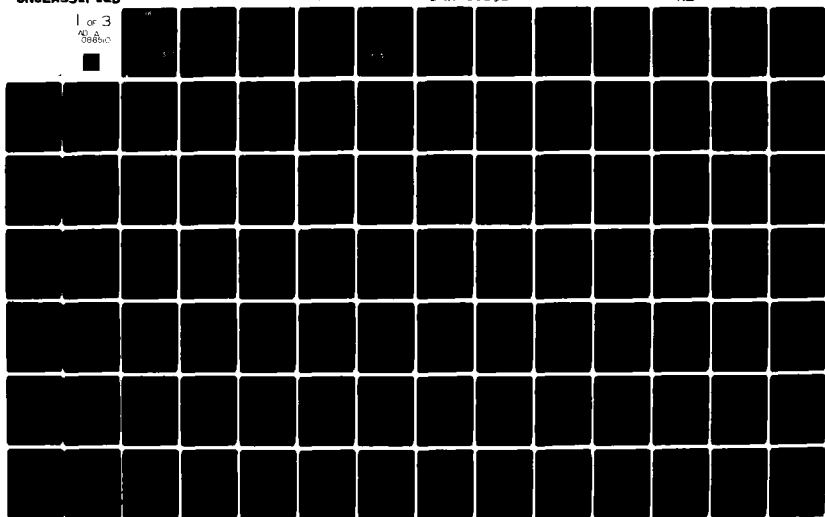
CIVIL SYSTEMS INC ALBUQUERQUE NM F/6 18/3  
MISERS BLUFF PHASE I GROUND SHOCK ANALYSIS OF THE MULTIPLE BURS--ETC(U)  
AUG 78 J S PHILLIPS, J L BRATTON DNA001-77-C-0301

UNCLASSIFIED

DNA-5089Z

NL

1 of 3  
AD-A  
088510



SL

(12)

LEVEL II

AD-E 300874<sup>9</sup>

DNA 5089Z

AD A088510

# MISERS BLUFF PHASE I GROUND SHOCK ANALYSIS OF THE MULTIPLE BURST EXPERIMENTS

James S. Phillips  
Jimmie L. Bratton  
Civil Systems, Incorporated  
2201 San Pedro, N.E.  
Bldg. 3, Suite 214  
Albuquerque, New Mexico 87110

15 August 1978

Interim Report for Period 1 January 1978—1 June 1978

CONTRACT No. DNA 001-77-C-0301

APPROVED FOR PUBLIC RELEASE;  
DISTRIBUTION UNLIMITED.

DTIC  
ELECTE  
S SEP 2 1980 D  
B

THIS WORK SPONSORED BY THE DEFENSE NUCLEAR AGENCY  
UNDER RDT&E RMSS CODE B344077462 H35KAXSX35510 H2590D.

Prepared for  
Director  
DEFENSE NUCLEAR AGENCY  
Washington, D. C. 20305

DDC FILE COPY

80 8 14 080

Destroy this report when it is no longer  
needed. Do not return to sender.

PLEASE NOTIFY THE DEFENSE NUCLEAR AGENCY,  
ATTN: TISI, WASHINGTON, D.C. 20305, IF  
YOUR ADDRESS IS INCORRECT, IF YOU WISH TO  
BE DELETED FROM THE DISTRIBUTION LIST, OR  
IF THE ADDRESSEE IS NO LONGER EMPLOYED BY  
YOUR ORGANIZATION.



(18) LNH, SBIE/

UNCLASSIFIED

SECURITY CLASSIFICATION OF THIS PAGE (When Data Entered)

19 REPORT DOCUMENTATION PAGE		READ INSTRUCTIONS BEFORE COMPLETING FORM
1. REPORT NUMBER DNA 5089Z, HL-HQ 78 51 P RD-A0885 10	2. GOVT ACCESSION NO.	3. RECIPIENT'S CATALOG NUMBER
4. TITLE (and Subtitle) 6 MISERS BLUFF PHASE I GROUND SHOCK ANALYSIS OF THE MULTIPLE BURST EXPERIMENTS.	5. TYPE OF REPORT & PERIOD COVERED 9 Interim Report for Period 1 Jan 78 - 1 Jun 78	6. PERFORMING ORG. REPORT NUMBER
7. AUTHOR(s) 10 James S. Phillips Jimmie L. Bratton	8. CONTRACT OR GRANT NUMBER(s) 15 DNA 001-77-C-0301	9. PROGRAM ELEMENT, PROJECT, TASK AREA & WORK UNIT NUMBERS 16 Subtask H35KAXSX355-10
9. PERFORMING ORGANIZATION NAME AND ADDRESS Civil Systems, Incorporated 2201 San Pedro, N.E., Bldg. 3, Suite 214 Albuquerque, New Mexico 87110	11. CONTROLLING OFFICE NAME AND ADDRESS Director Defense Nuclear Agency Washington, D.C. 20305	12. REPORT DATE 11 15 Aug 78
14. MONITORING AGENCY NAME & ADDRESS (if different from Controlling Office) 17 X3551	13. NUMBER OF PAGES 12 260	15. SECURITY CLASS (of this report) UNCLASSIFIED
16. DISTRIBUTION STATEMENT (of this Report) Approved for public release; distribution unlimited.		
17. DISTRIBUTION STATEMENT (of the abstract entered in Block 20, if different from Report)		
18. SUPPLEMENTARY NOTES This work sponsored by the Defense Nuclear Agency under RDT&E RMSS Code B344077462 H35KAXSX35510 H2590D.		
19. KEY WORDS (Continue on reverse side if necessary and identify by block number) Misers Bluff Prediction Methods High Explosive Test Wave Propagation Ground Shock Data Data Analysis		
20. ABSTRACT (Continue on reverse side if necessary and identify by block number) The multiple burst experiments of Misers Bluff Phase I provided the data base for the evaluation of the superposition principle for ground motions. In addition, this data will be used in the development of a general prediction procedure for the multiple burst environment.  Superposition of single burst waveforms is compared to the multiple burst waveforms on a component by component basis. Quantitative evaluation of these		

UNCLASSIFIED

SECURITY CLASSIFICATION OF THIS PAGE(When Data Entered)

20. ABSTRACT (Continued)

→ comparisons is made and presented for the three multiple burst experiments discussed in this report. In addition, state-of-the-art empirical predictions are compared in a like manner.

Phenomenology associated with these experiments is discussed and related to the waveforms observed in the various experiments. The understanding of this phenomenology will aid in the development of the prediction procedure for the multiple burst environment. In addition, recommendations aimed at furthering the understanding of the multiple burst phenomenology are presented. ↗

UNCLASSIFIED

SECURITY CLASSIFICATION OF THIS PAGE(When Data Entered)

## Preface

This Report was prepared by CSI, Albuquerque, New Mexico, under Contract DNA001-77-C-0301. This research was performed under Program Element T62710H, Project H35KAXS, Task Area X355, Work Unit 10, and was funded by the Defense Nuclear Agency. The Technical Monitor was Dr. George W. Ullrich, DNA.

Inclusive dates of Research were January 1978 through June 1978.

**DTIC**  
**ELECTE**  
**S** SEP 2 1980 **D**  
**B**

ACCESSION for	
NTIS	White Section <input checked="" type="checkbox"/>
DDC	Buff Section <input type="checkbox"/>
UNANNOUNCED	<input type="checkbox"/>
JUSTIFICATION	
BY	
DISTRIBUTION/AVAILABILITY CODES	
Dist.	AVAIL. and/or SPECIAL
<b>A</b>	

PERTINENT CONVERSION FACTORS - SI TO U. S. CUSTOMARY UNITS OF MEASUREMENT

<u>PARAMETERS</u>	<u>TO CONVERT FROM</u>	<u>TO</u>	<u>MULTIPLY BY</u>
Length	Meters (m)	Feet	3.281
Velocity	Meters/Second (mps)	Feet/Second	3.281
Unit Weight	Grams/Cubic Centimeter (G/cc)	Pounds/Cubic Foot	62.427
Yield	Terra Joules (TJ)	Kilotons	$2.391 \times 10^{-1}$
Volume	Cubic Meters ( $m^3$ )	Cubic Feet	35.315
Cratering Efficiency	Cubic Meters/Terra Joule ( $m^3/TJ$ )	Cubic Feet/Ton	6.770
Pressure	Mega Pascals (MPa)	Pounds/Square Inch	145
Impulse	Mega Pascals-Sec (MPa-sec)	Pounds/Square Inch-Sec	145

## TABLE OF CONTENTS

	<u>Page No.</u>
1. Introduction . . . . .	23
2. Experiment Description . . . . .	25
2.1 General . . . . .	25
2.2 Experiments . . . . .	25
2.3 Instrumentation . . . . .	34
3. Prediction of the Multiple Burst Ground Motion Environment . . . . .	41
3.1 General . . . . .	41
3.2 Computer Generated Predictions . . . . .	41
3.3 Single Burst Data Superposition . . . . .	43
3.3.1 Determination of Ranges and Selection of the Proper Bounding Waveforms . .	45
3.3.2 The Interpolation of the Timing of the Waveform . . . . .	47
3.3.3 Determination of Amplitude Modification Factor . . . . .	47
4. Comparison of Data & Predictions . . . . .	57
4.1 Airblast . . . . .	57
4.2 Ground Motion . . . . .	68
4.2.1 Introduction . . . . .	68
4.2.2 Accuracy of Superposition . . . . .	69
4.2.3 Representative Points of Comparison .	76
a) Array Center . . . . .	76
b) 1/2 The Charge Spacing . . . . .	88
c) Between Charges on the Bisector .	100
d) Charge Spacing Outside the Array on the Bisector . . . . .	113
4.3 Evaluation of Superposition . . . . .	120
4.3.1 Introduction . . . . .	120
4.3.2 Regions Where Superposition is Valid .	126
4.3.3 Region Where Superposition is Not Valid	127
a) Negative Airblast . . . . .	130
b) Cylindrical Convergence . . . . .	135
c) Comments . . . . .	143

TABLE OF CONTENTS (continued)

	<u>Page No.</u>
4.4 Stress Measurements . . . . .	143
4.5 Measurements in the Horizontal Plane . . .	145
5. Conclusions and Recommenations . . . . .	151
APPENDIX A . . . . .	A.1
APPENDIX B . . . . .	B.1
APPENDIX C . . . . .	C.1

## LIST OF ILLUSTRATIONS

<u>FIGURE</u>		<u>PAGE NO.</u>
1	Misers Bluff Phase I Test Bed Location .	26
2	Test Bed Plan - Phase I - Misers Bluff .	27
3	P-Wave Velocity Profile Interpreted from Crosshole, Uphole and Surface Refraction Seismic Data (Reference 3) . . . . .	28
4	S-Wave Velocity Profile Interpreted from Crosshole Seismic Data (Reference 3) . .	29
5	Simplified Seismic Profile of Misers Bluff Phase I Test Bed (Reference 3) . .	30
6	Additional Moisture Content Measure- ments . . . . .	31
7	Plan View of Gage Layout for MBI-4 . . .	35
8	Profile View of Gage Layout Along the Main Gage Line for MBI-4 . . . . .	36
9	Plan View of Gage Layout for MBI-6 . . .	37
10	Profile View of Gage Layout Along the Main Gage Line for MBI-6 . . . . .	38
11	Plan View of Gage Layout for MBI-8 . . .	39
12	Profile View of Gage Layout Along the Main Gage Line for MBI-8 . . . . .	40
13	Regions for which Procedural Differences in Superposition Predictions Exist . . .	44
14	Target Location for Illustrative Example of Superposition Prediction Procedure - From Event 6 . . . . .	46
15	Waveforms Used for Interpolation in the Superposition Prediction for the Target Point @ 31.70/0.46/270° . . . . .	48
16	Attenuation Curves Used for Determination of the Amplitude Modification Factors .	50

# LIST OF ILLUSTRATIONS (continued)

<u>FIGURE</u>		<u>PAGE NO.</u>
17	Modified Vertical Waveforms Used in the Superposition Prediction for the Target Point @ 31.70/0.46/270° . . . . .	51
18	Superposition Prediction for Vertical Motion at 31.70/0.46/270° . . . . .	52
19	Modified Horizontal Waveforms Used in the Superposition Prediction of Target Point @ 31.70/0.46/270° . . . . .	55
20	Superposition Prediction for Horizontal Motion at 31.70/0.46/270° . . . . .	56
21	Airblast Prediction Layouts for the Phase I Multiple Burst Experiments . . . . .	58
22	Comparison of Predicted and Measured Single and Multiple Burst Air Pressures for the Half Buried Configuration . . . . .	59
23	Comparison of Measured and Predicted Airblast Pressure & Impulse - MBI-6 . . . . .	61
24	Air Pressure Measurements on the 150° Azimuth - MBI-6 . . . . .	62
25	Comparison of Measured and Predicted Airblast Pressure & Impulse MBI-4 . . . . .	64
26	Comparison of Measured and Predicted Airblast Pressure & Impulse MBI-8 . . . . .	66
27	Magnitude and Duration of the Negative Phase of the Airblast for MBI-6 & MBI-4 . . . . .	67
28	Representative Points of Comparison for Predictions vs Data . . . . .	77
29	Waveform Comparison of Vertical Velocity at the Array Center - MBI-6 . . . . .	78
30	Waveform Comparison of Vertical Velocity at the Array Center - MBI-6 . . . . .	79
31	Waveform Comparisons of Vertical Velocity at the Array Center - MBI-8 . . . . .	80

# LIST OF ILLUSTRATIONS (continued)

<u>FIGURE</u>		<u>PAGE NO.</u>
32	Waveform Comparisons of Vertical Velocity at the Center of an Outside Array - MBI-8 . . . . .	81
33	Shock Spectra Comparisons of Vertical Velocity at the Array Center - MBI-6 .	84
34	Shock Spectra Comparisons of Vertical Velocity at the Array Center - MBI-4 .	85
35	Shock Spectra Comparisons of Vertical Velocity at the Array Center - MBI-8 .	86
36	Shock Spectra Comparisons of Vertical Velocity at the Center of an Outside Array - MBI-8 . . . . .	87
37	Waveform Comparisons of Vertical Velocity at 1/2 the Charge Spacing - MBI-6 . . . . .	89
38	Waveform Comparisons of Vertical Velocity at 1/2 the Charge Spacing - MBI-4 . . . . .	90
39	Waveform Comparisons of Vertical Velocity at 1/2 the Charge Spacing - MBI-8 . . . . .	91
40	Waveform Comparisons of Horizontal Velocity at 1/2 the Charge Spacing - MBI-6 . . . . .	92
41	Waveform Comparisons of Horizontal Velocity at 1/2 the Charge Spacing - MBI-4 . . . . .	93
42	Shock Spectra Comparisons of Vertical Velocity at 1/2 the Charge Spacing - MBI-6 . . . . .	95
43	Shock Spectra Comparisons of Vertical Velocity at 1/2 the Charge Spacing - MBI-4 . . . . .	96
44	Shock Spectra Comparisons of Vertical Velocity at 1/2 the Charge Spacing - MBI-8 . . . . .	97

# LIST OF ILLUSTRATIONS (continued)

<u>FIGURE</u>		<u>PAGE NO.</u>
45	Shock Spectra Comparisons of Horizontal Velocity at 1/2 Charge Spacing - MBI-6 . .	98
46	Shock Spectra Comparisons of Horizontal Velocity at 1/2 Charge Spacing - MBI-4 . .	99
47	Waveform Comparisons of Vertical Velocity Between Charges on the Bisector - MBI-6 .	101
48	Waveform Comparisons of Vertical Velocity Between Charges on the Bisector - MBI-4 .	102
49	Waveform Comparisons of Vertical Velocity Between Charges on the Bisector - MBI-8 .	103
50	Waveform Comparisons of Horizontal Velocity Between Charges on the Bisector - MBI-6 . . . . .	104
51	Waveform Comparisons of Horizontal Velocity Between Charges on the Bisector - MBI-4 . . . . .	105
52	Shock Spectra Comparisons of Vertical Velocity Between Charges on the Bisector - MBI-6 . . . . .	108
53	Shock Spectra Comparisons of Vertical Velocity Between Charges on the Bisector - MBI-4 . . . . .	109
54	Shock Spectra Comparisons of Vertical Velocity Between Charges on the Bisector - MBI-8 . . . . .	110
55	Shock Spectra Comparisons of Horizontal Velocity Between Charges on the Bisector - MBI-6 . . . . .	111
56	Shock Spectra Comparisons of Horizontal Velocity Between Charges on the Bisector - MBI-4 . . . . .	112

# LIST OF ILLUSTRATIONS (continued)

<u>FIGURE</u>		<u>PAGE NO.</u>
57	Waveform Comparisons of Vertical Velocity a Charge Spacing Outside the Array on a Bisector - MBI-6 . . . . .	114
58	Waveform Comparisons of Vertical Velocity a Charge Spacing Outside the Array on a Bisector - MBI-4 . . . . .	115
59	Waveform Comparisons of Vertical Velocity a Charge Spacing Outside the Array on a Bisector - MBI-8 . . . . .	116
60	Waveform Comparisons of Horizontal Velocity a Charge Spacing Outside the Array on a Bisector - MBI-6 . . . . .	117
61	Waveform Comparisons of Horizontal Velocity a Charge Spacing Outside the Array on a Bisector - MBI-4 . . . . .	118
62	Shock Spectra Comparisons of Vertical Ve- locity a Charge Spacing Outside the Array on a Bisector - MBI-6 . . . . .	121
63	Shock Spectra Comparisons of Vertical Ve- locity a Charge Spacing Outside the Array on a Bisector - MBI-4 . . . . .	122
64	Shock Spectra Comparisons of Vertical Ve- locity a Charge Spacing Outside the Array on a Bisector - MBI-8 . . . . .	123
65	Shock Spectra Comparisons of Horizontal Velocity a Charge Spacing Outside the Array on a Bisector - MBI-6 . . . . .	124
66	Shock Spectra Comparisons of Horizontal Velocity a Charge Spacing Outside the Array on a Bisector - MBI-4 . . . . .	125
67	Comparisons of Maximum Upward Velocities from MBI-4 and Superposition of MBI-2 . .	128
68	Comparison of Corresponding Upward Velocities from MBI-4 and Superposition of MBI-2 . .	129

# LIST OF ILLUSTRATIONS (continued)

<u>FIGURE</u>		<u>PAGE NO.</u>
69	Comparison of Corresponding & Maximum Velocities from MBI-6 and Superposition of MBI-1 . . . . .	131
70	Time Correlation of Negative Phase and Large Upward Motion of the Array Center - MBI-6 . . . . .	133
71	Time Phasing of Airblast and Large Upward Ground Motion - MBI-4 . . . . .	134
72	Peak Upward Motion Versus Range for MBI-4 & MBI-6 . . . . .	136
73	Comparison of Horizontal Stress Levels in the Single Burst and Multiple Burst Experiments . . . . .	138
74	Maximum Horizontal Displacements - MBI-6 . . . . .	139
75	Maximum Horizontal Displacements - MBI-4 . . . . .	140
76	Peak Horizontal Outward Velocity - MBI-6 . . . . .	141
77	Peak Horizontal Outward Velocity - MBI-4 . . . . .	142
78	Comparison of Single Burst and Multiple Burst Vertical Stress Waveforms on MBI-4 and MBI-6 . . . . .	144
79	Peak Positive and Negative Horizontal Stresses Measured in the Multiple Burst Experiments . . . . .	146
80	Comparison of Horizontal and Transverse Measurements for Phase I . . . . .	147
81	Comparison of Horizontal and Transverse Measurements for MBI-4 and MBI-8 at the Center of the Array . . . . .	149
82	Comparison of Horizontal and Transverse Measurements for MBI-6 at the Center of the Array . . . . .	150

## APPENDIX A

### LIST OF ILLUSTRATIONS

<u>FIGURE</u>		<u>PAGE NO.</u>
A.1	Comparison of MBI-4 Data and Super-imposed MBI-2 Data @ 0/1.52/0 Vertical Velocity . . . . .	A.2
A.2	Comparison of MBI-4 Data and Super-imposed MBI-2 Data @ 0/3.05/0 Vertical Velocity . . . . .	A.3
A.3	Comparison of MBI-4 Data and Super-imposed MBI-2 Data @ 0/6.10/0 Vertical Velocity . . . . .	A.4
A.4	Comparison of MBI-4 Data and Super-imposed MBI-2 Data @ 0/9.15/0 Vertical Velocity . . . . .	A.5
A.5	Comparison of MBI-4 Data and Super-imposed MBI-2 Data @ 0/12.20/0 Vertical Velocity . . . . .	A.6
A.6	Comparison of MBI-4 Data and Super-imposed MBI-2 Data @ 5.34/0.46/0 Vertical Velocity . . . . .	A.7
A.7	Comparison of MBI-4 Data and Super-imposed MBI-2 Data @ 5.34/0.46/0 Horizontal Velocity . . . . .	A.8
A.8	Comparison of MBI-4 Data and Super-imposed MBI-2 Data @ 5.34/0.46/270 Horizontal Velocity . . . . .	A.9
A.9	Comparison of MBI-4 Data and Super-imposed MBI-2 Data @ 10.68/0.46/270 Horizontal Velocity . . . . .	A.10
A.10	Comparison of MBI-4 Data and Super-imposed MBI-2 Data @ 19.22/0.46/254 Horizontal Velocity . . . . .	A.11

# APPENDIX A

## LIST OF ILLUSTRATIONS (continued)

<u>FIGURE</u>		<u>PAGE NO.</u>
A.11	Comparison of MBI-4 Data and Super-imposed MBI-2 Data @ 26.69/0.46/0 Horizontal Velocity . . . . .	A.12
A.12	Comparison of MBI-4 Data and Super-imposed MBI-2 Data @ 32.03/0.46/0 Vertical Velocity . . . . .	A.13
A.13	Comparison of MBI-4 Data and Super-imposed MBI-2 Data @ 32.03/0.46/0 Horizontal Velocity . . . . .	A.14
A.14	Comparison of MBI-4 Data and Super-imposed MBI-2 Data @ 42.70/0.46/0 Vertical Velocity . . . . .	A.15
A.15	Comparison of MBI-4 Data and Super-imposed MBI-2 Data @ 42.70/0.46/0 Horizontal Velocity . . . . .	A.16
A.16	Comparison of MBI-6 Data and Super-imposed MBI-1 Data @ 0/1.52/0 Vertical Velocity . . . . .	A.17
A.17	Comparison of MBI-6 Data and Super-imposed MBI-1 Data @ 0/3.05/0 Vertical Velocity . . . . .	A.18
A.18	Comparison of MBI-6 Data and Super-imposed MBI-1 Data @ 0/6.10/0 Vertical Velocity . . . . .	A.19
A.19	Comparison of MBI-6 Data and Super-imposed MBI-1 Data @ 0/9.15/0 Vertical Velocity . . . . .	A.20
A.20	Comparison of MBI-6 Data and Super-imposed MBI-1 Data @ 0/12.2/0 Vertical Velocity . . . . .	A.21

APPENDIX A  
LIST OF ILLUSTRATIONS  
(continued)

<u>FIGURE</u>		<u>PAGE NO.</u>
A.21	Comparison of MBI-6 Data and Super- imposed MBI-1 Data @ 9.15/0.46/0 Vertical Velocity . . . . .	A.22
A.22	Comparison of MBI-6 Data and Super- imposed MBI-1 Data @ 9.15/0.46/0 Horizontal Velocity . . . . .	A.23
A.23	Comparison of MBI-6 Data and Super- imposed MBI-1 Data @ 9.15/0.46/270 Horizontal Velocity . . . . .	A.24
A.24	Comparison of MBI-6 Data and Super- imposed MBI-1 Data @ 32.94/0.46 Horizontal Velocity . . . . .	A.25
A.25	Comparison of MBI-6 Data and Super- imposed MBI-1 Data @ 45.75/0.46/0 Horizontal Velocity . . . . .	A.26
A.26	Comparison of MBI-6 Data and Super- imposed MBI-1 Data @ 54.90/0.46/0 Vertical Velocity . . . . .	A.27
A.27	Comparison of MBI-6 Data and Super- imposed MBI-1 Data @ 54.90/0.46/0 Horizontal Velocity . . . . .	A.28
A.28	Comparison of MBI-6 Data and Super- imposed MBI-1 Data @ 73.2/0.46/0 Vertical Velocity . . . . .	A.29
A.29	Comparison of MBI-6 Data and Super- imposed MBI-1 Data @ 73.2/0.46/0 Horizontal Velocity . . . . .	A.30
A.30	Comparison of MBI-8 Data with MBI-4 Data and Superimposed MBI-2 Data @ 0/1.52/0 Vertical Velocity . . . . .	A.31
A.31	Comparison of MBI-8 Data with MBI-4 Data and Superimposed MBI-2 Data @ 0/3.05/0 Vertical Velocity . . . . .	A.32

APPENDIX A  
LIST OF ILLUSTRATIONS  
(continued)

<u>FIGURE</u>		<u>PAGE NO.</u>
A.32	Comparison of MBI-8 Data with MBI-4 Data and Superimposed MBI-2 Data @ 0/6.10/0 Vertical Velocity . . . . .	A.33
A.33	Comparison of MBI-8 Data with MBI-4 Data and Superimposed MBI-2 Data @ 0/12.20/0 Vertical Velocity . . . . .	A.34
A.34	Comparison of MBI-8 Data with MBI-4 Data and Superimposed MBI-2 Data @ 5.34/0.46/0 Vertical Velocity . . . . .	A.35
A.35	Comparison of MBI-8 Data with MBI-4 Data and Superimposed MBI-2 Data @ 5.34/0.46/0 Horizontal Velocity . . . . .	A.36
A.36	Comparison of MBI-8 Data with MBI-4 Data and Superimposed MBI-2 Data @ 32.03/0.46/0 Vertical Velocity . . . . .	A.37
A.37	Comparison of MBI-8 Data with MBI-4 Data and Superimposed MBI-2 Data @ 73.93/0.46/0 Vertical Velocity . . . . .	A.38

## APPENDIX B

### LIST OF ILLUSTRATIONS

<u>FIGURE</u>		<u>PAGE NO.</u>
B.1	Location of Shock Spectra Compari- sons for MBI-4 . . . . .	B.2
B.2	Evaluation Plot of Limiting Displace- ments - MBI-4 . . . . .	B.3
B.3	Evaluation Plot of Limiting Velocities - MBI-4 . . . . .	B.4
B.4	Evaluation Plot of Limiting Low Fre- quencies - MBI-4 . . . . .	B.5
B.5	Evaluation Plot of Limiting High Frequencies - MBI-4 . . . . .	B.6
B.6	Shock Spectra Comparison of MBI-4 and Superposition of MBI-2 @ 0/1.52/0 Vertical Velocity . . . . .	B.7
B.7	Shock Spectra Comparison of MBI-4 and Superposition of MBI-2 @ 0/3.05/0 Vertical Velocity . . . . .	B.8
B.8	Shock Spectra Comparison of MBI-4 and Superposition of MBI-2 @ 0/6.10/0 Vertical Velocity . . . . .	B.9
B.9	Shock Spectra Comparison of MBI-4 and Superposition of MBI-2 @ 0/9.15/0 Vertical Velocity . . . . .	B.10
B.10	Shock Spectra Comparison of MBI-4 and Superposition of MBI-2 @ 0/12.20/0 Vertical Velocity . . . . .	B.11
B.11	Shock Spectra Comparison of MBI-4 and Superposition of MBI-2 @ 5.34/0.46/0 Vertical Velocity . . . . .	B.12
B.12	Shock Spectra Comparison of MBI-4 and Superposition of MBI-2 @ 5.34/0.46/0 Horizontal Velocity . . . . .	B.13
B.13	Shock Spectra Comparison of MBI-4 and Superposition of MBI-2 @ 5.34/0.46/270 Horizontal Velocity . . . . .	B.14

## APPENDIX B

### LIST OF ILLUSTRATIONS (continued)

<u>FIGURE</u>	<u>PAGE NO.</u>
B.14      Shock Spectra Comparison of MBI-4 and Superposition of MBI-2 @ 19.25/0.46/ Vertical Velocity . . . . .	B.15
B.15      Shock Spectra Comparison of MBI-4 and Superposition of MBI-2 @ 19.25/0.46/ Horizontal Velocity . . . . .	B.16
B.16      Shock Spectra Comparison of MBI-4 and Superposition of MBI-2 @ 26.69/0.46/0 Vertical Velocity . . . . .	B.17
B.17      Shock Spectra Comparison of MBI-4 and Superposition of MBI-2 @ 26.69/0.46/0 Horizontal Velocity . . . . .	B.18
B.18      Shock Spectra Comparison of MBI-4 and Superposition of MBI-2 @ 32.03/0.46/0 Vertical Velocity . . . . .	B.19
B.19      Shock Spectra Comparison of MBI-4 and Superposition of MBI-2 @ 32.03/0.46/0 Horizontal Velocity . . . . .	B.20
B.20      Shock Spectra Comparison of MBI-4 and Superposition of MBI-2 @ 42.70/0.46/0 Vertical Velocity . . . . .	B.21
B.21      Location of Shock Spectra Comparisons for MBI-6 . . . . .	B.22
B.22      Evaluation Plot of Limiting Displace- ments - MBI-6 . . . . .	B.23
B.23      Evaluation Plot of Limiting Velocities - MBI-6 . . . . .	B.24
B.24      Evaluation Plot of Limiting Low Fre- quencies - MBI-6 . . . . .	B.25
B.25      Evaluation Plot of Limiting High Frequencies - MBI-6 . . . . .	B.26
B.26      Shock Spectra Comparison of MBI-6 and Superposition of MBI-1 @ 0/1.52/0 Vertical Velocity . . . . .	3.27

## APPENDIX B

### LIST OF ILLUSTRATIONS (continued)

<u>FIGURE</u>		<u>PAGE NO.</u>
B.27	Shock Spectra Comparison of MBI-6 and Superposition of MBI-1 @ 0/3.05/0 Vertical Velocity . . . . .	B.28
B.28	Shock Spectra Comparison of MBI-6 and Superposition of MBI-1 @ 0/6.10/0 Vertical Velocity . . . . .	B.29
B.29	Shock Spectra Comparison of MBI-6 and Superposition of MBI-1 @ 0/9.15/0 Vertical Velocity . . . . .	B.30
B.30	Shock Spectra Comparison of MBI-6 and Superposition of MBI-1 @ 0/12.20/0 Vertical Velocity . . . . .	B.31
B.31	Shock Spectra Comparison of MBI-6 and Superposition of MBI-1 @ 9.15/0.46/0 Vertical Velocity . . . . .	B.32
B.32	Shock Spectra Comparison of MBI-6 and Superposition of MBI-1 @ 9.15/0.46/0 Horizontal Velocity . . . . .	B.33
B.33	Shock Spectra Comparison of MBI-6 and Superposition of MBI-1 @ 32.94/0.46/ Vertical Velocity . . . . .	B.34
B.34	Shock Spectra Comparison of MBI-6 and Superposition of MBI-1 @ 32.94/0.46/ Horizontal Velocity . . . . .	B.35
B.35	Shock Spectra Comparison of MBI-6 and Superposition of MBI-1 @ 45.75/0.46/0 Vertical Velocity . . . . .	B.36
B.36	Shock Spectra Comparison of MBI-6 and Superposition of MBI-1 @ 45.75/0.46/0 Horizontal Velocity . . . . .	B.37
B.37	Shock Spectra Comparison of MBI-6 and Superposition of MBI-1 @ 54.90/0.46/0 Vertical Velocity . . . . .	B.38

# APPENDIX B

## LIST OF ILLUSTRATIONS (continued)

<u>FIGURE</u>		<u>PAGE NO.</u>
B.38	Shock Spectra Comparison of MBI-6 and Superposition of MBI-1 @ 54.90/0.46/0 Horizontal Velocity . . . . .	B.39
B.39	Shock Spectra Comparison of MBI-6 and Superposition of MBI-1 @ 73.20/0.46/0 Vertical Velocity . . . . .	B.40
B.40	Shock Spectra Comparison of MBI-6 and Superposition of MBI-1 @ 73.20/0.46/0 Horizontal Velocity . . . . .	B.41
B.41	Location of Shock Spectra Comparisons for MBI-8 . . . . .	B.42
B.42	Evaluation Plot of Limiting Displace- ments - MBI-8 . . . . .	B.43
B.43	Evaluation Plot of Limiting Velocities - MBI-8 . . . . .	B.44
B.44	Evaluation Plot of Limiting Low Fre- quencies - MBI-8 . . . . .	B.45
B.45	Evaluation Plot of Limiting High Frequencies - MBI-8 . . . . .	B.46
B.46	Shock Spectra Comparison of MBI-8 and MBI-4 @ 0/1.52/0 Vertical Velocity . . .	B.47
B.47	Shock Spectra Comparison of MBI-8 and MBI-4 @ 0/3.05/0 Vertical Velocity . . .	B.48
B.48	Shock Spectra Comparison of MBI-8 and MBI-4 @ 0/6.10/0 Vertical Velocity . . .	B.49
B.49	Shock Spectra Comparison of MBI-8 and MBI-4 @ 0/12.20/0 Vertical Velocity . . .	B.50
B.50	Shock Spectra Comparison of MBI-8 and MBI-4 @ 5.34/0.46/ Vertical Velocity . .	B.51
B.51	Shock Spectra Comparison of MBI-8 and MBI-4 @ 5.34/0.46/ Horizontal Velocity . . . . .	B.52

## APPENDIX C

### LIST OF ILLUSTRATIONS

<u>FIGURE</u>		<u>PAGE NO.</u>
C.1	Overpressure Waveforms Measured on Bisector, MBI-4 . . . . .	C.3
C.2	Overpressure Waveforms Measured on Charge Line, MBI-4 . . . . .	C.4
C.3	Overpressure Waveforms Measured on Charge Line MBI-6 . . . . .	C.6
C.4	Overpressure Waveforms Measured on Charge Line, MBI-8 . . . . .	C.8
C.5	Overpressure Waveforms Measured on Bisector, MBI-8 . . . . .	C.9

# LIST OF TABLES

<u>TABLE</u>		<u>PAGE NO.</u>
1	Objectives of The Multiple Burst Experiments . . . . .	32
2	Misers Bluff Phase I Test Program . . .	33
3	Summary of Superposition Accuracy at the Center of the Charge Array . . . .	70
4	Summary of Superposition Accuracy Inside the Charge Array - Vertical Motions . . . . .	71
5	Summary of Superposition Accuracy Inside the Charge Array - Horizontal Motions . . . . .	72
6	Summary of Superposition Accuracy Outside the Charge Array - Vertical Motions . . . . .	73
7	Summary of Superposition Accuracy Outside the Charge Array - Horizontal Motions . . . . .	74
8	Summary of Prediction Accuracy at the Center of the Charge Array . . . .	82
9	Summary of Prediction Accuracy at a Range of 1/2 the Charge Spacing . . . .	94
10	Summary of Prediction Accuracy at the Location Inbetween Charges on a Bisector . . . . .	106
11	Summary of Prediction Accuracy at the Location of a Charge Spacing Outside the Charge Array on the Bisector . . . . .	119

APPENDIX C  
LIST OF TABLES

<u>TABLE</u>		<u>PAGE NO.</u>
C1	Peak Airblast Parameters Measured in MBI-4 . . . . .	C.2
C2	Peak Airblast Parameters Measured in MBI-6 . . . . .	C.5
C3	Peak Airblast Parameters Measured in MBI-8 . . . . .	C.7

1.

## INTRODUCTION

The Multiple Aim Point basing concept for the proposed MX weapon system derives its survivability by creating more targets than can be attacked one-on-one. The current estimates of the deployment pattern for the MX system places neighboring aim points from 1220 meters to 2134 meters apart for a "baseline" threat. For most geologic conditions this distance corresponds to a ground motion environment within the "transition" or "plateau" region (Reference 1). In this region there is little or no attenuation of ground motion with range, so that peak amplitudes of motion are relatively insensitive to distance from the source. Preliminary estimates of the effect of this multiburst phenomenon, assuming the superposition principal to be valid, indicated that un-attacked elements of the system may be subjected to a greater ground motion environment than that which results for a single burst at the design miss distance (Reference 2).

Currently no generally accepted method exists for predicting ground motions from multiple bursts. An evaluation of the superposition assumption performed by the Data Analysis Working Group (DAWG) prior to Misers Bluff and, using the very limited available data indicated that superposition of the effects of a single burst is not a satisfactory estimate of the multiburst effects. In general, superposition underestimated the period of oscillatory ground motion and under (however occasionally over) estimated the peak amplitudes (Reference 2).

The two phase Misers Bluff test program was designed to provide an experimental data base upon which a waveform synthesis procedure for predicting HE multiburst effects in a layered geology is to be developed.

Phase I consisted of a series of small yield single and multiple burst experiments. The approach used in the analysis of Phase I was to treat the single-burst experiments as an evaluation of the state-of-the-art of empirical prediction techniques, and to utilize the multiple-burst experiments as an evaluation of the superposition of the data from the single-burst experiments to describe the ground motion environment for the multiburst experiments. The results of the evaluation of these procedures will then be synthesized to provide a updated prediction procedure for multiburst events. This procedure will then be used for pretest predictions, and evaluated in the higher yield experiments and different geology of Phase II.

The analysis of the single burst experiments was reported in Reference 3. The subject of this companion report is the analysis of the multiple burst experiments in Phase I.

Experimental layouts are presented in Section 2. Procedures for the derivation of superposition predictions and a discussion of these procedures are contained in Section 3. Comparison of data and predictions are shown in Section 4. Section 5 presents conclusions and recommendations.

## 2. EXPERIMENT DESCRIPTION

### 2.1 GENERAL

Location of the test bed for Phase I of Misers Bluff was the Queen 15 site on the White Sands Missile Range (WSMR), New Mexico, approximately 1200 meters east of the Pre-Dice Throw (PDT-II) test bed (Figure 1). The locations of the various ground zeros within the test bed area are shown in Figure 2. Geologic properties of the site were described in Reference 3. P-wave, S-wave, and the simplified profiles of the test site are presented in Figures 3 through 5. Additional water content measurements, made for the near surface soils to gage the seasonal variations in rainfall and weather conditions, are presented in Figure 6 (References 4 and 5).

### 2.2 EXPERIMENTS

There were three multiple burst experiments conducted during Phase I. Objectives of these experiments are listed in Table 1 (Ref. 2). The dates and configurations of these experiments and their relation to the other experiments in Phase I are shown in Table 2.

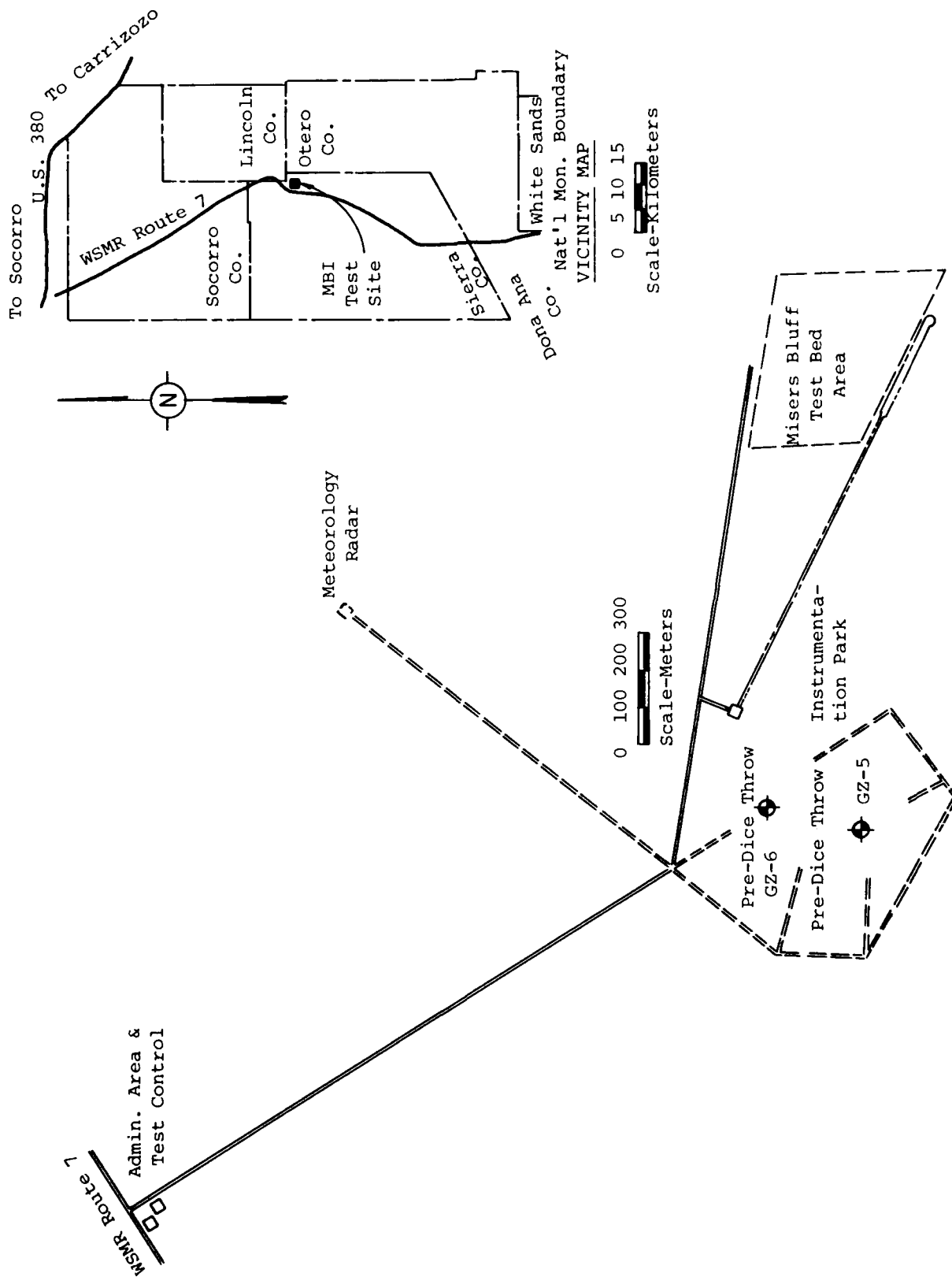


Figure 1. Misers Bluff Phase I Test Bed Location

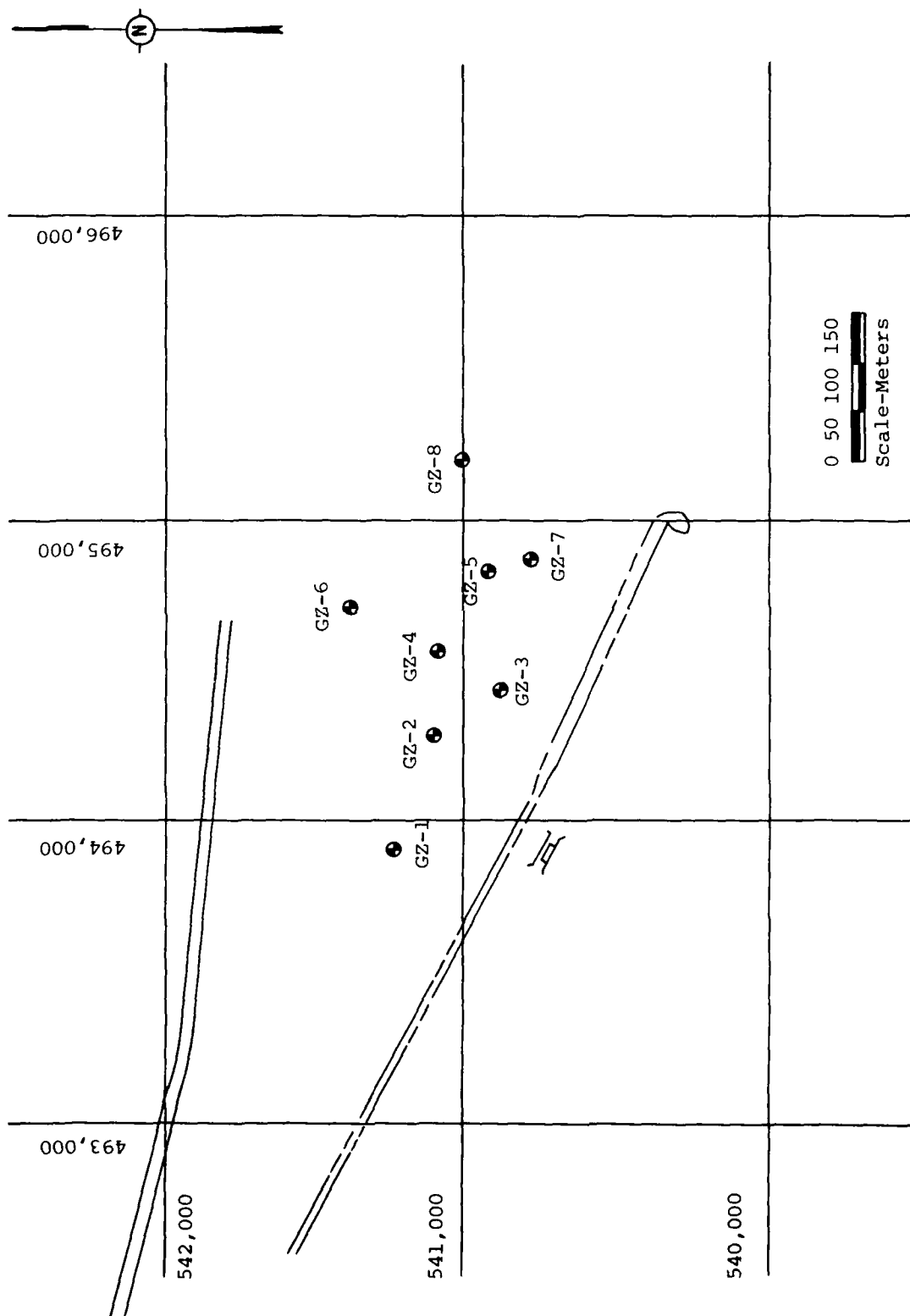
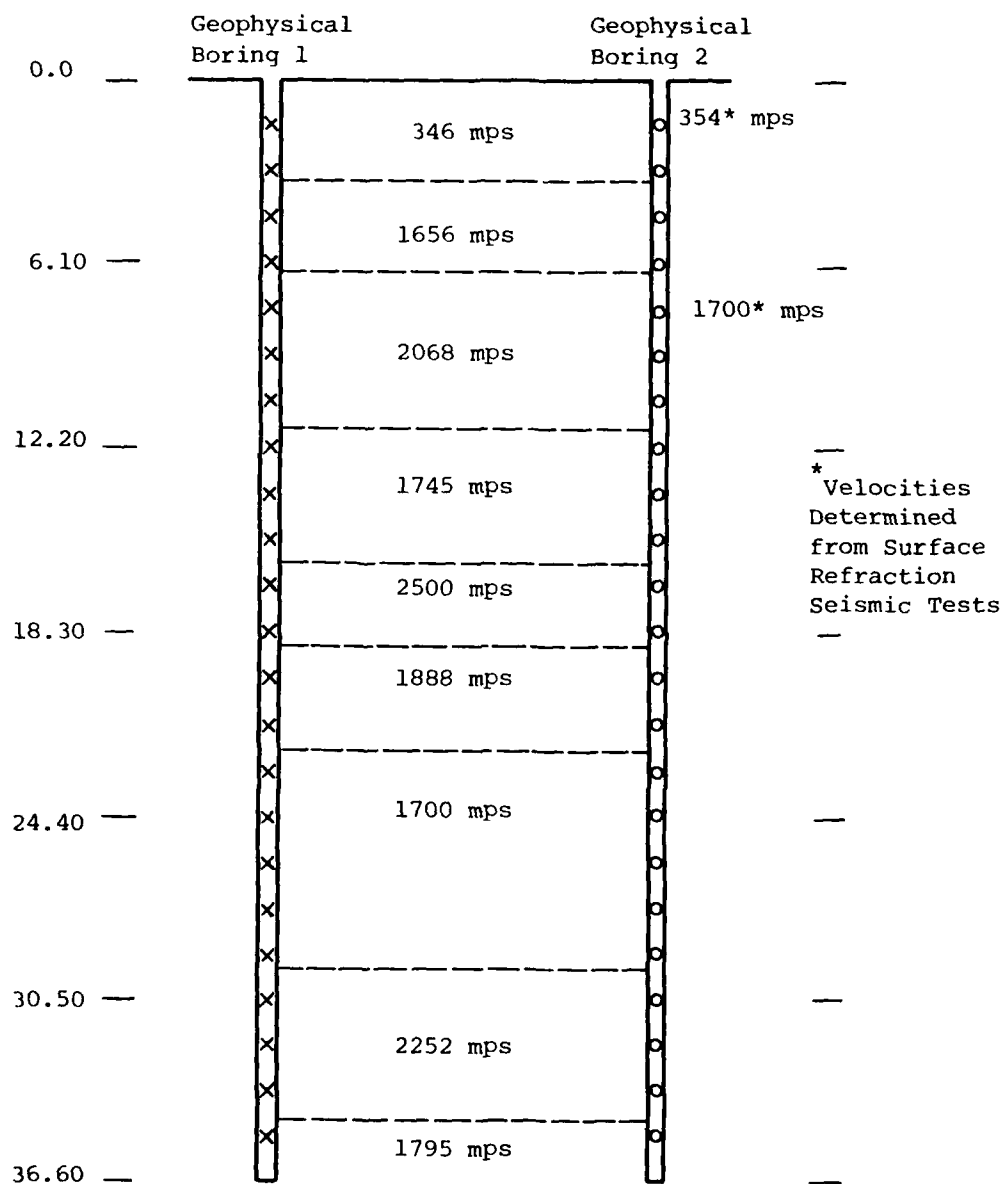


Figure 2. Test Bed Plan - Phase I - Misers Bluff

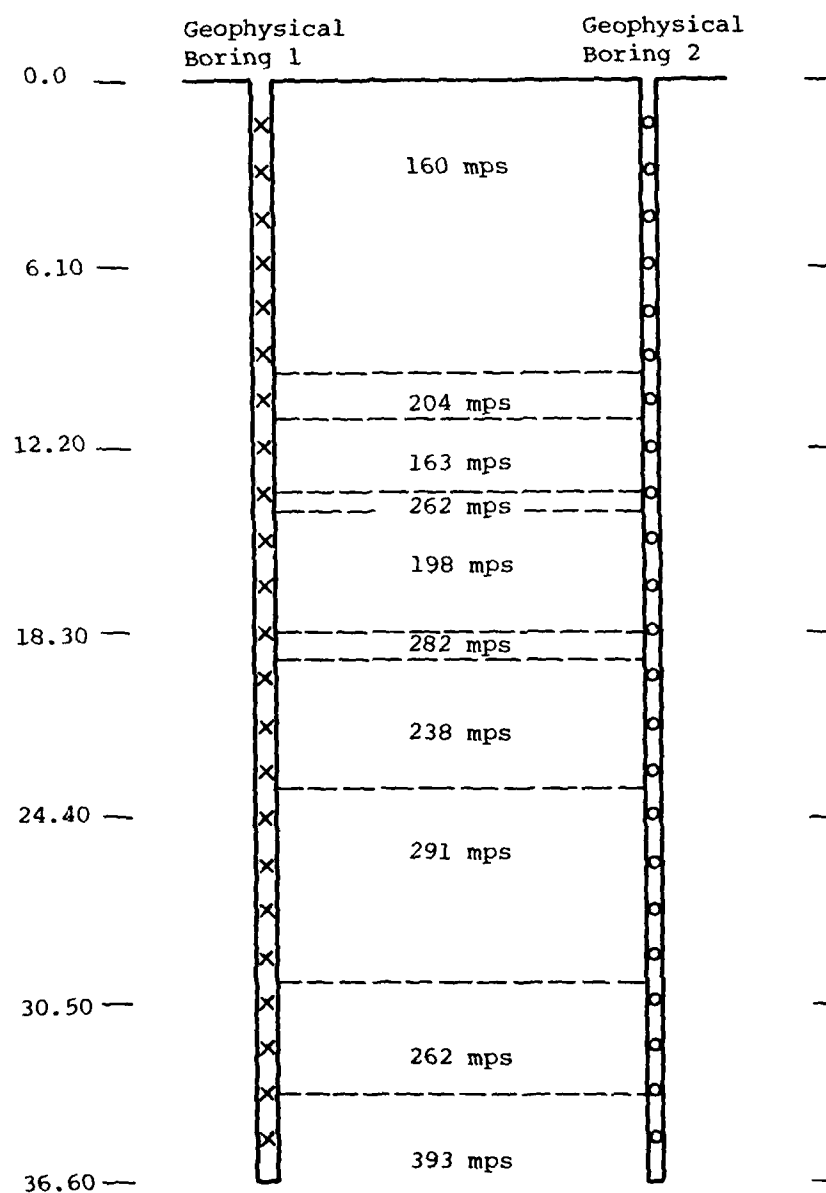


Legend

X Seismic Source

O Geophone Location

Figure 3. P-wave Velocity Profile Interpreted from Cross-hole, Uphole and Surface Refraction Seismic Data (from Reference 3)



Legend

X Seismic Source Location  
O Geophone Location

Figure 4. S-wave Velocity Profile Interpreted from Cross-hole Seismic Data (from Reference 3)

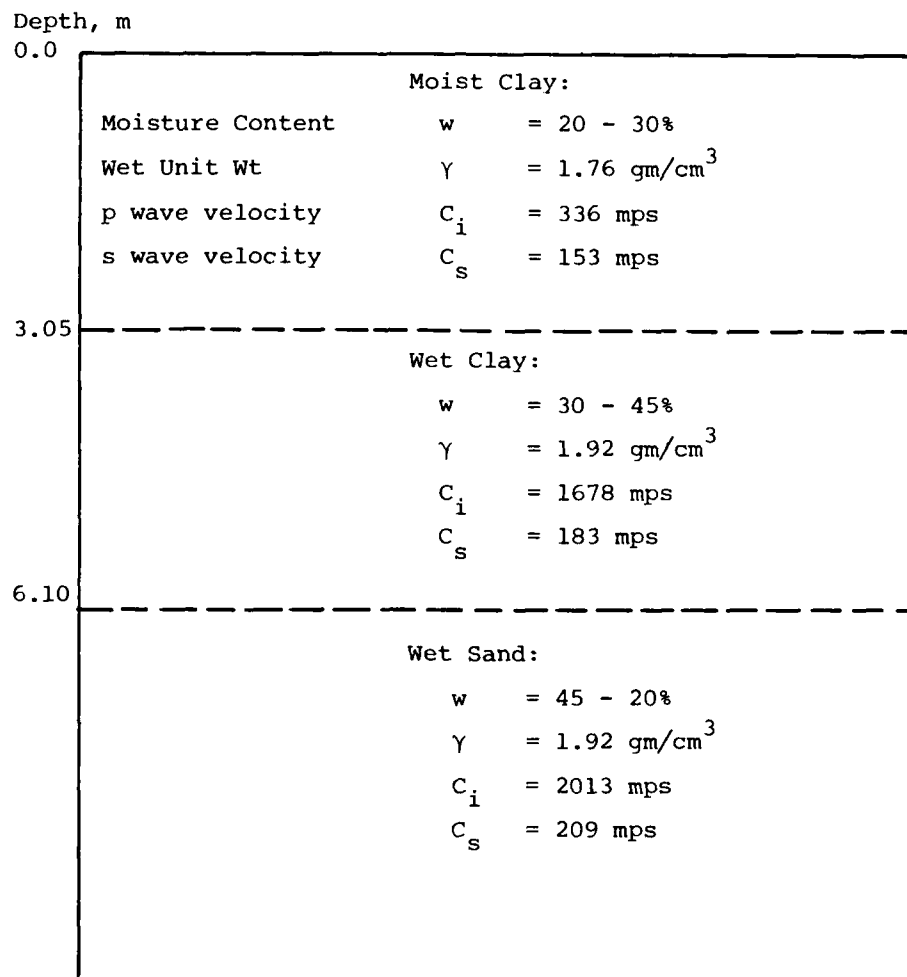


Figure 5. Simplified Seismic Profile of Misers Bluff  
Phase I Test Bed (Reference 3)

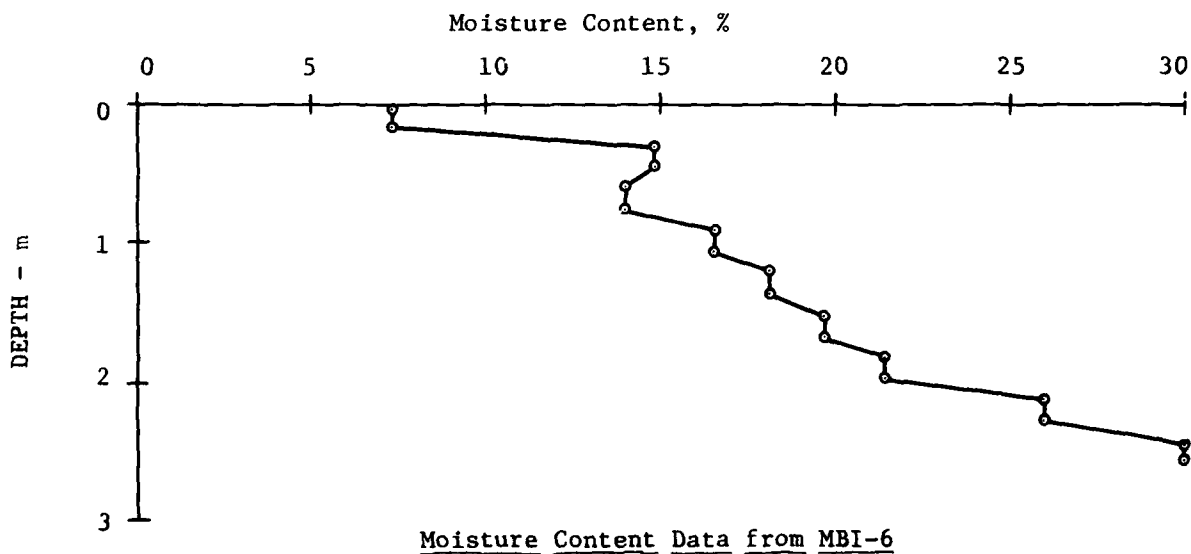
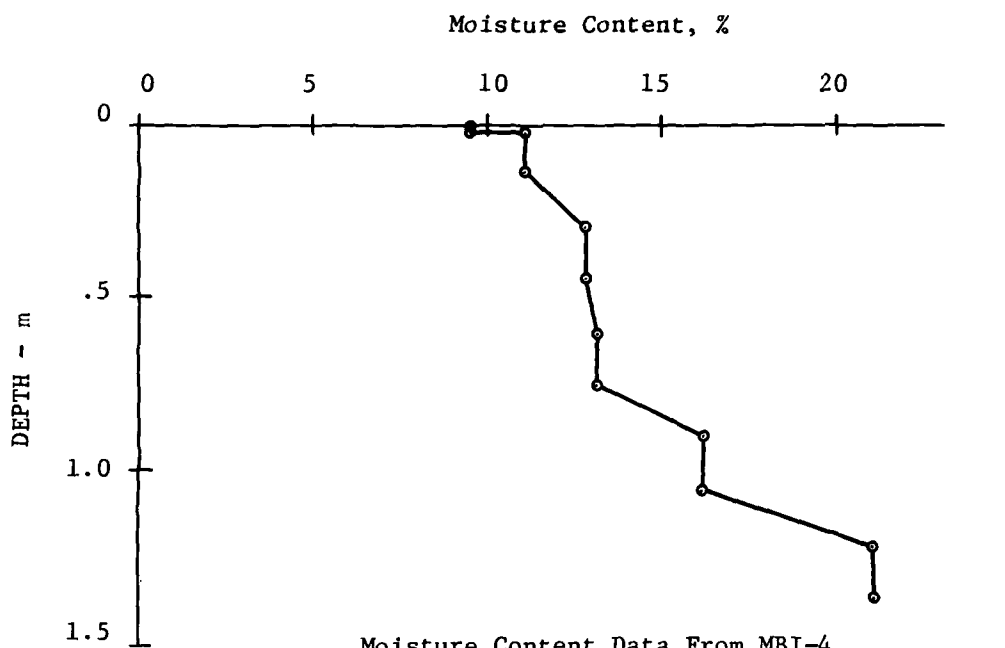


Figure 6: Additional Moisture Content Measurements Made for Events 4 and 6

Table 1. OBJECTIVES OF MISERS BLUFF PHASE I  
MULTIPLE BURST EXPERIMENTS

<u>Event</u>	<u>Objective</u>
MBI-4	Provide data for waveform synthesis model and identification of height of burst phenomena differences in multiburst configurations.
MBI-6	Provide data for waveform synthesis model.
MBI-8	Resolve importance of more distant charges on "local" multiburst phenomena; provide data for assessing reproducibility, symmetry, etc., because configuration contains seven identical 6-charge arrays.

TABLE 2. MISERS BLUFF PHASE I TEST PROGRAM

EVENT	NO. OF CHARGES	YIELD/CHARGE	CHARGE CONFIGURATION	DATE
MBI-1	1	$2.09 \times 10^{-3}$ TJ (1000 lb)	Half Buried $\oplus$	2 August 1977
MBI-2	1	$2.09 \times 10^{-3}$ TJ (1000 lb)	Surface Tangent $\underline{Q}$	15 August 1977
MBI-3	1	$2.09 \times 10^{-3}$ TJ (1000 lb)	Half Buried $\oplus$	23 August 1977
MBI-4	6	$2.09 \times 10^{-3}$ TJ (1000 lb)	Surface Tangent $\underline{Q}$	7 September 1977
MBI-5	1	$2.09 \times 10^{-3}$ TJ (1000 lb)	Tangent Below $\overline{O}$	20 September 1977
MBI-6	6	$2.09 \times 10^{-3}$ TJ (1000 lb)	Half Buried $\oplus$	13 October 1977
MBI-7	1	$5.35 \times 10^{-4}$ TJ (256 lb)	Half Buried $\oplus$	25 October 1977
MBI-8	24	$2.09 \times 10^{-3}$ TJ (1000 lb)	Surface Tangent $\underline{Q}$	7 December 1977

### 2.3 Instrumentation

Plan and profile views of the instrumentation layouts for these experiments are shown in Figures 7 through 12. Instruments used in these events were Endevco Accelerometers, Sandia DX and Bell and Howell velocity gages, Kulite air pressure gages, and WES SE stress gages. Capabilities and limitations of these instruments are discussed in Reference 6.

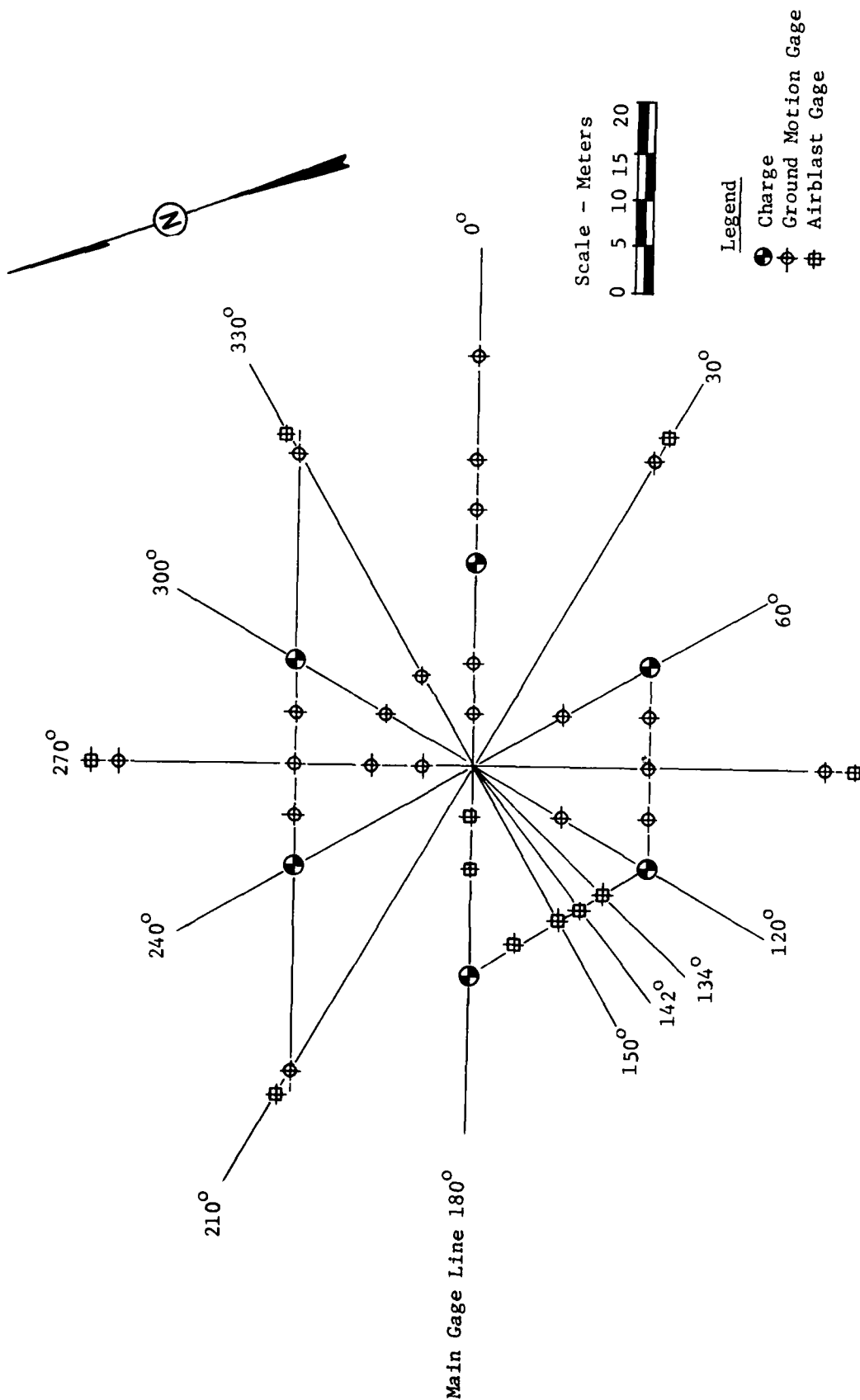


FIGURE 7: Plan View of Gage Layout for MBI-4

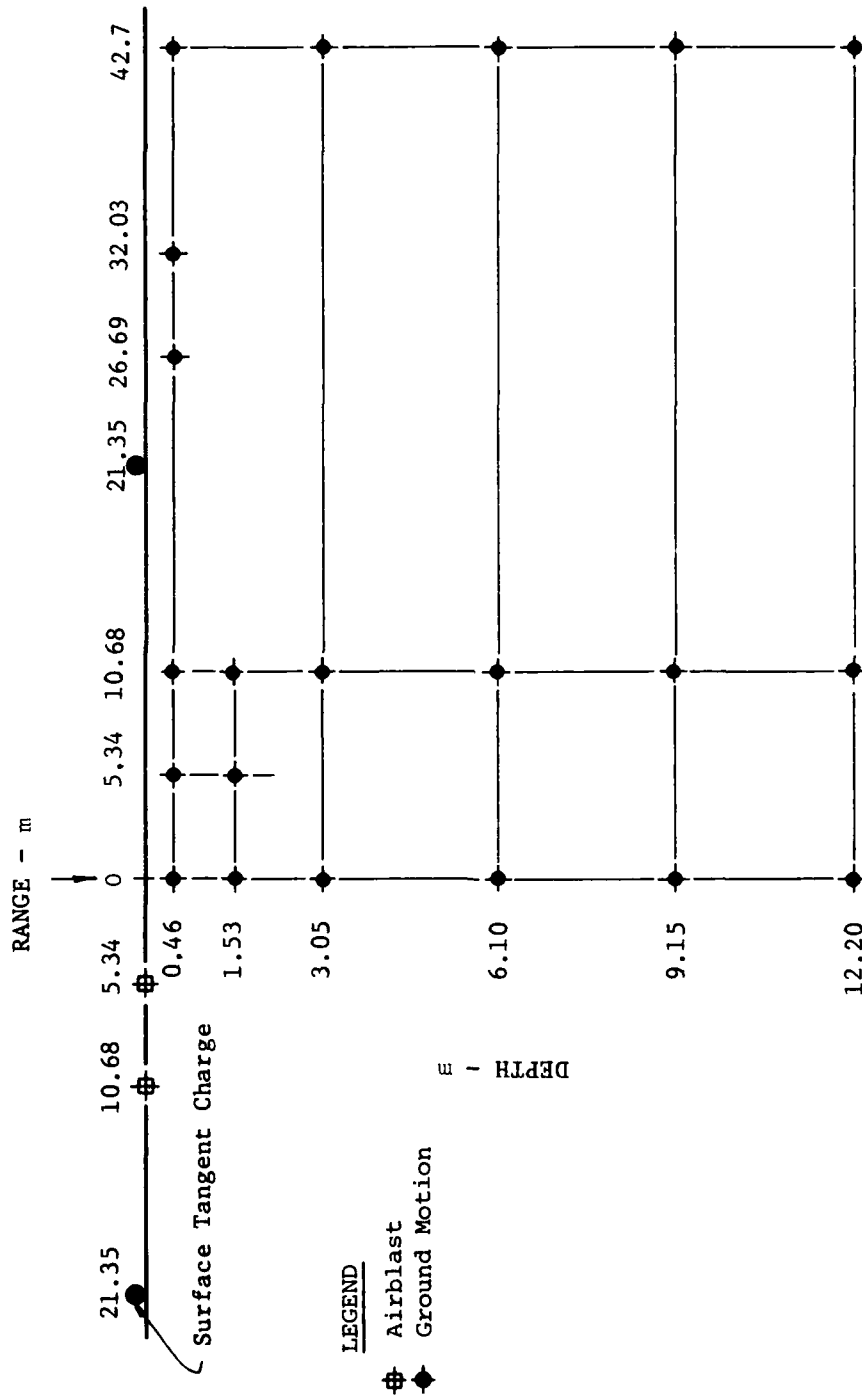


FIGURE 8: Profile View of Gage Layout Along the Main Gage Line for MBI-4

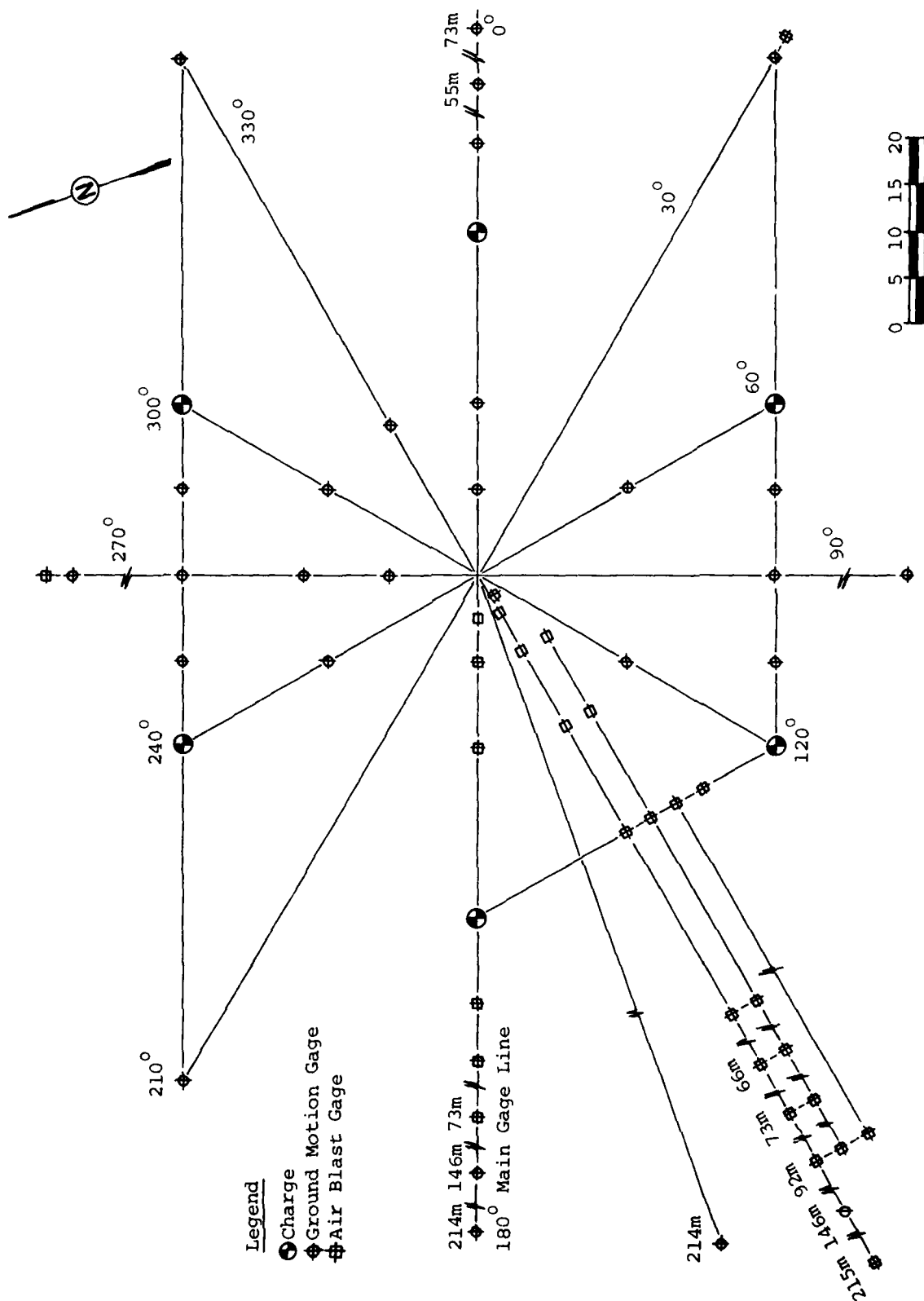


FIGURE 9: Plan View of Gage Layout for MBI-6

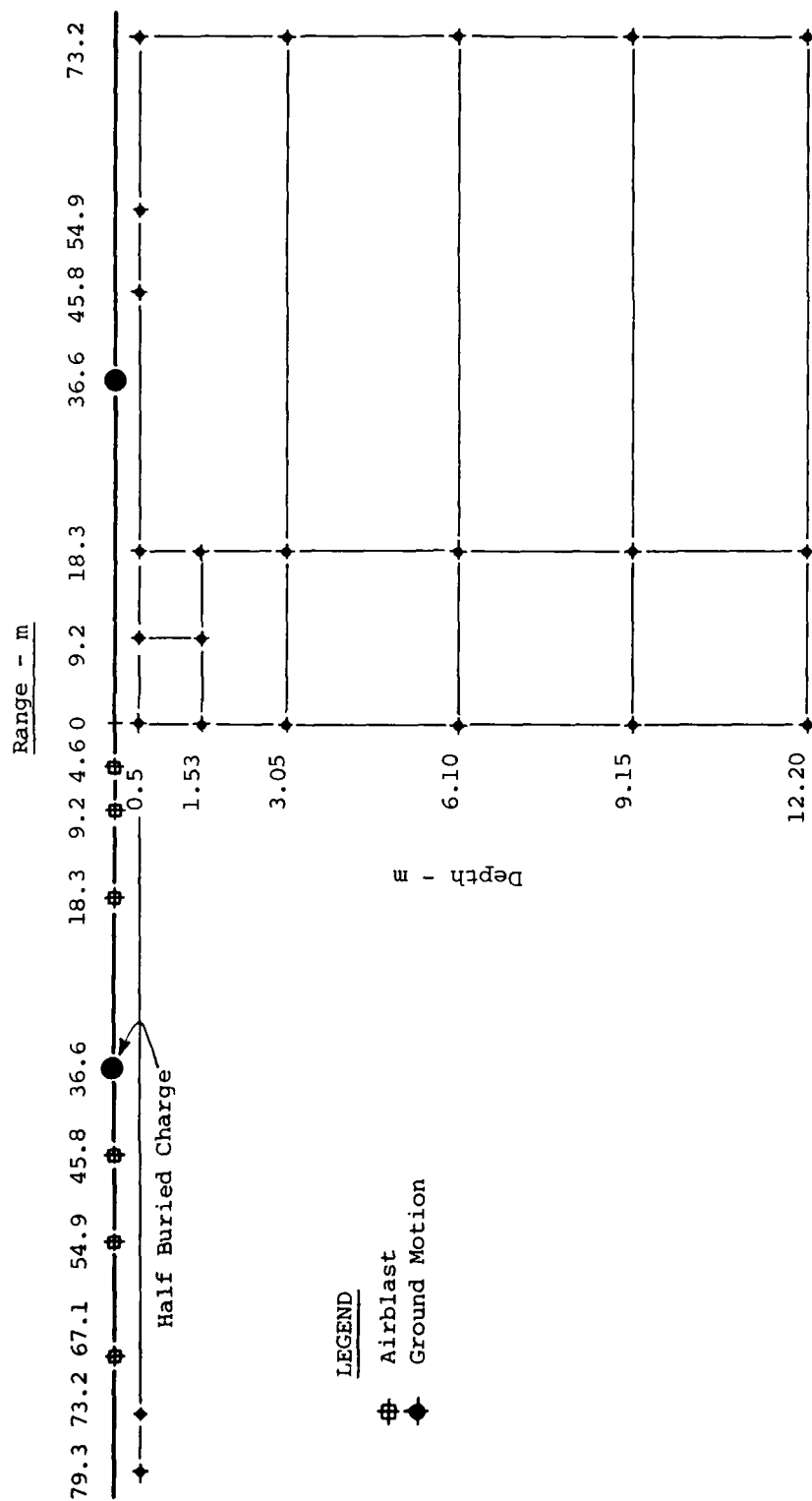


FIGURE 10: Profile View of Gage Layout Along the Main Gage Line for MBI-6

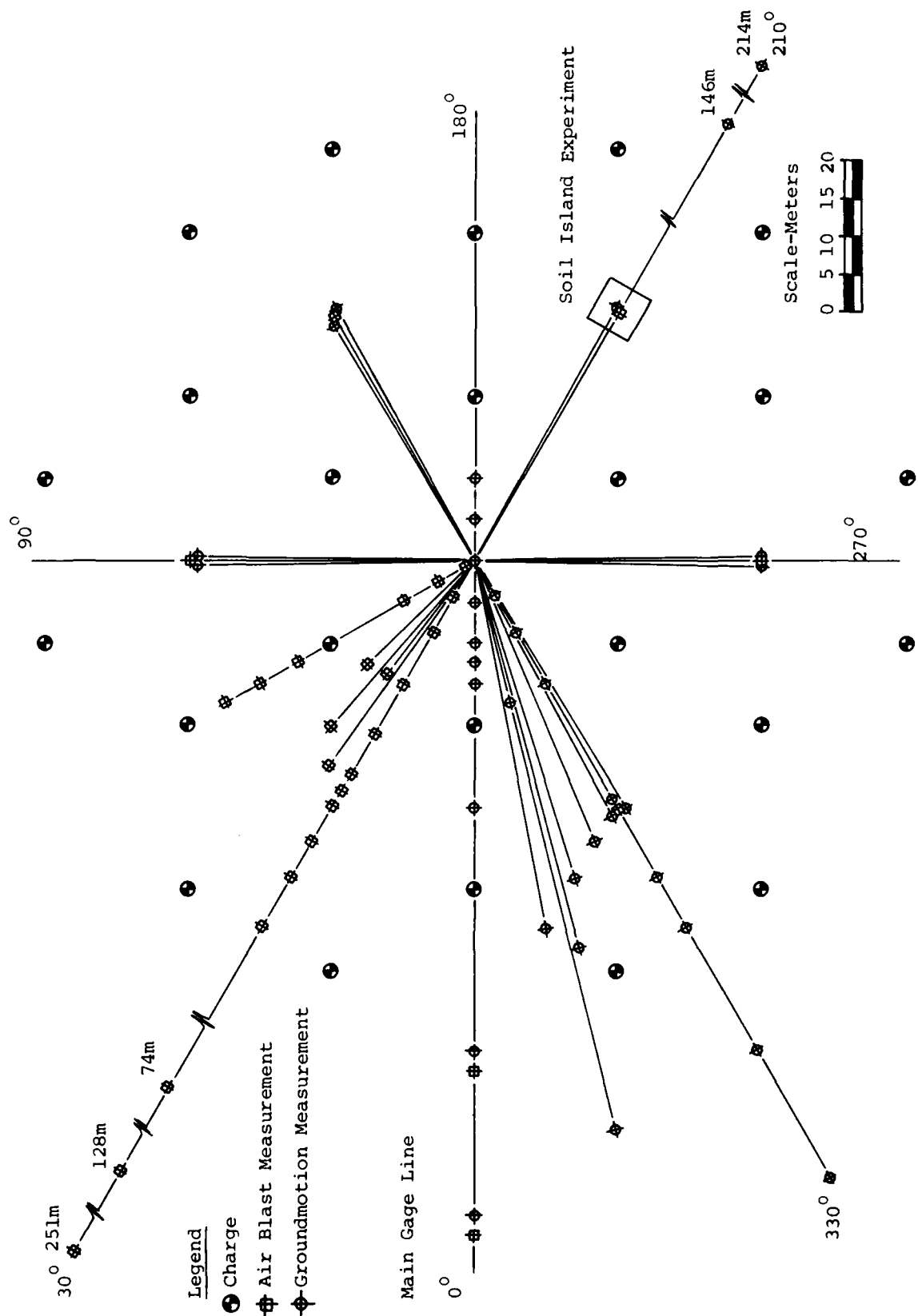


FIGURE 11: Plan View of Gage Layout for MBI-8

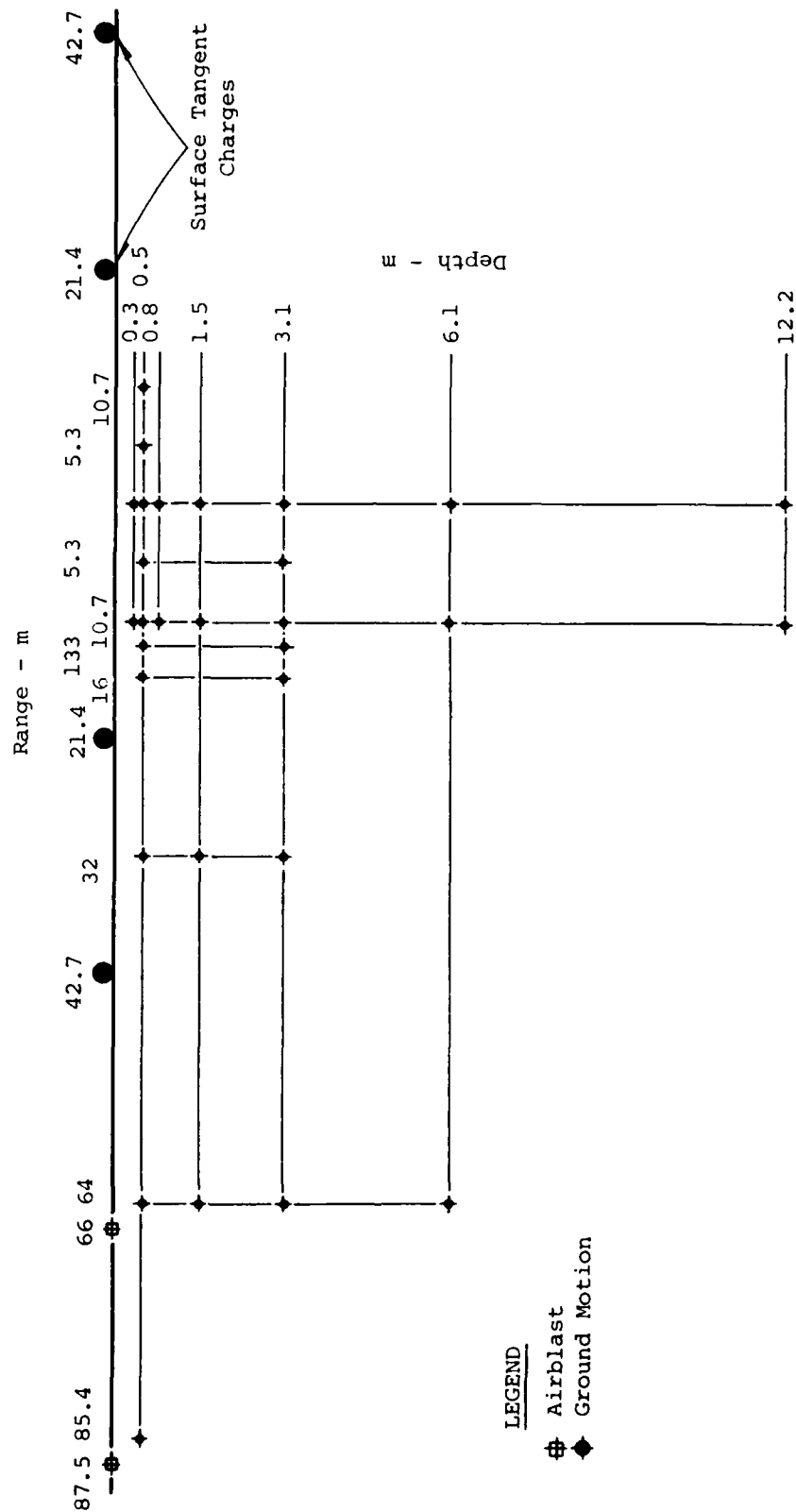


FIGURE 12: Profile View of Gage Layout Along the Main Gage Line for MBI-8

### 3. PREDICTION OF THE MULTIPLE BURST GROUND MOTION ENVIRONMENT

#### 3.1 GENERAL

Two techniques were utilized in the prediction of the ground motion environment for the multiple burst experiments. The first approach was a superposition of the effects of single bursts using the empirical methods discussed in Reference 3. This was accomplished by modifying the "WAVE-ADDER" code (Reference 7) to utilize the empirical procedures used in predicting the Phase I experiments. The second approach was the superposition of data from the appropriate Phase I single burst experiment to describe the ground motion in the multiple burst experiment. Both methods will be discussed below, with the major emphasis placed on superposition of data.

#### 3.2 COMPUTER GENERATED PREDICTIONS

Two codes were used in conjunction for the prediction of the multiple burst experiments. These were the Low Altitude Multiple Burst (LAMB) model and the CSI modified version of the "WAVE-ADDER", the RDA superposition program (Reference 7).

LAMB, which models the nonlinear characteristics of the atmosphere after the detonation of multiple nuclear bursts, was used to calculate the airblast environment. Since the LAMB code was developed for the prediction of nuclear events, an HE/NE equivalency factor of 2 was assumed (i.e., HE is twice as effective as NE in producing airblast). This is generally accepted practice below the 2.0 MPa overpressure level.

The "WAVE-ADDER" code calculates the vertical components of ground motion due to the detonation of each of the several bursts then superimposes these components at the desired gage locations to form the composite vertical waveform.

The original version of the "WAVE-ADDER" was set up to calculate the airblast environment internally by superposition. The LAMB model provides a more accurate description of the airblast environment because it treats the highly nonlinear nature of the equation of state of the air. Because of this the "WAVE-ADDER" was modified to accept as input the peak overpressure, and impulse from LAMB to use in the calculation of the air slap component of ground motion.

Another change made in the "WAVE-ADDER" code occurred in the calculation of the air slap induced displacements. Originally the code used the yield of the individual charges to calculate the displacement due to a particular charge, then superimposed displacements due to all charges to determine the multiple burst environment. Observation of peak impulse and overpressure as calculated by LAMB indicated that use of the single burst yield in this manner would lead to gross underestimation of air slap displacements. The approach finally adopted was to determine an effective yield at the target point location. This yield was cube root scaled from the impulse calculated by LAMB by the following equation:

$$W_e = \left( \frac{I_L}{I_{SB}} \right)^3 W_{SB}$$

where

$W_e$  = the effective yield

$I_L$  = peak impulse computed by LAMB

$I_{SB}$  = the impulse that would occur for a single burst at the peak overpressure calculated by LAMB at the point in question

$W_{SB}$  = the single burst yield

These additions only affected the values of the air slap related particle velocity and displacement. The general character of the Air Slap Signature (Ref. 7) remained unchanged. (i.e. the multiple peak nature of the airblast was ignored)

The second modification to the "WAVE-ADDER" was to add the Higgins method (Ref. 8) for calculation of the vertical oscillatory motions.

The vertical ground motion prediction made by the "WAVE-ADDER" then is the superposition of the air slap signature and the Higgins oscillatory component signature.

The prediction of horizontal motions involved modification of the vertical air slap motions by the equations given in Reference 9. The oscillatory component was determined by Higgins method (as in Ref. 3) for each charge and then all oscillatory waveforms were superimposed with the air slap signature to form the predicted waveform.

Comparison of these predictions and the data will be made in Section 4.

### 3.3 SINGLE BURST DATA SUPERPOSITION PREDICTIONS

There are basically three procedures for making predictions of this type depending upon the location of the gage in question. For discussion purposes the procedures will be classed as, at the array center, off center but greater than  $1/4$  the charge spacing from an individual charge, and at  $1/4$  or less the charge spacing away from the closest charge ( $1/4$  CS). (See Figure 13)

The procedures for the on-center and  $1/4$ -CS locations are straight forward. The prediction of the on-center points involve only the vertical gages, since in theory the horizontal motions will cancel. The vertical prediction is arrived at by the multiplication of the waveform amplitudes registered by the gages at the single burst range equal to the charge spacing of the multiburst array, by the number of "nearest" charges in the array (for all experiments presented here the number of charges was 6). At the  $\leq 1/4$  CS locations the prediction simply becomes the single burst waveform at the appropriate location from the single charge experiment. At this distance, the effect of the nearest charge is so great that the other charges

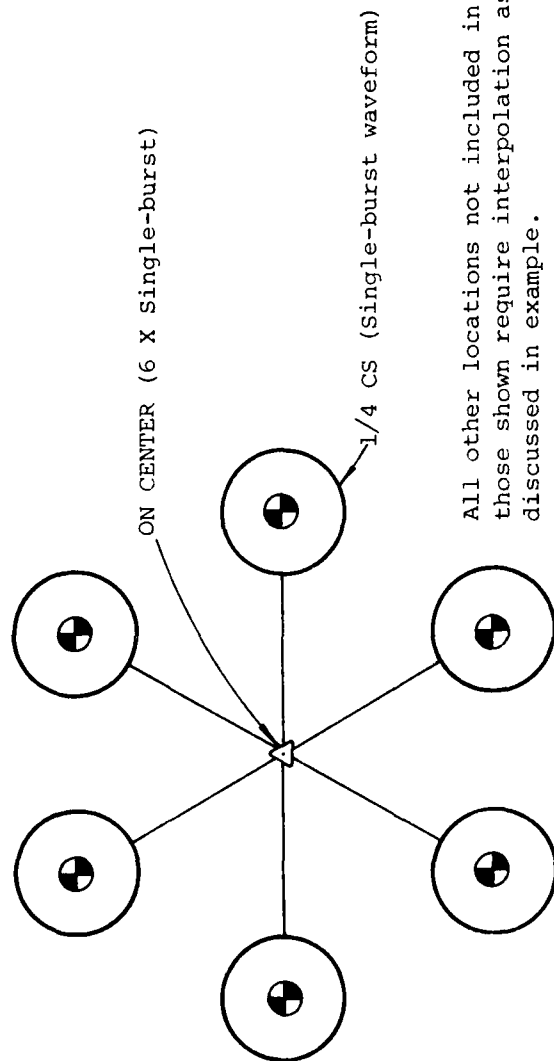


Figure 13: Regions for which procedural differences in superposition predictions exist.

in the array have a negligible effect on the waveform. This is true for both the horizontal and vertical motions.

In theory, the prediction of the intermediate locations is straight forward. Data from a single burst experiment at ranges corresponding to the distances from the target point to each charge are superimposed. In practice, however, the procedure is much more complicated because data from the required single burst locations are not available. As a result it is necessary to construct waveforms which represent data at the required locations. This involves interpolation and extrapolation of existing data. Since the waveforms are made up of components with differing attenuation rates and propagation speeds and the linear variation of the physics involved is not guaranteed, the construction of these waveforms is somewhat tenuous.

The following example is as an illustration of the procedure utilized. The target point chosen for this example was taken from a six charge array where the spacing was 36.60m (MBI-6). The location at this point was on the 270° azimuth at a range of 21.70m and 0.46m in depth. The spatial orientation of the problem is presented in Figure 13.

The procedure used for the prediction of the vertical waveform was broken down into three general areas. They were as follows:

3.3.1      Determination of Ranges and the Selection of the Proper Bounding Waveforms: The determination of ranges was a simple process. For this example there were only three different ranges involved due to the symmetry of the problem. These ranges are shown on Figure 14 as  $R_1 = 18.30\text{m}$ ,  $R_2 = 48.42\text{m}$ , and  $R_3 = 65.98\text{m}$ . For  $R_1$  there was no need to select bounding waveforms as the single burst experiment had a measurement at this exact location.

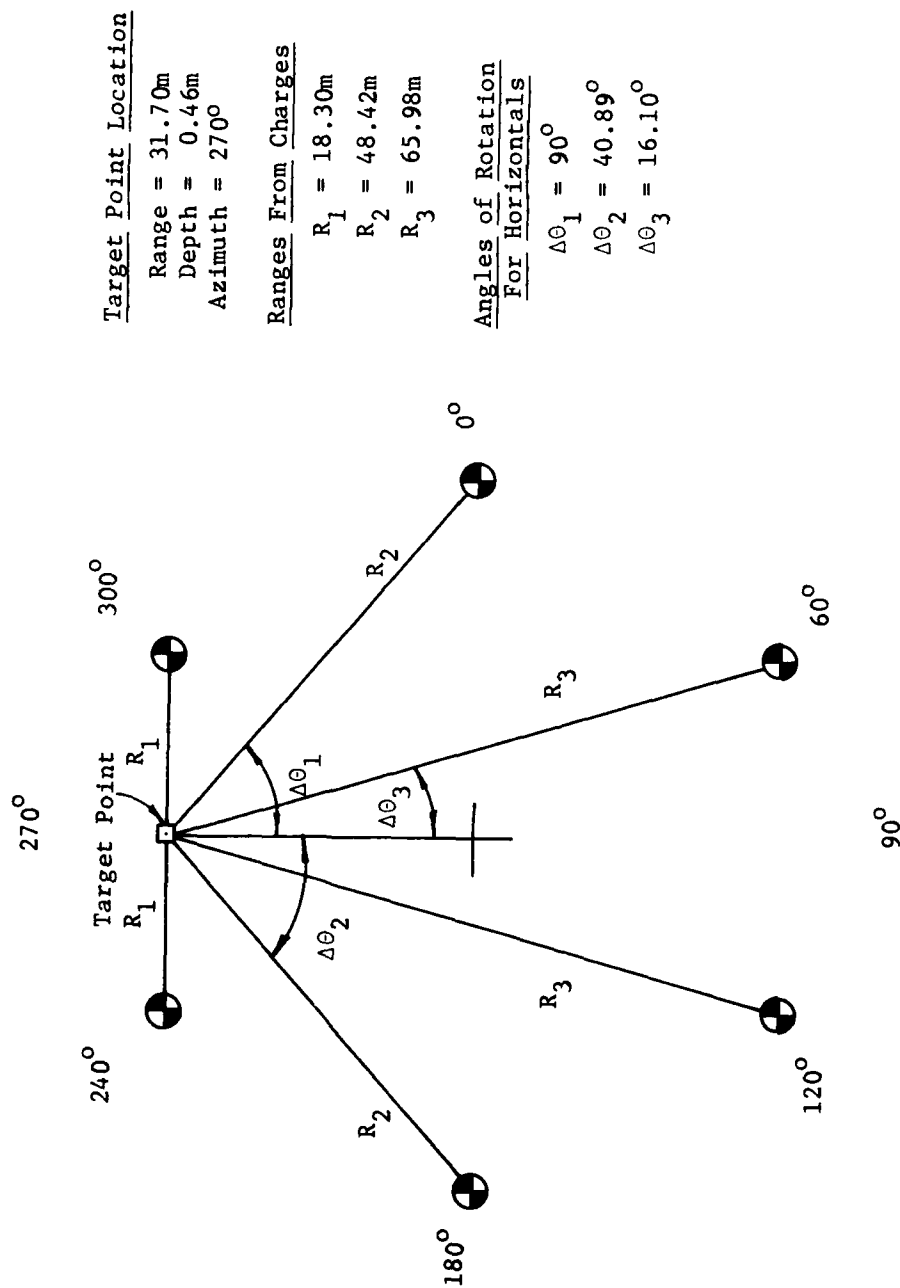


FIGURE 14: Target Location for Illustrative  
 Example of the Superposition  
 Prediction Procedure - From  
 Event 6

For  $R_2$  and  $R_3$ , the closest bounding waveforms were at the ranges of 45.75m and 73.20m. These waveforms are shown in Figure 15a.

3.3.2 The Interpolation of the Timing of the Waveform: For the determination of the timing of the waveform, the waveform was divided into three components. These were first arrival (outrunning), high frequency (airslap) and low frequency (oscillatory component). Arrival times for these components on the two bounding waveforms are indicated by the arrows in Figure 15a. Arrival times for these three components were linearly interpolated from the closest bounding waveform. The arrival times were calculated to be 45 msec for the first arrival, 88 msec for high frequency and 233 msec for low frequency at  $R_2$ . For  $R_3$  the arrival times were calculated to be 48 msec for the first arrival, 138 msec for high frequency and 285 msec for low frequency.

3.3.3 Determination of Amplitude Modification Factors: Waveform amplitudes were modified by factors for both the high and low frequency components. These factors were determined by the general equation:

$$(AM)_V = \frac{V'_V}{V_V} \quad (N)$$

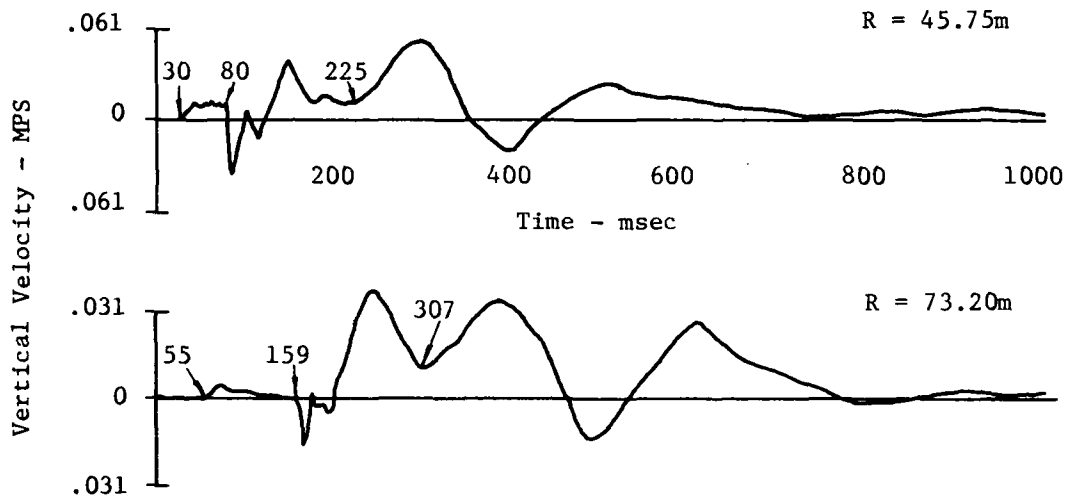
where

$(AM)_V$  = vertical amplitude modification factor

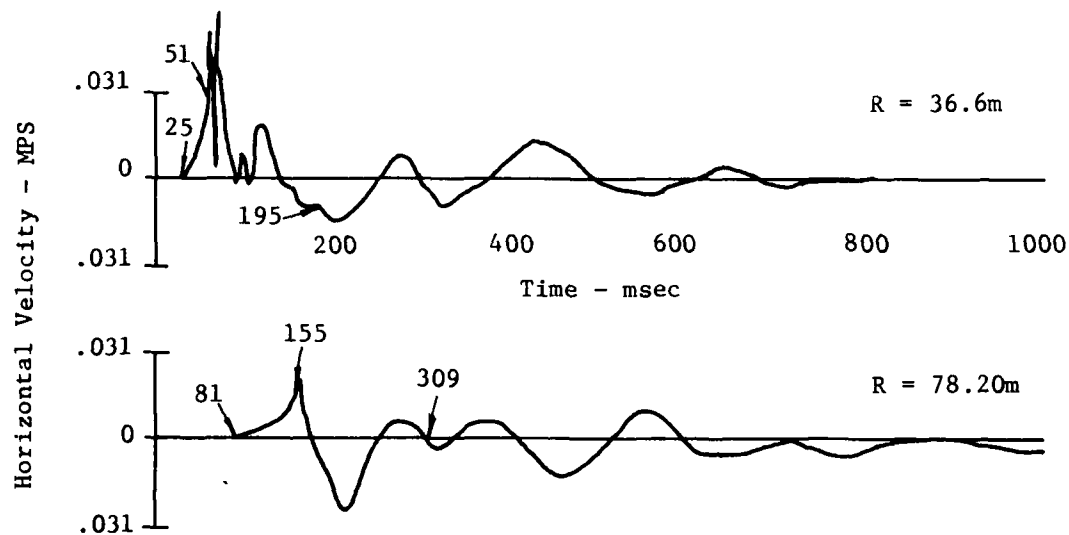
$V'_V$  = vertical velocity at the range in question  
(determined from an attenuation curve)

$V_V$  = vertical velocity at the nearest bounding  
single burst location

$N$  = number of charges involved at the range  
in question



a) Vertical Waveforms From MBI-1 Used for Interpolation of Target Point at  $R=31.7$ ;  $Z=0.46$ ;  $\Theta=270^\circ$



b) Horizontal Waveform From MBI-1 Used for Interpolation of Target Point at  $31.70/0.46/270^\circ$

FIGURE 15: Waveforms Used for Interpolation in the Superposition Prediction for the Target Point @  $R=31.70$ ;  $Z=0.46$ ;  $\Theta=270^\circ$

In this example  $V_v^1$  and  $V_v$  are taken from Figure 16 which presents the attenuation curves for both high frequency and low frequency components. The values for  $(AM)_v$  at  $R_2$  were determined to be 1.8 for high frequency and 2.0 for low frequency. At  $R_3$  these values were 2.25 for high frequency and 2.31 for low frequency.

All modifications discussed above were then incorporated into the nearest bounding waveforms for  $R_2$  and  $R_3$  (for  $R_2$  the nearest bounding waveform was at 45.75m and for  $R_3$  it was 73.20m). The results of these modifications are shown in Figure 17. Shown on Figure 18 is the composite waveform which is the superposition prediction for the vertical motion at this target point.

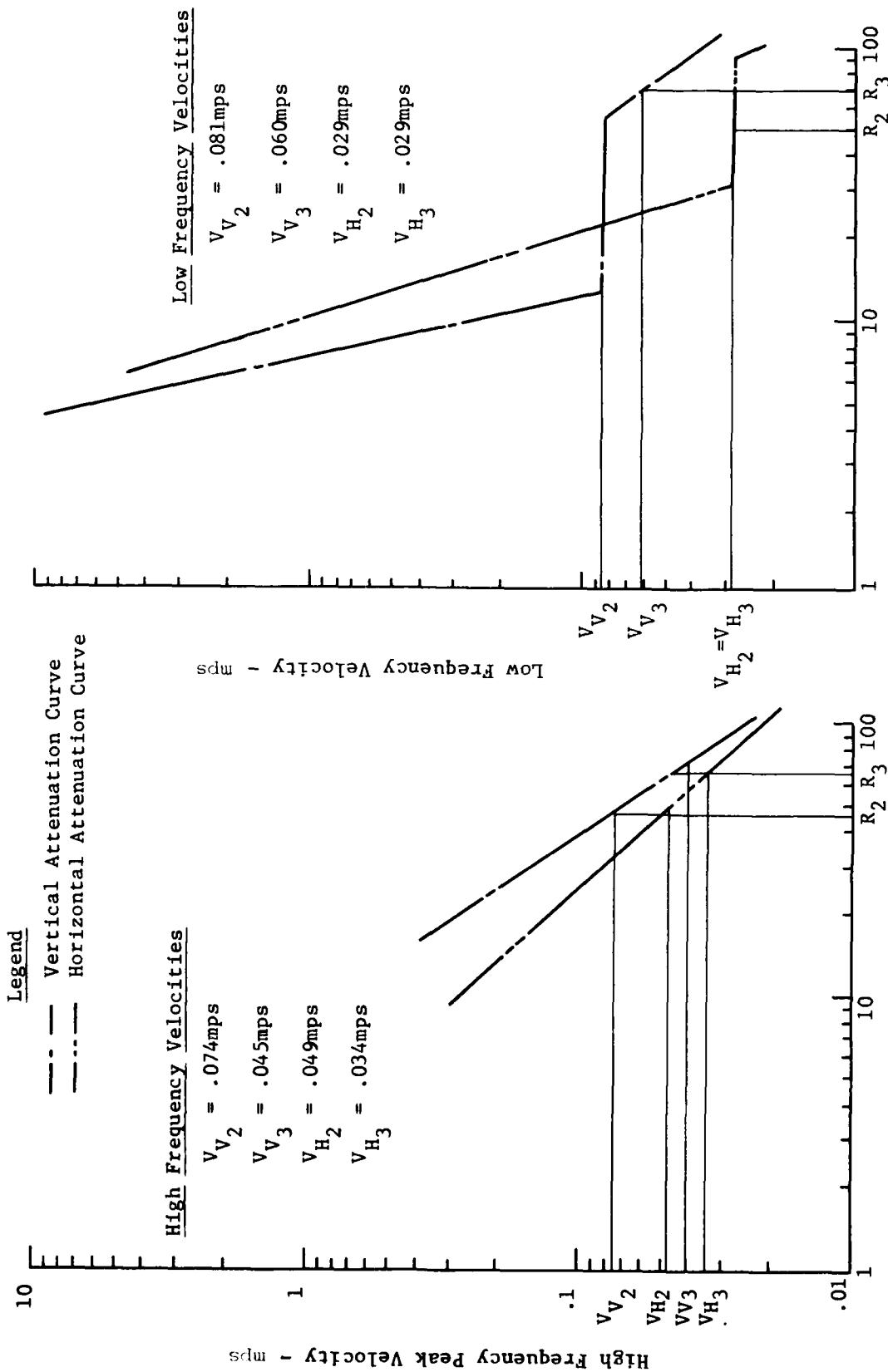


FIGURE 16: Attenuation Curves Used for Determination of the Amplitude Modification Factors (Ref 1)

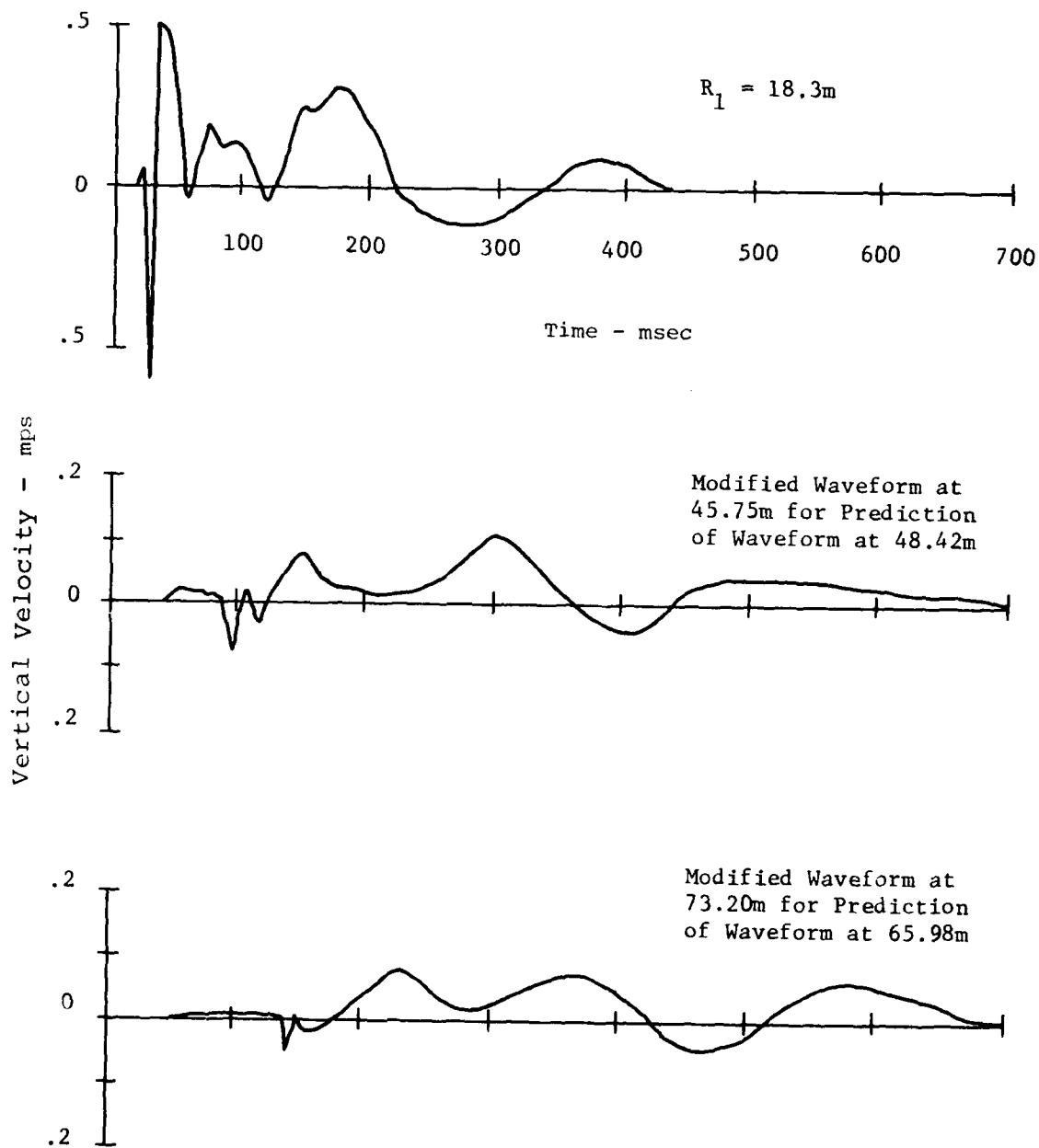


FIGURE 17: Modified Vertical Waveforms Used  
in the Superposition Prediction  
of Target Point  $\theta R=31.70$ ;  $Z=0.46$ ;  
 $\theta=270^\circ$

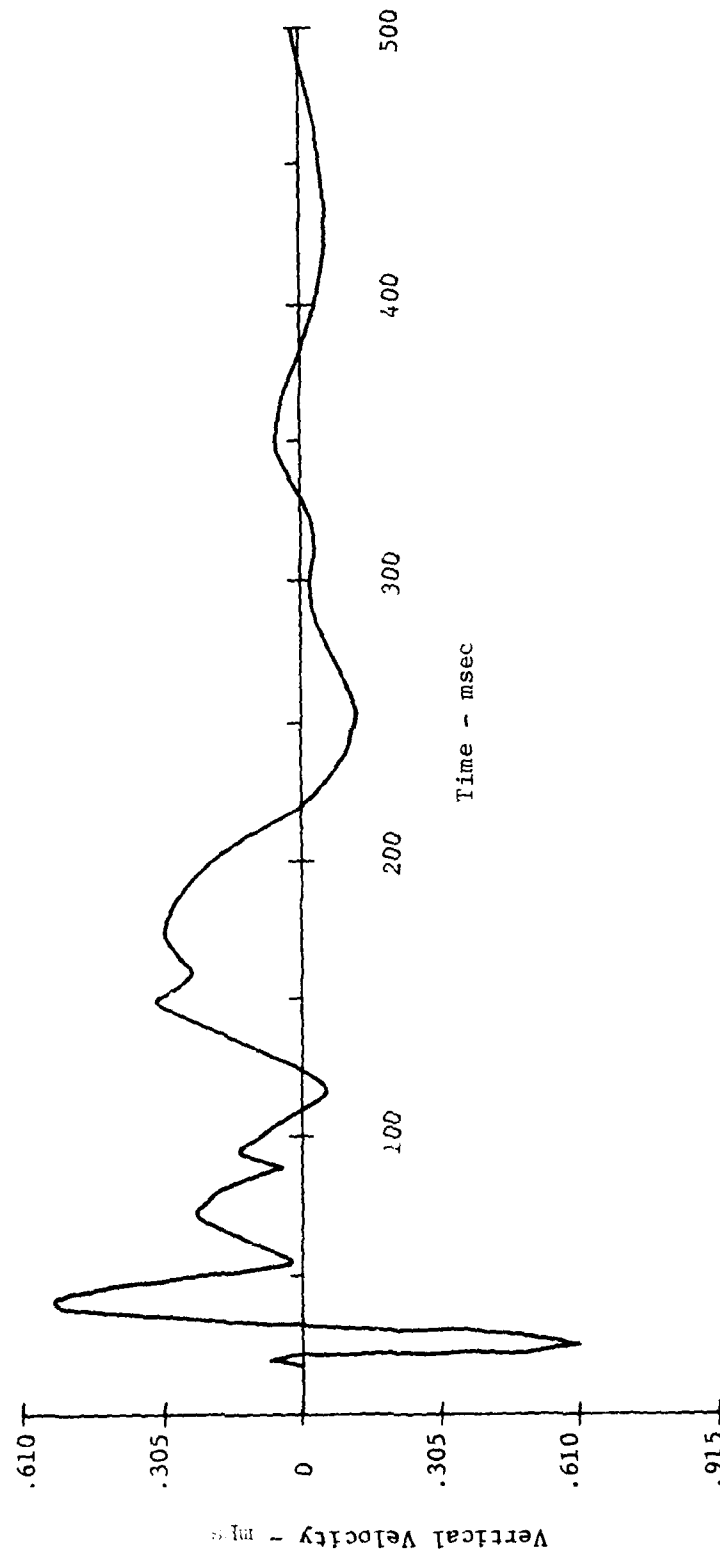


FIGURE 12: Superposition Prediction for Vertical Motion at  $R=31.70$ ;  $Z=0.46$ ;  $\theta=270^\circ$

The procedure used for the prediction of the horizontal waveform was identical to the procedure used for the vertical waveform as far as determination of ranges, selection of waveforms, and interpolation of timing. For this example the ranges of interest are only  $R_2$  and  $R_3$ . The charges at  $R_1$  in theory will cancel. The bounding waveforms used for the interpolation process are shown in Figure 15b (the bounding waveforms used for horizontal motions are different from the vertical because of the lack of useable horizontal data at the 45.75m range). The arrival times for the interpolated waveforms are 30 msec for the first arrival, 54 msec for high frequency, and 280 msec for low frequency at  $R_2$  and 70 msec for the first arrival, 134 msec for high frequency, and 286 msec for low frequency at  $R_3$ .

The difference in the prediction procedures for horizontal and vertical motions came in the calculation of the amplitude modification factor. The general equation used for the horizontal modification factor was:

$$(AM)_H = \frac{V'_H}{V_H} (N) (\cos \Delta \theta)$$

where

$(AM)_H$  = horizontal amplitude modification factor

$V'_H$  = horizontal velocity at range in question  
(taken from attenuation curve - Figure 9)

$V_H$  = horizontal velocity at nearest single  
burst bounding waveform

$N$  = number of charges involved at the range  
in question

$\Delta \theta$  = angle of rotation necessary to rotate  
single burst horizontal gage orientation  
to match the multiple burst horizontal  
gage orientation.

For this example the horizontal gages on the single burst experiment were oriented such that the positive direction of measurement was outward from the charge. The multiple burst gage orientation was such that the positive direction of measurement was outward from the center of the array. The resulting angles for each range are shown on Figure 14. The modification factors were then calculated to be 1.09 for high frequency and 1.51 for low frequency at  $R_2$ , and 2.18 for high frequency and 1.92 for low frequency at  $R_3$ . The modified waveforms are shown on Figure 19 and final superposition waveforms are shown in Figure 20.

It should be recognized that the major limitation of this procedure is the experimenter's choice of the single burst waveform that will be used to interpolate from. In all cases where the single burst waveform is modified to form an interpolated waveform, only the single burst waveform that is the closest bounding waveform should be used, or significant errors could develop. This is especially true where ground motion is undergoing the transition from a waveform dominated by high frequency airblast related motion to the classic outrunning waveform. Extrapolation of waveforms leads to questionable results and should be avoided.

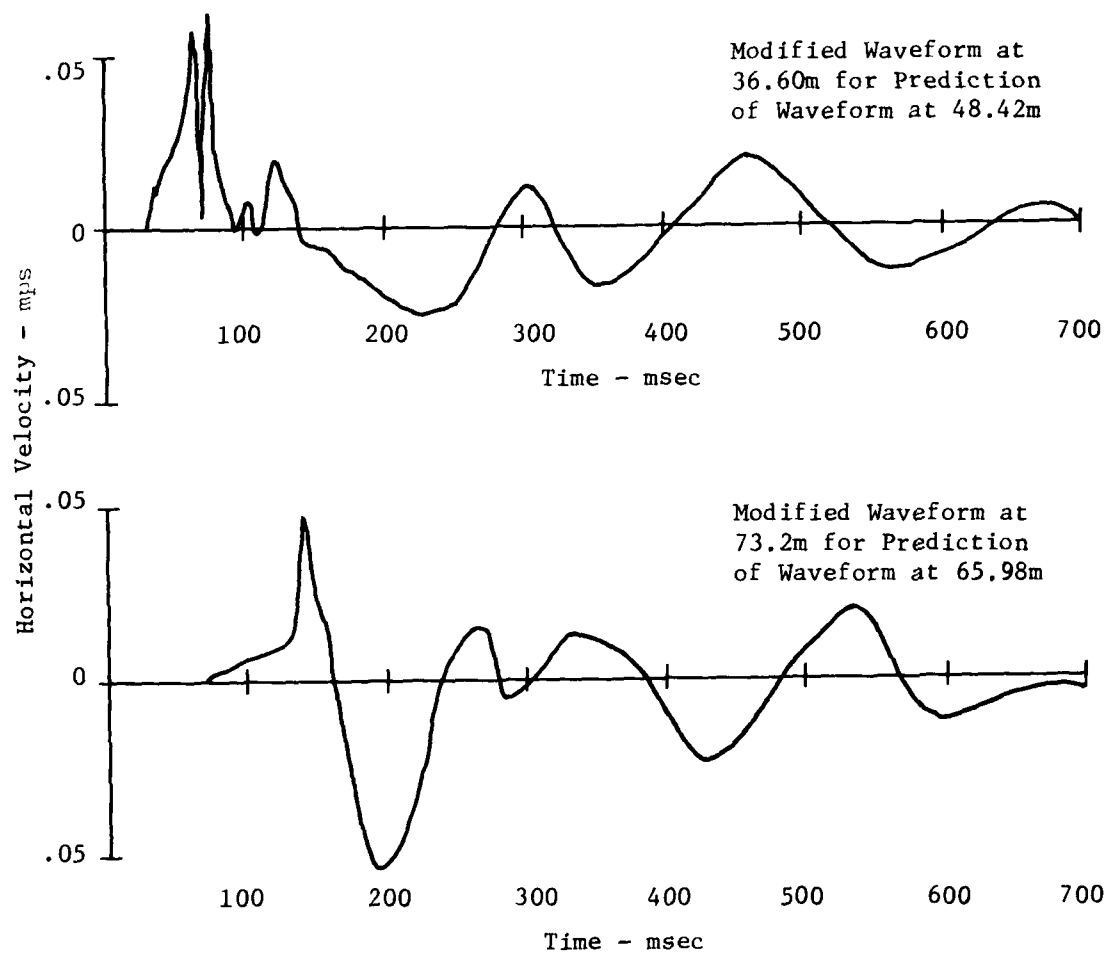


FIGURE 19: Modified Horizontal Waveforms Used in the Superposition Prediction of Target Point @  $R=31.70$ ;  $Z=0.46$ ;  $\Theta=270^\circ$

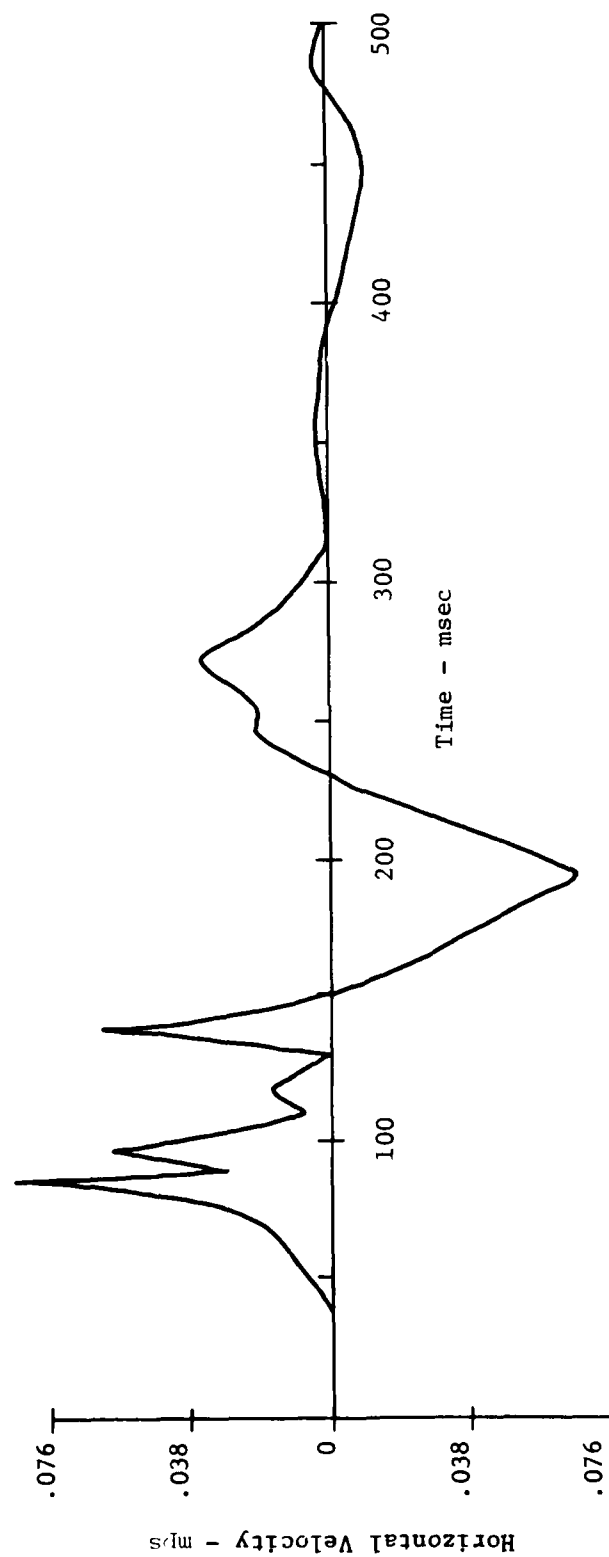


FIGURE 20: Superposition Prediction for Horizontal Motion at  $R=31.70$ ;  $Z=0.46$ ;  $\Theta=270^\circ$

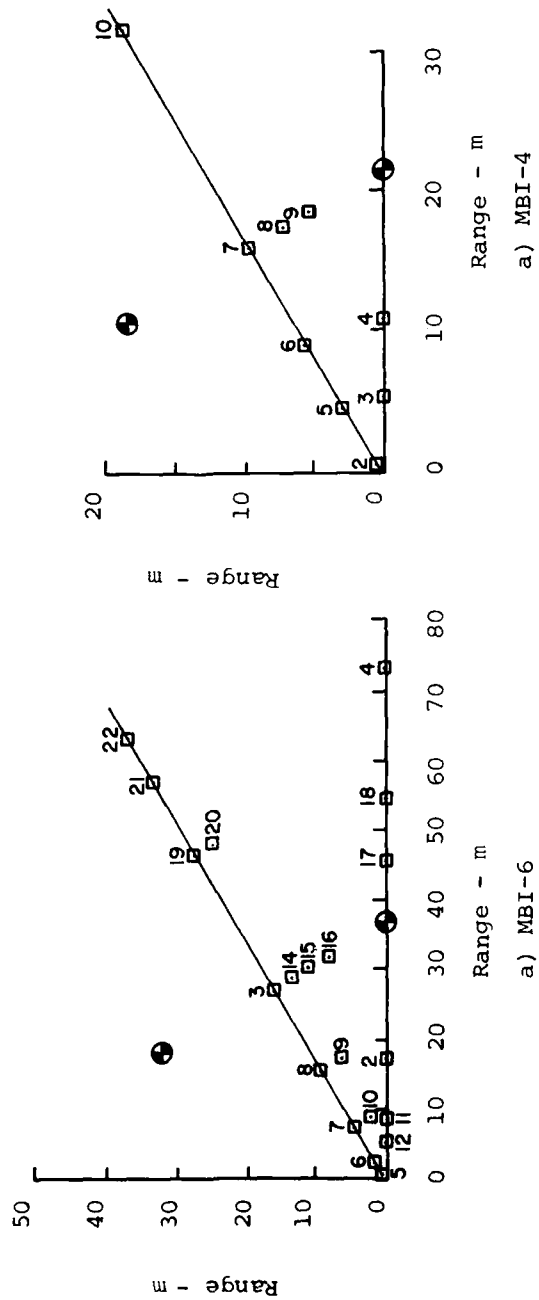
#### 4. COMPARISON OF DATA & PREDICTIONS

##### 4.1 AIRBLAST

As was stated in the previous section, the airblast predictions were performed using the LAMB model and assuming the  $2.09 \times 10^{-3} \text{ TJ}$  (0.5T) HE sphere could be approximated by  $4.18 \times 10^{-3} \text{ TJ}$  (1.0T) of nuclear energy. This factor of equivalence is commonly used in HE airblast evaluation although a better fit is possible by varying the factor for different overpressure regions.

All the instrumentation locations have been folded into one  $30^\circ$  segment as shown on Figure 21, so that gages at geometrically redundant locations are shown as one point. The first peak for a number of these locations will be determined only by the nearest charge with the effects of other charges arriving later. To evaluate the LAMB prediction of the multiburst effects it is necessary to evaluate how well it treats the single burst incident blast. First peaks determined by a single charge from a number of the gages are plotted in Figure 22 along with the single burst data from MBI-1, MBI-3 and MBI-7 (scaled). The LAMB predictions for those same locations are also shown. The MBI-6 data agree very well with the single burst data falling about 20% below the empirical prediction. The LAMB predictions on the other hand vary from 50 to 100% greater than the data with the better agreement at the lower overpressures.

Since the calculated overpressures are greater than measured, the reflection factor, which is a multiplicative factor, will also be higher than that actually occurring.



# LEGEND

- Charge
- AF Gage Location

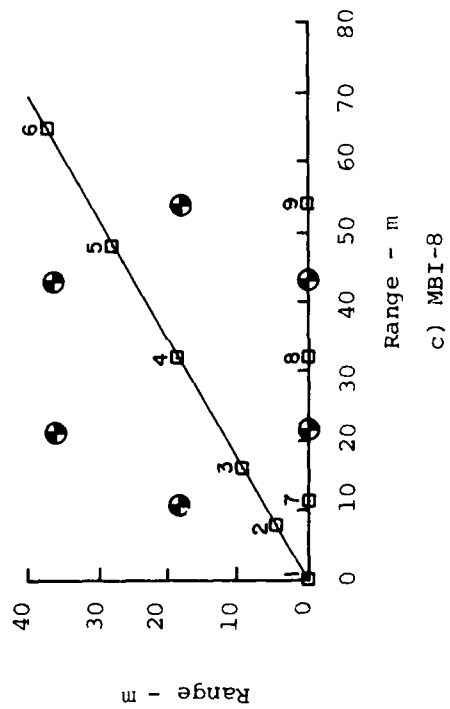


FIGURE 21: Airblast Prediction layouts for the Phase I Multiple Burst Experiments

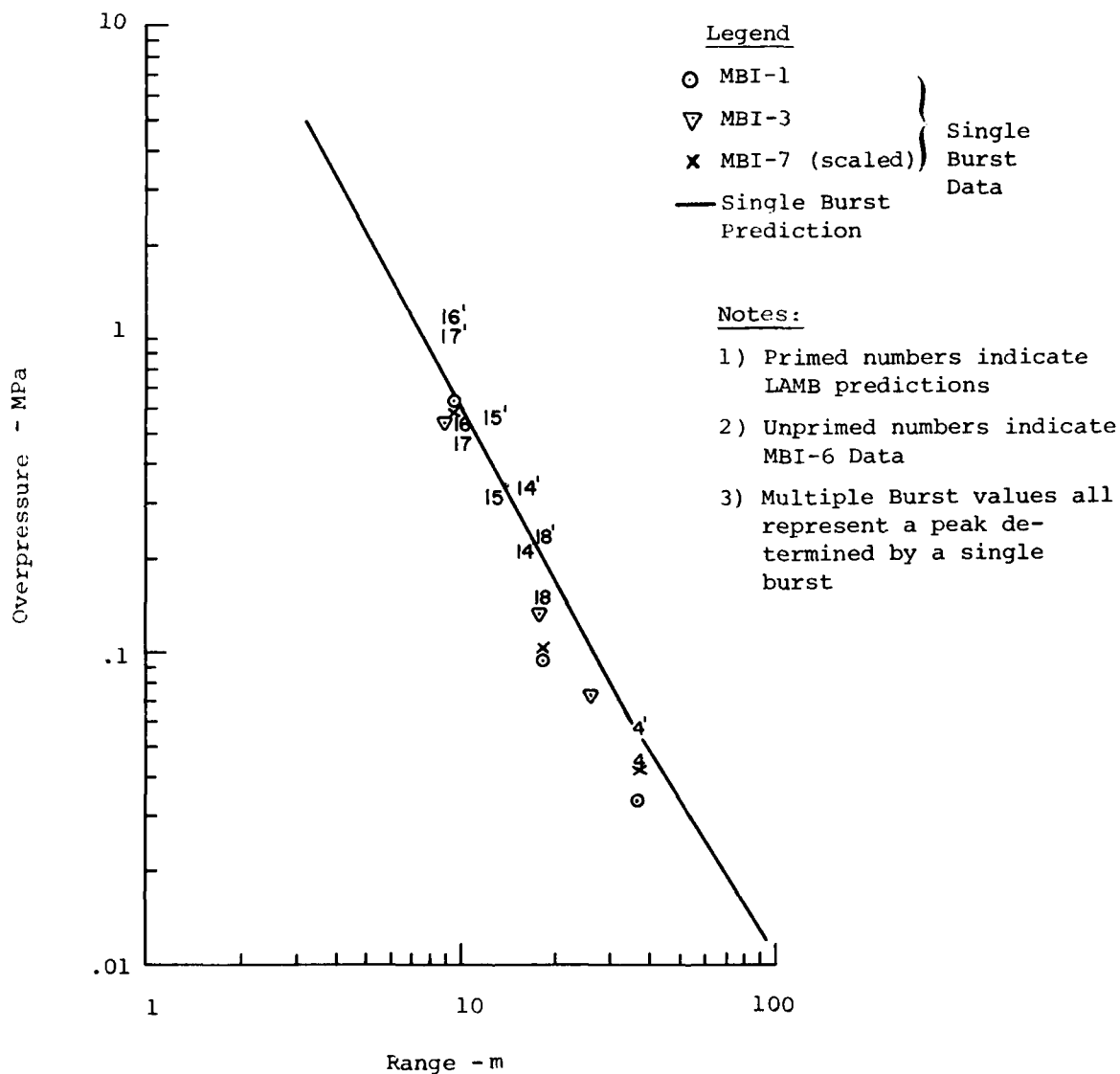


FIGURE 22: Comparison of Predicted and Measured Single and Multiple Burst Air Pressure for the Half Buried Configuration

This should result in significant overestimation of the peak pressures. The six charge, half buried experimental data (MBI-6) and calculations are compared in Figure 23. The solid lines shown represent the ideal situation (i.e., prediction and data equal). The predicted overpressures average only about 18% greater than measured. This suggests that the LAMB code may be underestimating the shock on shock interaction effects.

The comparison of total impulses is also shown in Figure 23 LAMB also overpredicted the impulse as would be expected from the discussion above. The impulse at target point 5 (.915m off center) is  $3.5 \times 10^{-3}$  MPa-sec. Since the six bursts arrive with approximate simultaneity at this point, the waveform looks like a classical single burst waveform. This combination of pressure and impulse would be equivalent to a single burst yield of  $3.85 \times 10^{-3}$  TJ (0.92T).

Measured pressure-time histories along a bisector ( $\theta=150^\circ$ ) are shown in Figure 24 (additional pressure time histories may be found in Appendix C). Note that the range is measured from the center of the array. The very different nature of the waveform in the center half of the array is illustrated by the first three waveforms. The first record shows the three distinct arrivals (each from 2 charges) occurring very closely in time due to the small offset (0.915m) from the array center. There is little time for decay of the overpressure before the later arrivals so that the peak overpressure occurs with the third arrival. The single burst incident pressure at this range is 0.36 MPa. The first peak is 0.103 MPa indicating a reflection factor of 1.44 for the two bursts (an increase of 44% over superposition). The second step is 0.131 MPa and the third step is 0.266 MPa. This increase in pressure associated with each pair of charges reflects the effect of the preshocked nature of the air. The resultant peak pressure of 0.414 MPa is only slightly less than the 0.473 MPa which would be estimated from the rule of thumb; (i.e., incident overpressure multiplied by the number of bursts and the reflection factor).

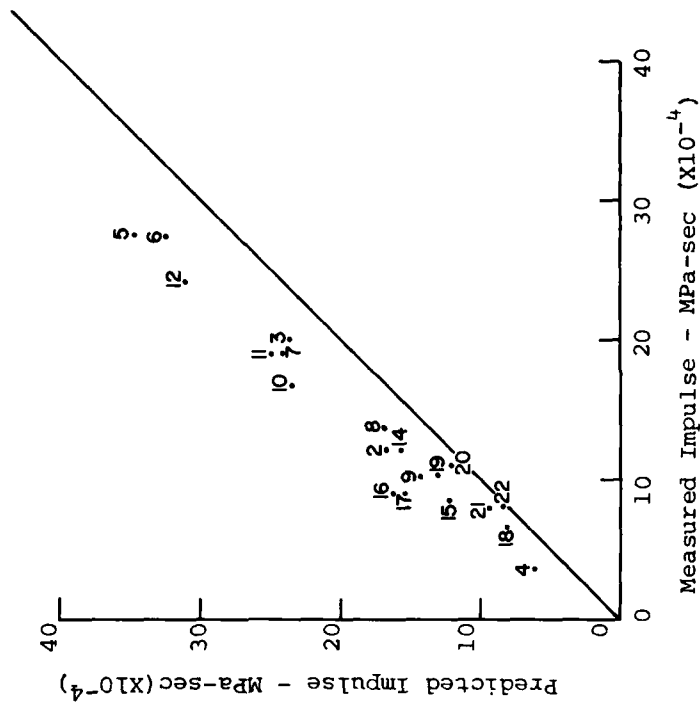
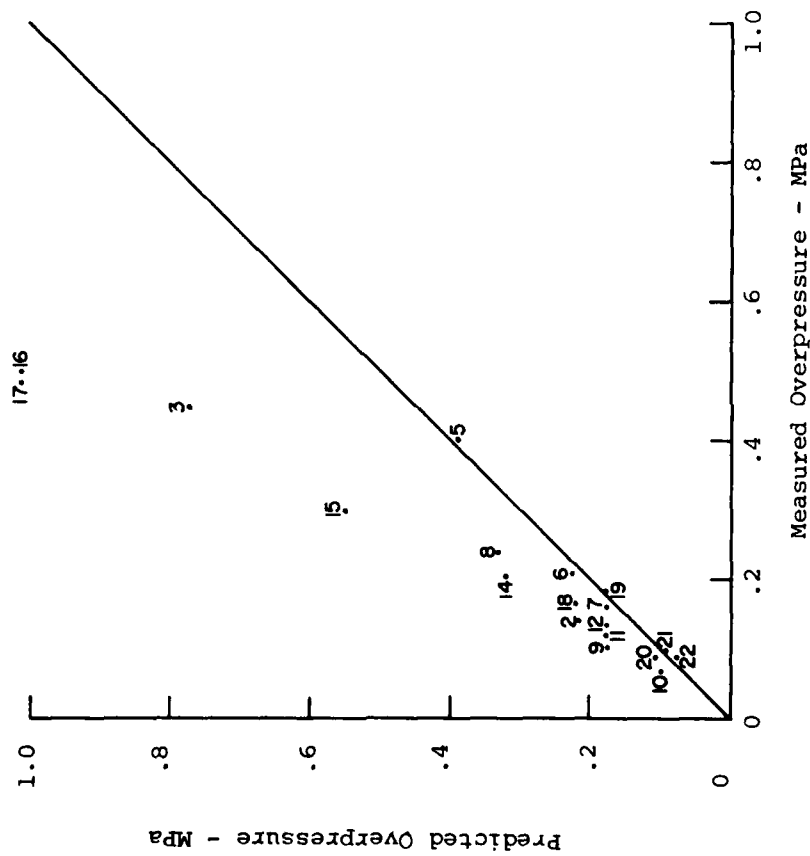


FIGURE 23: Comparison of Measured and Predicted Airblast Pressure & Impulse - MBI-6

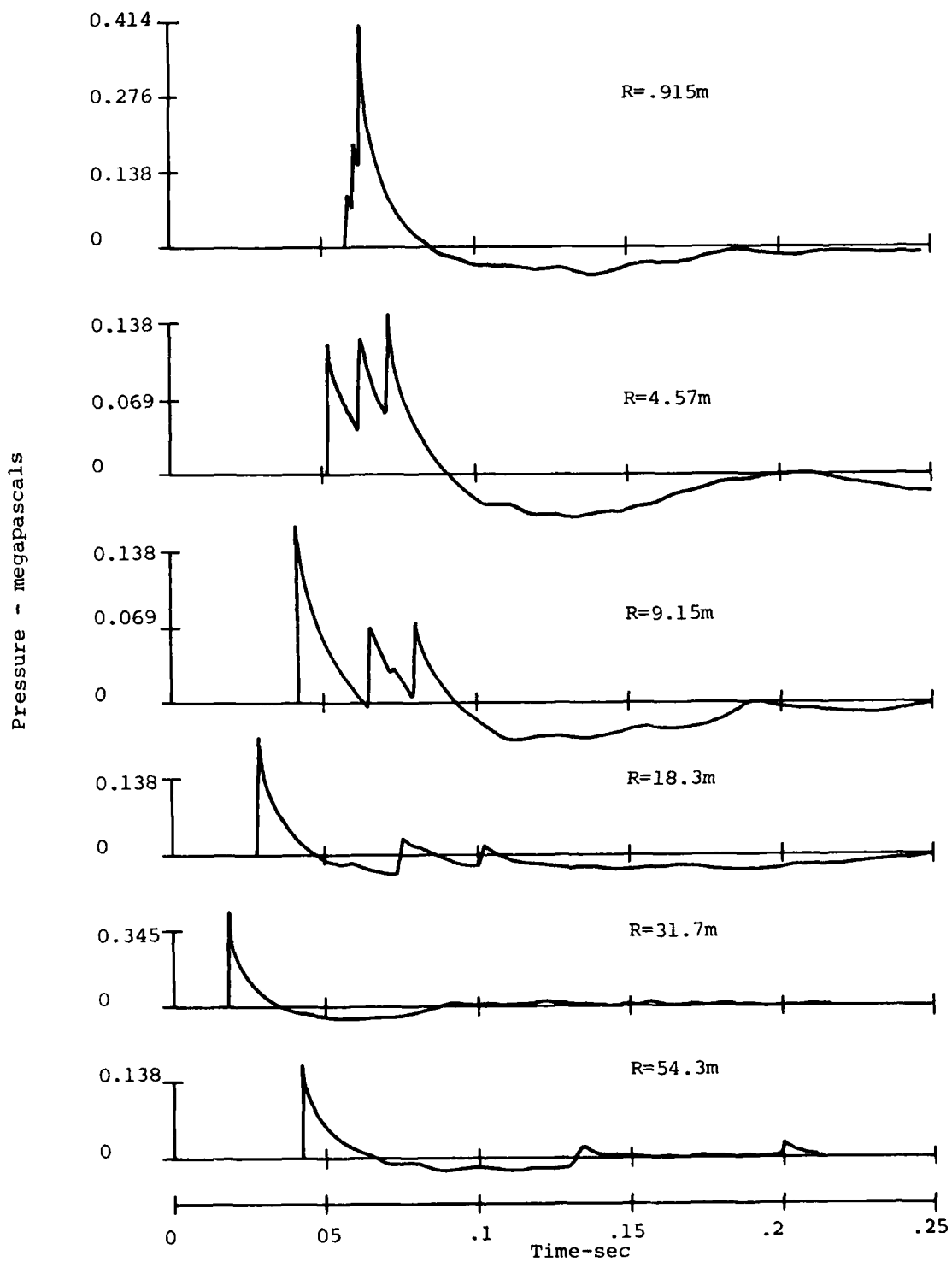


FIGURE 24: Air Pressure Measurements on the  $150^\circ$  Azimuth - MBI-6

The record from 4.57 m range also indicates the simultaneity of bursts (only 3 arrivals) but the decay between arrivals is significant, resulting in three peaks of nearly the same amplitude. This trend continues until the 9.15 m range where the initial pulse has decayed to zero pressure before the second wave arrives. Directly between 2 charges (31.71 m range) the pulse looks very much like a single burst waveform. The incident pressure of 0.172 MPa is reflected to 0.462 MPa which is significantly less than the rule of thumb estimate of 1.069 MPa. The LAMB prediction for this location was 0.766 MPa indicating this gage for some reason may be underrecording.

The comparisons of calculated and measured overpressure and impulse for the six charge surface tangent experiment (MBI-4) is shown in Figure 25 (pressure time histories may be found in Appendix C). Examination of the points where the first peak is controlled by a single charge (pts 4, 8, 9) indicates that LAMB is overestimating the single burst peak pressure above 1 MPa and underestimating it below 1 MPa. Since all the shock on shock interactions occur below 1 MPa, LAMB would be expected to underestimate the multiburst peak pressures. This is true except for target point 10, therefore, data scatter does not explain these exceptions. The waveforms along the bisector (150°) indicates that there was a little jitter in the detonation times.

The total impulse at all target points controlled by multiple burst interactions. The data are generally within  $\pm 20\%$  of the LAMB calculated values with no apparent systematic trend.

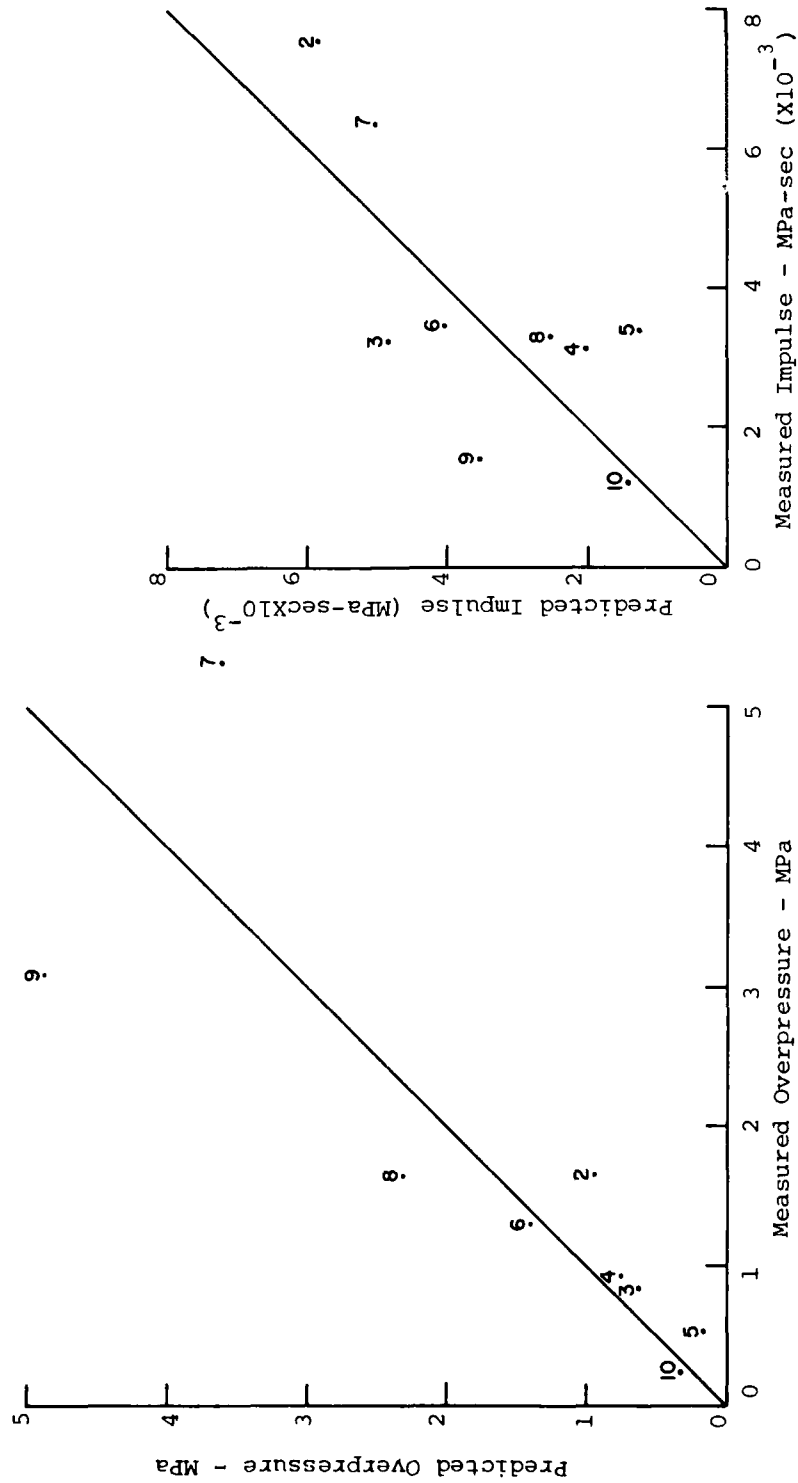


FIGURE 25: Comparison of Measured and Predicted Airblast Pressure & Impulse MBI-4

The air pressure instrumentation layout shown in Figure 21C shows 6 of the 24 charges of MBI-8. Point 1 represents the center of the outside 6 hexagons. With the exception of these center points, the multiple burst model (LAMB) overpredicted the peak pressure (Figure 26). The first peaks from points 7 and 9 are a result of the closest single burst and are overpredicted by about 40% by LAMB. The outside centerpoints (pt 4) are the only measurements made at the exact center of a hexagon and are significantly underpredicted. The large data scatter in these measurements are probably the result of jitter in the detonation times. Impulses at all target points were underpredicted.

The negative portion of the airblast has received little attention in the past. However, study of the ground motions indicates that the negative pressure may be playing an important role in near surface region.

The maximum underpressure and duration of the negative phases for MBI-6 and MBI-4 are shown in Figure 27. Range has been plotted as distance from the nearest charge, therefore, a range of 21.3 m on MBI-4 represents the array center and also a point on a bisector outside the array (a second center on event 8). Comparisons with the LAMB code were not made because matching this phase of the airblast was not included in the LAMB development. Data from the single burst events are shown for comparison, however. The best single burst data were available for MBI-1. Near the charge the Event MBI-6 amplitude appears to be controlled by the single burst and the 20% difference is probably data scatter. Outside the array at one charge spacing the multiple burst value is approximately twice the single burst at the array center, the multiple burst value is approximately 8 times the single burst value for both MBI-6 and MBI-4. This suggests that superposition is a reasonable

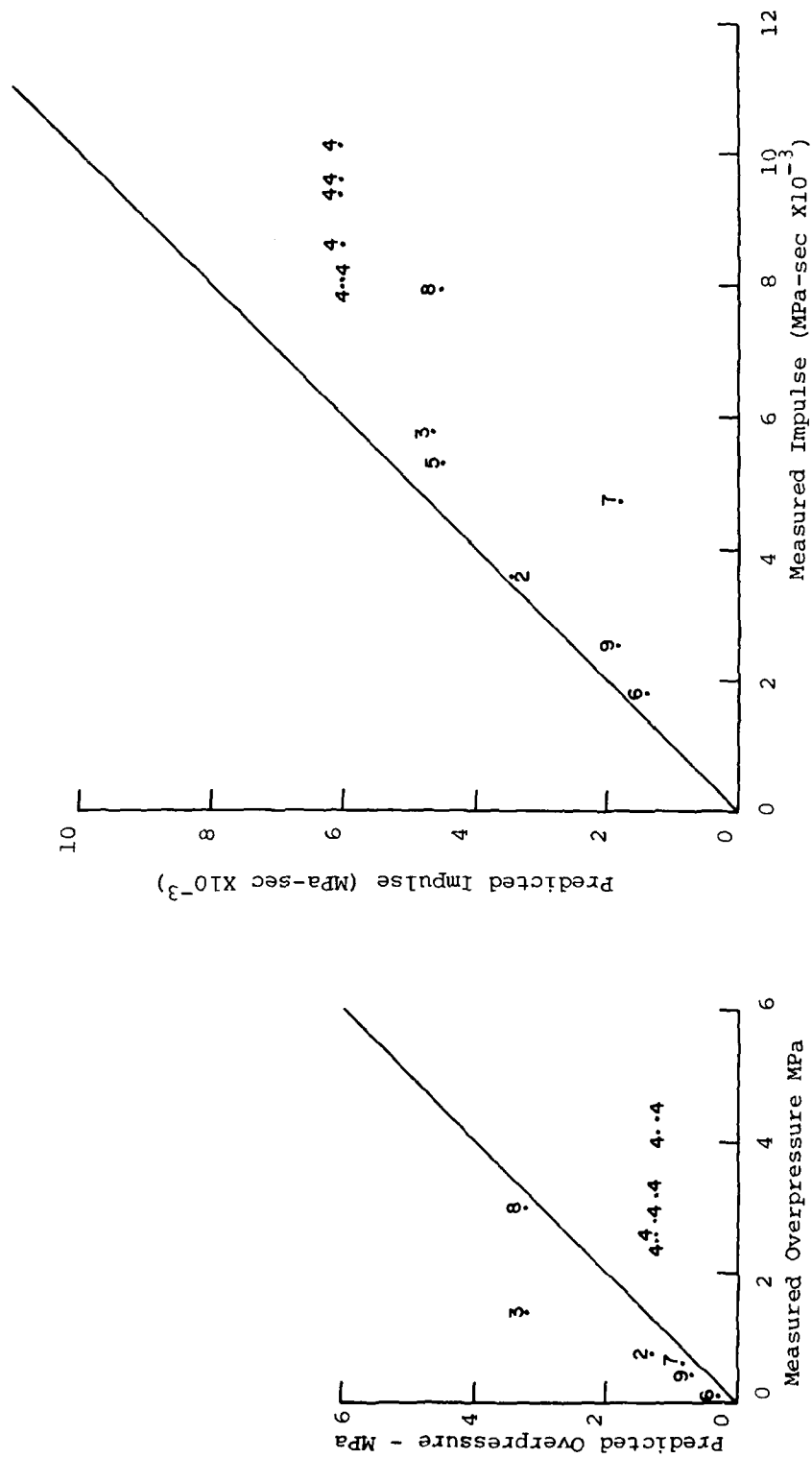
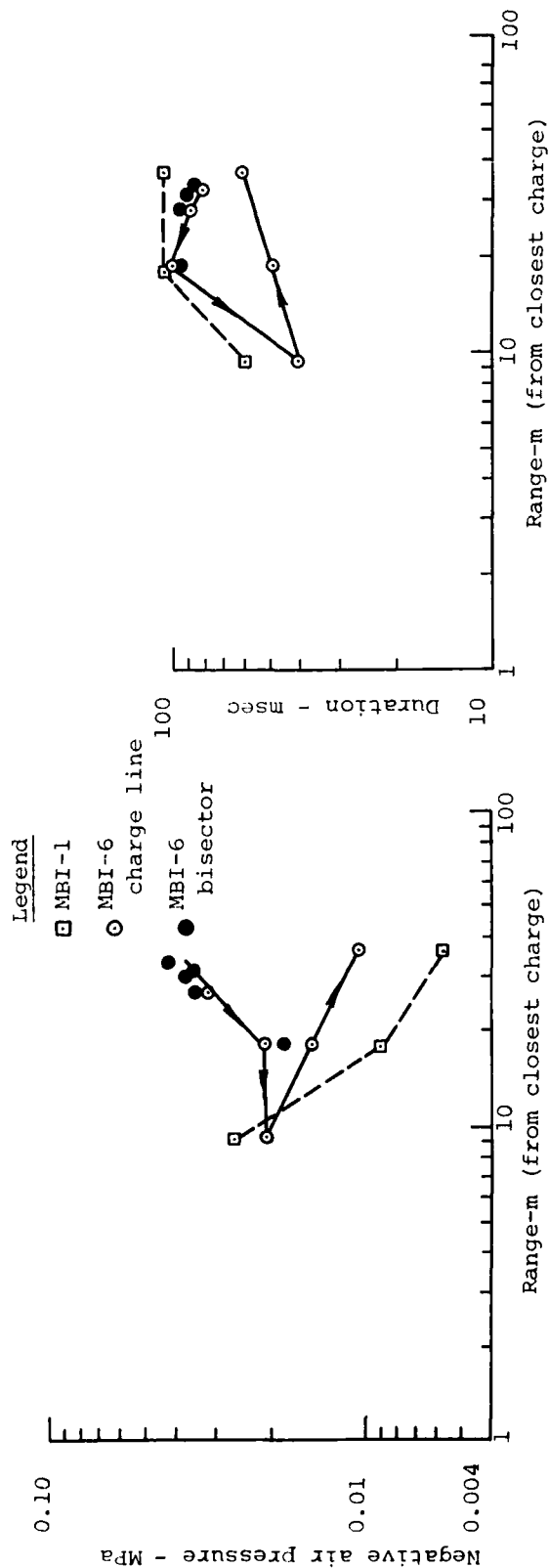
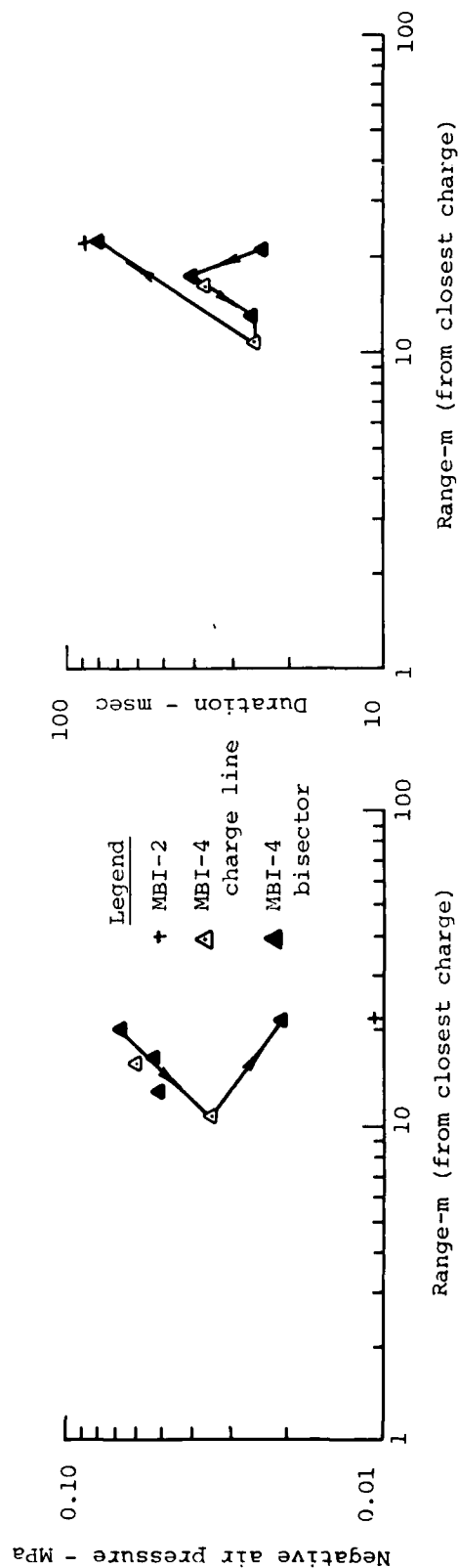


FIGURE 26: Comparison of Measured and Predicted Airblast Pressure & Impulse MBI-8



a) MBI-6



b) MBI-4

FIGURE 27: Magnitude and duration of Negative Phase of the air blast for MBI-6 and MBI-4

approximation of the peak negative pressures as long as the combined negative pressure does not exceed an atmosphere. Durations for the multiburst experiments on the other hand, appear to be upperbounded by the single burst experiments. This would be expected at points off the array center due to the arrival of positive pulses from more distant charges. However, superposition would also lead to this result.

Event MBI-8 data are not presented because of the numerous arrivals during the negative phase, but the data appears to support the observations presented above (see the pressure time histories from MBI-8 included in Appendix C).

In summary, it appears that using a  $4.18 \times 10^{-3} \text{ TJ}$  (1.0T) nuclear airblast to approximate a  $2.09 \times 10^{-3} \text{ TJ}$  (0.5T) high explosive airblast leads to an overestimate of the high explosive airblast in the pressure regions of interest in this study. However, it should be noted that the empirical prediction also overestimated the peak pressures for the half buried and tangent below events of Phase I. In light of this it is difficult to make definitive statements concerning the accuracy of the LAMB airblast model. It appears, however, that the tendency is for LAMB to underestimate the shock-on-shock interactions. The waveforms it predicts however are very similar and the impulse generally agree with the data better than the peak pressures indicating the duration are somewhat longer than measured.

Superposition of the single burst negative pressure leads to a good estimate of the multiple burst negative pressure measurements.

## 4.2 GROUND MOTIONS

### 4.2.1 Introduction

An assumption inherent in the multiburst predictions made by both the empirical and superposition techniques is that the phenomenology may be superimposed. An evaluation of this assumption will be discussed in Section 4.3.

This section presents the comparisons made between the empirical predictions, superposition predictions, and the multiple burst experimental data. To make comparisons the waveforms were divided into two basic components. These were the high frequency (air slap) component and the low frequency (oscillatory) component. These components were broken down into characteristics such as time of arrival, frequency or period, peak values, etc. and these individual characteristics were then compared. These comparisons were grouped into three locations. These were the array center, inside the array, and outside the array.

#### 4.2.2 Accuracy of Superposition

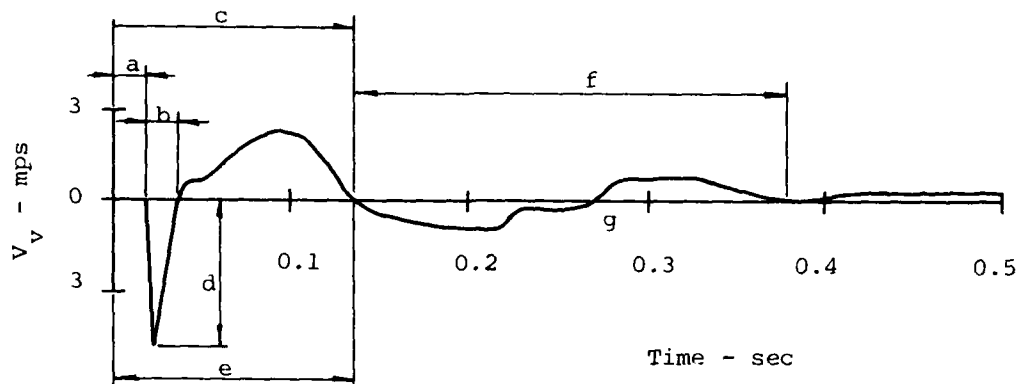
The following discussion is based on several waveforms comparing superposition and data from the three multiple burst experiments. These waveform comparisons are presented in Appendix. The results of the waveform comparison study are presented in Tables 3 through 7. It is noted here that the figures in the tables represent the percentage difference of the data and superposition with the data used as the base. When the data was consistently over or under predicted an average of the scatter is shown. If the data was both under and over predicted then the range of the scatter is shown.

From the study of these Tables the following conclusions may be made:

- The accuracy of superposition is not considered acceptable at the center of the charge array at depths above the phreatic surface. From Table 3 the general trend in the three experiments is toward an underprediction in all the characteristic components.

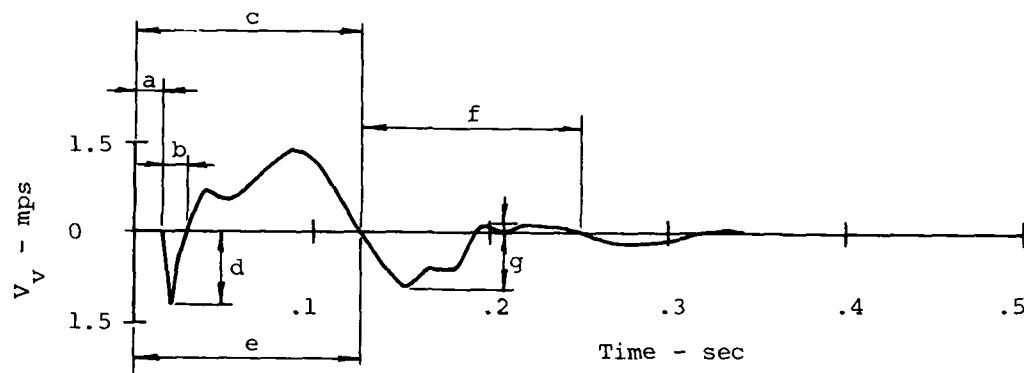
- Below the phreatic surface the accuracy of superposition improves and is considered acceptable (generally within 20%).

TABLE 3: Summary of Superposition Accuracy at the Center of the Charge Array



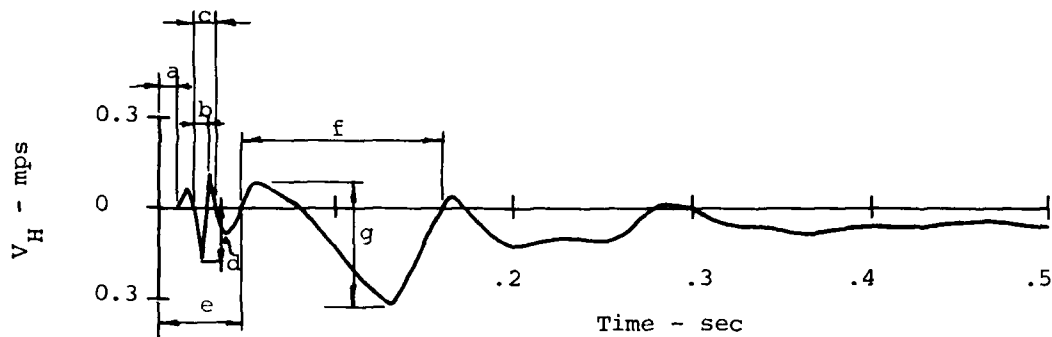
Component	MBI-4	MBI-6	MBI-8
1. Above Phreatic Surface			
Air Slap			
a) Time of arrival	0%	0%	0%
b) Pulse width	0%	0%	-25%
c) Period	-80%	-85%	-60%
d) Peak	-29%	-66%	-60%
Oscillatory Component			
e) Time of arrival	-11%	-22%	+ 5%
f) Period	-55%	+30%	-16%
g) Peak	-61%	-53%	-60%
2. Below Phreatic Surface			
Air Slap			
a) Time of arrival	+40%	+ 4%	+20%
b) Pulse width	-11%	- 4%	+10%
c) Period	- 5%	-12%	-15%
d) Peak	-16%	+13%	-39%
Oscillatory Component			
e) Time of arrival	- 5%	+12%	-20%
f) Period	+34%	-12%	+20%
g) Peak	-30%	- 8%	-24%

TABLE 4: Summary of Superposition Accuracy Inside the Charge Array - Vertical



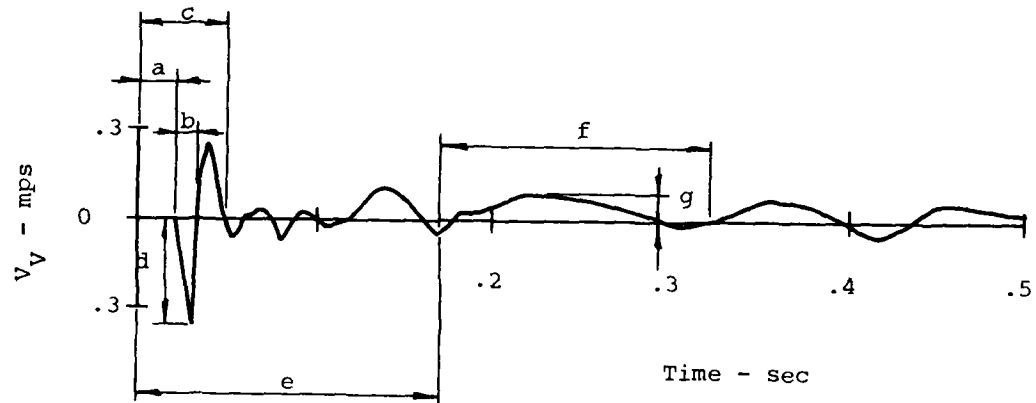
Component	MBI-4	MBI-6	MBI-8
Air Slap			
a) Time of arrival	+22 %	- 7%	0%
b) Pulse width	+13 %	- 9%	+40%
c) Period	-40 %	+155%	-26%
d) Peak	+38, -65%	- 10%	+70%
Oscillatory Component			
e) Time of arrival	-16 %	- 23%	-47%
f) Period	-11 %	- 7%	-29%
g) Peak	-40 %	+ 43%	-24%

TABLE 5: Summary of Superposition Accuracy Inside  
the Charge Array - Horizontal



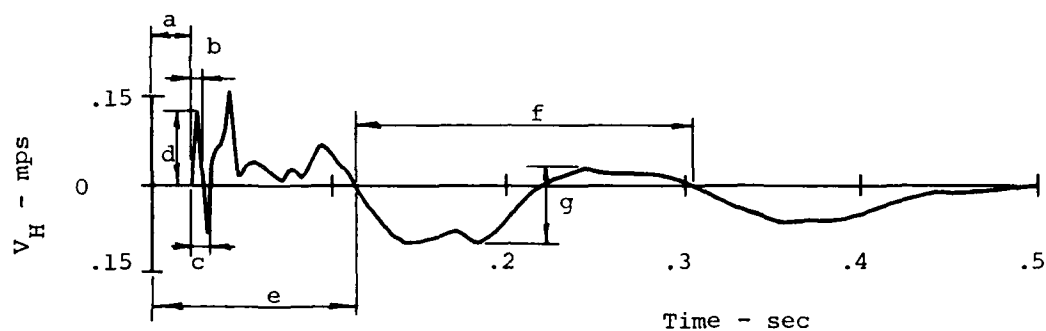
Component	MBI-4	MBI-6	MBI-8
Air Slap			
a) Time of arrival	0,+150%	+ 20%	+127%
b) Pulse width	+ 45%	+ 50%	- 33%
c) Period	- 20,+ 30%	- 45%	+ 20%
d) Peak	-195,+ 52%	-15,+137%	- 40%
Oscillatory Component			
e) Time of arrival	- 11,+ 96%	+ 20%	- 12%
f) Period	+ 24%	+ 5%	- 26%
g) Peak	- 8,+ 72%	- 35%	- 10%

TABLE 6: Summary of Superposition Accuracy Outside the Charge Array - Vertical



Component	MBI-4	MBI-6	MBI-8
Air Slap			
a) Time of arrival	-13 %	0 %	0%
b) Pulse width	+ 8%	-13 %	-13%
c) Period	-45,+29%	-26,+ 7%	-20%
d) Peak	+12%	-33 %	- 5%
Oscillatory Component			
e) Time of arrival	+16%	-15 %	- 6%
f) Period	+28%	-15,+28%	+32%
g) Peak	+70%	-43,+68%	+80%

TABLE 7: Summary of Superposition Accuracy Outside the Charge Array - Horizontal



Component	MBI-4	MBI-6	MBI-8
Air Slap			
a) Time of arrival	0%	0%	0%
b) Pulse width	0%	0%	0%
c) Period	+15%	-26,+23%	+35%
d) Peak	+75%	-26,+36%	
Oscillatory Component			
e) Time of arrival	7,+18%	$\pm$ 5%	9%
f) Period	-10 %	-20 %	0%
g) Peak	+20%	-15 %	-32%

- Inside the charge array and above the phreatic surface, superposition is not considered acceptable (Tables 4 & 5). This region can be divided into two areas however. At ranges that are between the center and  $1/2$  the charge spacing away from the center, the comparison of the data with superposition is not much different from the comparison made of the center point. However at ranges greater than  $1/2$  the charge spacing, superposition is exhibiting a definite trend of improvement.

- At locations outside the charge array, superposition accuracy is considered to be satisfactory. (Tables 6 & 7).

In addition to the study of the waveforms, calculation of the frequency domain data of superposition was compared to that performed on the multiple burst data. The method of comparison was to determine the limiting spectra, primarily displacements and velocities. The shock spectra and evaluation plots are presented in Appendix B.

From a study of the material in Appendix B, the following statements may be made:

- The limiting vertical velocities do not, in general, lend themselves to broad generalization, but the trend of improved accuracy below the phreatic surface is reinforced.

- Limiting vertical displacements are poorly described by superposition at near surface center locations, but with increased depth the accuracy is greatly improved. For the other locations, the displacements are generally underpredicted.

- Limiting horizontal velocities are within a factor of 2 of the data.

- Limiting horizontal displacements generally are within a factor of 2 of the data, but also a possible tendency of overprediction by superposition is shown.

#### 4.2.3 Representative Points of Comparison

The locations chosen to illustrate the ability of both the empirical methods and superposition to describe the multiple burst environment were at the array center, at a range from the center of  $1/2$  the charge spacing, between charges on the bisector, and at a range of one charge spacing outside the array on the bisector (See Fig. 28). The decision to use these locations was based on the conclusions drawn concerning the accuracy of superposition.

##### a) Array Center

Figures 29 through 31 present the waveform comparisons made for the center points in the various experiments. Table 8 summarizes the accuracy of both methods.

Generally both methods are accurate in predicting the arrival time of the air slap signal. The downward peak is underpredicted by both methods as is the period of the first cycle. Pulse width of the downward signal was consistently overpredicted by the empirical method and consistently underpredicted by superposition.

The most noticeable difference in the predictions of the high frequency component and the data involve the large magnitude and long duration signal after the downward air slap. Both methods are rather poor in the prediction of this effect. The empirical method does a better job in the prediction of the duration of this signal than does superposition, but both methods underpredict this peak by about the same amount.

The oscillatory motions predicted by both methods are similar to what was measured. However, both methods tend to underpredict the peak motions and generally underpredict the period of oscillation.

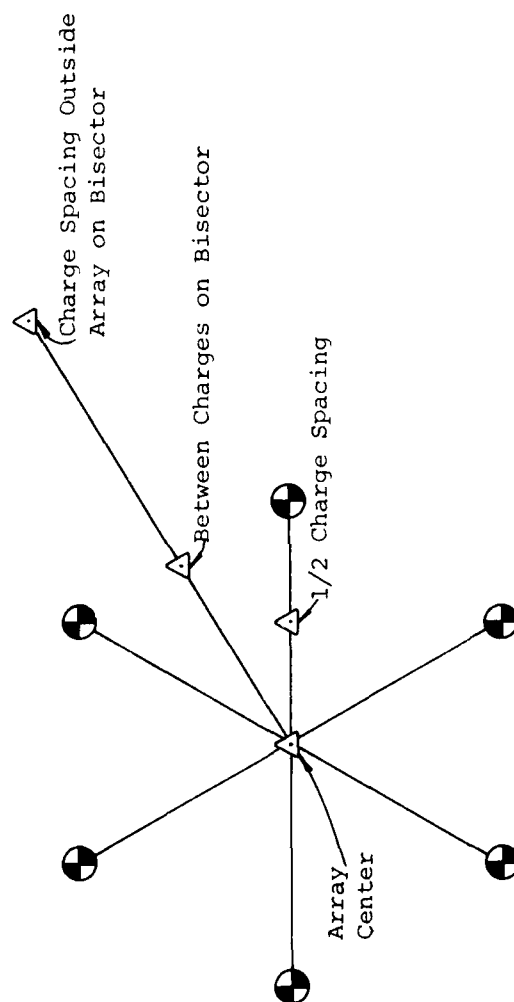


Figure 28: Representative Points of Comparison for Predictions vs Data

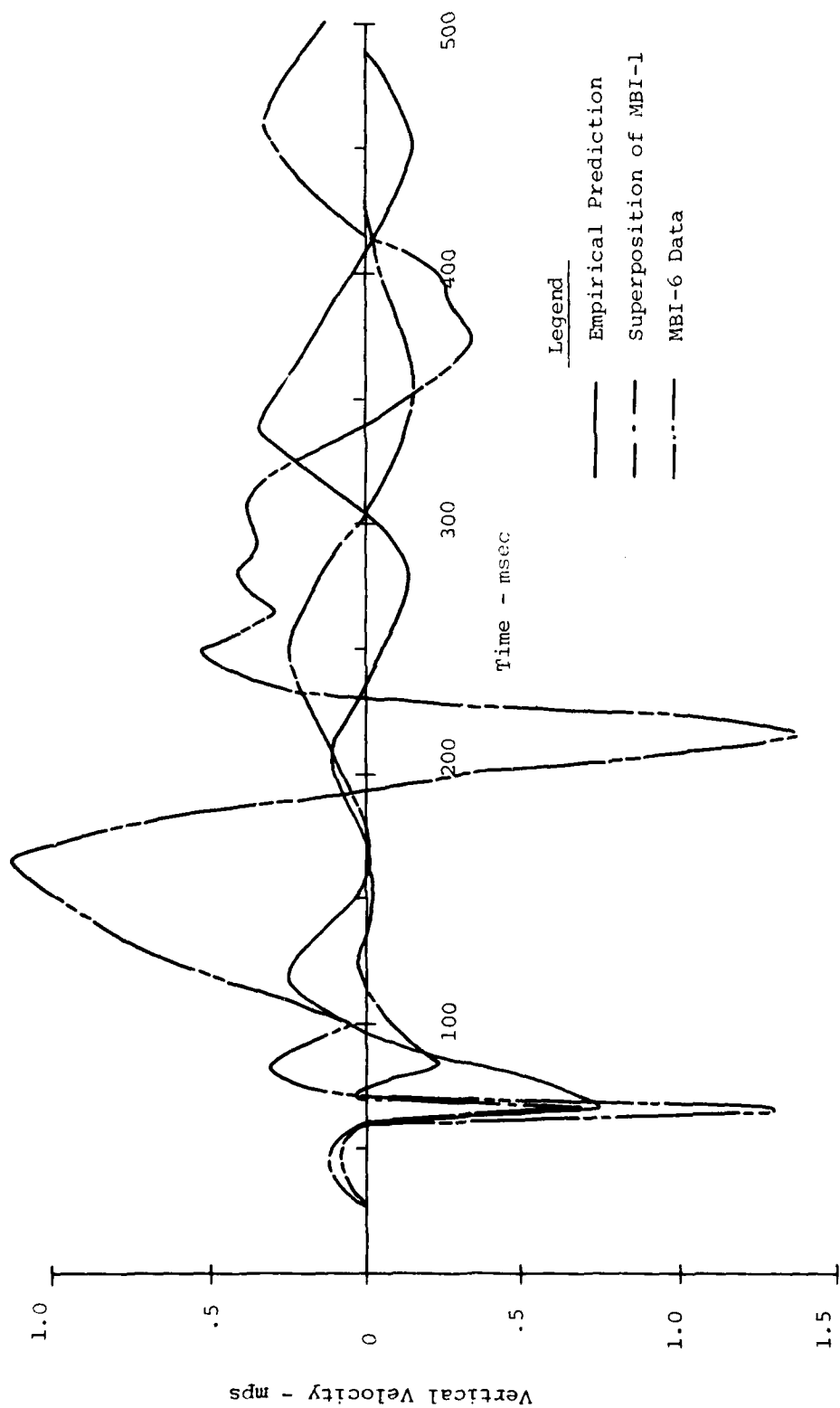


FIGURE 29: Waveform Comparison of Vertical Velocity of the Array Center - MBI-6

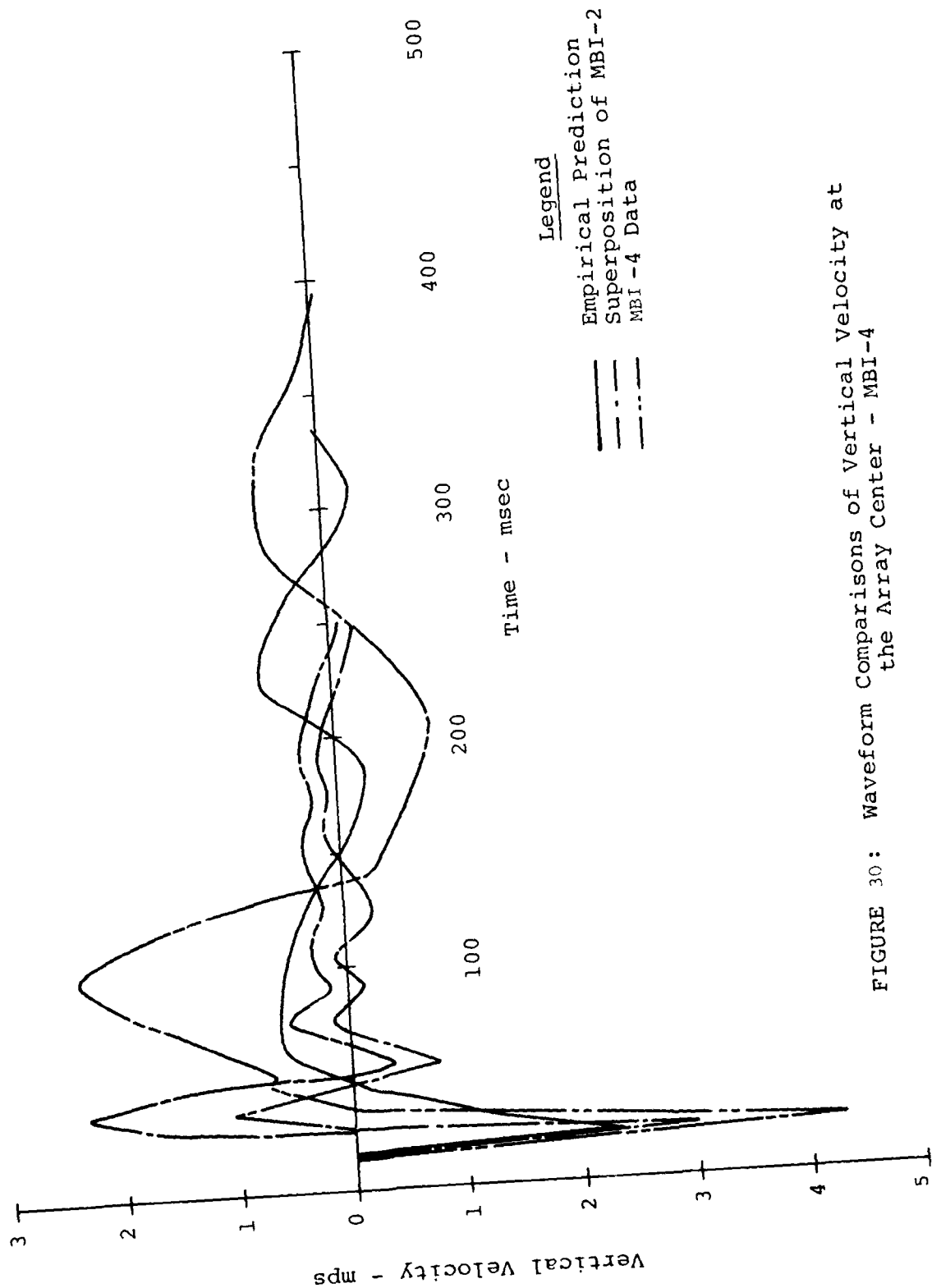


FIGURE 30: Waveform Comparisons of Vertical Velocity at the Array Center - MBI-4

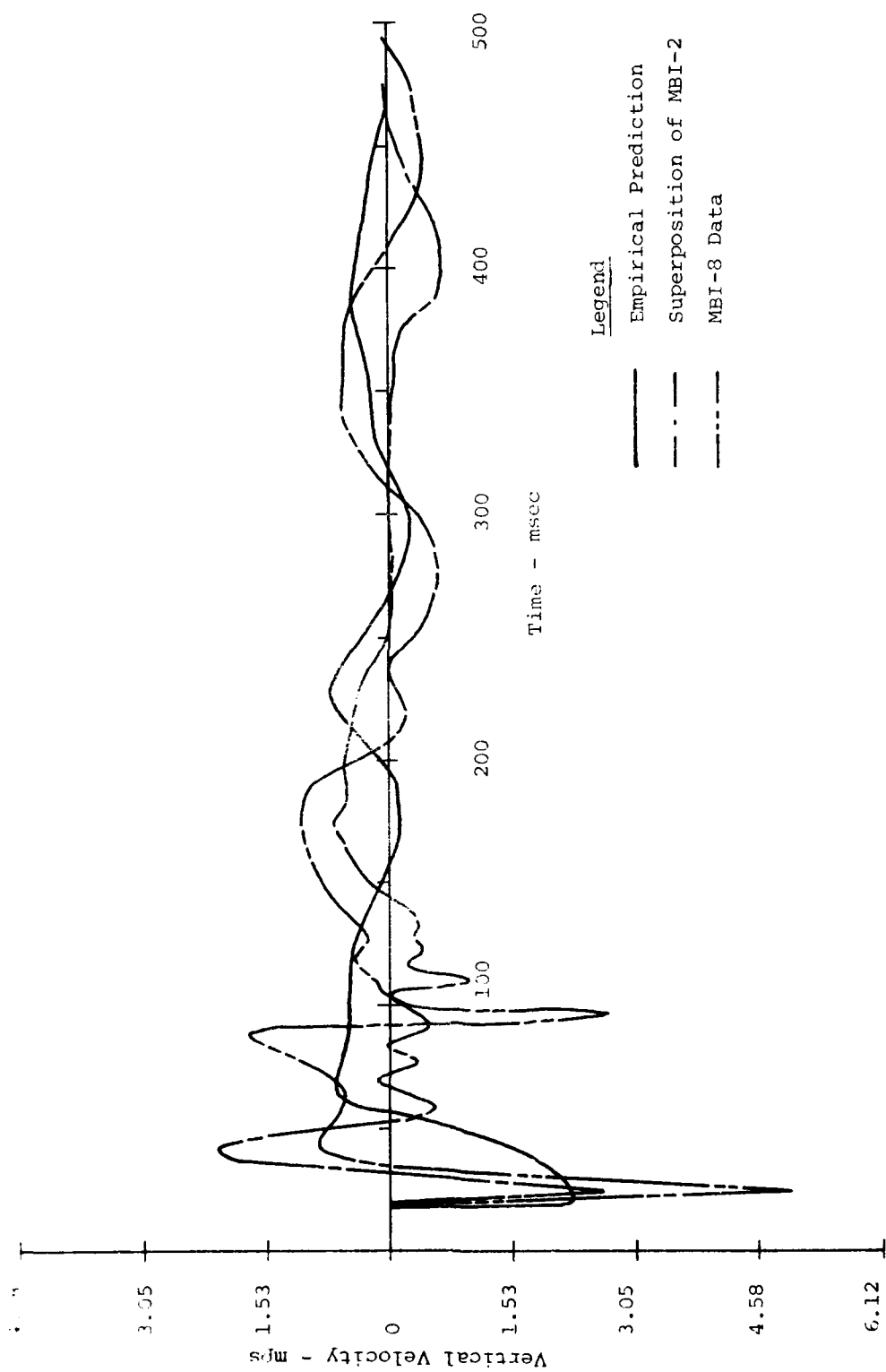


FIGURE 31: Waveform Comparisons of Vertical Velocity at the Array Center - MBI-8

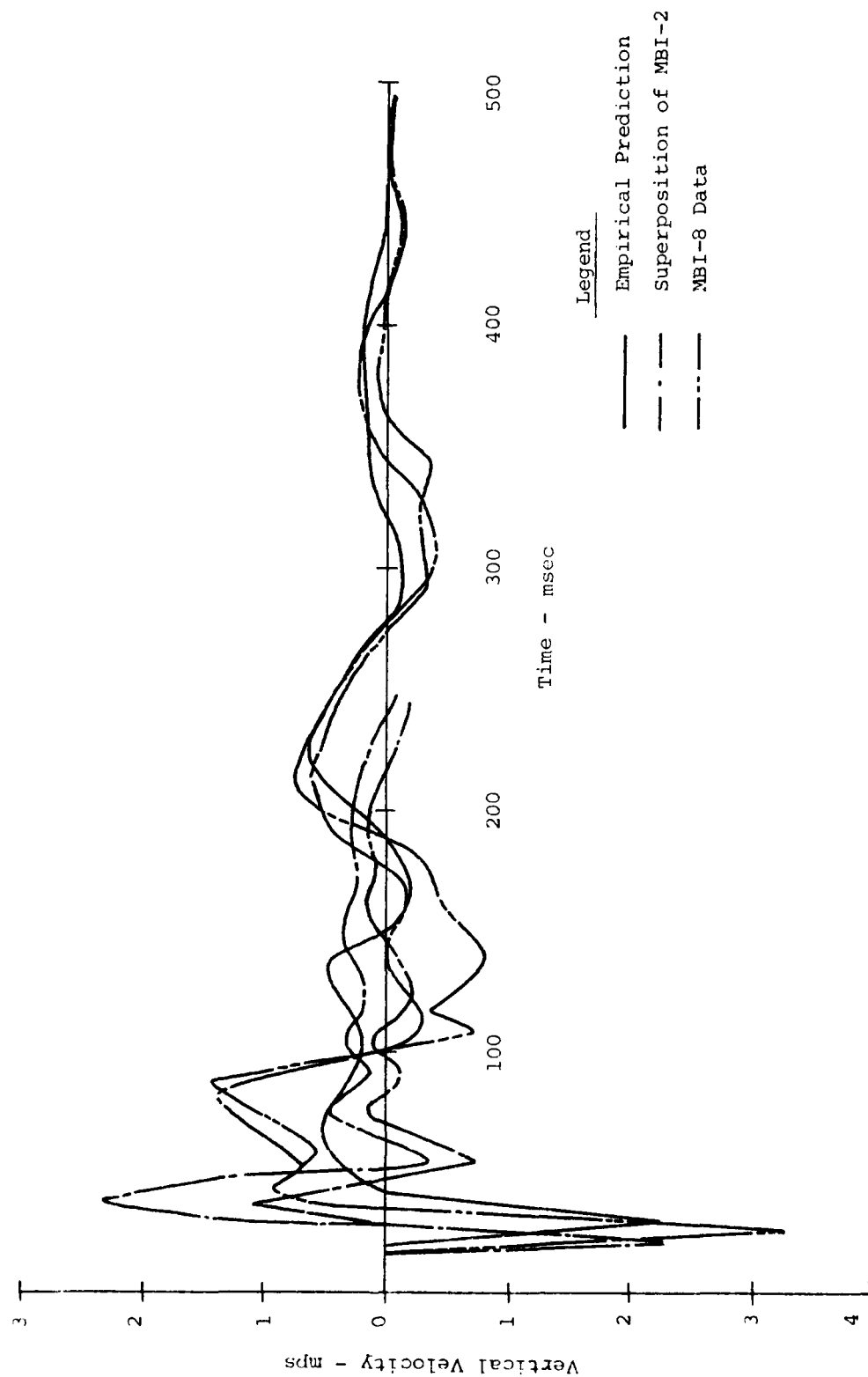


FIGURE 32: Waveform Comparisons of Vertical Velocity at the Center of an Outside Array - MBI-8

Table 8: Summary of Prediction Accuracy of the Center of Charge Array

Component	MBI-4		MBI-6		MBI-8	
	Super-position	Empirical	Super-position	Empirical	Super-position	Empirical
1) Vertical Air Slap						
a) Time of arrival	0%	+ 5%	0%	0%	0%	0%
b) Pulse width	-43%	+40%	0%	+260%	-27%	+157%
c) Period	-80%	+15%	-85%	- 28%	-60%	- 70%
d) Peak	-29%	-45%	-42%	- 39%	-46%	- 86%
Oscillatory Component						
e) Time of arrival	-11%	+20%	-22%	+ 34%	+ 5%	+ 51%
f) Period	-55%	-50%	+30%	- 3%	-16%	- 82%
g) Peak	-61%	-60%	-53%	- 41%	-60%	- 32%

Shock spectra comparisons which correspond to the waveform comparisons discussed above, are presented in Figures 33 through 36. In general shock spectra of the multiple burst data has two distinct peaks. One at low frequency (between 1Hz and 10Hz) and one at the higher frequencies (between 10Hz and 100). These are due, respectively, to the large upward motion at the center and the air slap peak. The predicted shock spectra generally have one peak at the higher frequencies.

For simplicity in comparing the shock spectra the limiting displacement and velocity values and low frequency were determined, and these individual values compared.

For limiting velocities, superposition of MBI-1 and the empirical prediction for MBI-6 both yielded approximately the same values and both were underpredicted. For both MBI-4 and MBI-8 superposition provided more accurate limiting velocities than did their empirical counterparts. The superposition predictions for these events are well within a factor of 2 of the data whereas, the empirical predictions were underpredicted by a larger factor. In all cases the general trend is for both prediction procedures to underpredict.

Limiting displacements at the center points in all events were underpredicted. This was due to the very large upward motion observed in the data. The only event that produced a limiting displacement within a factor of 2 of the data was MBI-8. This was due to the arrival of the airblast from the second ring of charges cutting short the large upward surge and thus limiting the displacement.

The limiting low frequencies were neither consistently under or over predicted by either method and generally fell within a factor of 2 of the data.

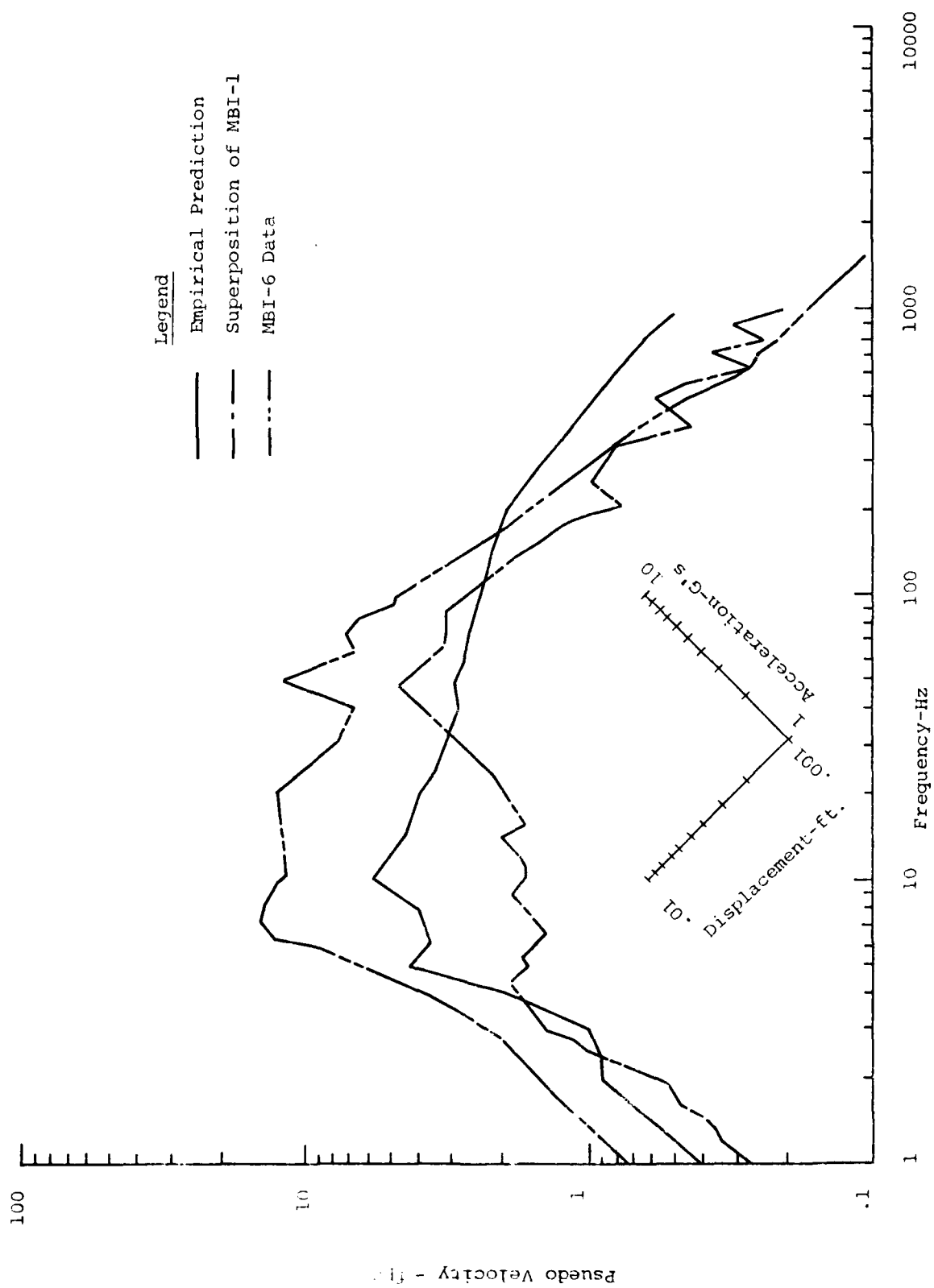


FIGURE 33: Shock Spectra Comparisons of Vertical Velocity  
at the Array Center - MBI-6

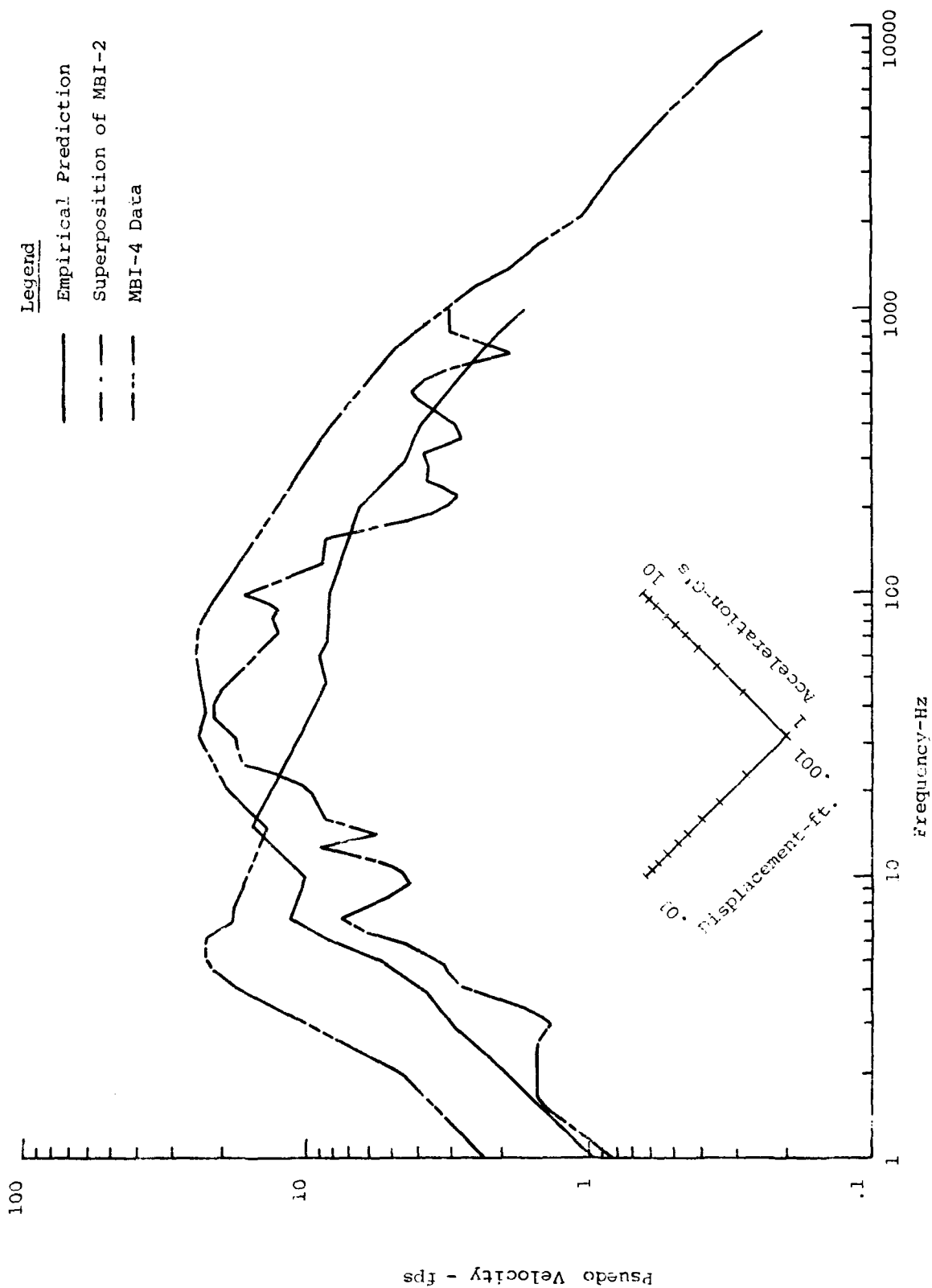


FIGURE 34: Shock Spectra Comparisons of Vertical Velocity at the Array Center - MBI-4

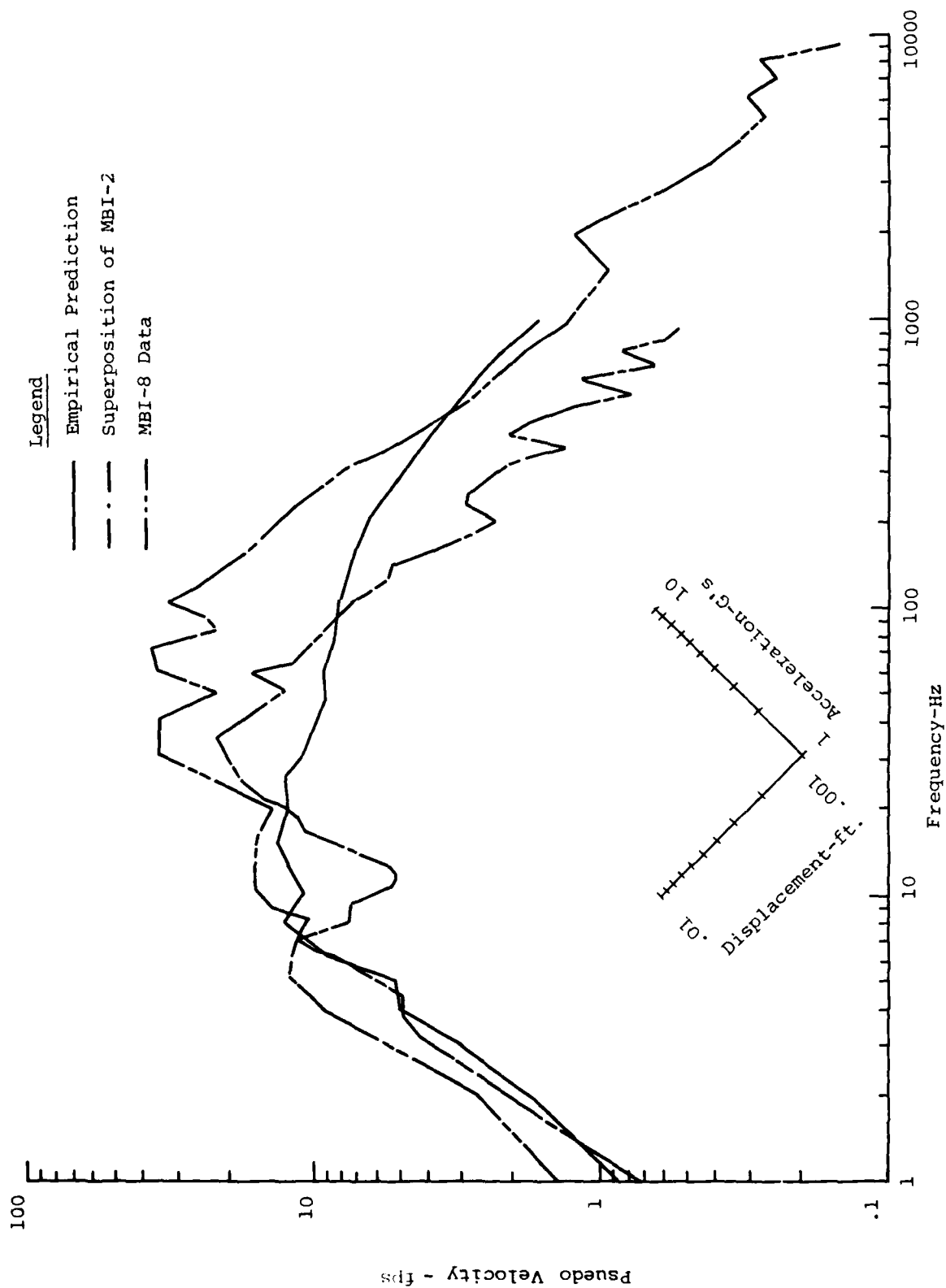


FIGURE 35: Shock Spectra Comparisons of Vertical Velocity at the Array Center - MBI-8

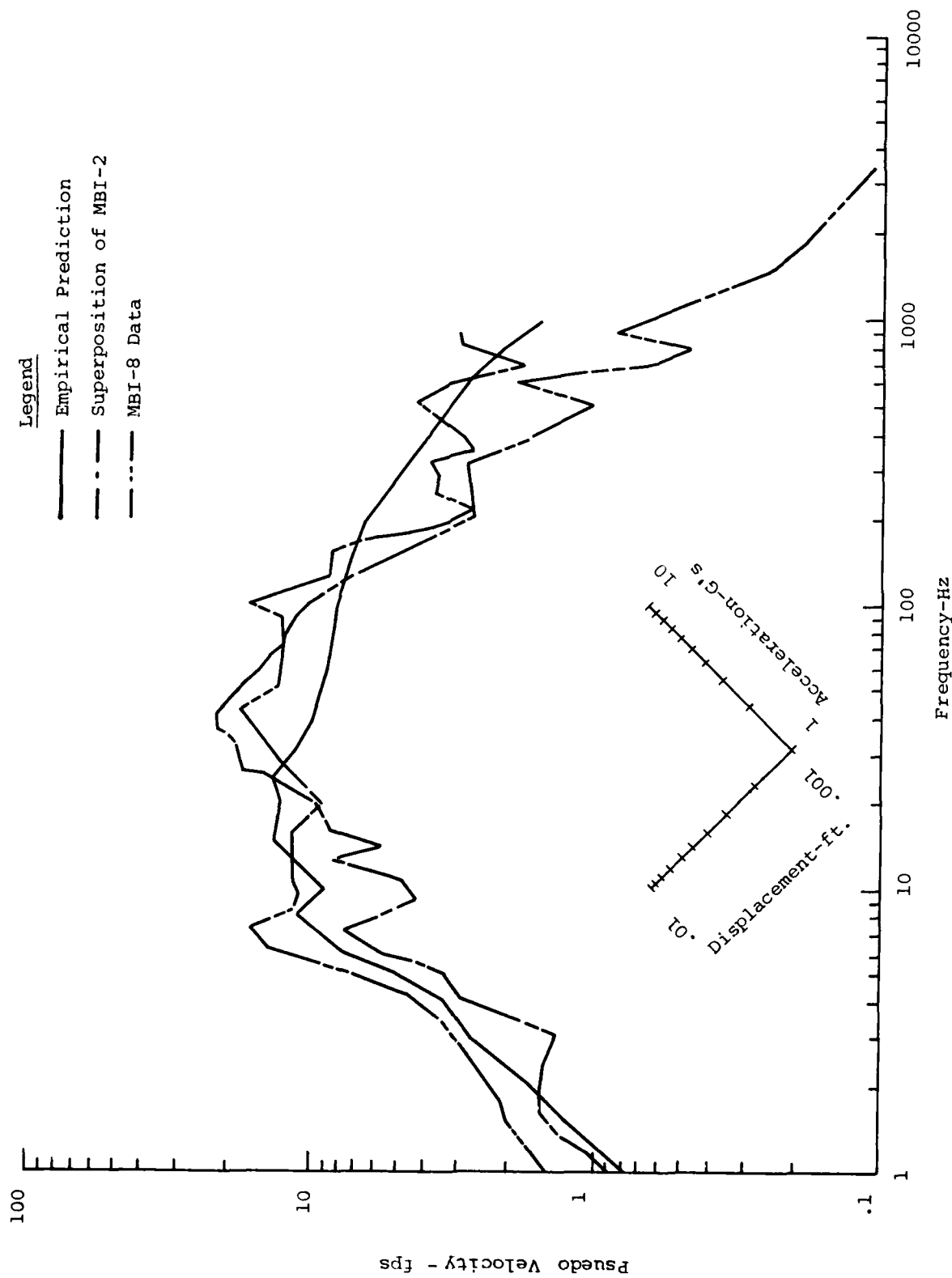


FIGURE 36: Shock Spectra Comparisons of Vertical Velocity at the Center of an Outside Array - MBI-8

It appears from the comparisons presented for this gage location, that neither superposition nor the empirical methods produce consistently better results. Both tend to underpredict peak values, overpredict the high frequencies, and underpredict the oscillatory period.

b)  $1/2$  the Charge Spacing

Waveform comparisons made for this location are shown in Figures 37 through 41. The summary of these comparisons is presented in Table 9.

In general, prediction of the vertical motion by both methods is improved slightly. The air slap peaks are still not accurate but they are generally becoming closer to the measured values. The period of the air slap motion is improving and the upward peak is not as greatly underpredicted as at the center of the array. The oscillatory component predicted by both methods compare equally with the data. Again there is a slight improvement of the prediction at this location over what was predicted at the center point.

The prediction of the horizontal motion is about as good as the prediction of the vertical motions. However, the air slap period predicted by the empirical methods is poor. This is mainly due to the airblast induced shear wave that is not modeled empirically. The superposition prediction contains this shear wave and, therefore, does a better job at predicting the period. The other characteristics of this component are predicted with about the accuracy of the vertical motions, as is the oscillatory component.

The shock spectra corresponding to the waveforms discussed above are shown in Figure 42 through 46.

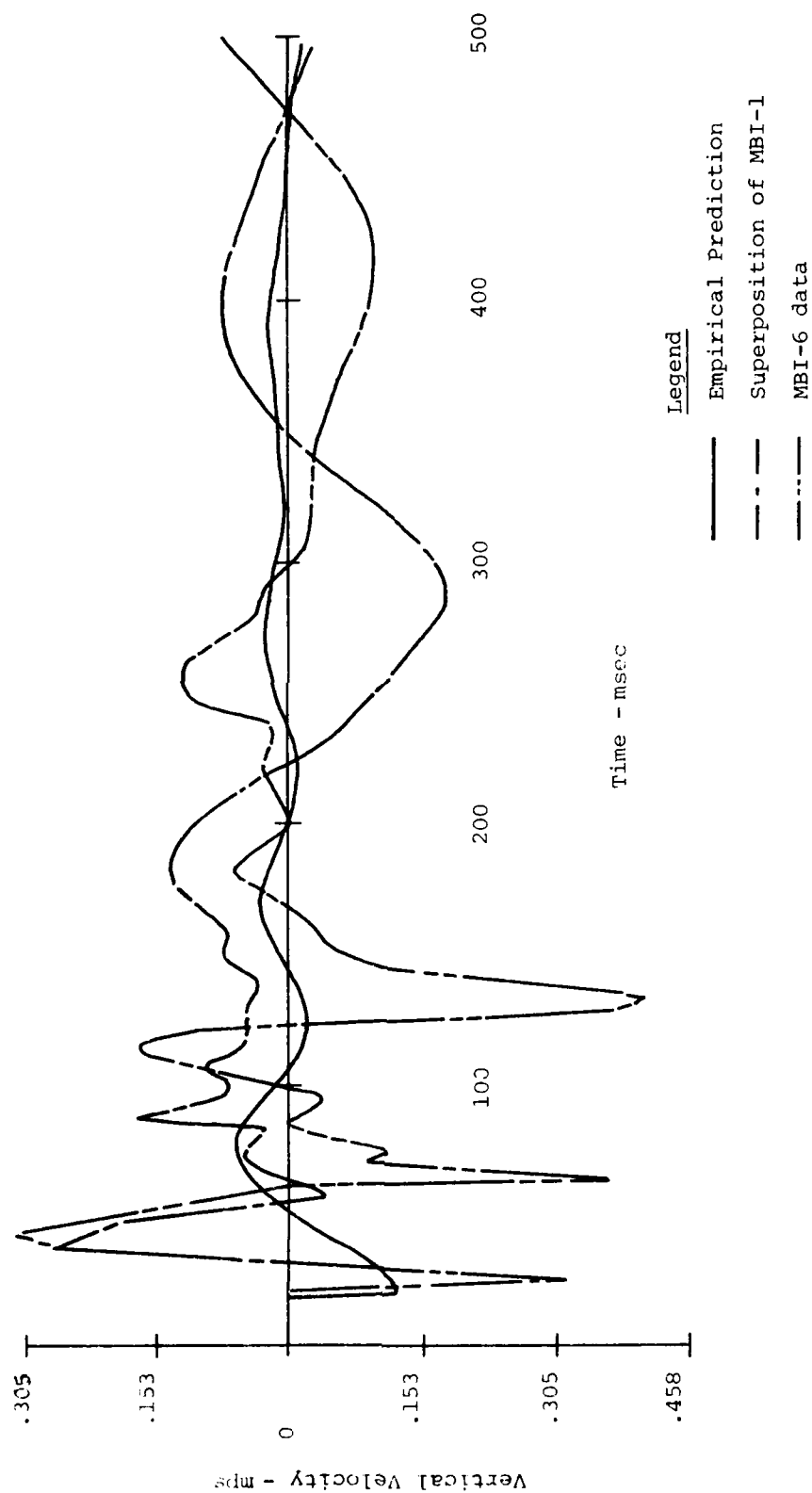


FIGURE 37: Waveform Comparison of Vertical Velocity  
at 1/2 the Charge Spacing - MBI-6

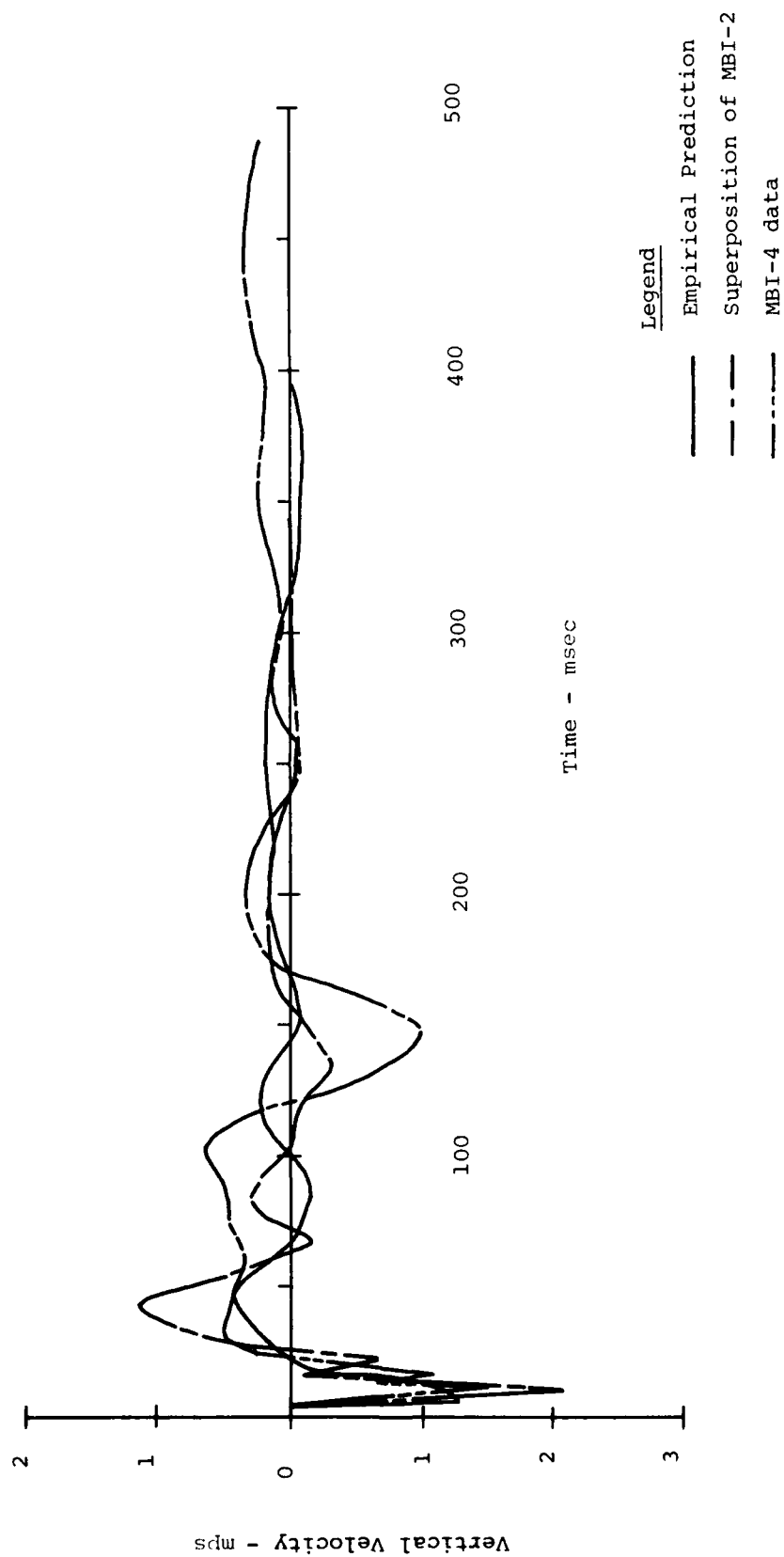


FIGURE 38: Waveform Comparison of Vertical Velocity  
at 1/2 the Charge Spacing - MBI-4

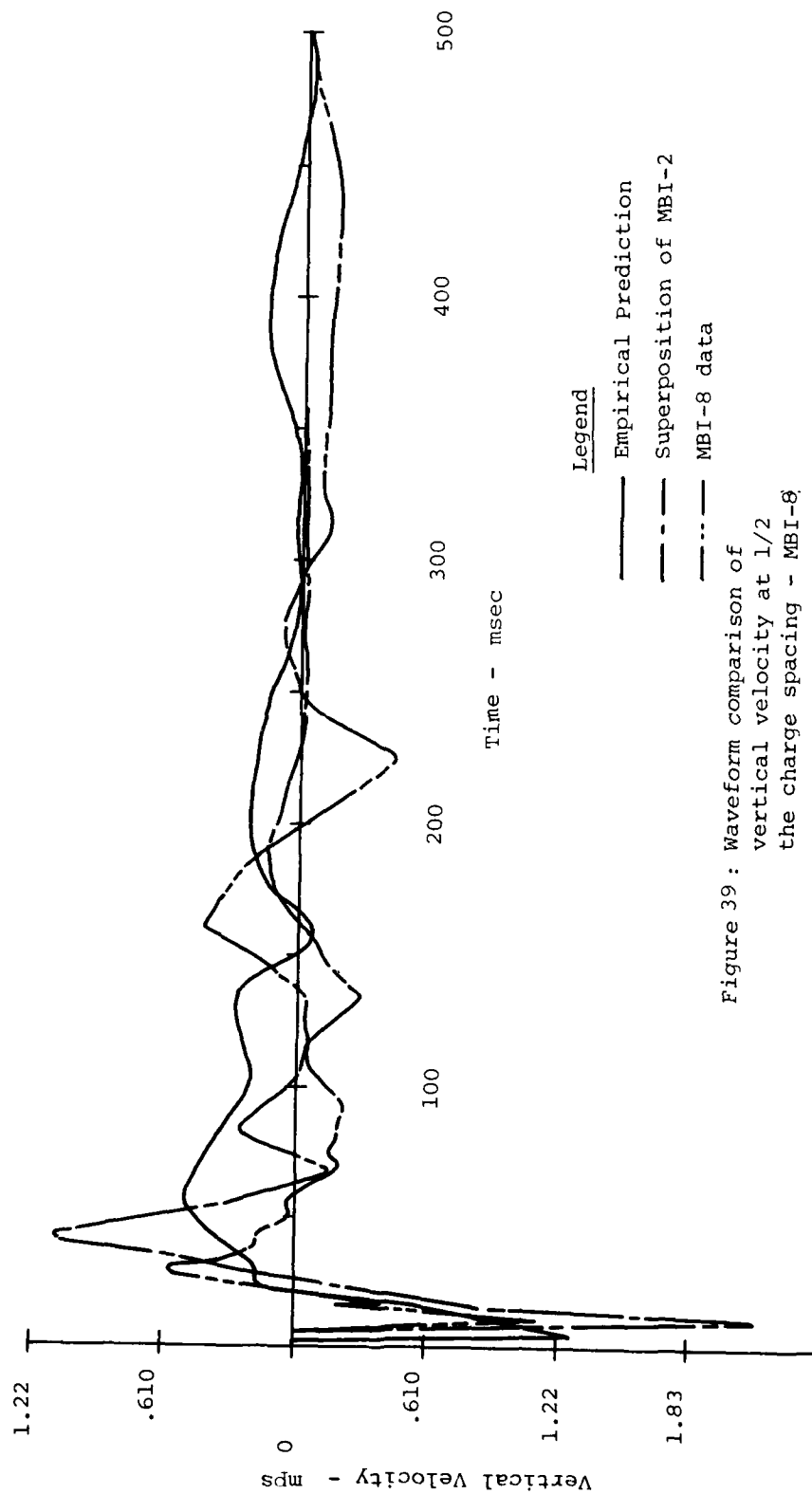


Figure 39: Waveform comparison of  
vertical velocity at 1/2  
the charge spacing - MBI-8.

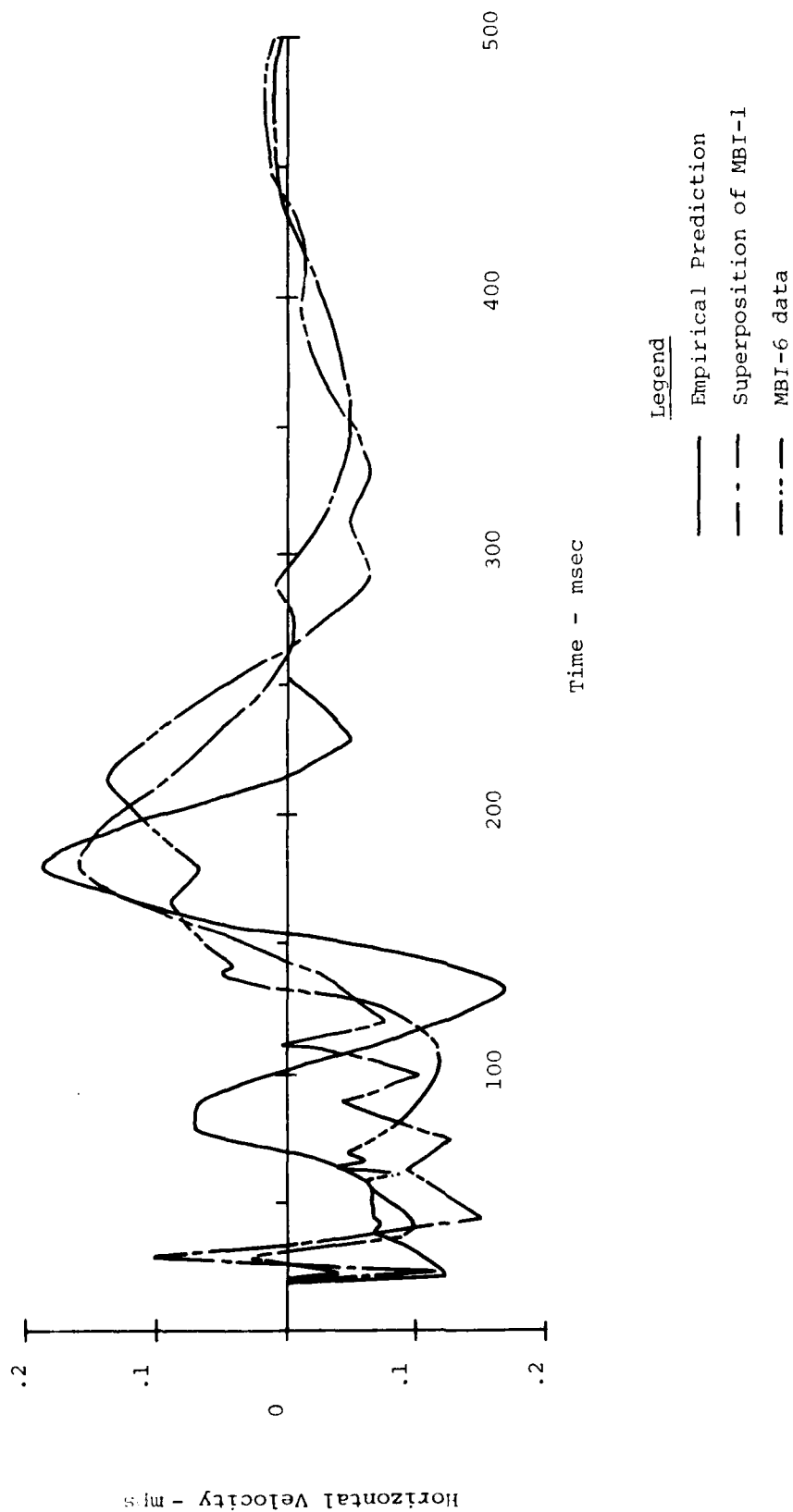


Figure 40: Waveform comparison of horizontal velocity at 1/2 the charge spacing-MBI-6

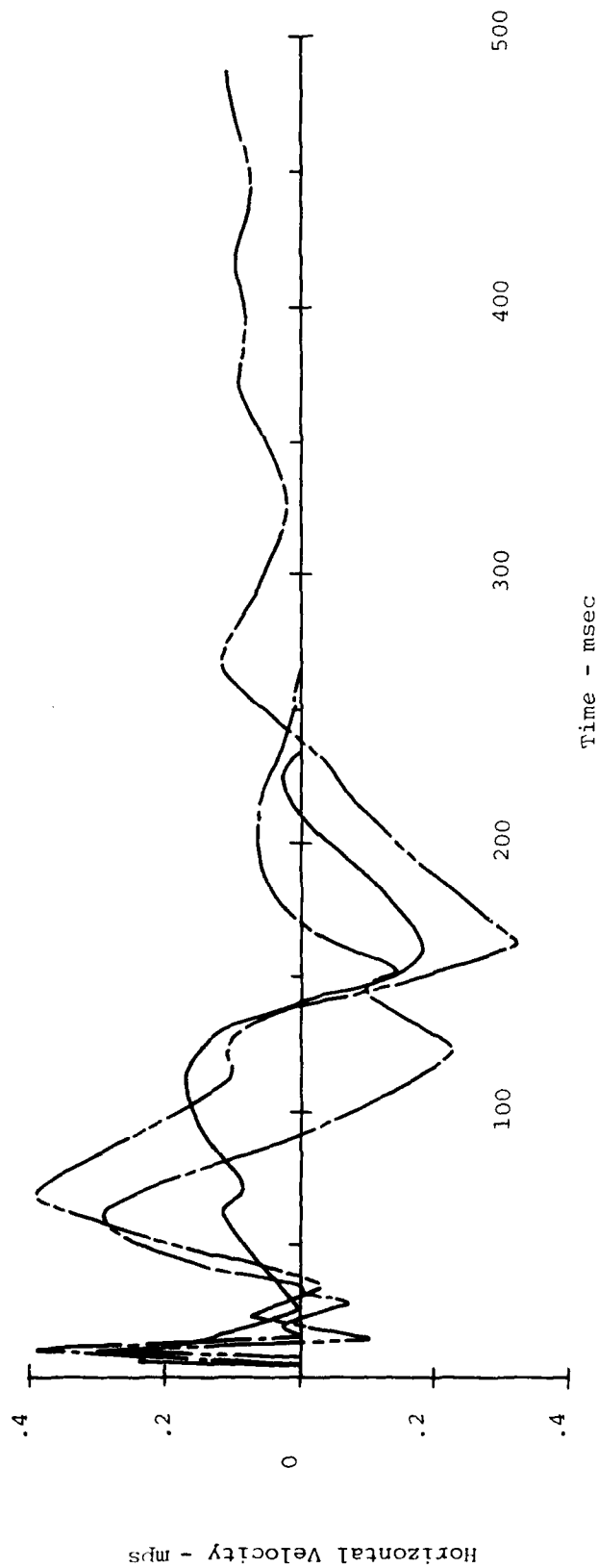


Figure 41: Waveform comparison of horizontal velocity at 1/2 the charge spacing - MBI-4

AD-A088 510

CIVIL SYSTEMS INC ALBUQUERQUE NM

F/6 18/3

WISERS BLUFF PHASE I GROUND SHOCK ANALYSIS OF THE MULTIPLE BURS-ETC(U)

AUG 78 J S PHILLIPS, J L BRATTON

DNA001-77-C-0301

UNCLASSIFIED

DNA-5089Z

NL

2 OF 3

AD-A

000011

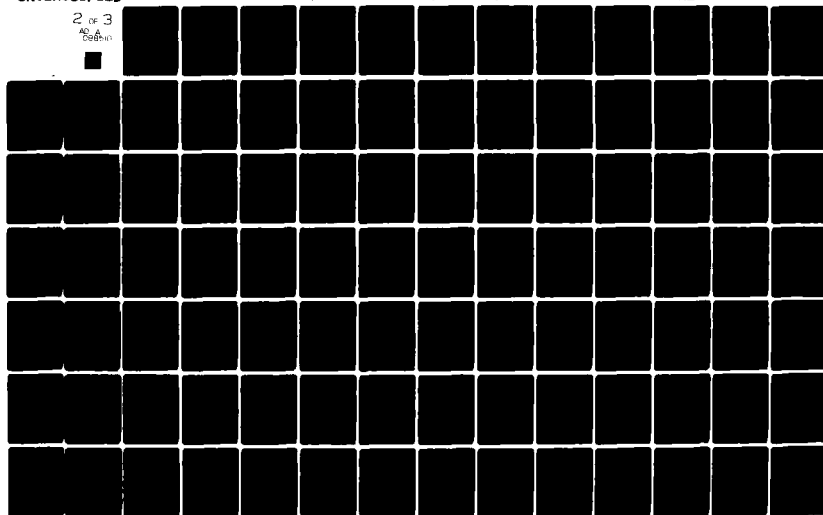


TABLE 9: Summary of Prediction Accuracy at a range of 1/2 the charge spacing

Component	MBI-4		MBI-6		MBI-8	
	Super- position	Empirical	Super- position	Empirical	Super- position	Empirical
1) Vertical Air Slap						
a) Time of ar- rival	+66%	- 20%	0%	- 12%	0%	- 52%
b) Pulse width	+ 7%	+ 10%	0%	+171%	+33%	+ 27%
c) Period	-46%	- 47%	-36%	- 23%	+ 4%	+180%
d) Peak	+38%	- 15%	-11%	- 61%	+83%	+ 14%
Oscillatory Component						
e) Time of ar- rival	-18%	+ 25%	-20%	- 27%	+22%	+ 22%
f) Period	-27%	- 25%	-31%	- 67%	+77%	+ 56%
g) Peak	-62%	- 81%	+42%	- 79%	-77%	- 73%
2) Horizontal Air Slap						
a) Time of ar- rival	0%	0%	0%	0%		
b) Pulse width	+60%	+320%	0%			
c) Period	- 4%	+193%	0%	+ 9%		
d) Peak	+18%	- 21%	-42%			
Oscillatory Component						
e) Time of ar- rival	-13%	- 38%	- 7%	+ 8%		
f) Period	-33%	- 8%	+ 5%	-66%		
g) Peak	+36%	- 4%	- 4%	+14%		

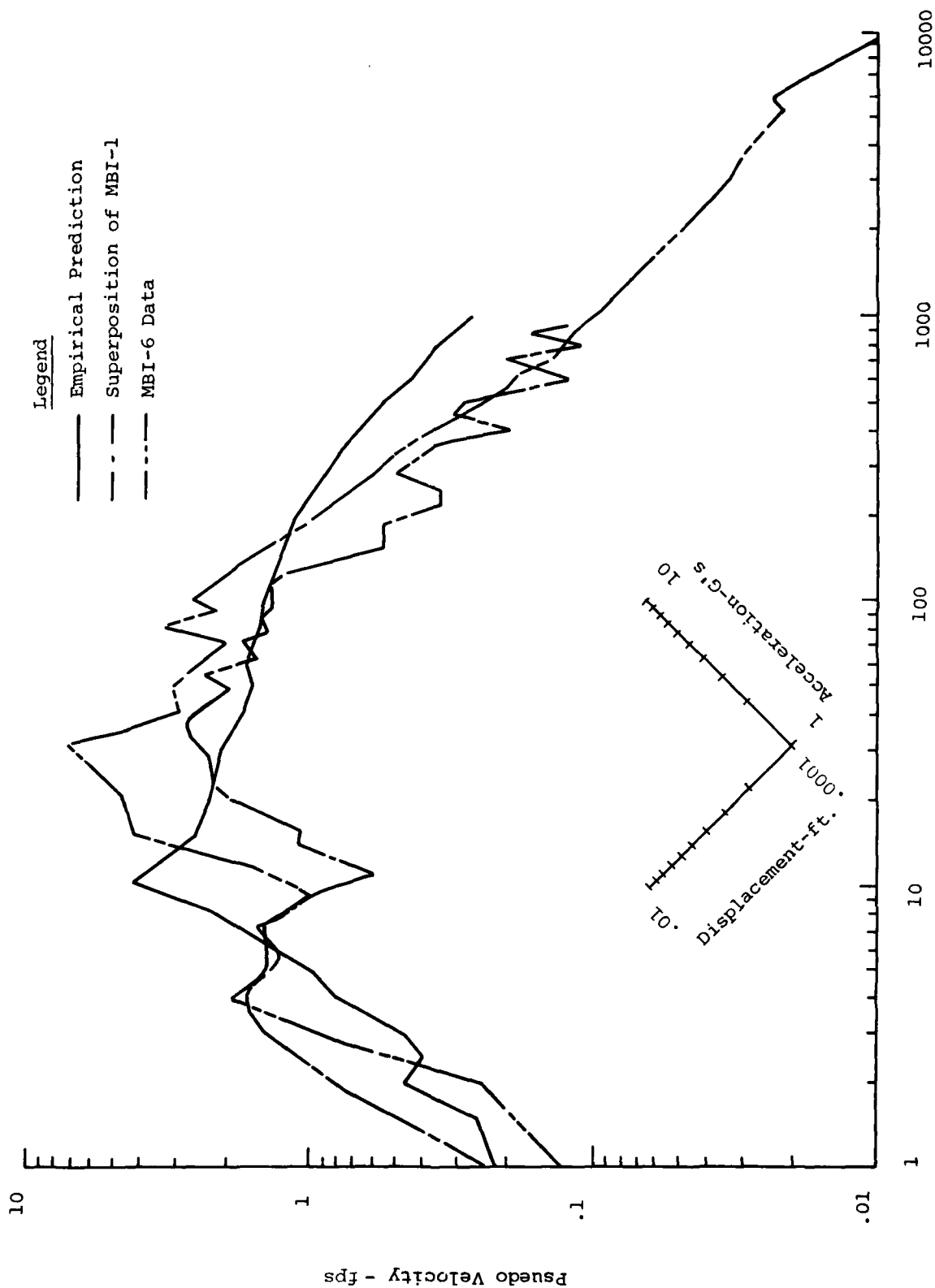


FIGURE 42: Shock Spectra Comparisons of Vertical Velocity at 1/2  
Charge Spacing - MBI-6

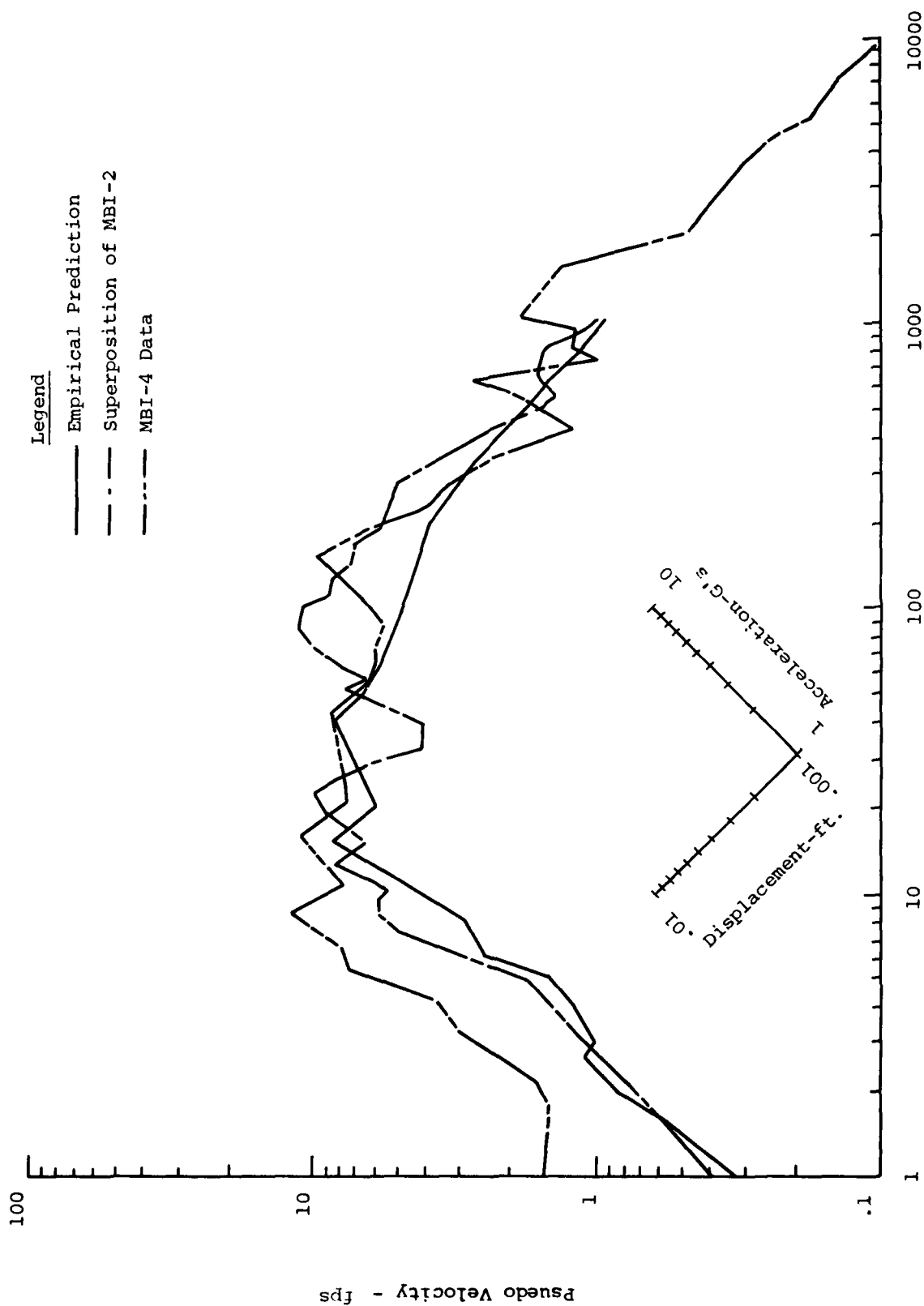


FIGURE 43: Shock Spectra Comparisons of Vertical Velocity at 1/2 Charge Spacing - MBI-4

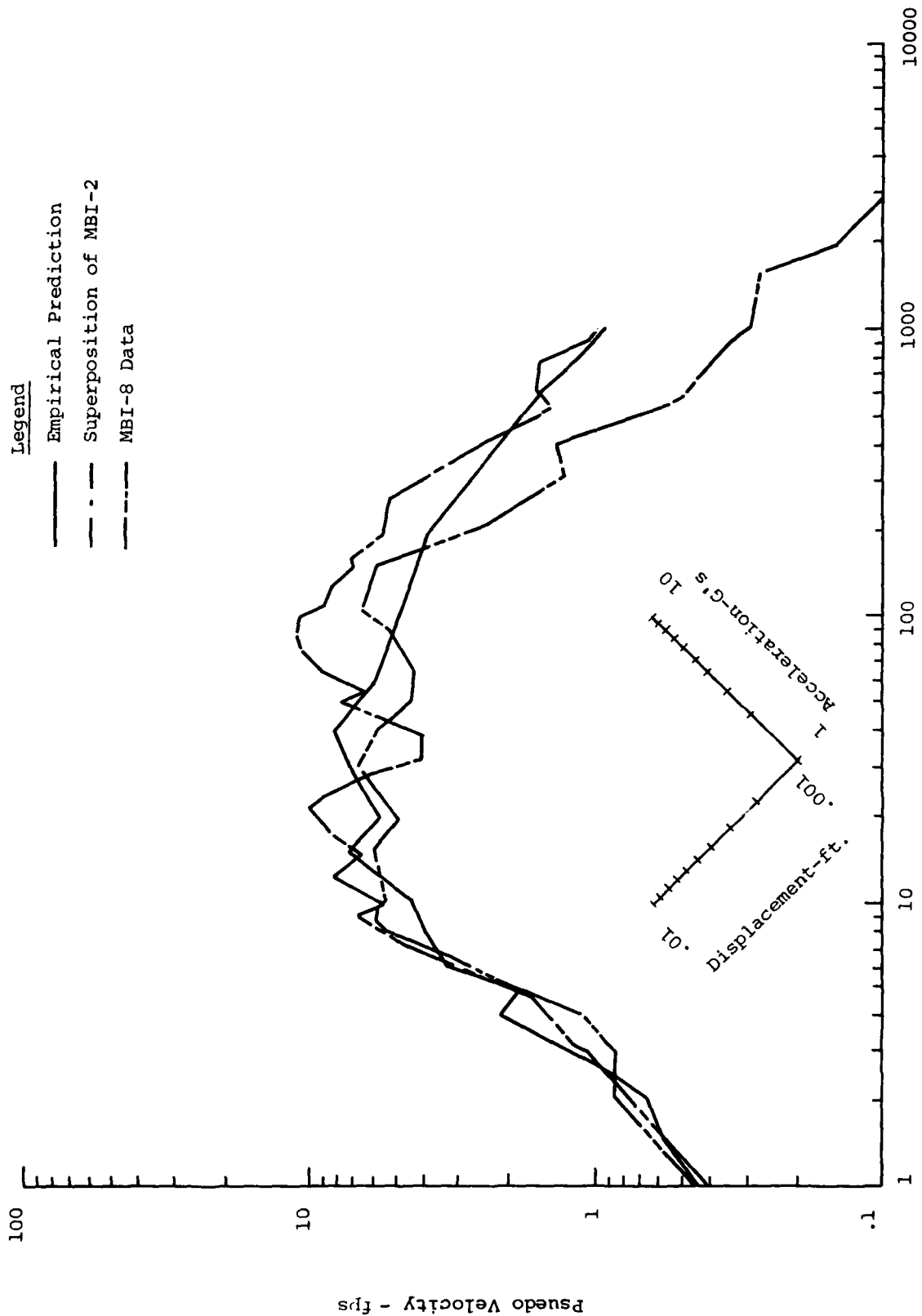


FIGURE 44: Shock Spectra Comparisons of Vertical Velocity at 1/2 Charge Spacing - MBI-8

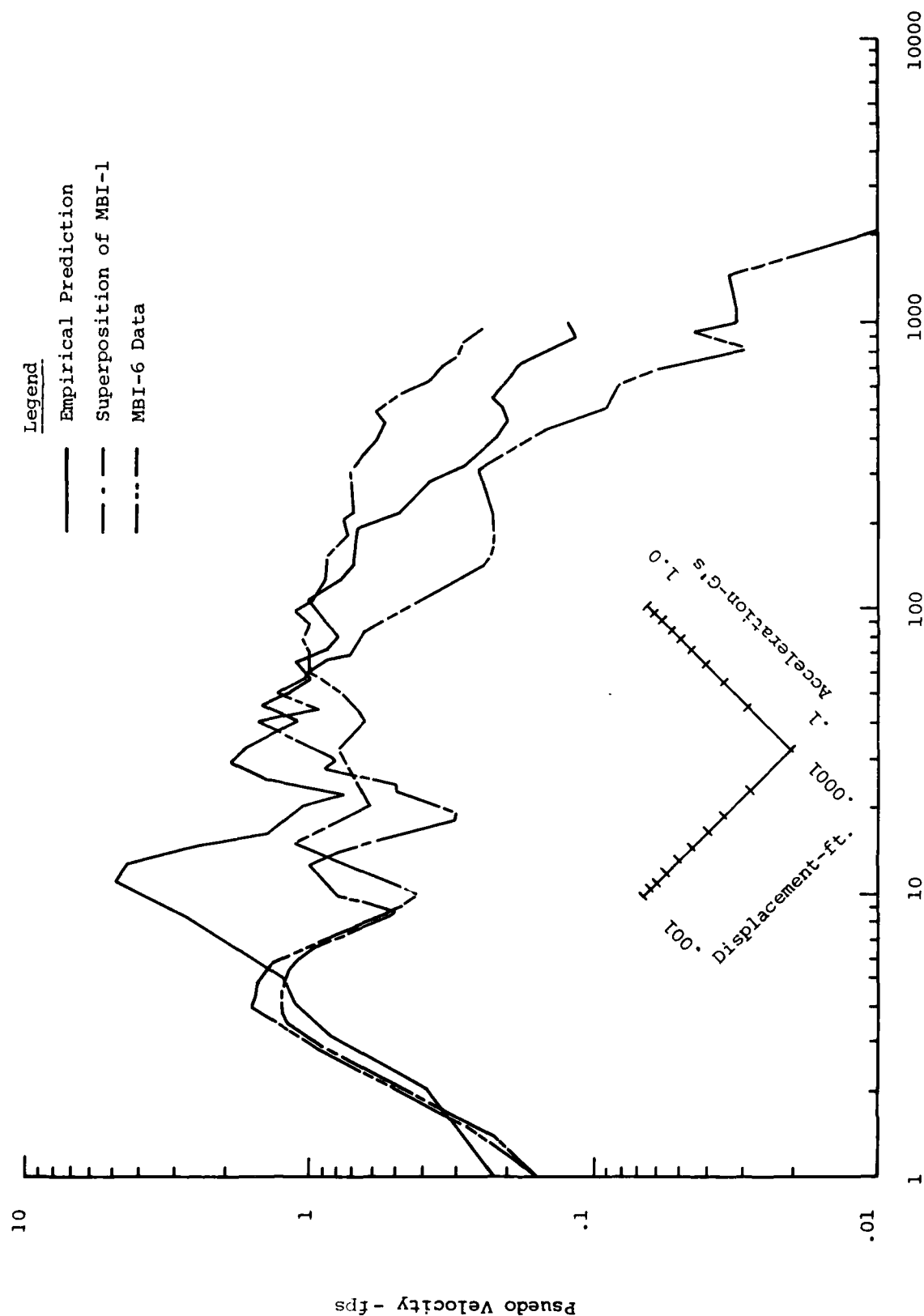


FIGURE 45: Shock Spectra Comparisons of Horizontal Velocity at 1/2 Charge Spacing - MBI-6

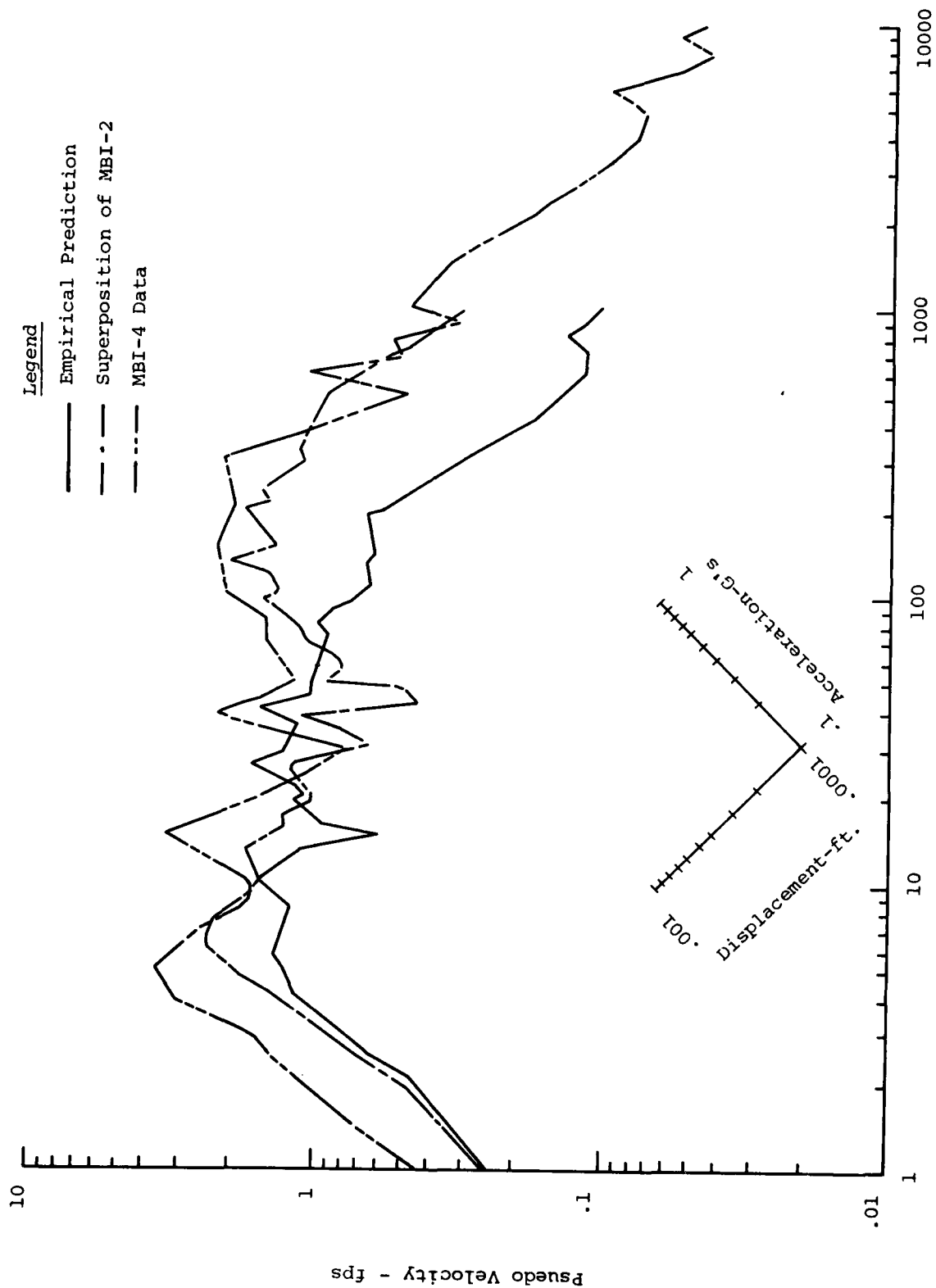


FIGURE 46: Shock Spectra Comparisons of Horizontal Velocity at 1/2 Charge Spacing - MBI-4

The general shapes of the spectra of vertical waveforms are similar. The limiting displacement, velocity, and low frequency values determined for these spectra do indicate some trends. For displacements it appears that superposition is more accurate, however, all predictions (superposition and empirical) underpredict this limiting displacement. As far as the limiting velocity is concerned, neither method appears more accurate. For MBI-4 and MBI-8 the superposition prediction is higher than the empirical, however this is reversed on MBI-6, indicating no apparent trend. It is interesting to note that both the empirical and superposition predictions for MBI-4 and MBI-8 are within a factor of 2 of the data, while both predictions for MBI-6 are well below that kind of accuracy. The limiting low frequencies do not follow any specific trend, however, on MBI-4 and MBI-8 they are "overpredicted" and on MBI-6 they are "underpredicted".

The limiting values determined from the horizontal shock spectra comparisons lead to some interesting observations. The limiting velocity values predicted by superposition was generally within a factor of two for the multiple burst events. The empirical predictions were not quite as well behaved. For MBI-6 this value was three times the data value and on MBI-4 it was about 1/3 of the data value. Limiting displacements were accurately predicted by both methods for MBI-6, but there was a consistent underprediction for MBI-4. Limiting low frequencies were generally overpredicted, but within about a factor of two of the data.

#### c) Between Charges on the Bisector

Figures 47 through 51 show the waveform comparisons made for this location. The summary of the comparisons is presented in Table 10.

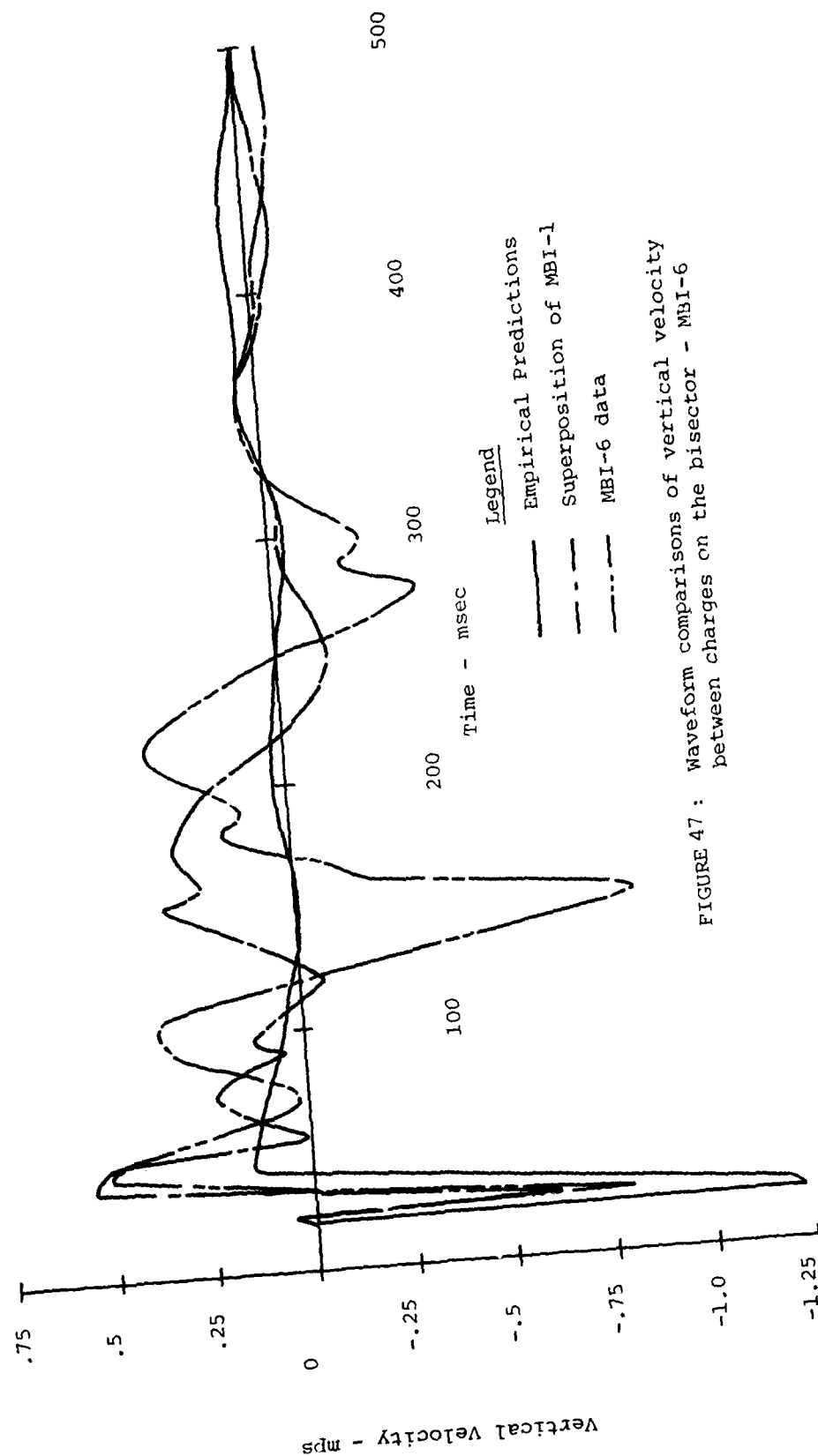


FIGURE 47 : Waveform comparisons of vertical velocity between charges on the bisector - MBI-6

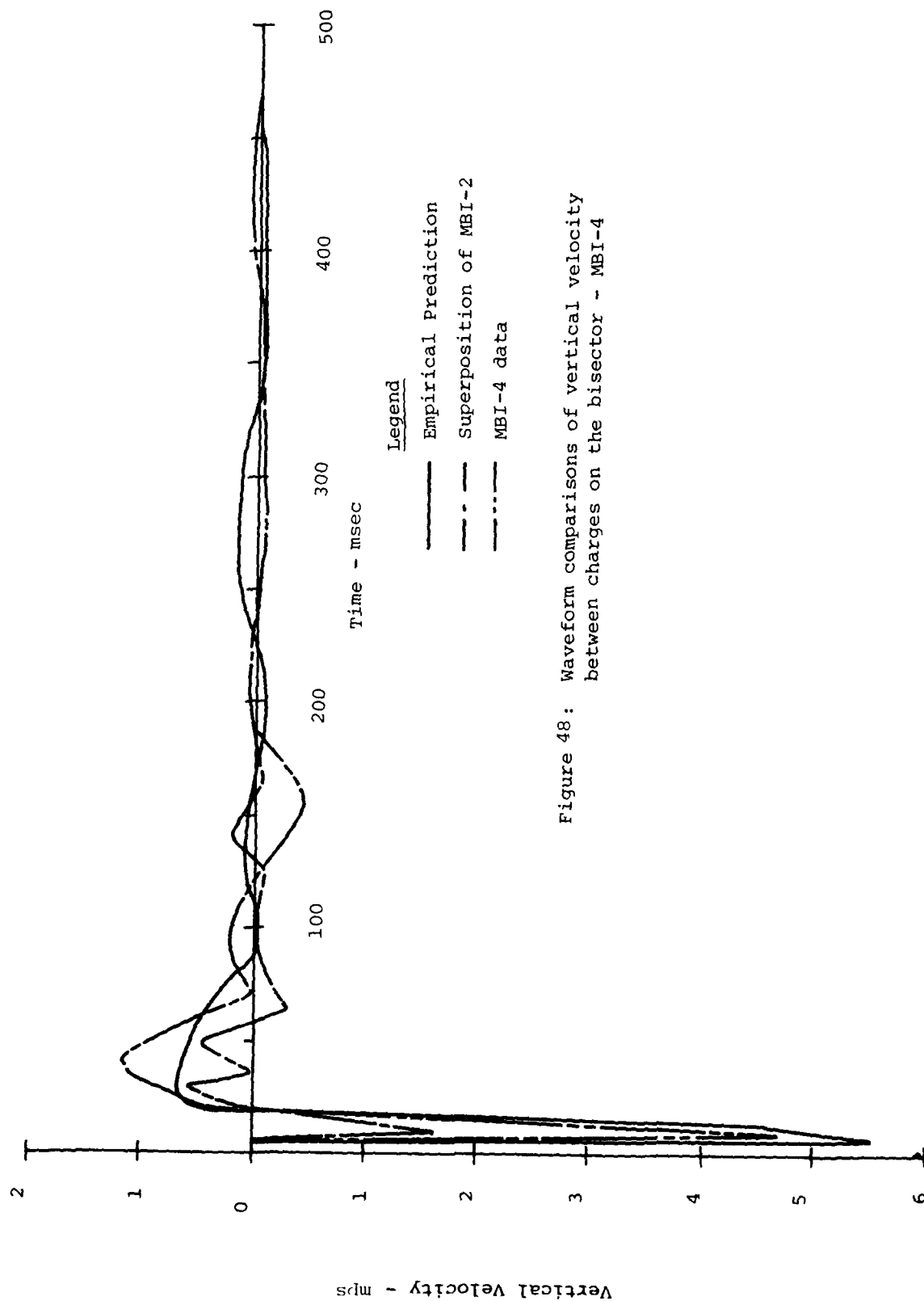


Figure 48: Waveform comparisons of vertical velocity between charges on the bisector - MBI-4

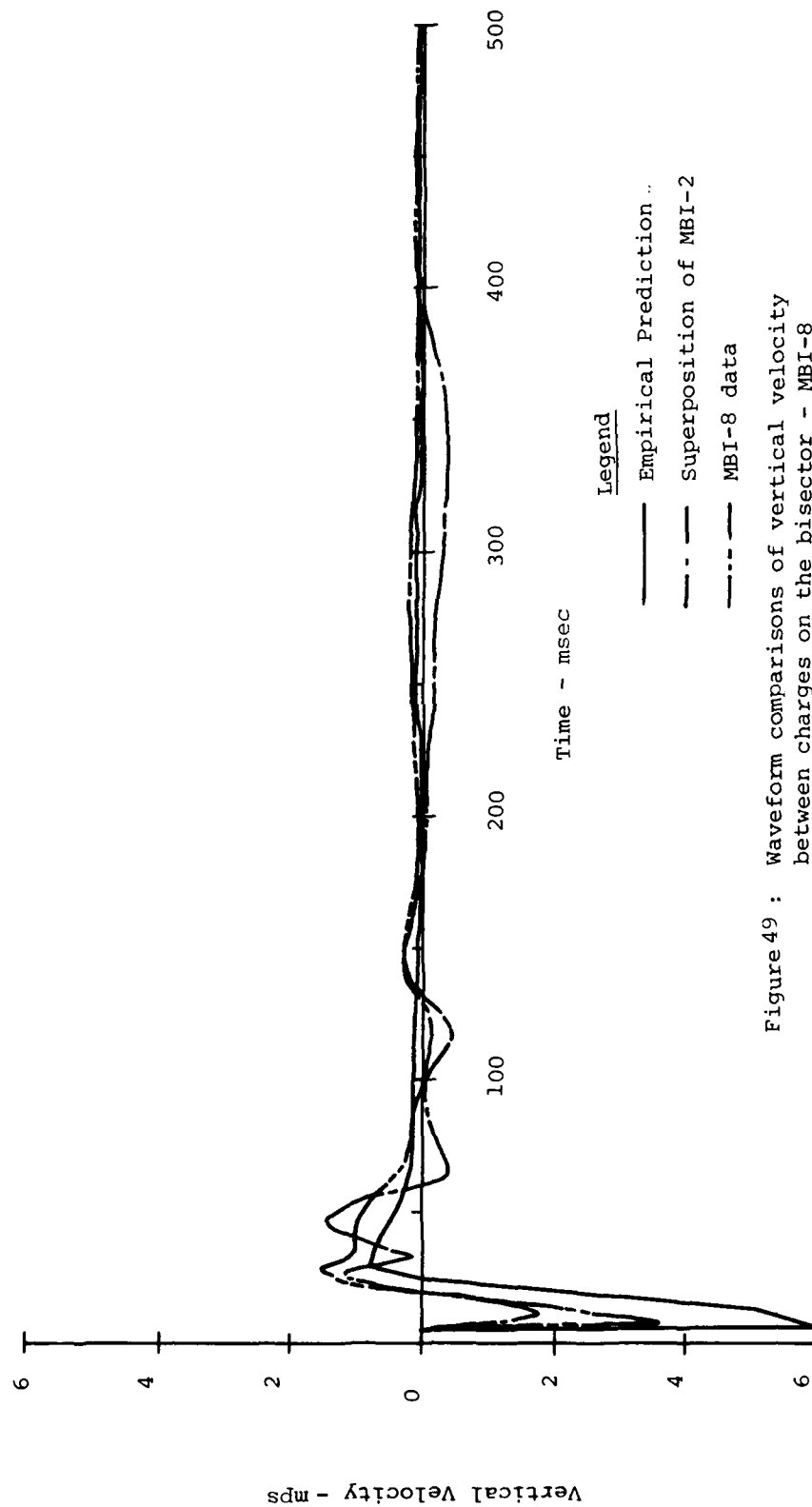


Figure 49 : Waveform comparisons of vertical velocity  
between charges on the bisector - MBI-8

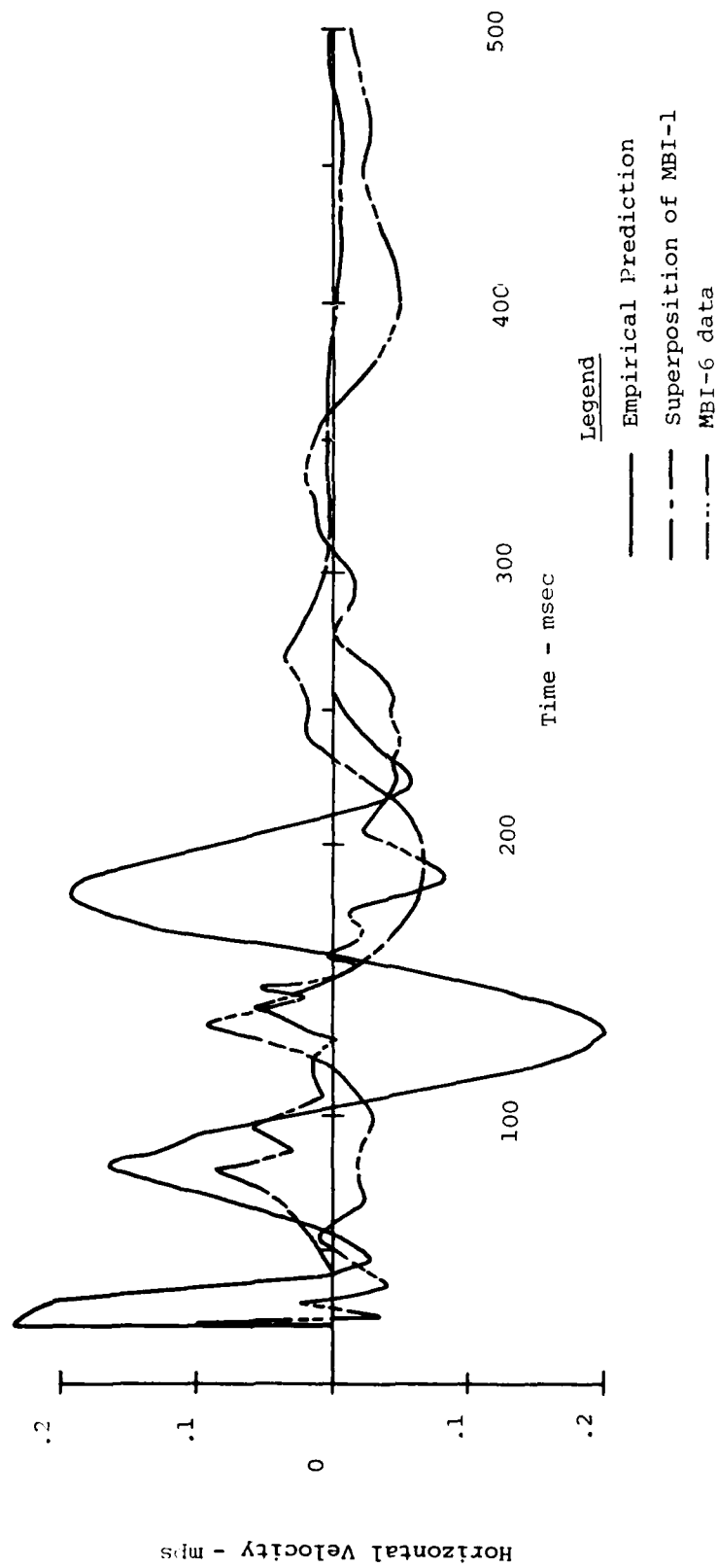


FIGURE 50: Waveform Comparisons of Horizontal Velocity between charges on the bisector - MBI-6

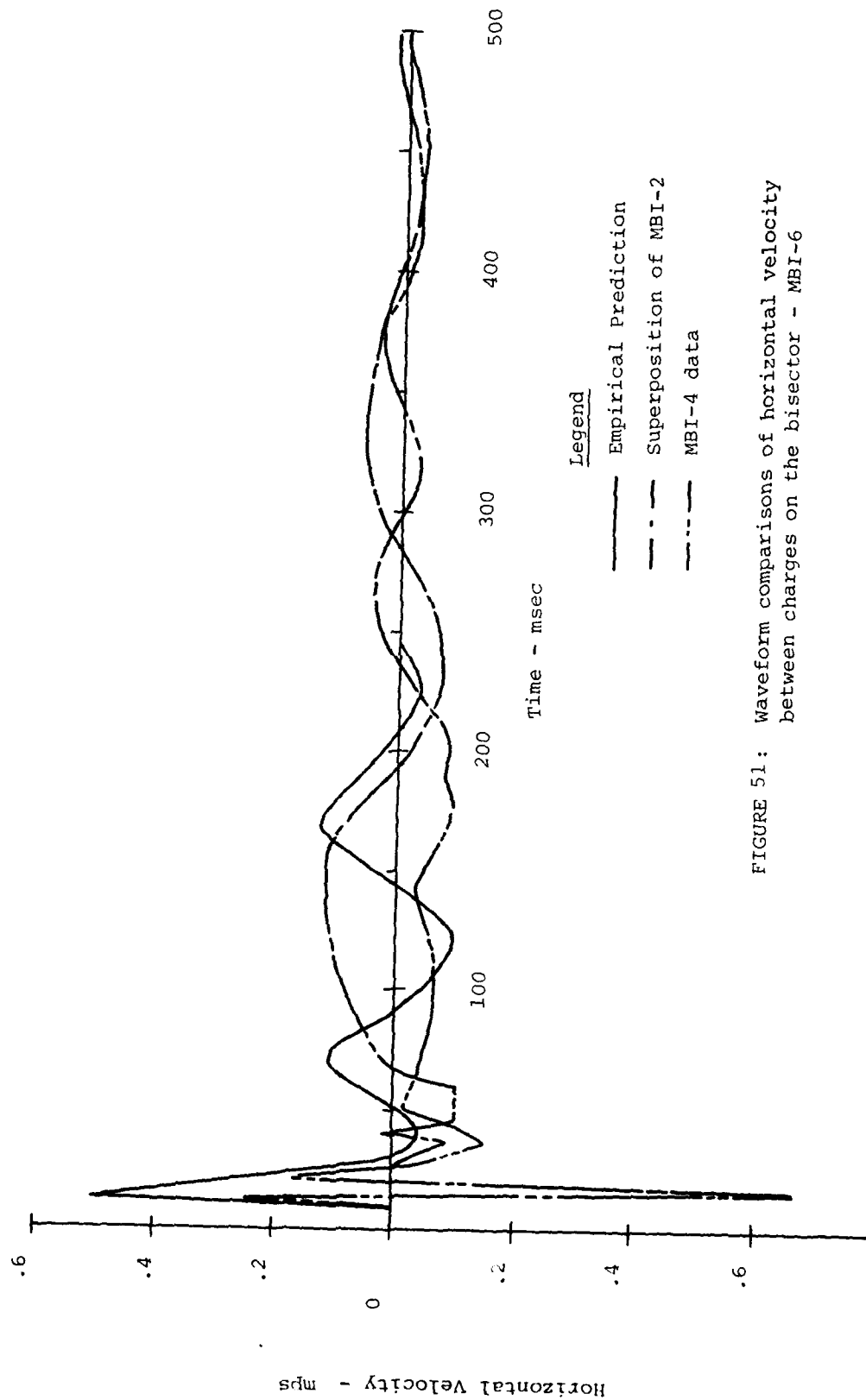


FIGURE 51: Waveform comparisons of horizontal velocity between charges on the bisector - MBI-6

TABLE 10: Summary of Prediction Accuracy at the location between charges on the bisector

Component	MBI-4		MBI-6		MBI-8	
	Super-position	Empirical	Super-position	Empirical	Super-position	Empirical
1) Vertical Air Slap						
a) Time of ar-rival	0%	-33%	0%	+ 3%	0%	0%
b) Pulse width	0%	+ 4%	-18%	+77%	-13%	+33%
c) Period	+15%	+42%	- 7%	+17%	-48%	+68%
d) Peak	-65%	+17%	-25%	+49%	-54%	+39%
Oscillatory Component						
e) Time of ar-rival	-13%	+66%	-26%	- 3%		
f) Period	-57%	0%	+28%	0%		
g) Peak	-37%	-71%	+68%	-82%		
2) Horizontal Air Slap						
a) Time of ar-rival	+260%	0%	+85%	0%		
b) Pulse width	+150%	+320%				
c) Period						
d) Peak	- 60%	+108%	-17%	+133%		
Oscillatory Component						
e) Time of ar-rival	- 19%	- 38%	0%	- 31%		
f) Period	+110%	- 5%	-24%	- 48%		
g) Peak	+ 53%	+ 88%	+ 2%	+283%		

The vertical air slap component is better predicted for this location than those discussed previously. The improvement for this component is in the timing aspect. Arrival times, pulse widths, and periods are all better predicted than at other locations. Air slap peaks are consistently underpredicted by superposition and consistently overpredicted by the empirical methods.

The prediction of the vertical oscillatory component for this location has about the same accuracy as the other locations. Neither method appears to be consistently better.

Horizontal air slap motions were poorly predicted by both methods. The largest failure of superposition is in the arrival time. This occurs because the effects of the two closest charges are assumed to cancel due to symmetry. From the waveforms shown, this is obviously not the case. The empirical prediction is just the vertical air slap modified as recommended in Reference 10. Since this is the case, the arrival time is the same as the vertical and, therefore, more like the data than was superposition. The peak motions were generally overpredicted by the empirical methods and underpredicted by superposition.

The oscillatory component was more accurately predicted than the air slap and in general within the accuracy that has been shown for the other locations. The oscillatory peaks are consistently overpredicted by both methods.

Shock spectra comparisons that correspond to the waveforms in the previous discussion are presented in Figures 52 and 56.

The general shapes of these spectra for vertical motions are more similar than any of the previous comparisons. The limiting displacements of these spectra are generally underpredicted by superposition. The empirical prediction of MBI-4

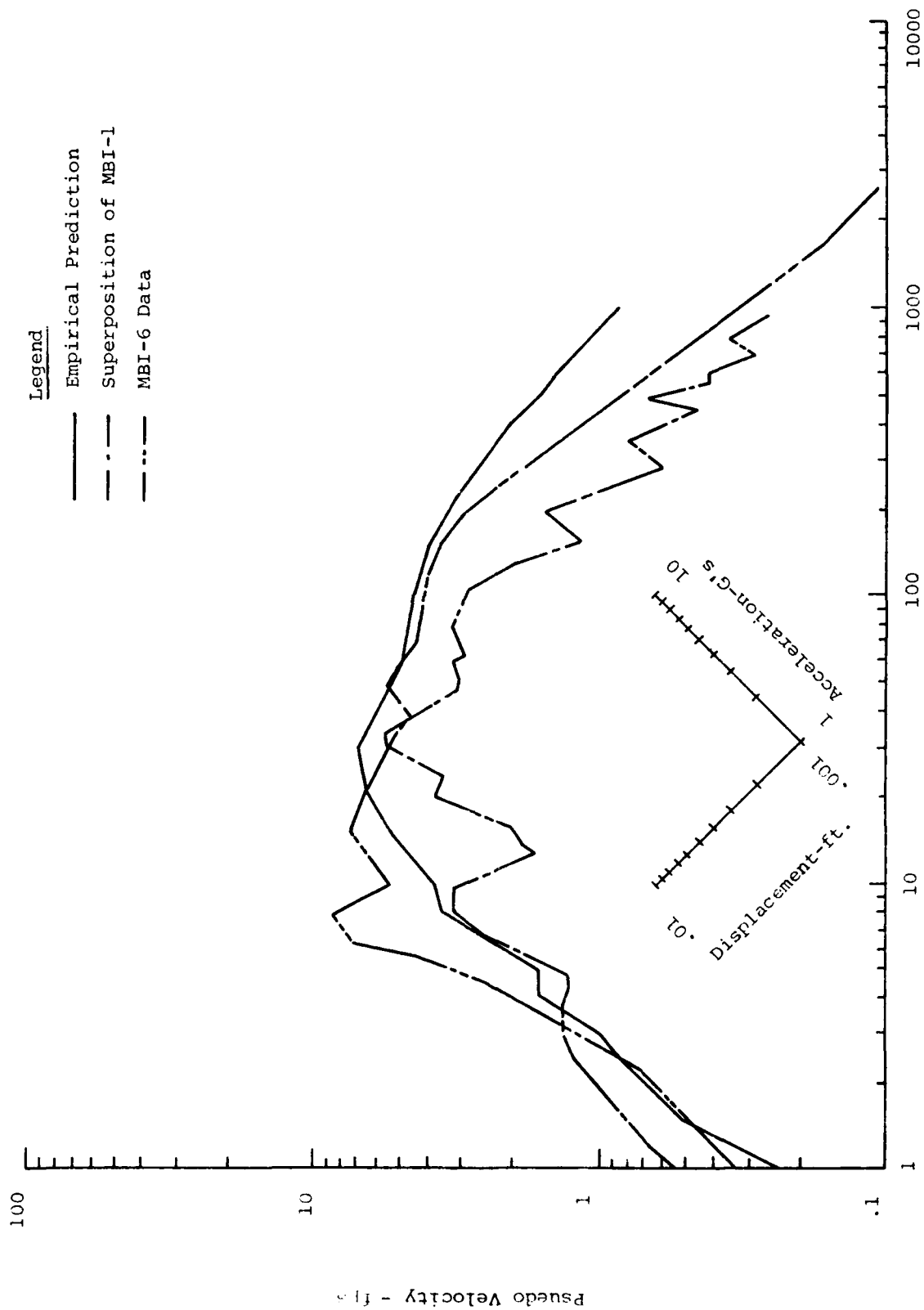


FIGURE 52: Shock Spectra Comparisons of Vertical Velocity between charges on the bisector - MBI-6



FIGURE 53: Shock Spectra Comparisons of Vertical Velocity between charges on the bisector - MBI-4

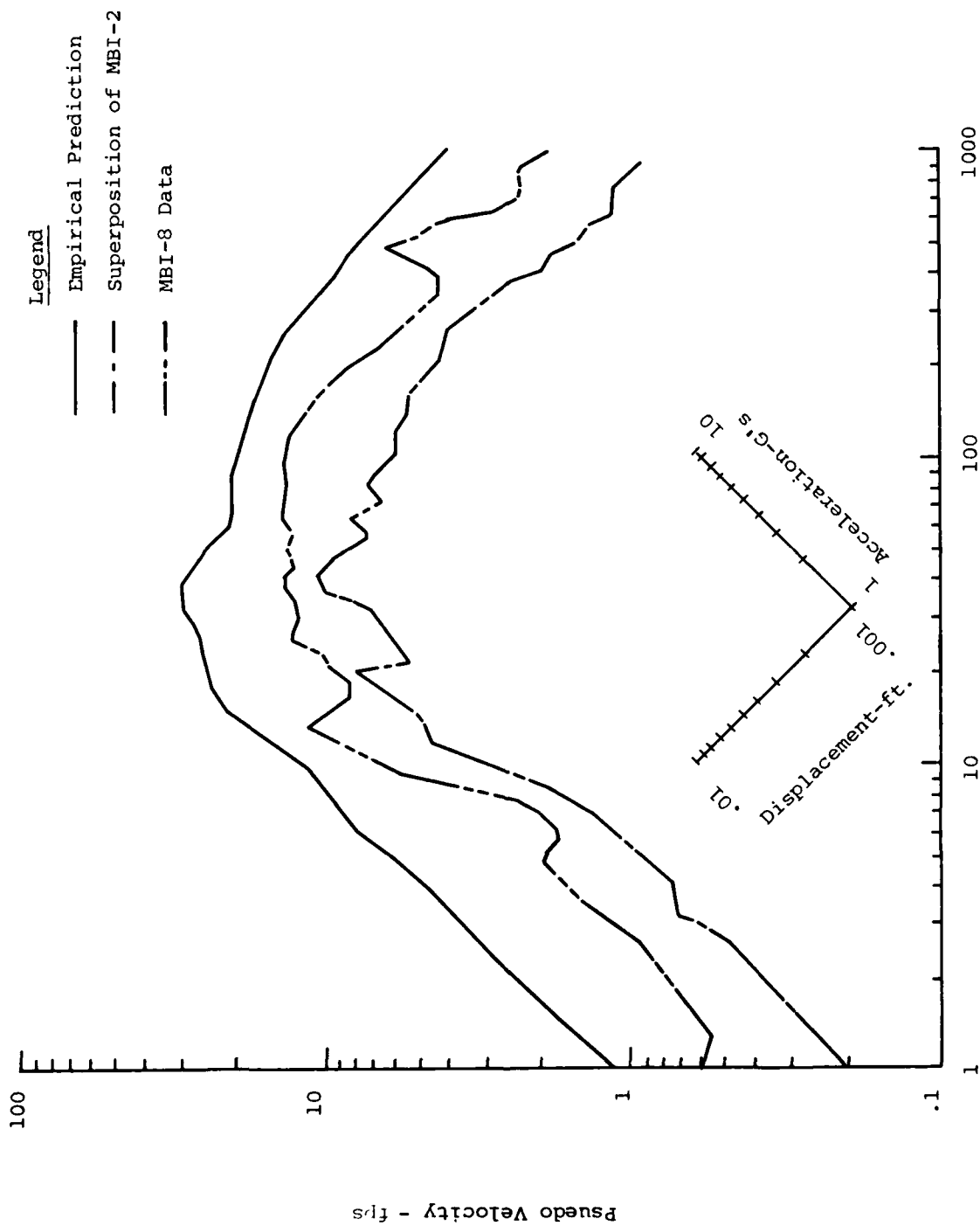


FIGURE 54: Shock Spectra Comparisons of Vertical Velocity between charges on the bisector - MBI-8

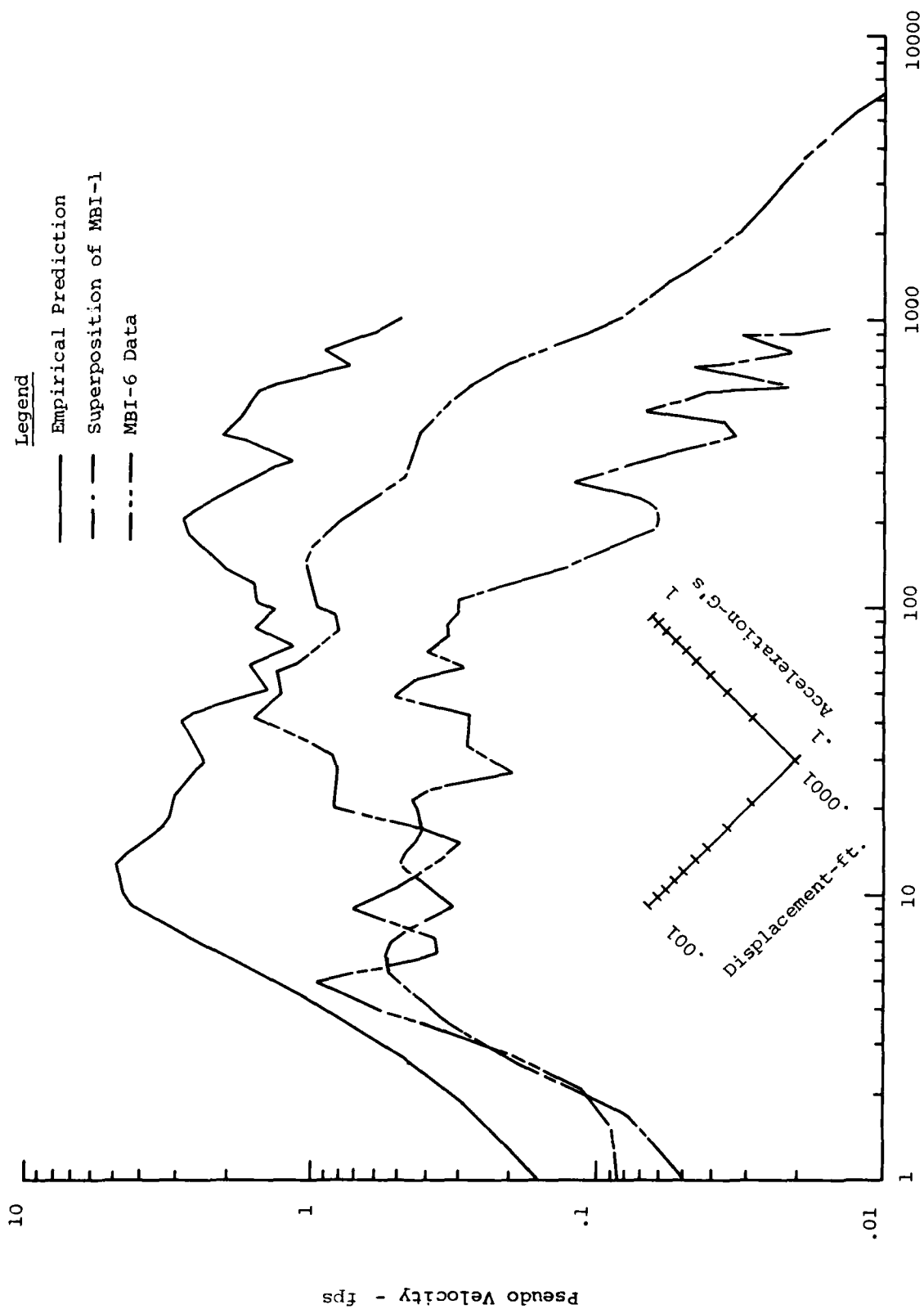


FIGURE 55: Shock Spectra Comparisons of Horizontal Velocity between charges on the bisector - MBI-6

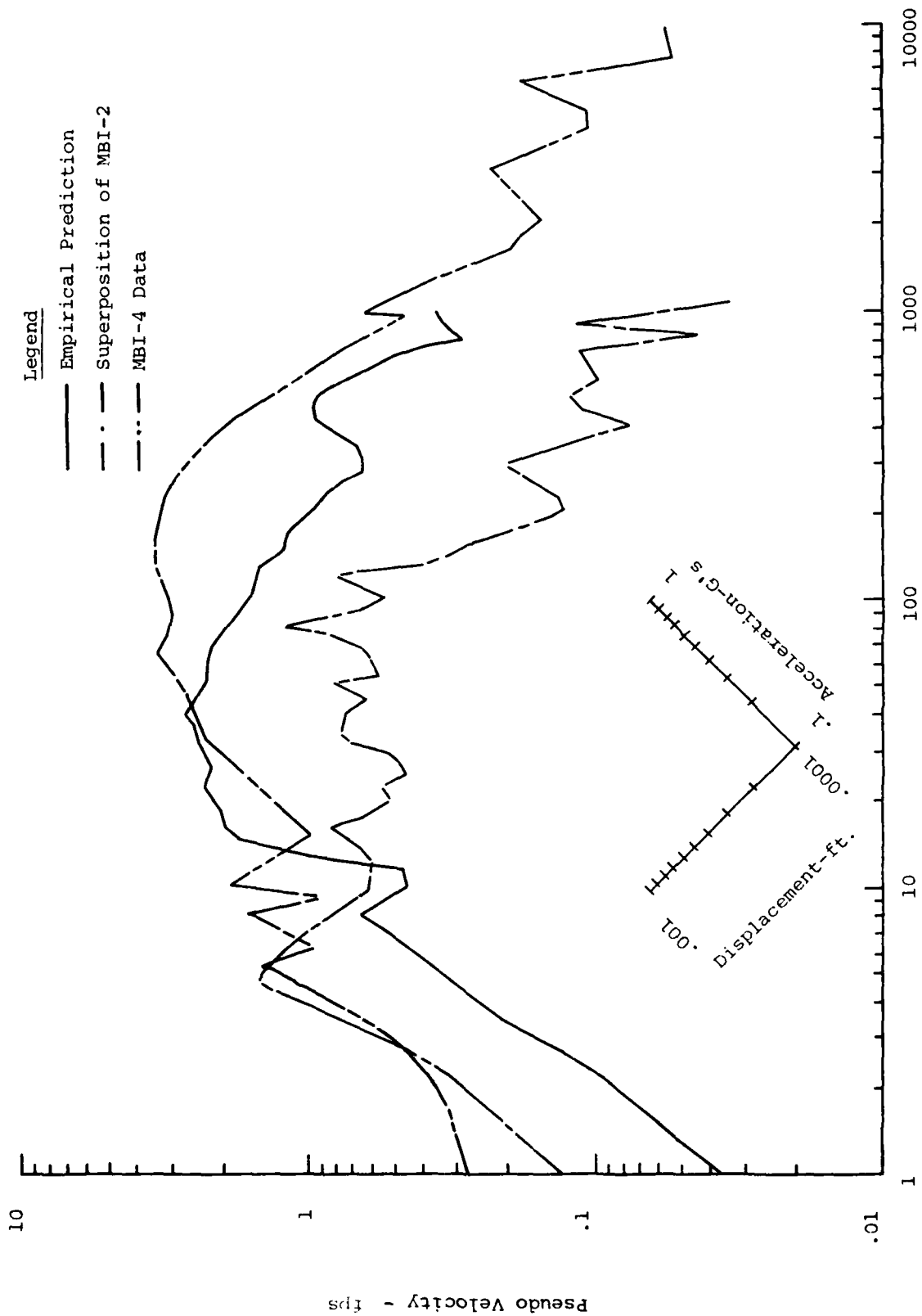


FIGURE 56: Shock Spectra Comparisons of Horizontal Velocity between charges on the bisector MBI-4

and MBI-8 overpredicts this quantity. Neither method produces consistently better results. Limiting velocities are generally predicted within a factor of two by both methods with neither showing greater accuracy. Limiting low frequency was generally overpredicted but still on the average within a factor of two of the data.

The horizontal shock spectra yielded limiting velocities which were consistently underpredicted by superposition. The empirical prediction overpredicted this value by 3 times the data value on MBI-6, but on MBI-4 the empirical prediction was within a factor of 2 of the data. The limiting displacements do not lend themselves to general statements. The limiting low frequencies indicate the trend for superposition to underpredict low frequencies while the empirical method overpredicts the low frequencies.

d) Charge Spacing Outside the Array on the Bisector

The waveform comparisons used in this discussion are shown in Figures 57 through 61. Table 11 presents the summary of the accuracy of the two prediction methods.

For this location superposition predicts the vertical air slap component well as compared to the other locations and the empirical prediction. The empirical prediction is poor in both period and pulse width.

Again the oscillatory component is as accurately predicted as at the other locations. Both the empirical method and superposition yield about the same success.

The superposition prediction for the horizontal air slap component is very good. Timing is generally accurate and peak values are reasonably close. The empirical prediction of this component is poor.

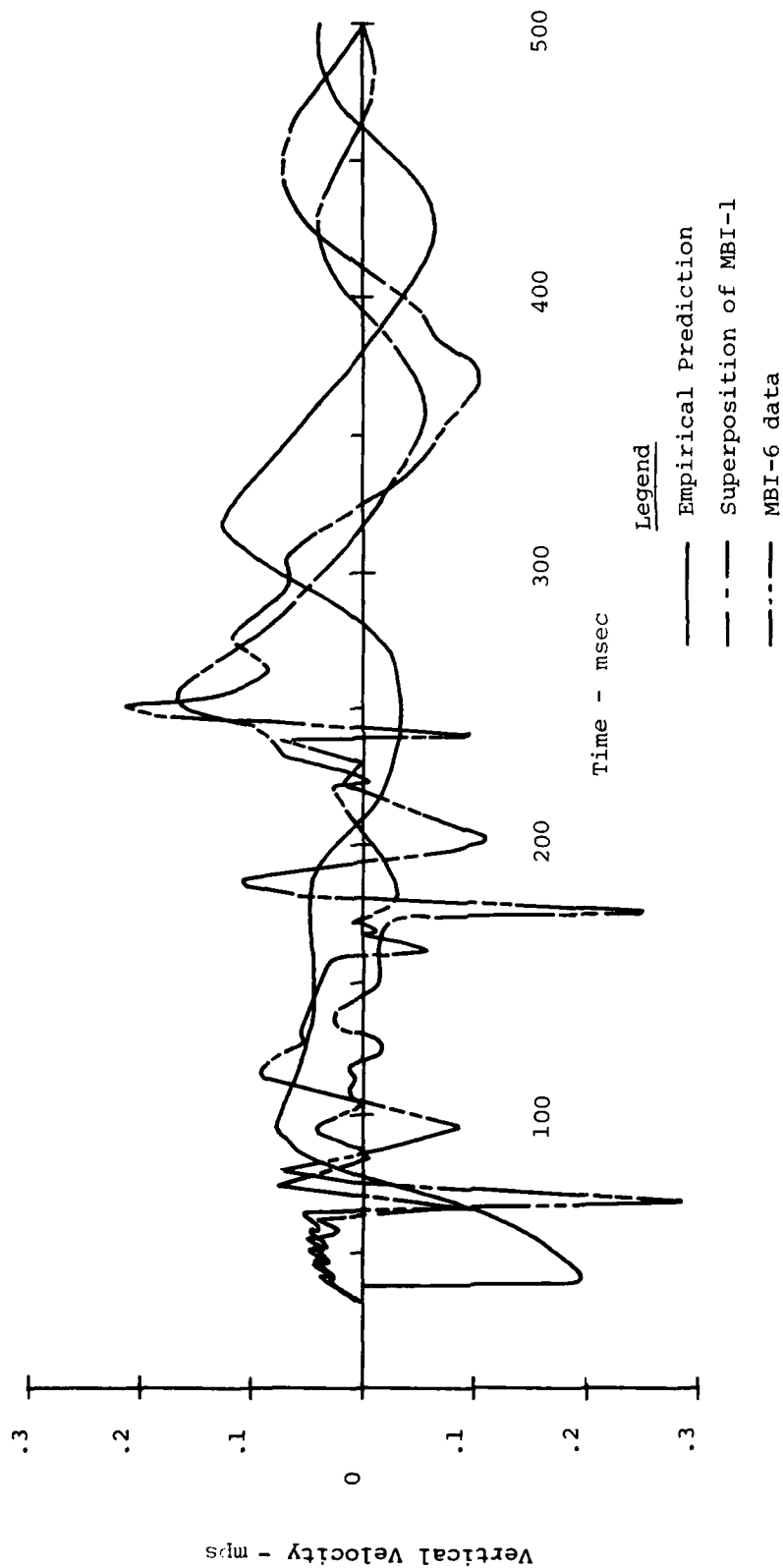


Figure 57 : Waveform comparisons of  
vertical velocity a charge  
spacing outside the array on  
a bisector - MBI- 6

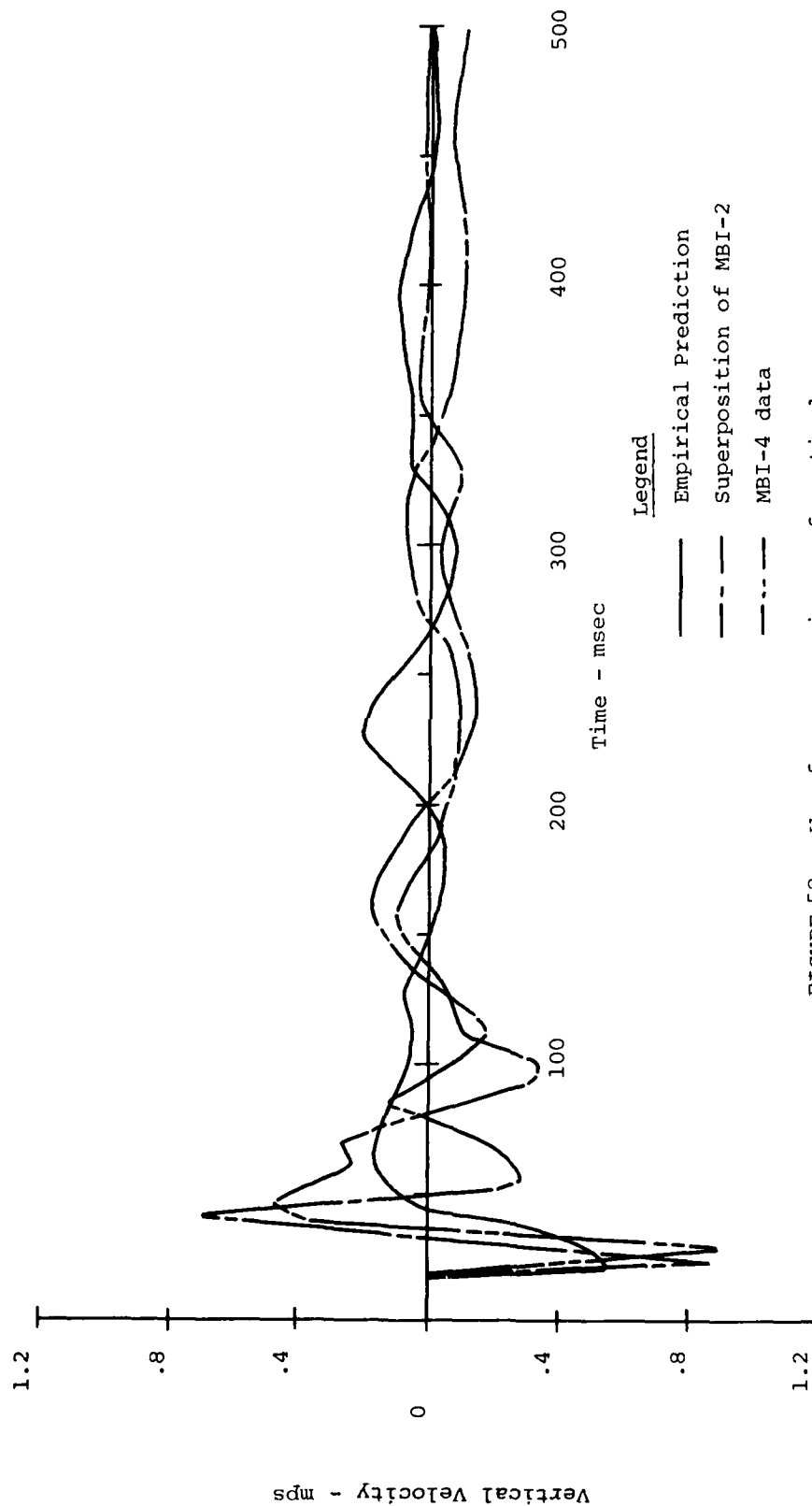


FIGURE 58: Waveform comparisons of vertical velocity a charge spacing outside the array on a bisector - MBI-4

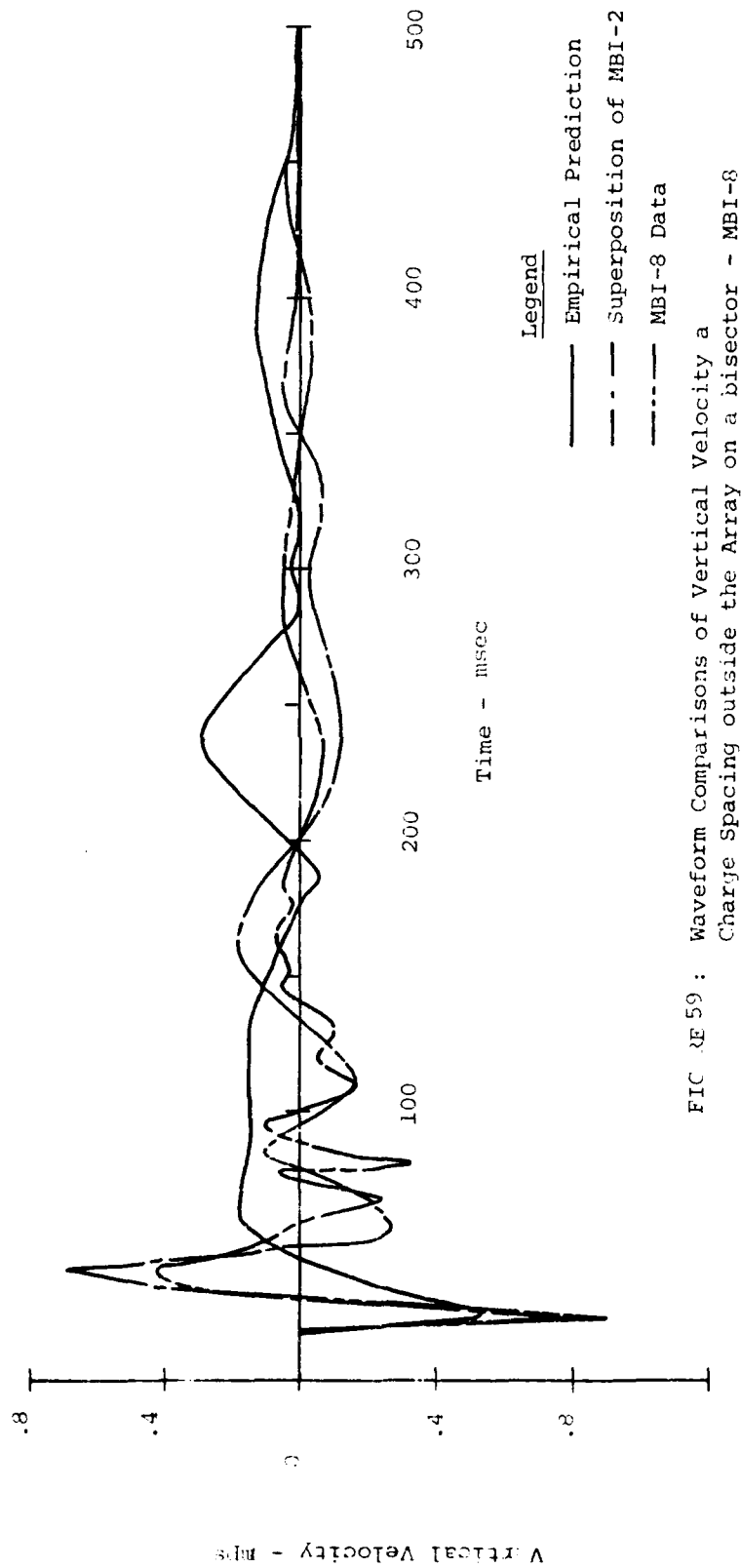


FIG 4E 59 : Waveform Comparisons of Vertical Velocity a  
Charge Spacing outside the Array on a bisector - MBI-8

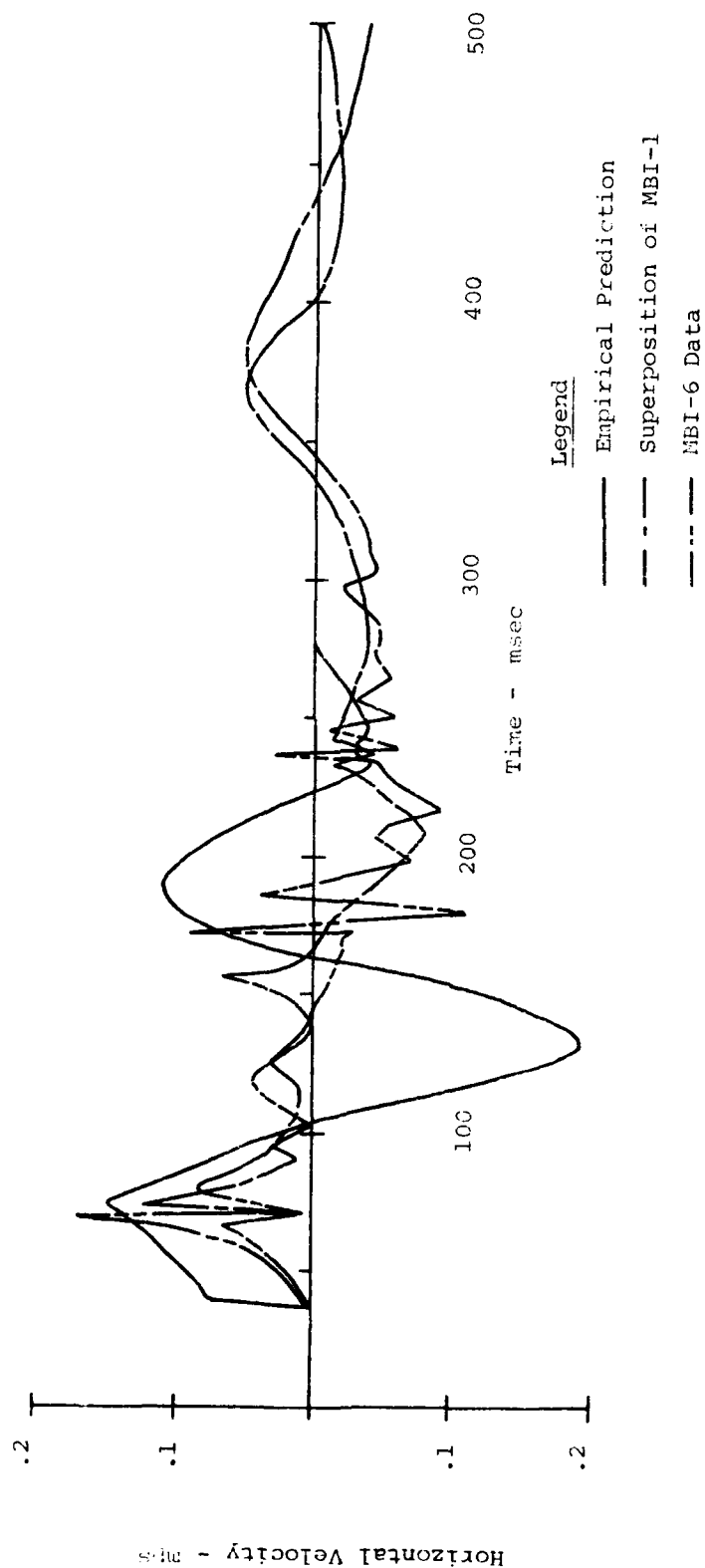


FIGURE 60 : Waveform Comparisons of Horizontal Velocity a Charge Spacing outside the array on a bisector - MBI-6

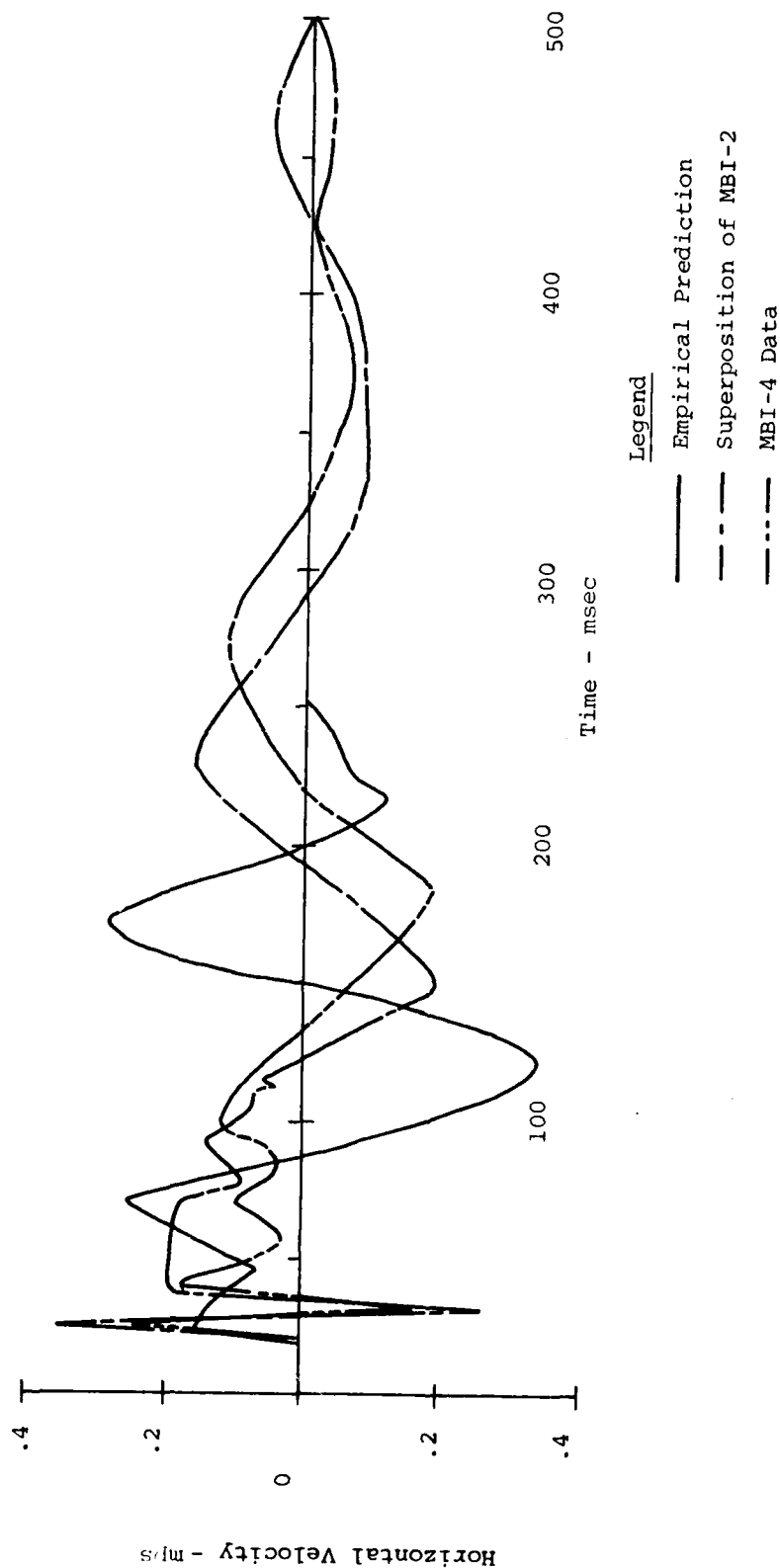


FIGURE 61: Waveform Comparisons of Horizontal Velocity a Charge Spacing outside the array on a bisector - MBI-4

TABLE 11: Summary of Prediction Accuracy at the location a charge spacing outside the charge array on the bisector

Component	MBI-4		MBI-6		MBI-8	
	Super-position	Empirical	Super-position	Empirical	Super-position	Empirical
1) Vertical Air Slap						
a) Time of ar-rival	-13%	- 15%	0%	- 44%	0%	0%
b) Pulse width	+ 8%	+108%	-20%	+300%	+12.5%	+133%
c) Period	-45%	+121%	-26%	+612%	- 25%	+300%
d) Peak	- 2%	- 40%	-66%	- 32%	- 2%	- 42%
Oscillatory Component						
e) Time of ar-rival	+16%	+ 43%	- 2%	+ 17%	- 5%	+ 40%
f) Period	+28%	- 8%	-15%	- 13%	+ 40%	+ 4%
g) Peak	+70%	+ 40%	-43%	- 40%	+ 3%	+ 9%
2) Horizontal Air Slap						
a) Time of ar-rival	0%	+ 16%	0%	- 18%		
b) Pulse width			+67%			
c) Period			+30%			
d) Peak	-26%	- 9%	+80%	- 20%		
Oscillatory Component						
e) Time of ar-rival	- 3%	- 52%	- 2%	- 30%		
f) Period	-32%	- 37%	-13%	- 40%		
g) Peak	-29%	+ 29%	+ 9%	+ 92%		

The prediction of the low frequency component by superposition is good. Timing is reasonable and peaks are quite accurate. Empirical predictions of this component are generally too large in magnitude and out of phase.

The shock spectra comparisons corresponding to the waveforms discussed above are shown in Figures 62 and 66.

The vertical waveforms yield spectra that are generally the same shape. The limiting values of displacement are generally predicted within a factor of 2. Superposition appears to do a better job in predicting limiting velocities than does the empirical prediction. Superposition is within a factor of 2 of the data whereas the empirical is below that measure of accuracy. The limiting low frequencies do not appear to follow a trend. Superposition is predicting higher values than does the empirical method and it is interesting to note all events produced a limiting low frequency value of about 10 Hz in the data for this particular location.

The limiting velocity determined from the horizontal shock spectra was overpredicted by the empirical method for these events. Superposition was not quite as consistent. MBI-6 was underpredicted while MBI-4 was overpredicted. For the limiting displacements both prediction methods have a tendency to overpredict, but in this particular case both methods were within a factor of 2 of the data. Limiting low frequencies were overpredicted for MBI-4 and underpredicted for MBI-6.

#### 4.3 EVALUATION OF SUPERPOSITION

##### 4.3.1 Introduction

It was stated at the outset that one of the primary objectives of this report is to evaluate the validity of the

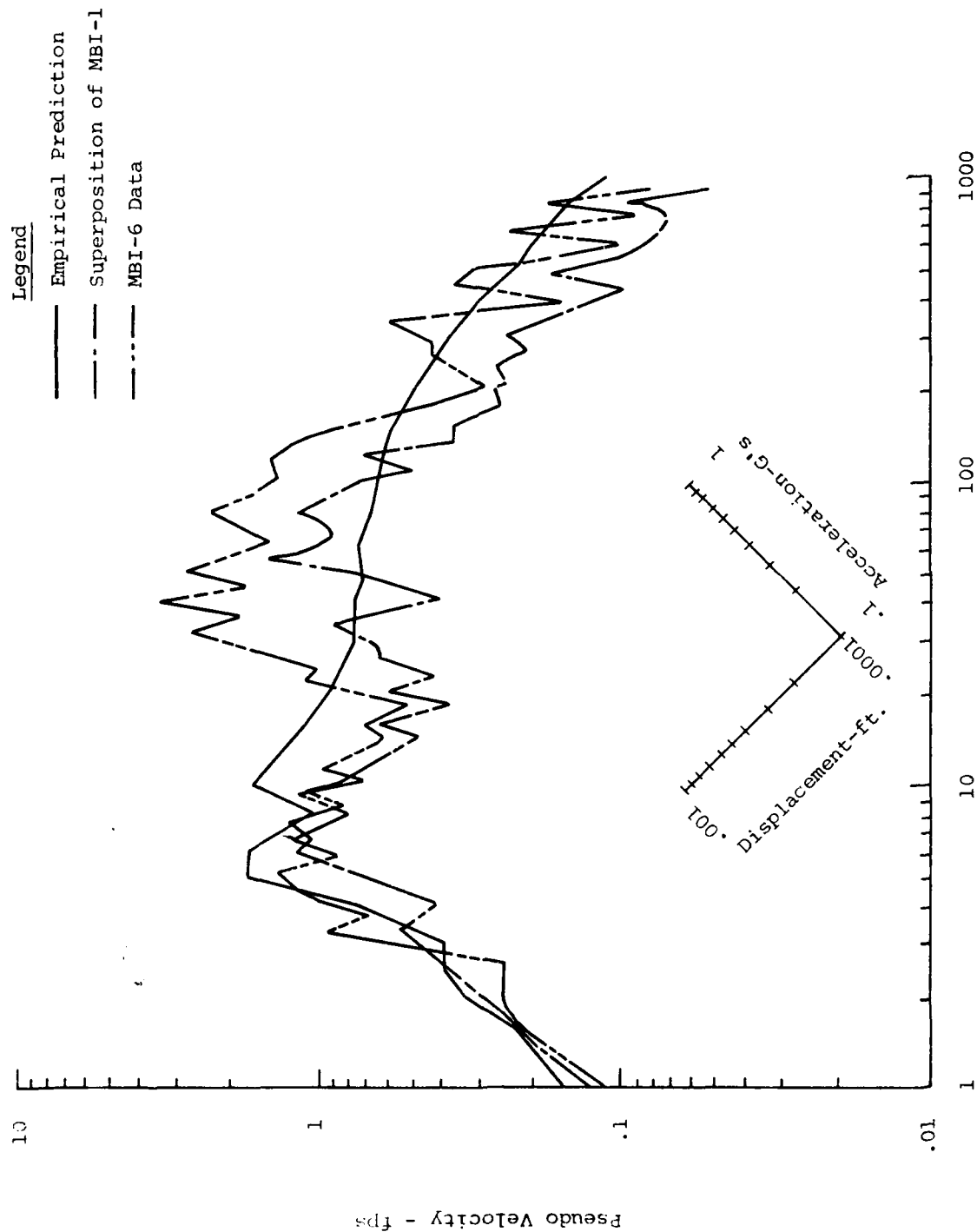


FIGURE 62: Shock Spectra Comparisons of Vertical Velocity a charge spacing outside the array on a bisector - MBI-6

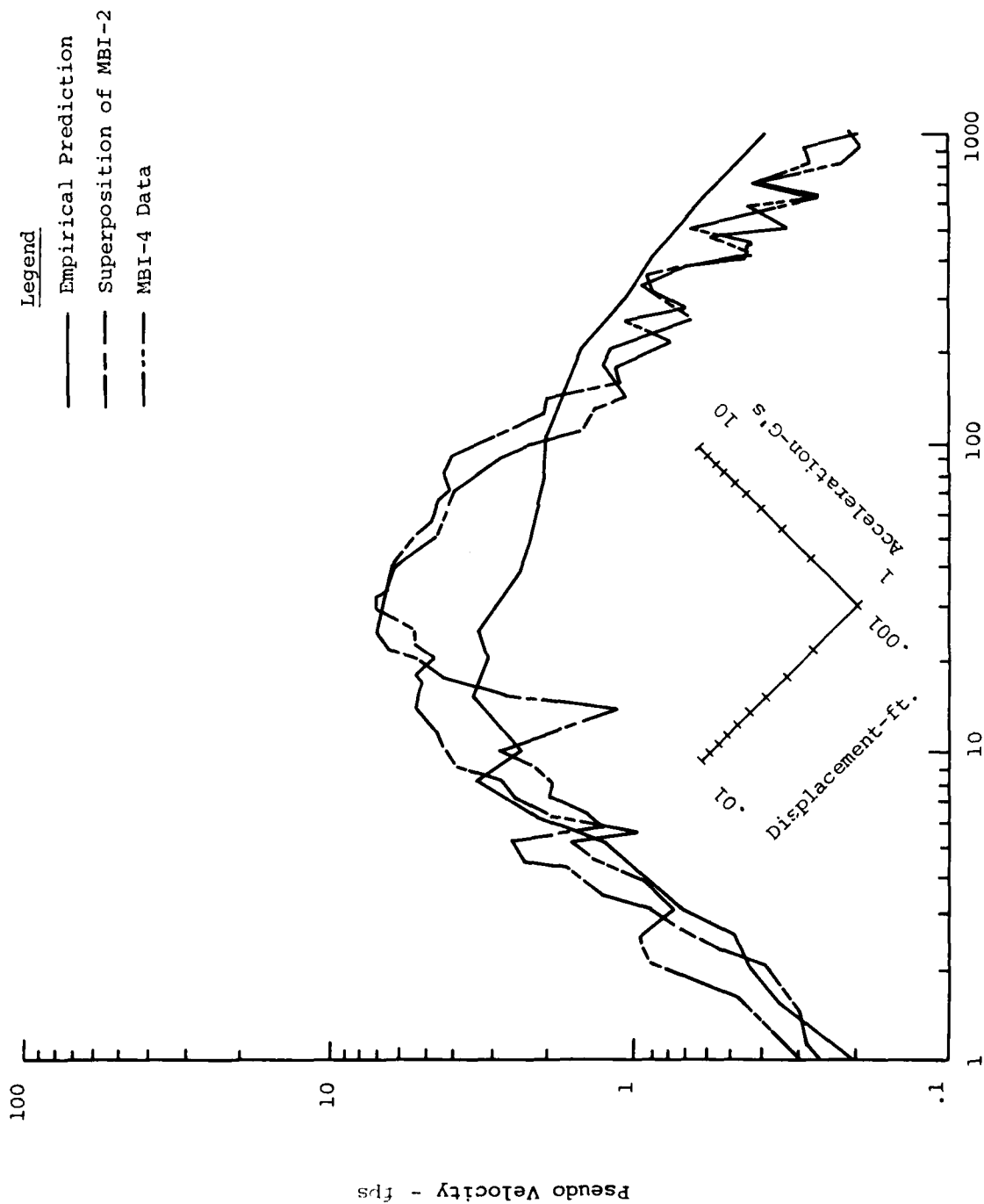


FIGURE 63: Shock Spectra Comparisons of Vertical Velocity a charge spacing outside the array on a bisector - MBI-4

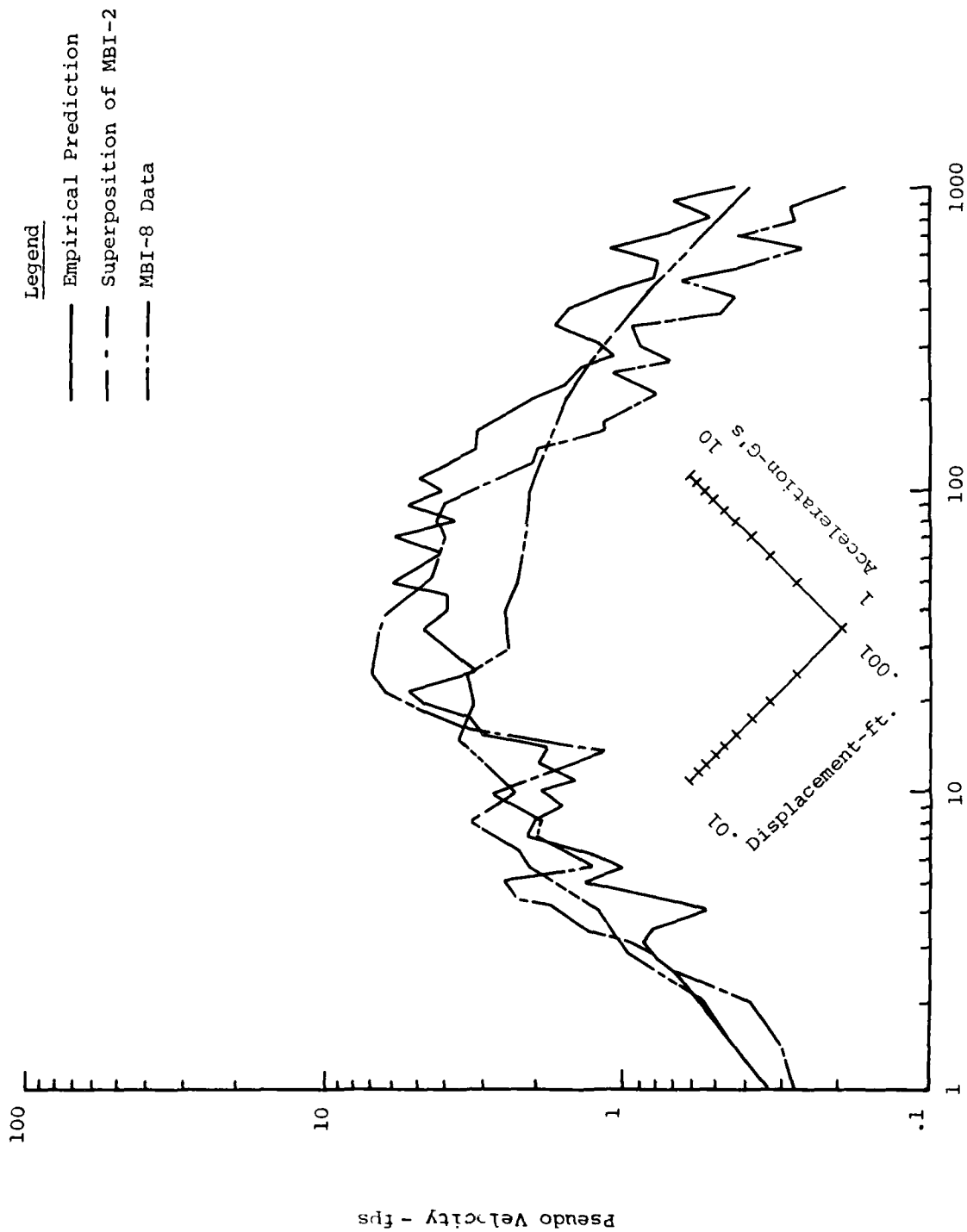


FIGURE 64: Shock Spectra Comparisons of Vertical Velocity a charge spacing outside the array on a bisector - MBI-8

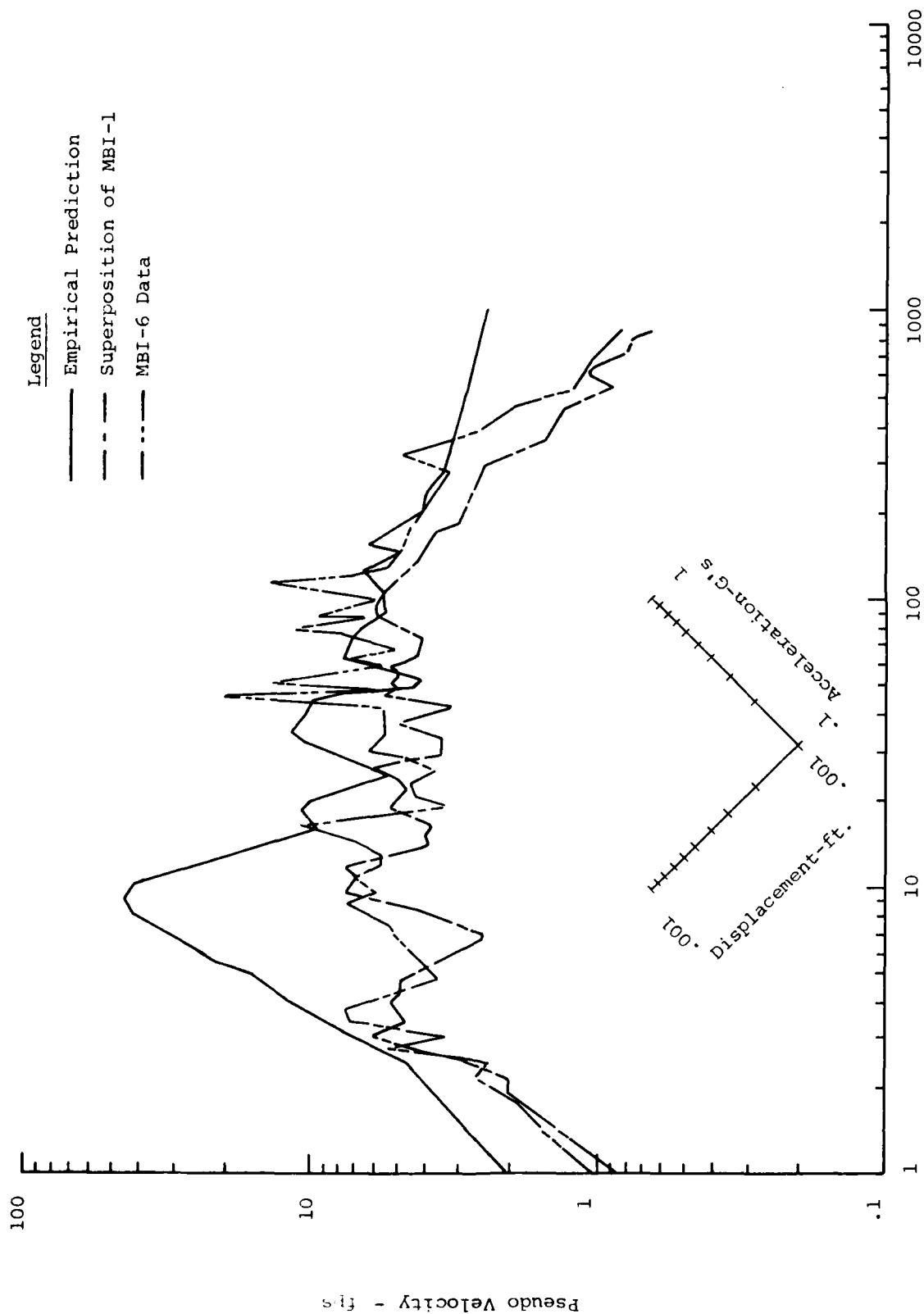


FIGURE 65: Shock Spectra Comparisons of Horizontal Velocity a charge spacing outside the array on a bisector - MBI-6

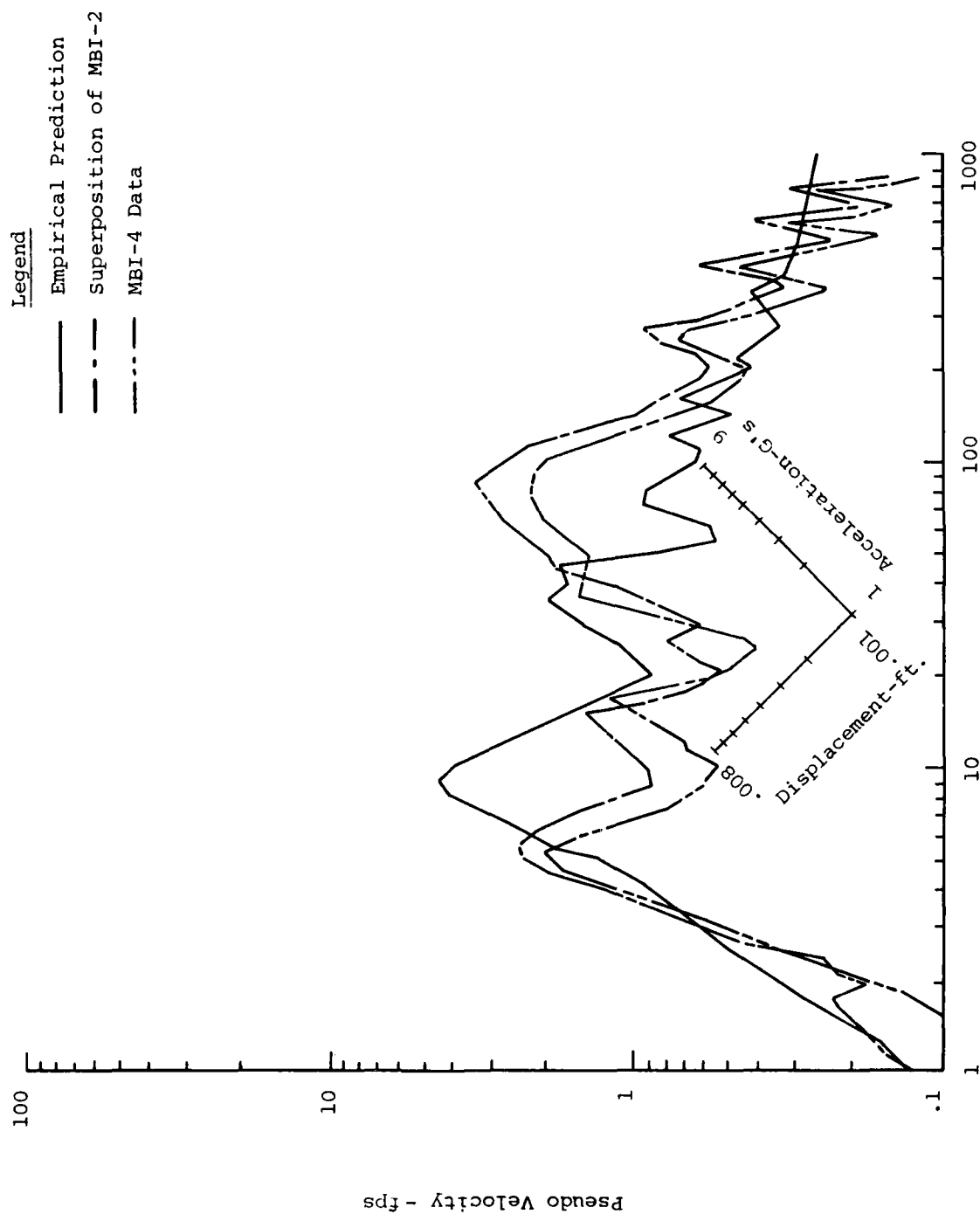


FIGURE 66: Shock Spectra Comparisons of Horizontal Velocity a charge spacing outside the array on a bisector - MBI-4

superposition assumption. That is, where do the nonlinear interaction effects become significant and where is the response primarily a linear phenomena. Implied in this objective, is the determination of the controlling factors of the nonlinear behavior and the attempt to define these factors quantitatively.

#### 4.3.2 Regions Where Superposition is Valid

The superposition assumption was found to be valid in three regions. These are summarized below:

a) At depths below the phreatic surface. For this region, the isolation of the gages from the surface airblast is thought to be the major cause of the validity of superposition. The motion in this region is a directly coupled signal and an upstream airblast signal. These signals are not dominated by the overhead surface airblast and the various shock on shock interaction as the nearer surface gages, and therefore, behave in a more linear elastic manner.

b) Outside the charge array. The success of superposition in this region is attributed to the behavior of the airblast. At these locations the nonlinear interactions of the airblast from different charges have become negligible and, therefore, the observed phenomena exhibits a character similar to the single burst experiments.

c) Inside the charge array at the range greater than one half the charge spacing from the center. This particular region is not as clear cut as the regions previously discussed. Inside the charge array, superposition

is showing a definite trend of improvement as distance from the array center increases. This improvement is due to a decrease in interaction of the overhead airblast. That is to say at the center of the array, the interaction is a maximum. This location is also the most poorly predicted. As a range from the array center increases, interaction decreases and the prediction becomes more accurate. As the range from the array center approaches the charge spacing the response becomes dominated by a single charge. This is obvious by the observation of the ground motion waveforms measured at locations of  $3/4$  charge spacing away from the array center. These waveforms are essentially the same as the single burst waveforms measured at comparable locations.

#### 4.3.3 Region Where Superposition is Not Valid

The region of invalidity of superposition can be defined by a circle, with a radius equal to one half the charge spacing, centered at the array center, and above the water table. The failure of superposition is noticeable in both the horizontal and vertical motions, however, it is most pronounced on the vertical waveforms and is manifested by the large upward, long duration signal that was discussed in Section 4.2.

Figures 67 and 68 illustrate some of the characteristics of this signal. Figure 67 shows the peak upward velocities recorded and predicted for MBI-4. At first glance, it appears that superposition does a good job of predicting the motion, however the peak motion on the superposition prediction is a combination of the reflected and recovery peak from the airblast signal. This peak is of much shorter duration than the signal on the multiple burst experiment. Figure 68 shows a comparison

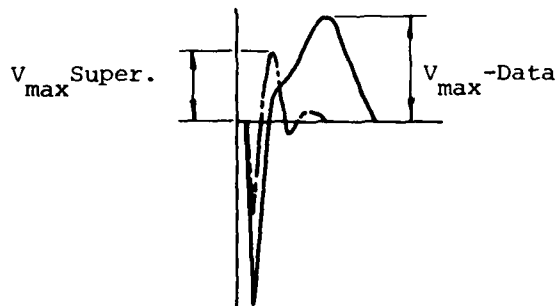
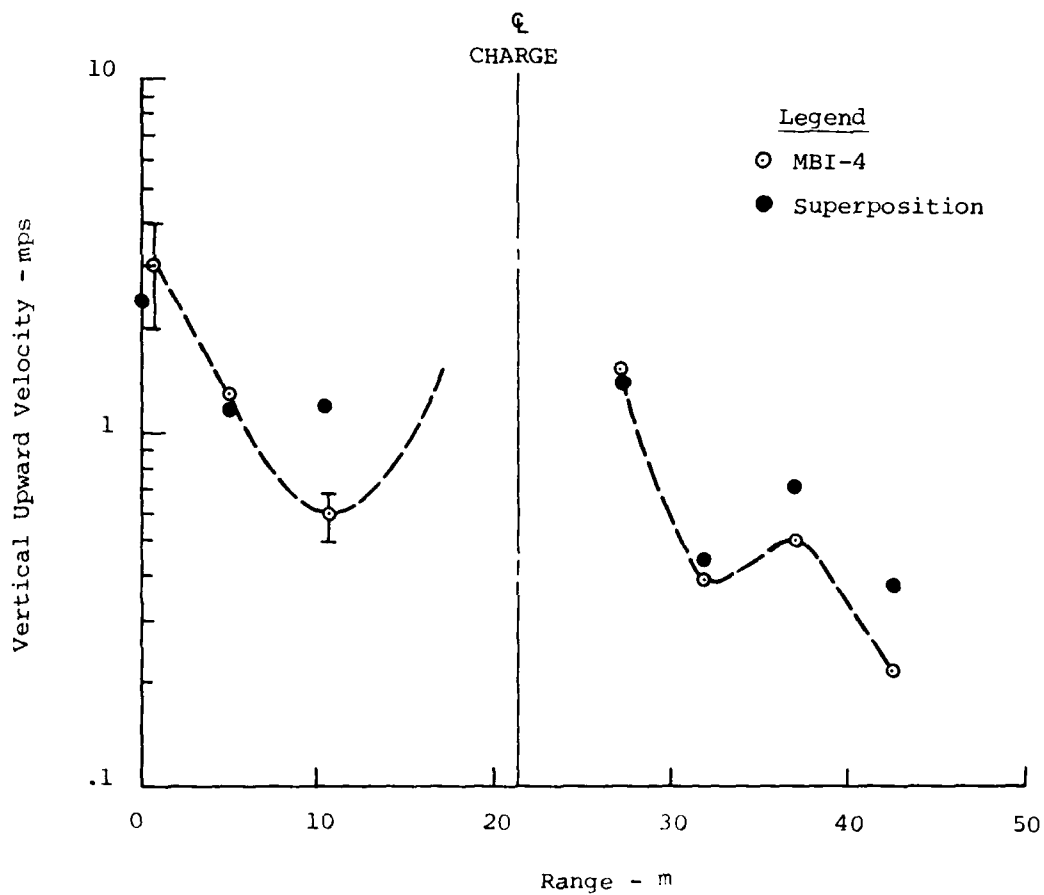


FIGURE 67: Comparison of Maximum Upward Velocities from MBI-4 and Superposition of MBI-2

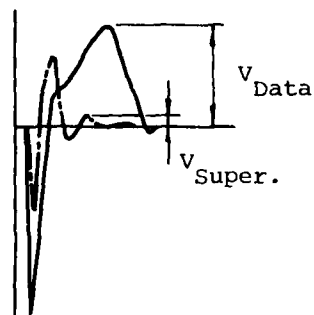
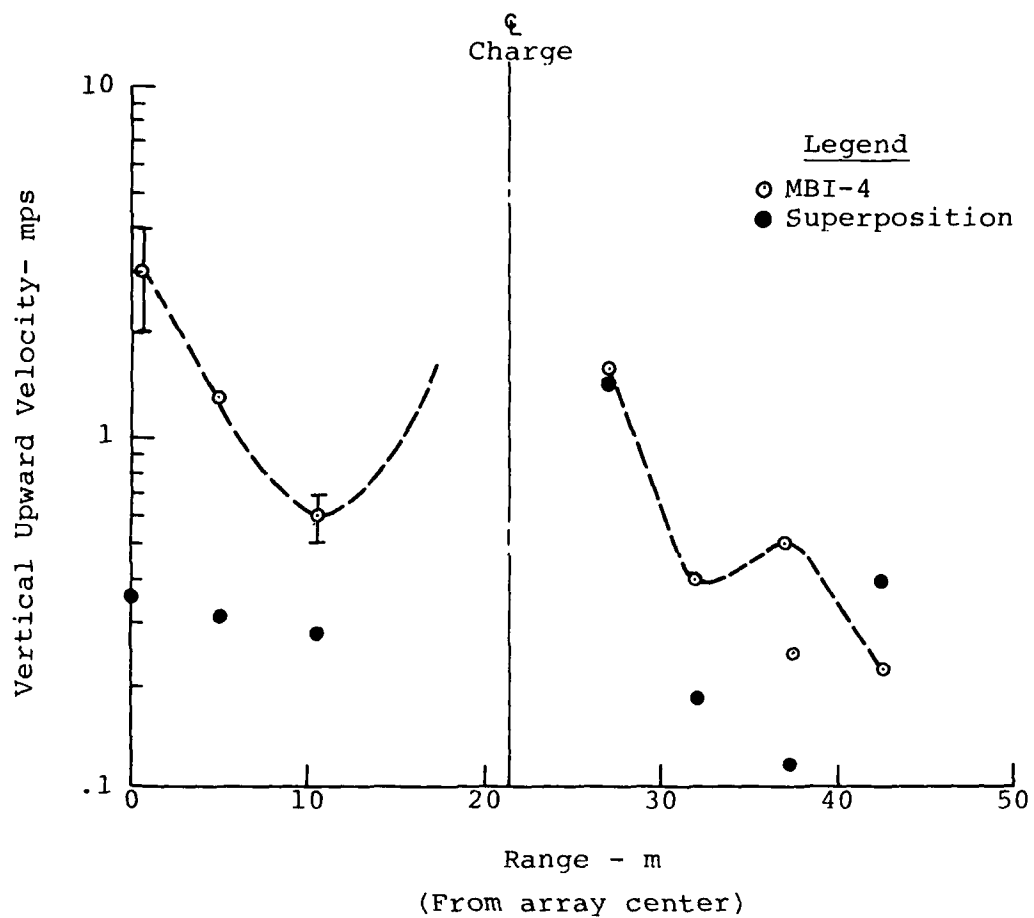


FIGURE 68: Comparison of Corresponding Upward Velocities from MBI-4 and Superposition of MBI-2

of the peak in the superposition prediction that corresponds to the peak in the multiple burst data. As is obvious, the superposition prediction is not satisfactory.

Figure 69 makes these same comparisons for MBI-6. In this case the maximum upward peak is the corresponding peak. As can be seen, there is an interesting difference between this figure and the two previous figures, i.e., the superposition prediction appears to be much better. There still is a large difference at the center points, but at the other points of comparison the agreement is well within acceptable accuracy. Although this seems to indicate that superposition is better for this configuration and spacing, it must be borne in mind that even though peaks are similar to superposition waveforms exhibit a different character than the MBI-6 data.

At the current time there are two major theories as to the cause of this large upward motion. These are the major negative phases of the airblast waveform and cylindrical convergence.

a) Negative Airblast

The negative airblast theory (Reference 9) contends that as the negative pressure passes over the location of interest it causes the air in the soil pores to expand. This expansion then forces the soil particles near the surface upward into the partial vacuum near the surface. A study of the data from MBI-4 and MBI-6 was made to evaluate this theory. MBI-8 was not used in this study because of the termination of the negative phase by the additional charges present in that experiment.

The major supportive evidence for the negative phase theory comes from the timing of the negative phase and the large upward motion. A representative comparison of the ground

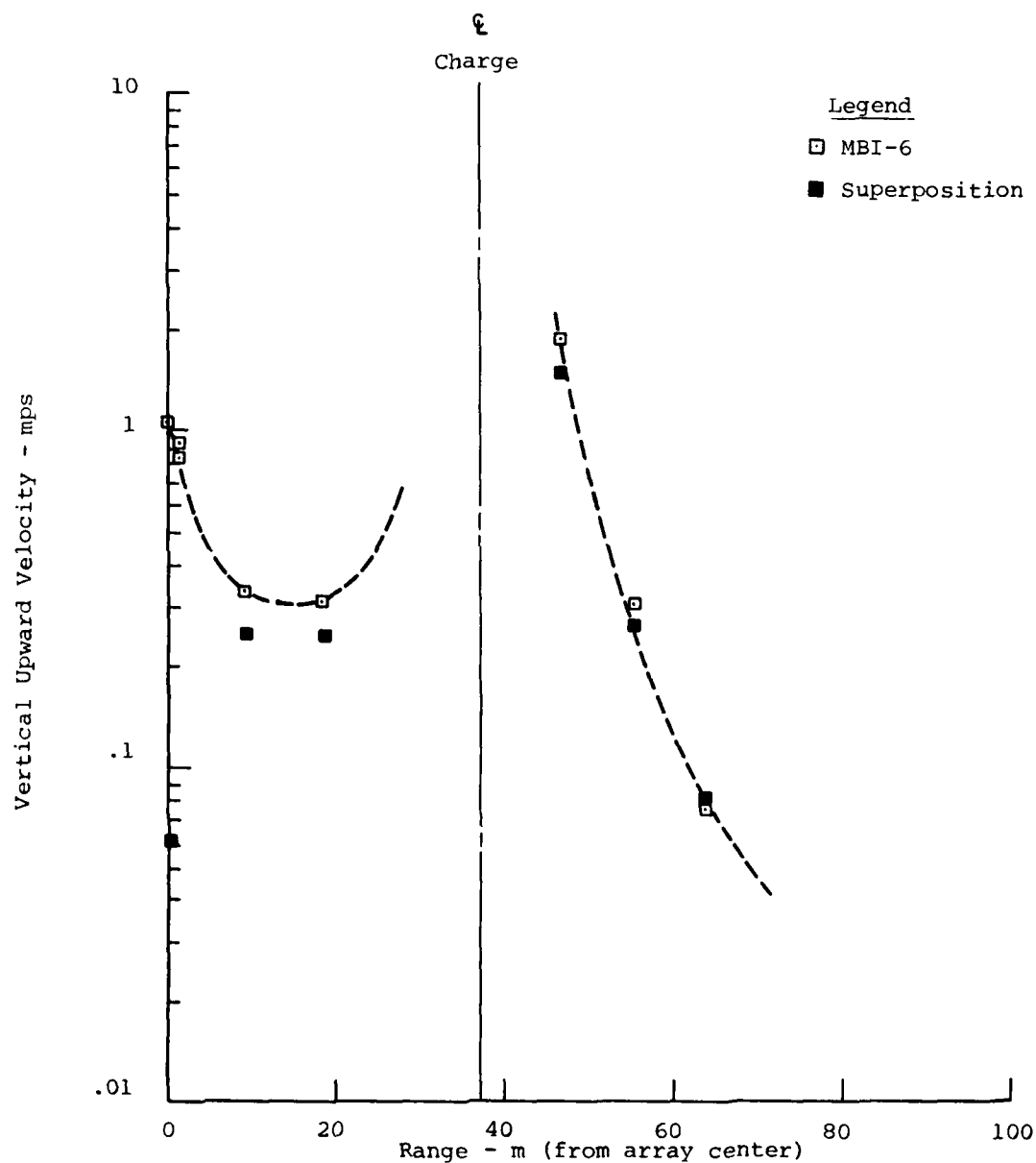


FIGURE 69: Comparison of corresponding and maximum velocities from MBI-6 and superposition of MBI-1

motion waveform and the airblast waveform is shown in Figure 70. It is obvious from this figure that both the negative phase and the large upward surge are occurring within the same time frame. Figure 71 shows the arrival times of the positive and negative phases of the airblast as well as the arrival time of the upward motion seen in the near surface waveforms. From this figure it is seen that the arrival time curves of the negative phase and the ground motion parallel one another at a difference of about 20 msec. This implies a propagation velocity to the .46 m depth on the order of 23 mps. The positive phase is propagating to the same depth at velocities on the order of 146 mps. This difference indicates an extremely dilated material.

To acquire a "feel" for the extent of dilation the material would experience a calculation using the following equation (Reference 10) was made:

$$\rho = \frac{\sigma}{\Delta V C_L}, \text{ where } \rho = \text{the density of the material}$$

$\sigma$  = measured underpressure

$\Delta V$  = measured velocity of the upward signal

$C_L$  = measured wave speed as determined from the arrival time of the upward signal at the 0.46 m and 1.53 m depths.

This calculation was carried out for both MBI-4 and MBI-6 and the results are shown below:

Event	Location	Meas. $\Delta V$ (mps)	Meas. $C_L$ (mps)	Meas. $\sigma$ (MPa)	Calc. $\rho$ (gm/cc)	$\rho_o$ (gm/cc)
MBI-4	Center	1.952	107	.052	.249	1.76
	1/4 Charge Spacing	0.955	137	.053	.406	1.76

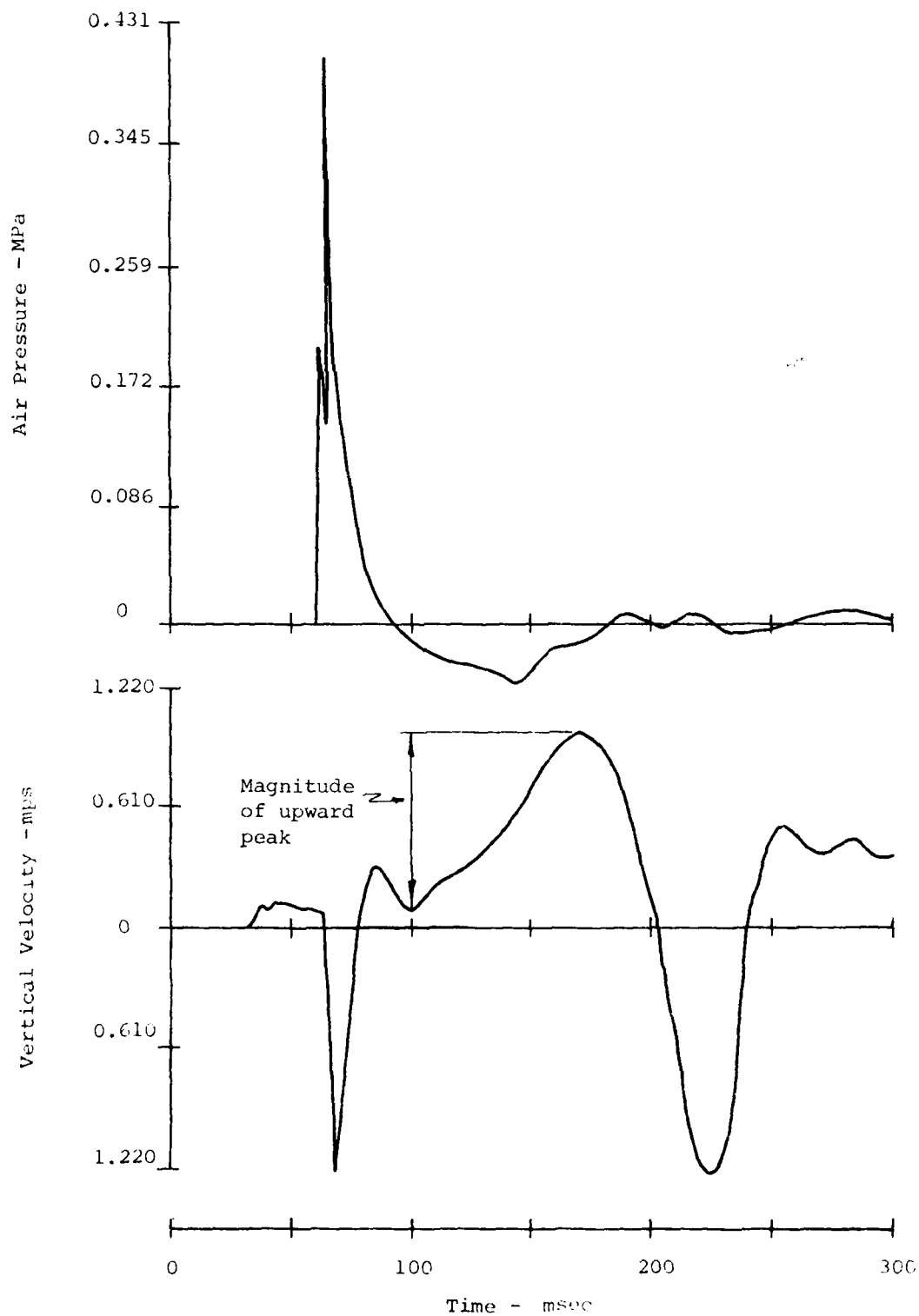


FIGURE 70 : Time Correlation of negative phase and large upward motion at the array "center" - MBI-6

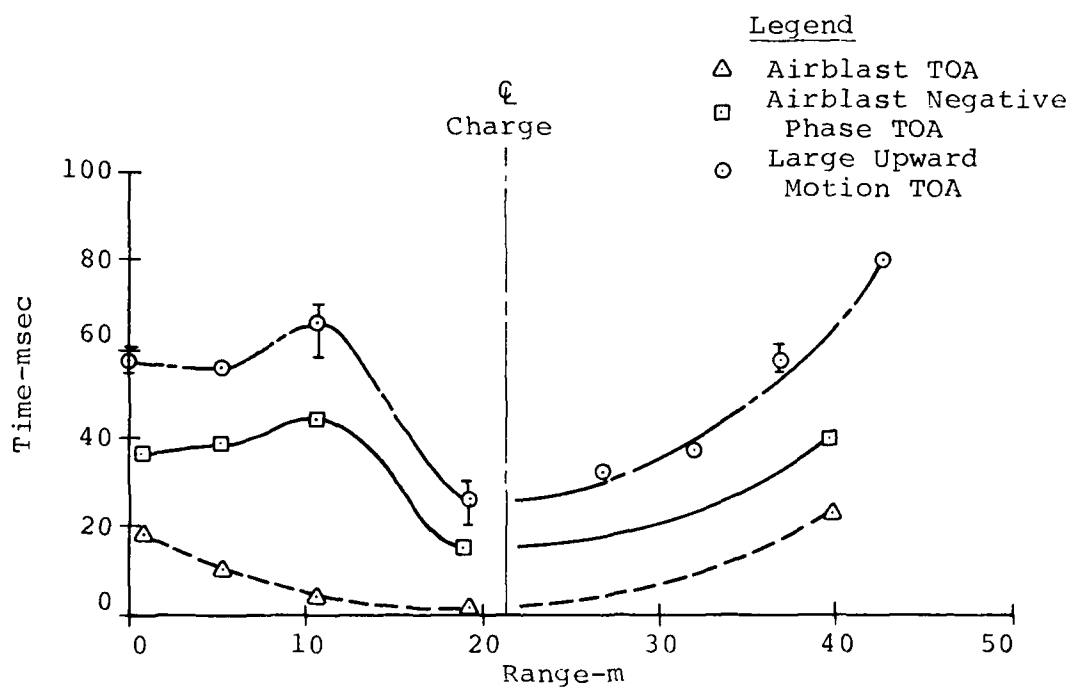


Figure 71: Time Phasing of Airblast and Large Upward Ground Motion - MBI-4

<u>Event</u>	<u>Location</u>	<u>Meas. <math>\Delta V</math></u>	<u>Meas. <math>C_L</math></u>	<u>Meas. <math>\sigma</math></u>	<u>Calc. <math>\rho</math></u>	<u><math>\rho_o</math></u>
MBI-6	1/2 Charge Spacing	0.342	178	.028	.461	1.76
	Center	0.903	178	.043	.268	1.76
	1/4 Charge Spacing	0.499	56	.025	.896	1.76

These calculations indicate that the density varies as distance from the center increases. For both experiments, the calculated density is about 1/8 the original. In MBI-4, this increases to only about 1/4 of the original density and the 1/2 charge spacing location. In MBI-6 the density increased to approximately 1/2 the original density and the 1/4 charge spacing location (the 1/2 charge spacing was not used as the upward signal was difficult to isolate).

An interesting point to note is the comparison of the underpressure measured at the center and 1/4 charge spacing location in MBI-4. These locations experienced approximately the same value of underpressure and yet the center point yielded an upward velocity almost twice that at the 1/4 charge spacing location. This seems to indicate some additional physics not accounted for by the negative phase alone.

#### b) Cylindrical Covergence

This theory contends that these large upward motions are a result of free surface spall which result from the very high stress levels that exist near the center of the charge array. These high stresses are caused by the interaction of the direct and reflected (from the center) waves which result due to the convergent nature of the geometry.

In studying the MBI-4 and MBI-6 data one of the most supportive pieces of evidence is Figure 72. This shows the magnitude of the upward velocity from 1/2 the charge spacing to the center. As can be observed, the trend is for this peak to increase by as much as a factor of 5 on the ranges of interest.

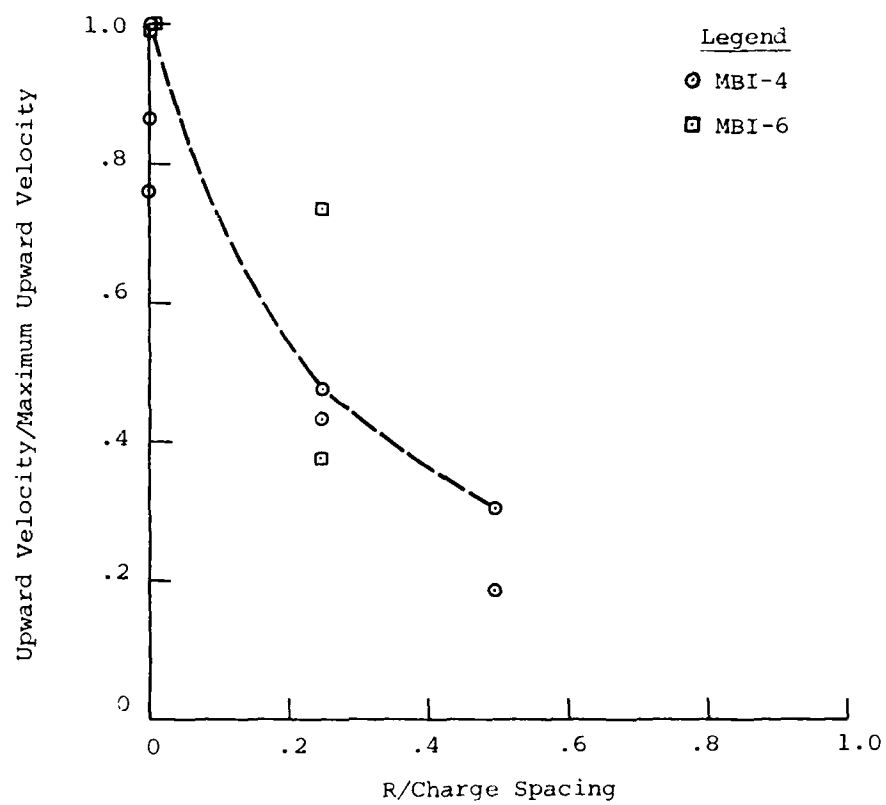


FIGURE 72: Peak upward motion versus range for MBI-4 and MBI-6

Another indication of cylindrical convergence is shown in Figure 73. This figure shows the horizontal stress data recorded in the center of one of the outside arrays on MBI-8 and compares this to the stress level recorded on Event 2 at an equivalent distance from a charge. This comparison indicates that stress levels are somewhat higher than would be expected from straight superposition. The positive stress values measured at the 1.52 m depth on MBI-8 are approximately 7 times what was measured on MBI-2, and the negative stress values on MBI-8 are approximately 8 times those measured on MBI-2. The gages at the 6.10 m depth on MBI-8 measured a positive horizontal stress of about 5 times the MBI-8 gages at 1.52 m depth and about 37 times the value measured at the 1.52 m depth on MBI-2. The negative horizontal stress measured at this greater depth produced similar differences (i.e., 6 times the MBI-8 1.52 m depth data and 48 times the MBI-2 1.52 m data). These higher stress levels seem to point to a cylindrical convergence type of phenomena. Horizontal motions also indicate that cylindrical convergence is occurring. Figures 74 and 75 show the maximum horizontal displacements from MBI-6 and MBI-4. The most interesting thing to note here is the magnitude of these displacements at the center of the charge array. When these are compared with the single burst values at an equivalent location it is seen that the multiple burst displacements vary from 2.5 times (MBI-6) to about 15 times (MBI-4) the single burst data. This indicates a substantial horizontal momentum at the center of the array. Figures 76 and 77 show the peak outward horizontal velocity for MBI-6 and MBI-4. In both these figures the trend for increased horizontal motion as the center is approached. This again is indicative of increased horizontal momentum at the center.

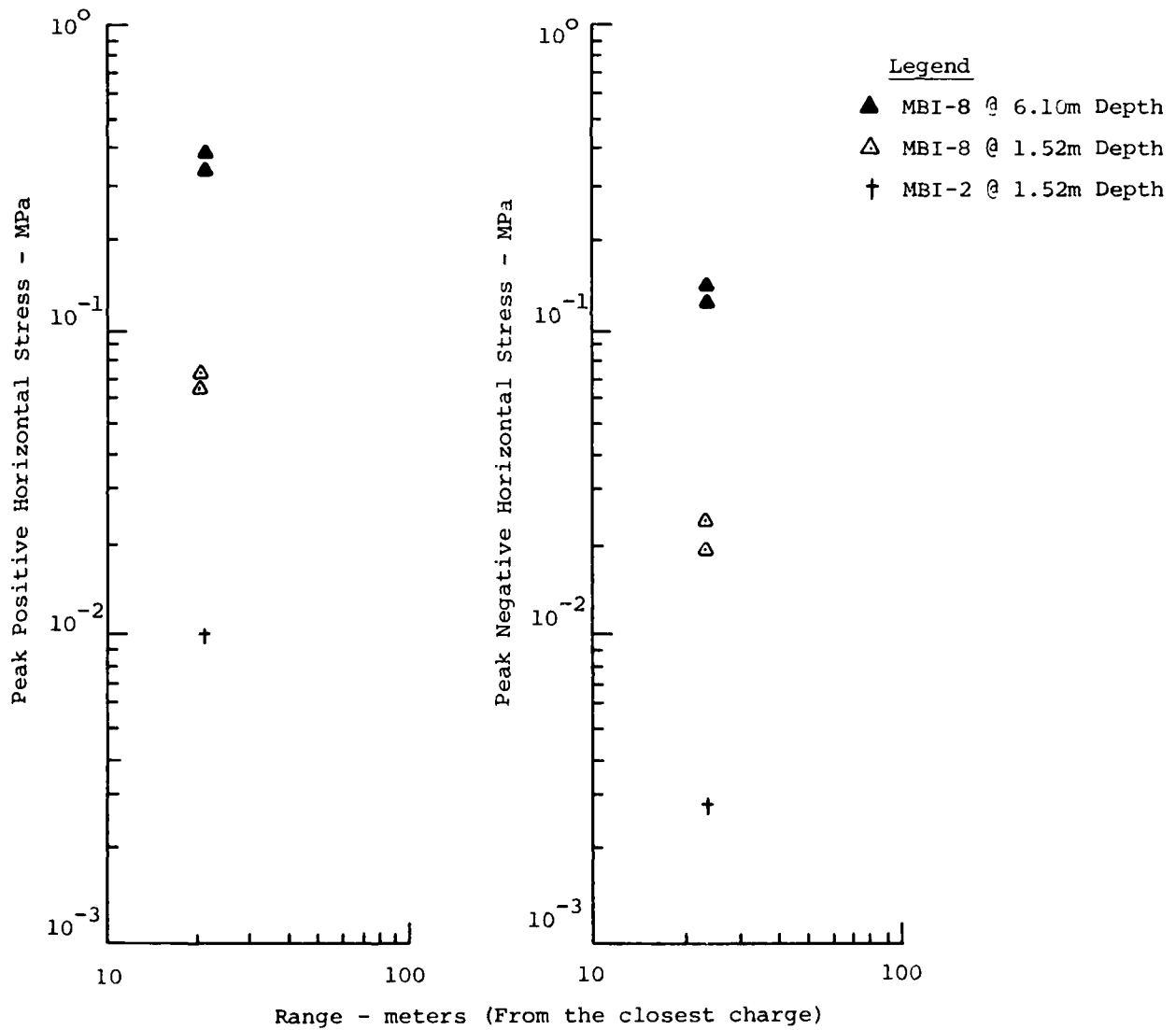


FIGURE 73: Comparison of Horizontal stress levels in the single burst and multiple burst experiments

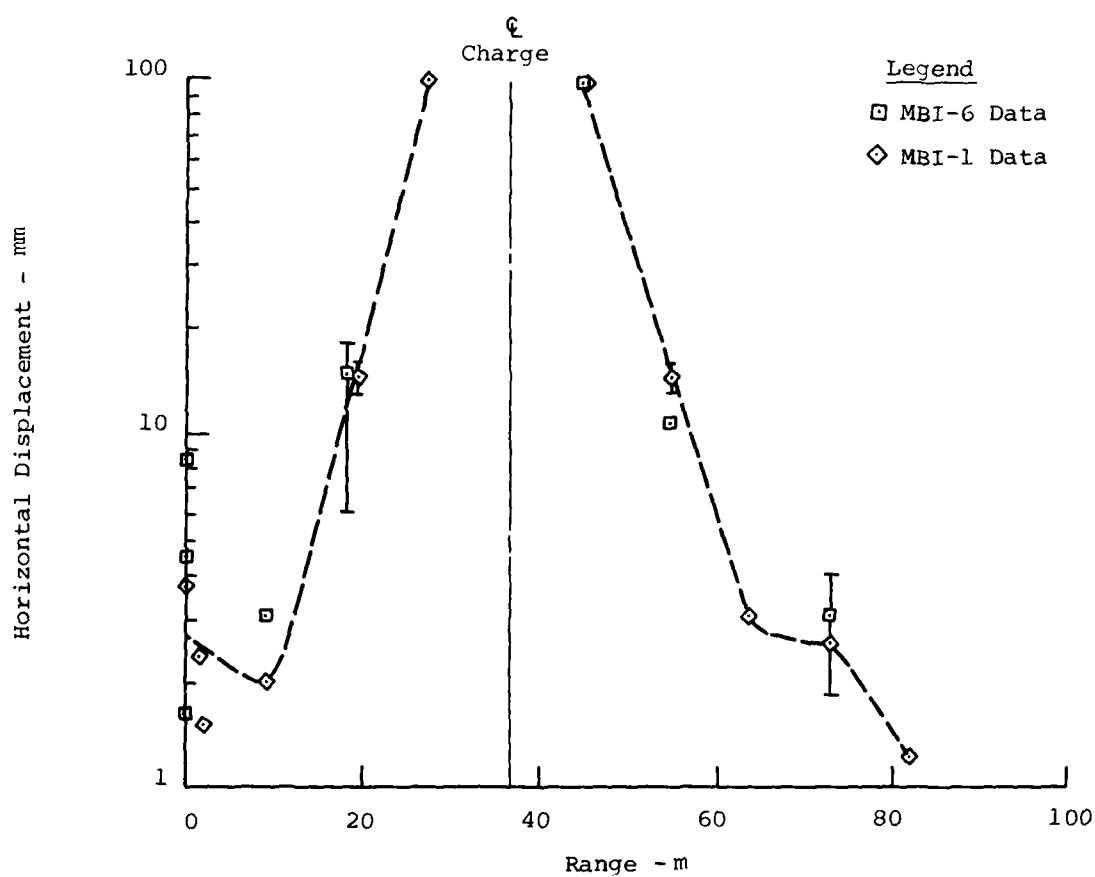


FIGURE 74: Maximum Horizontal Displacements - MBI-6

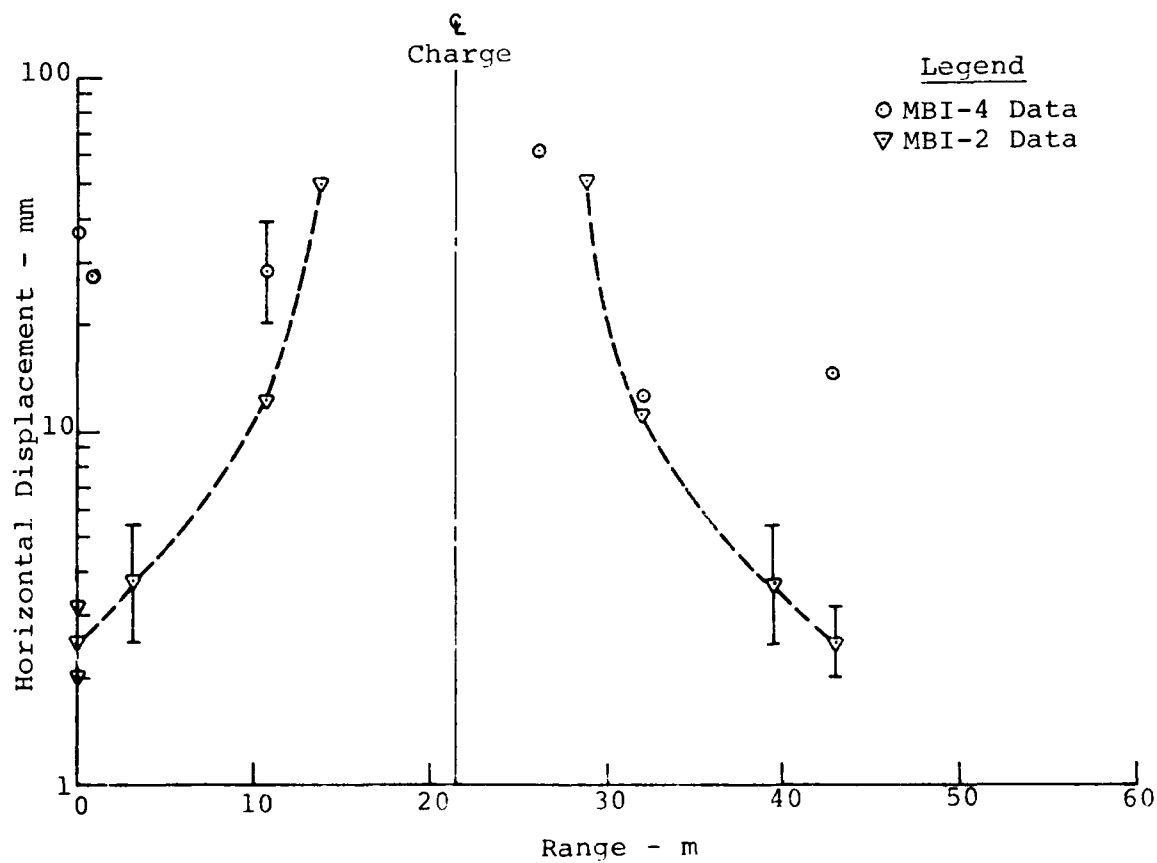


FIGURE 75: Maximum Horizontal Displacement - MBI-4

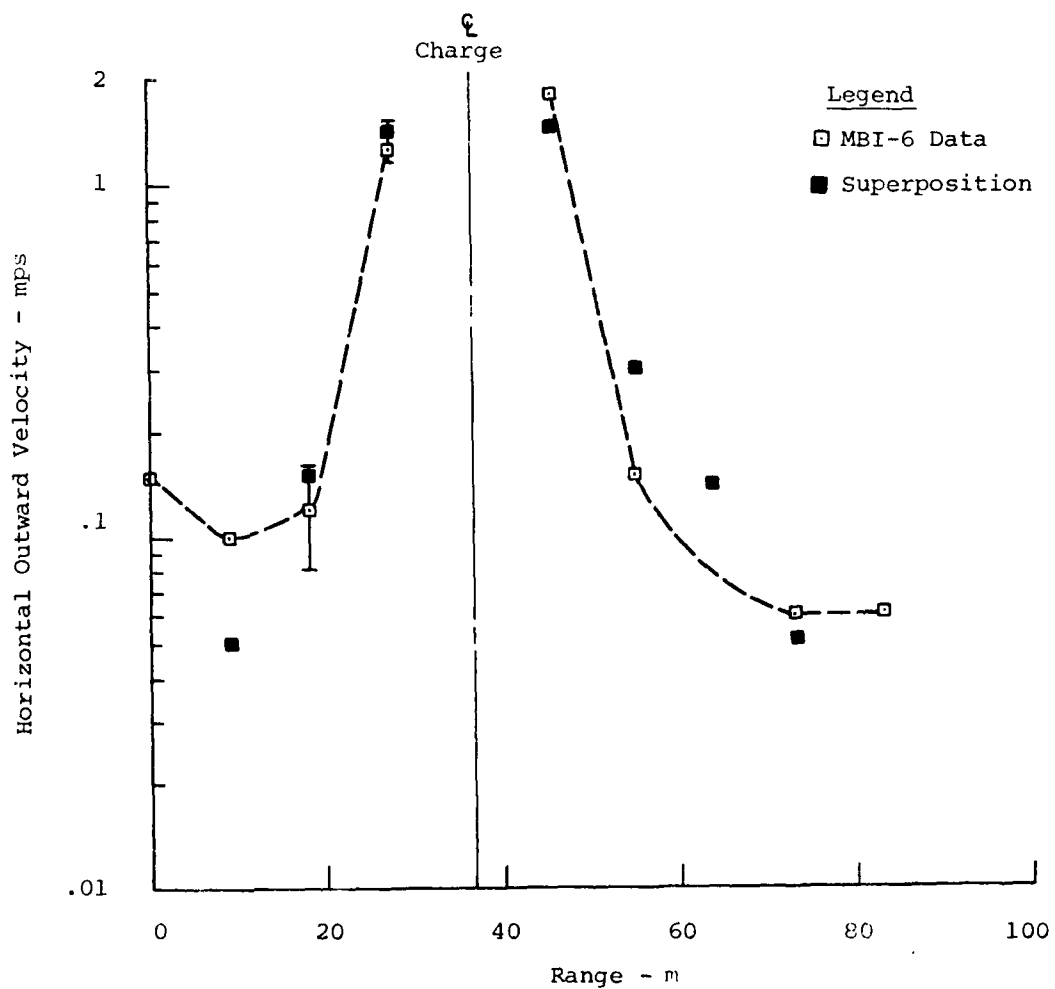


FIGURE 76: Peak Horizontal Outward Velocity - MBI-6

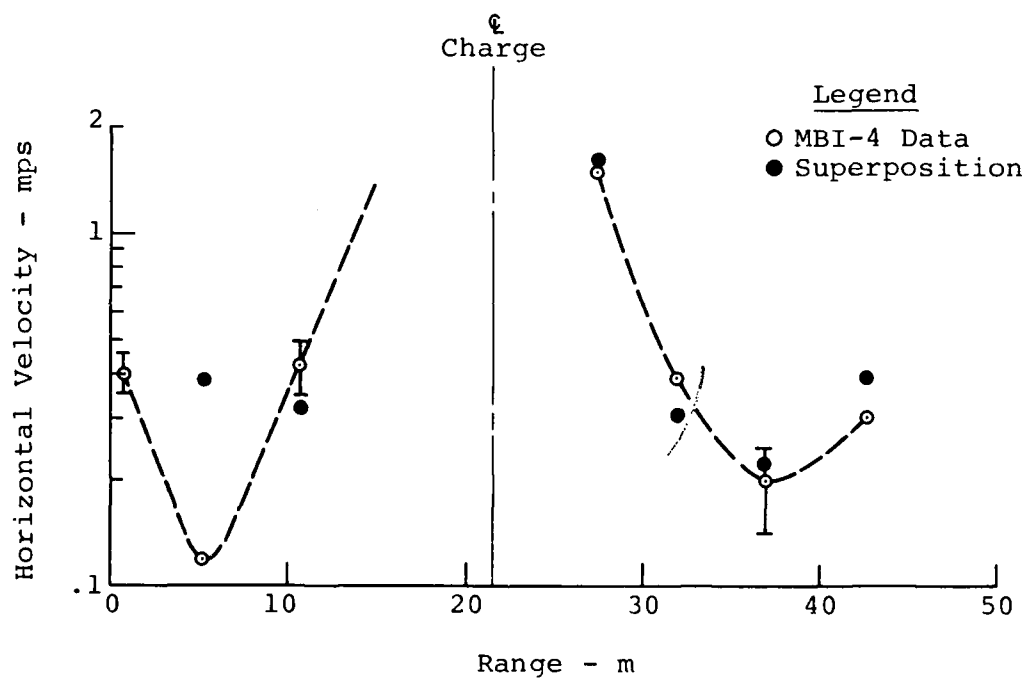


FIGURE 77: Peak Horizontal Outward Velocity - MBI-4

One of the major shortcomings of this theory is the timing aspect of the signal. In general for the theory to hold it should propagate upward and inward toward the center. In looking at the signal on the MBI-4 data the propagation appears to be downward rather than upward at all three locations. Although the motion is propagating inward toward the center at the .46 m depth it appears that at the 1.52 m depth the propagation is in the opposite direction. The MBI-6 data indicates propagation to be outward for both depths mentioned above.

#### c) Comments

Of the theories discussed above, it appears that the negative phase of the air pressure is more important for these experiments than the cylindrical convergence. However, in the nuclear case the air pressures may be less negative (due to the large difference in the mass of the explosive products) and this might well reverse the relative importance of the two effects. In addition, the pore air effect will remain a near surface effect (limited to a - 1 tour) while the wave convergence effects may scale.

#### 4.4 Stress Measurements

Stress measurements for the multiple burst experiments were quite limited, and quality of the data taken was generally poor. However, some observations may be made concerning the stress levels.

Only two vertical stress measurements were made on these experiments. These were at the 1/2 charge spacing location on MBI-4 and MBI-6. The recorded waveforms from these multiple burst experiments are compared with the appropriate single burst waveform in Figure 78. The character of the single and multiple burst waveforms are similar and the stress levels are not much different in the comparison mode for MBI-4 and MBI-2. However, the magnitude of the waveform recorded in MBI-6 is much lower than the MBI-1 waveform and, therefore, of questionable validity.

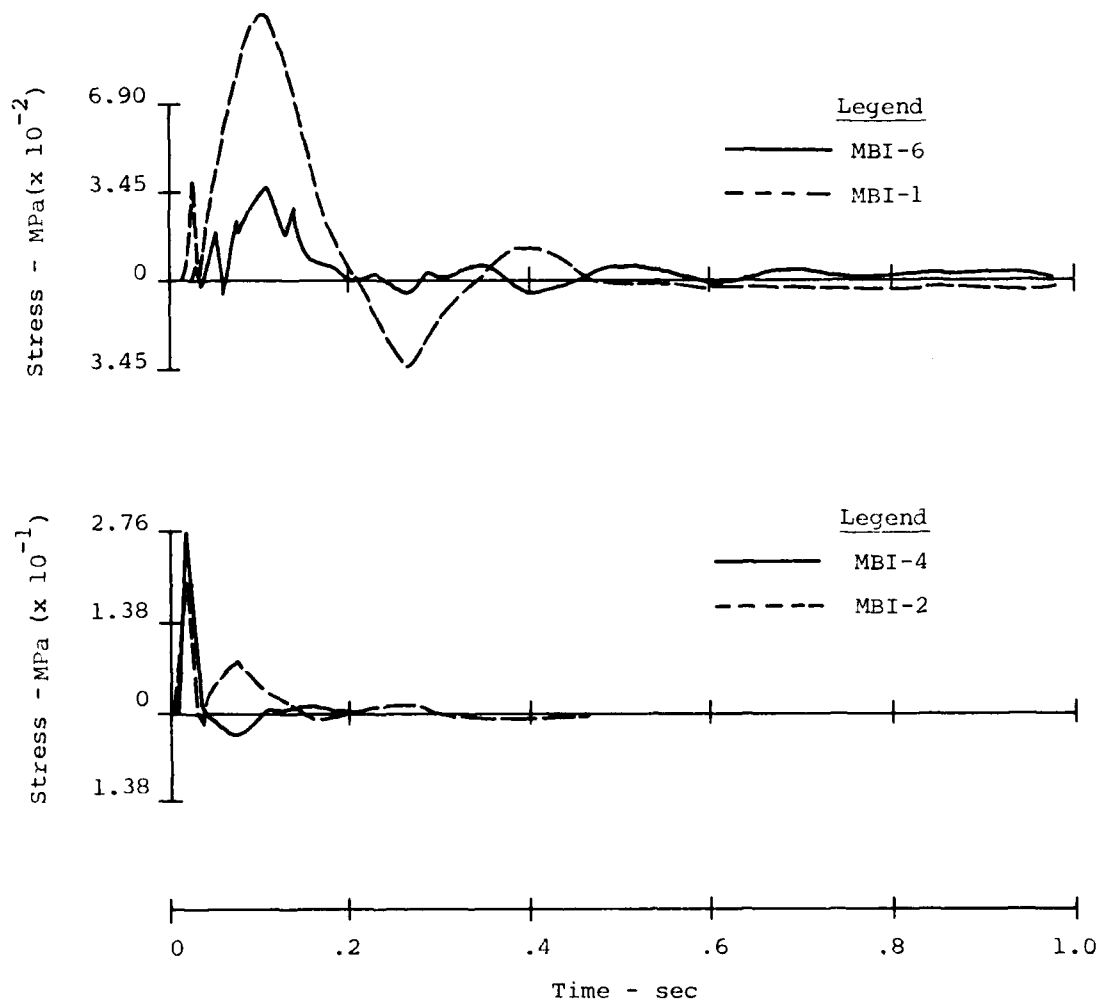


FIGURE 78: Comparison of Single Burst and Multiple Burst Vertical stress waveforms on MBI-4 and MBI-6

Horizontal stress measurements were made on MBI-4, MBI-6, and MBI-8. The peak positive and negative stress values recorded are shown on Figure 79. (The appropriate single burst measurements are shown also.) Again the data is at 1/2 the charge spacing on MBI-4 and MBI-6. The differences between the stress levels in the multiple burst environment and the single burst environment are not great. The horizontal stress measurement for MBI-8 was at the center of one of the outside arrays. The differences in the single burst stress level and the multiple burst stress level at this location are sizeable and were discussed in Section 4.3.3.

#### 4.5 Measurements in the Horizontal Plane

In studying the multiple burst experiments it became obvious that the horizontal (radial) and transverse measurements were yielding similar peak values and exhibiting approximately the same amount of scatter. Due to these observations these data were analyzed together.

Figure 80 presents the horizontal and transverse data measured at comparable locations in the three experiments. The locations were "normalized" by the charge spacing (e.g., center points are plotted at  $R/C_s = 1$ ). Generally, the scatter for the transverse measurements is about the same as the horizontal measurements. This is apparently true for all three experiments. This figure also indicates the velocity measured by these gages is approximately the same in the two directions of measurement. Another observation is that there is very little attenuation in these motions as the range approaches the charge spacing (i.e., inside the array). As the range becomes greater than the charge spacing there is a more "normal" type of attenuation taking place.

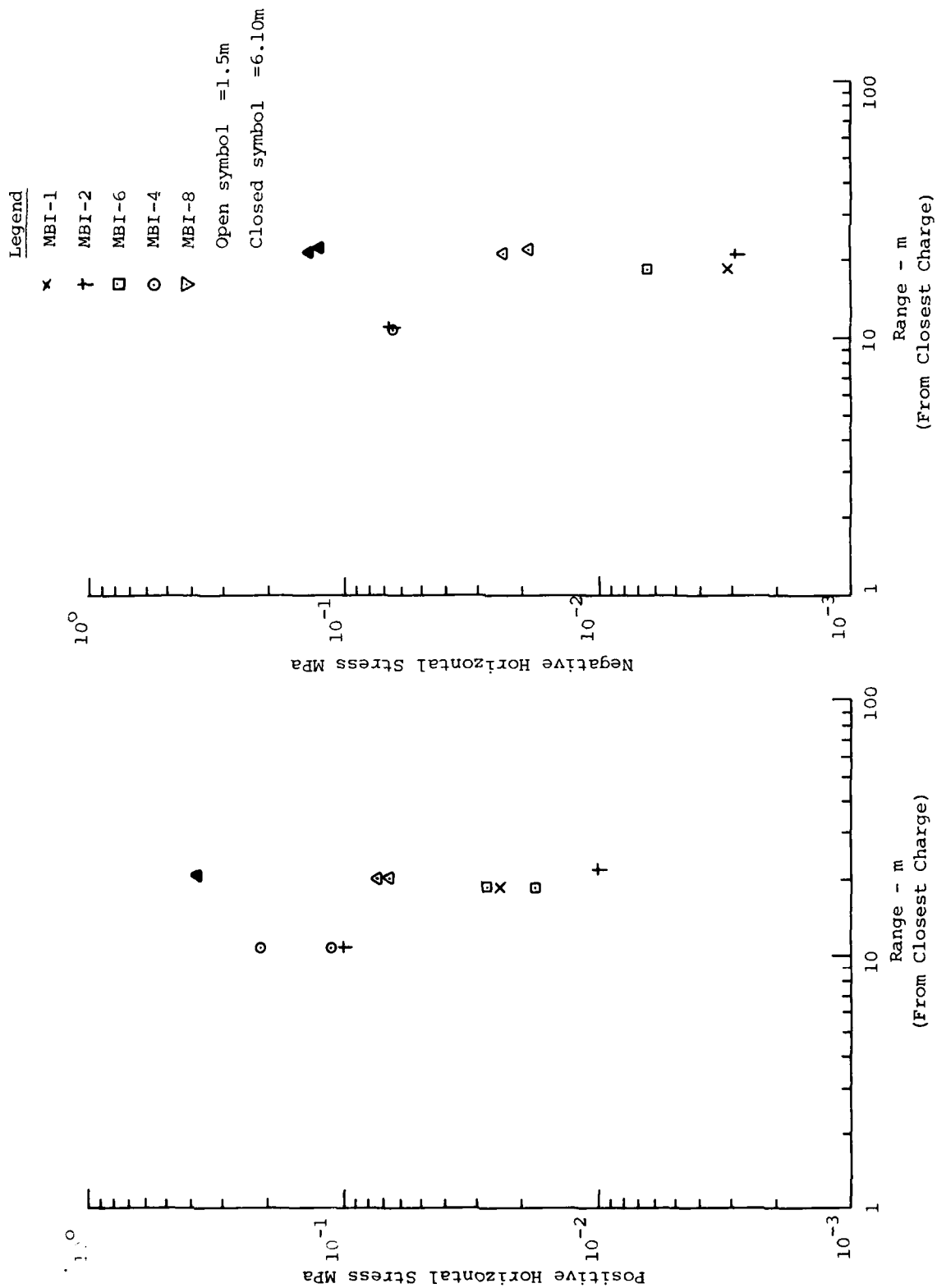


FIGURE 79: Peak Positive and Negative Horizontal Stresses  
Measured in the Multiple Burst Experiments

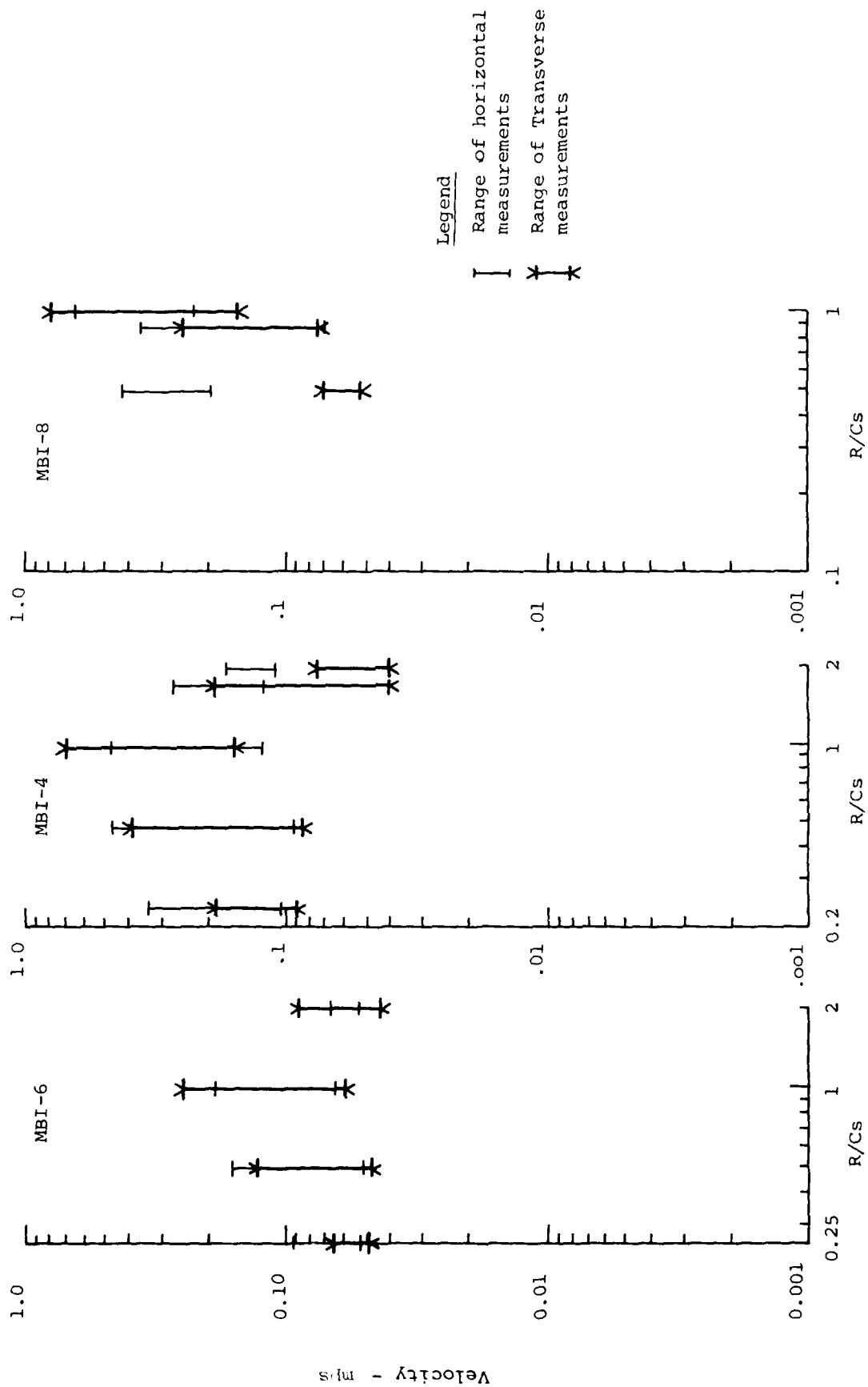


FIGURE 80: Comparison of Horizontal and Transverse measurements for Phase I

The behavior with depth of the transverse and horizontal motions at the center of the charge arrays are shown in Figures 81 and 82. Theoretically, these gages should measure zero velocity, as all horizontal motions at the exact center should cancel. This is obviously not the case and is due in part to the nonhomogeneity and anisotropy of the site. Another contributing factor was that all the desired measurements at the center of the array could not be fit into one measurement hole at the exact array center. The gages that could not be placed at the exact center were placed at 0.915 m away from the center. This eccentricity in the gage placement would have a tendency to enhance these measured horizontal motions. The actual behavior of these gages is not unlike those mentioned above. That is, in magnitude the two measurements are similar and the amount of scatter is about the same. Also, the attenuation rates with depth are all approximately equal for both transverse and horizontal measurements for all three experiments.

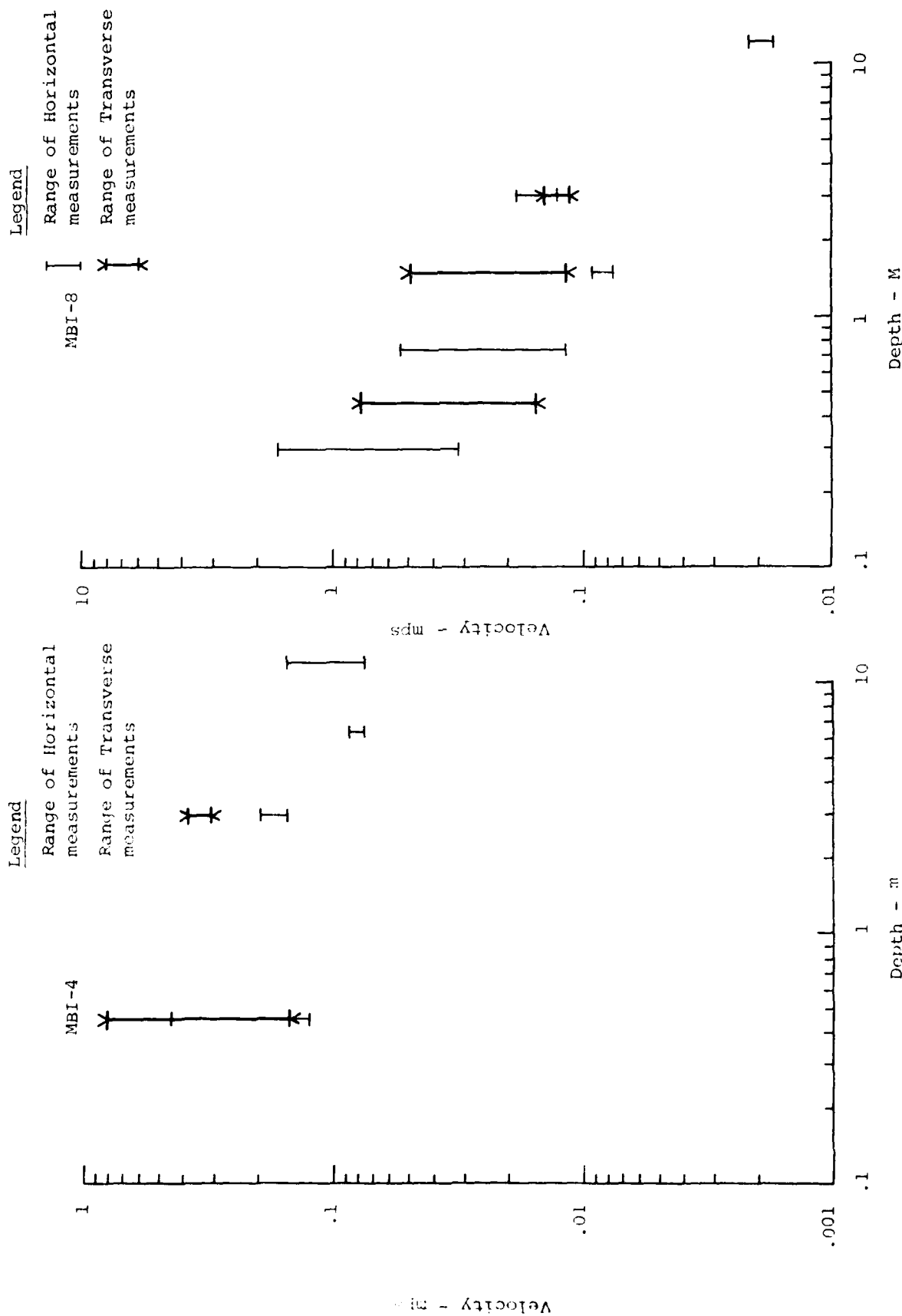


FIGURE 81: Comparison of Horizontal and Transverse measurements for MBI-4 and MBI-8 at the center of the array

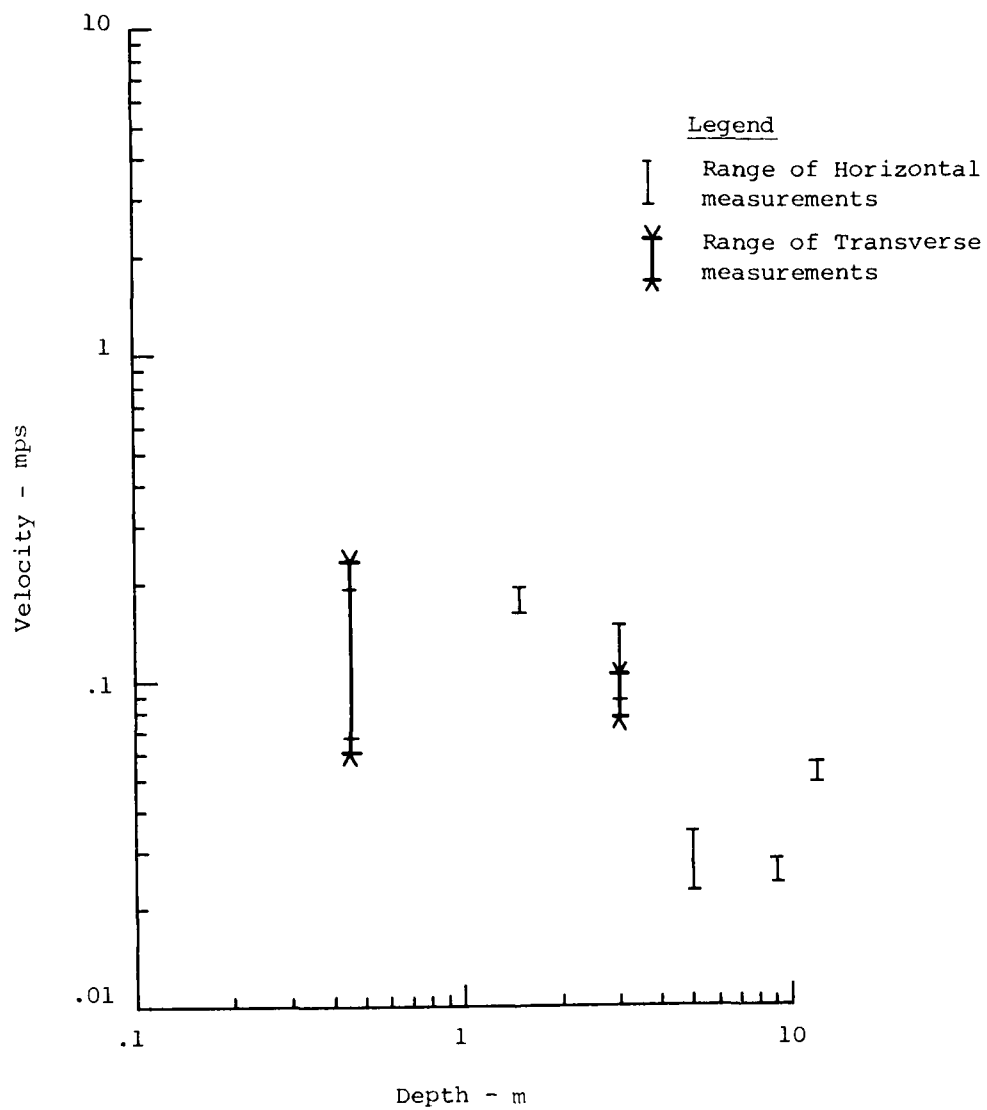


FIGURE 82: Comparison of Horizontal and Transverse measurements for MBI-6 at the center of the array

5.

## CONCLUSIONS AND RECOMMENDATIONS

From the previous discussions it is obvious that our understanding of the multiple burst environment is far from complete. However, our understanding has improved as a result of these experiments.

One of the main objectives of the Phase I multiple burst experiments was to determine the regions in which the superposition assumption is valid. From the study of the data the following conclusions about the superposition assumption were drawn:

- a) Superposition is satisfactory at all locations and depths investigated outside the charge array;
- b) All depths below the phreatic surface are adequately described by superposition;
- c) At the near surface gage locations inside the array and at ranges greater than  $1/2$  the charge spacing, superposition is not as accurate as at the previous locations, but shows a definite trend of improvement with increasing distance from the array center.
- d) Failure of superposition occurs at all gage locations above the phreatic surface within a circle having a radius of  $1/2$  the charge spacing centered at the array center.

The two theories discussed in Section 5.3 were attempts to explain the failure of superposition, but it is doubtful that either of these theories alone explain this failure.

Another objective, was the development of a procedure to predict the multiple burst environment in a more general sense. For this reason the procedures exercised in Misers Bluff Phase I will be used in Phase II. In analyzing the Phase I data it was obvious that the empirical prediction procedures were inadequate in the region where superposition failed; however, they were generally no worse or better than superposition for

most of these locations. The current prediction procedure could be modified empirically to produce results consistent with the Phase I Misers Bluff experiments in the region where superposition fails. However, this empirical "fix" would lead to results of low confidence when the procedure was applied to the nuclear case. The analysis of the data from Phase II of Misers Bluff will broaden the data base and hopefully help in generalizing the prediction procedure.

In the conduct of Phase I areas which totally lack understanding become obvious. These are the areas which hold the key to a complete understanding of the multiple burst phenomena. Therefore, it is recommended that the following areas be studied in detail:

- Horizontal Motions: As was obvious from the waveform comparisons presented in 4.2, the current empirical prediction procedures do not adequately treat the horizontal air slap phenomena. It is felt that a complete study of this is necessary if the multiple burst environment (or single burst for that matter) is to be completely specified.

- Spall or dilation: This effect is playing an important role in the behavior of the near surface materials and additional study of the phenomenon is required.

- Failure of Superposition: The airblast negative phase seems to dominate the Misers Bluff data and may be masking other mechanisms that contribute to the failure of superposition. An experimental program is needed to address the relative importance of the two theories presented in Section 4.3.

## REFERENCES

1. Bratton, J.L., The Effect of Subsurface Layers on the Simulation of Shock Waves in the Ground, Fourth International Symposium on the Military Application of Blast Simulation, AWRE, Foulness, September 1974.
2. The Data Analysis Working Group, A Review of High Explosive Testing to Investigate Ground Motions Pertinent to the MX Multiple Aimpoint Systems, DAWG-TR-1, May 13, 1977
3. Phillips, J.S. and Bratton, J.L., Misers Bluff Phase I: Single Burst Experiments: Ground Shock Analysis, Defense Nuclear Agency, To Be Published.
4. Benson, K. and Babcock, S., Quick Look Report for MBI-4, Air Force Weapons Laboratory, October 1977.
5. Benson, K. and Babcock, S., Quick Look Report for MBI-6, Air Force Weapons Laboratory, November 1977.
6. Murrel, D.W., Misers Bluff Series; Phase I, Ground Shock and Airblast Measurements Data Report, June 1978, U.S. Army Engineer Waterways Experiment Station, Misc. Paper N-78-4
7. Hurdle, P.M. and Port, R.J., MX Multiburst Ground Motion Study, RDA-TR-104806-007, October 1977
8. Higgins, C.J. and Schreyer, H.L., An Analysis of Out-running Ground Motion, AFWL-TR-74-220, Air Force Weapons Laboratory, May 1975
9. Ullrich, G.W., "Airblast/Ground Motion Effects from Simultaneous Detonation of High Explosive Charges," Nuclear Technology Digest, Vol. 1, Air Force Weapons Laboratory, 1978
10. Crawford, R.E., Higgins, C.J., and Bultmann, E.H., The Air Force Manual for Design and Analysis of Hardened Structures, AFWL-TR-74-102, Air Force Weapons Laboratory, October 1974

APPENDIX A

A.1

PRECEDING PAGE BLANK-NOT FILLED



FIGURE A.1: Comparison of MBI-4 Data and Superimposed MBI-2 Data  
@ 0/1.52/0 Vertical Velocity

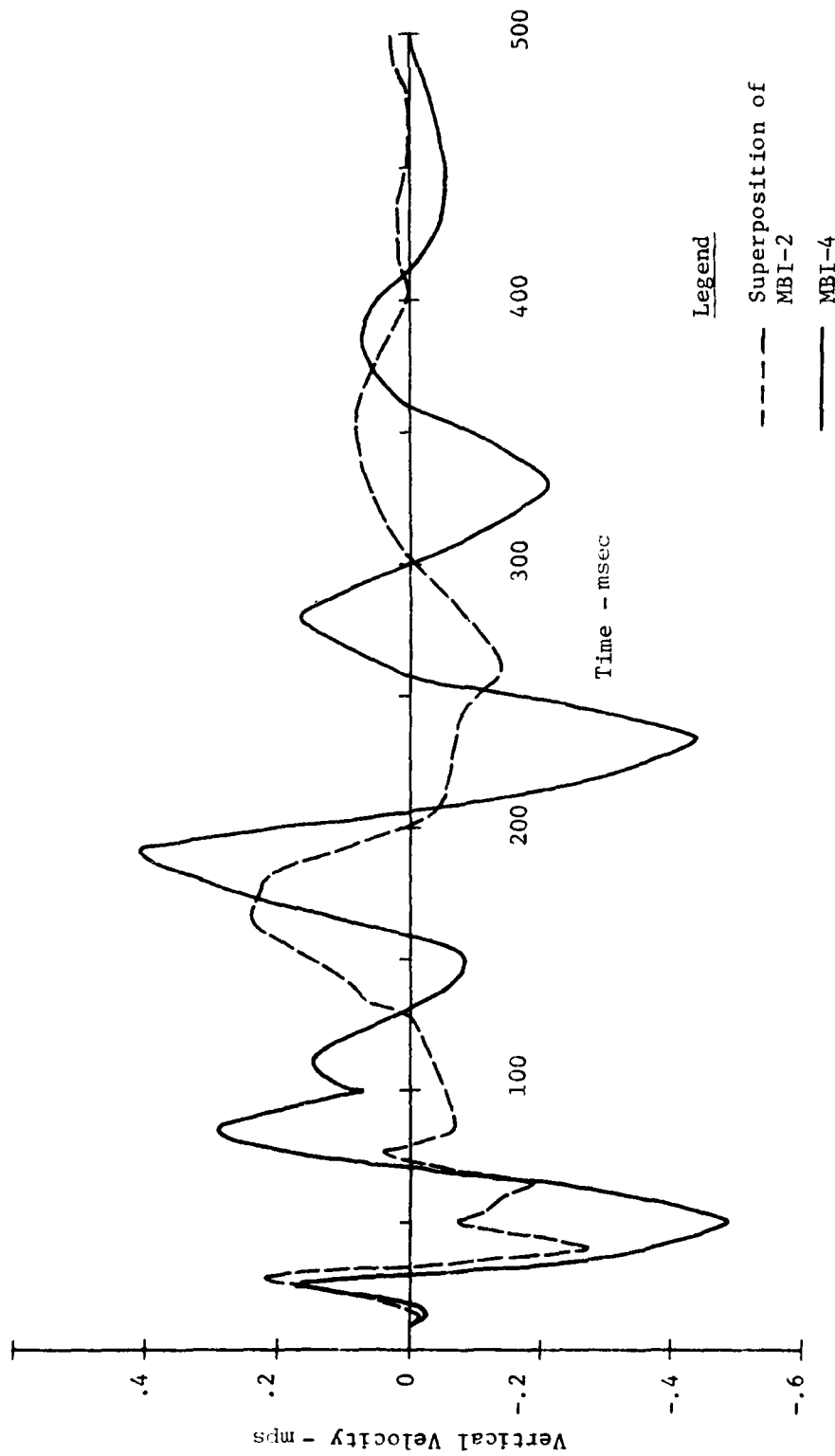


FIGURE A.2: Comparison of MBI-4 Data and Superimposed MBI-2 Data @ 0/3.05/0 Vertical Velocity

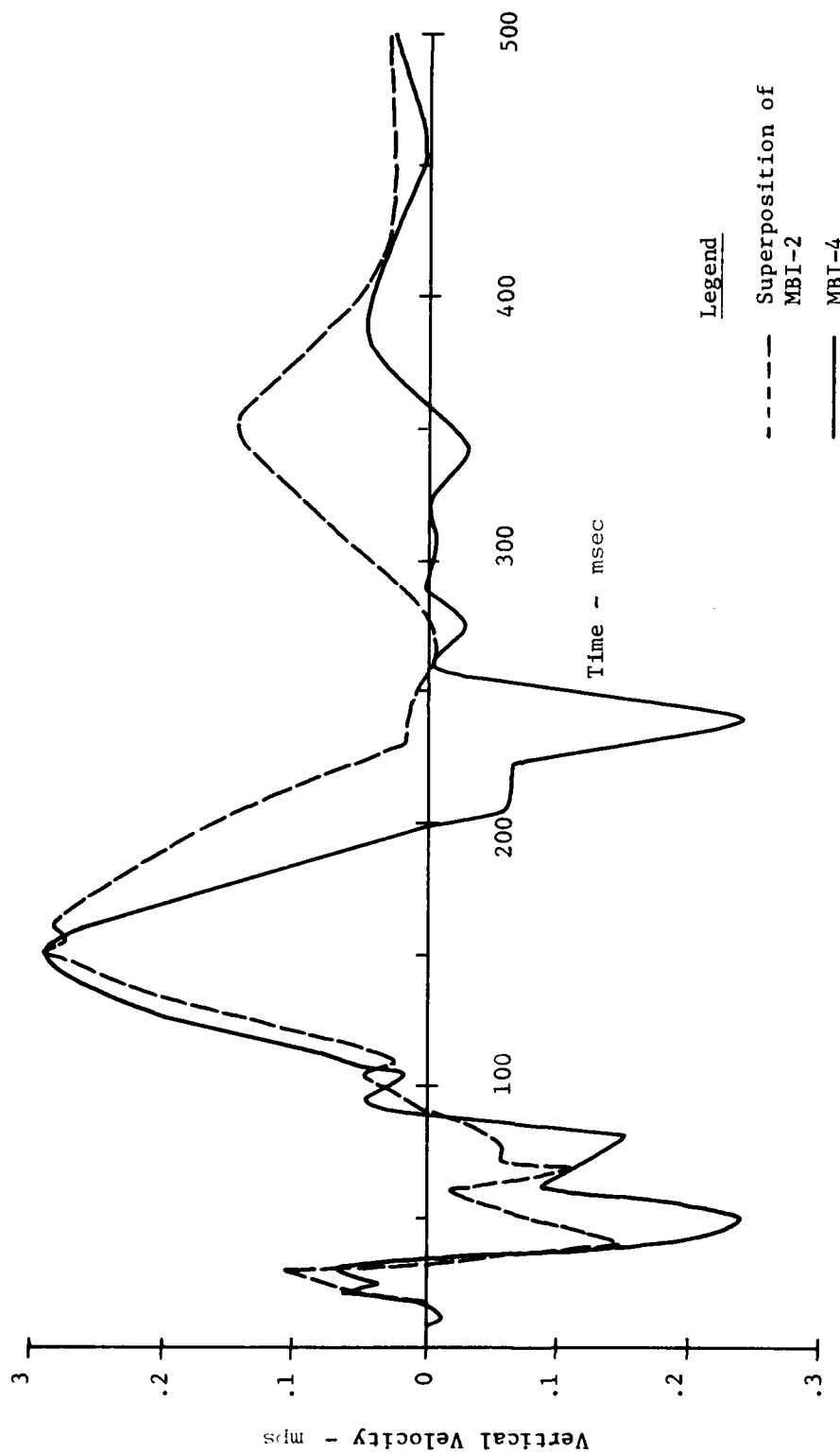


FIGURE A.3: Comparison of MBI-4 Data and Superimposed MBI-2 Data @ 0/6.10/0 Vertical Velocity

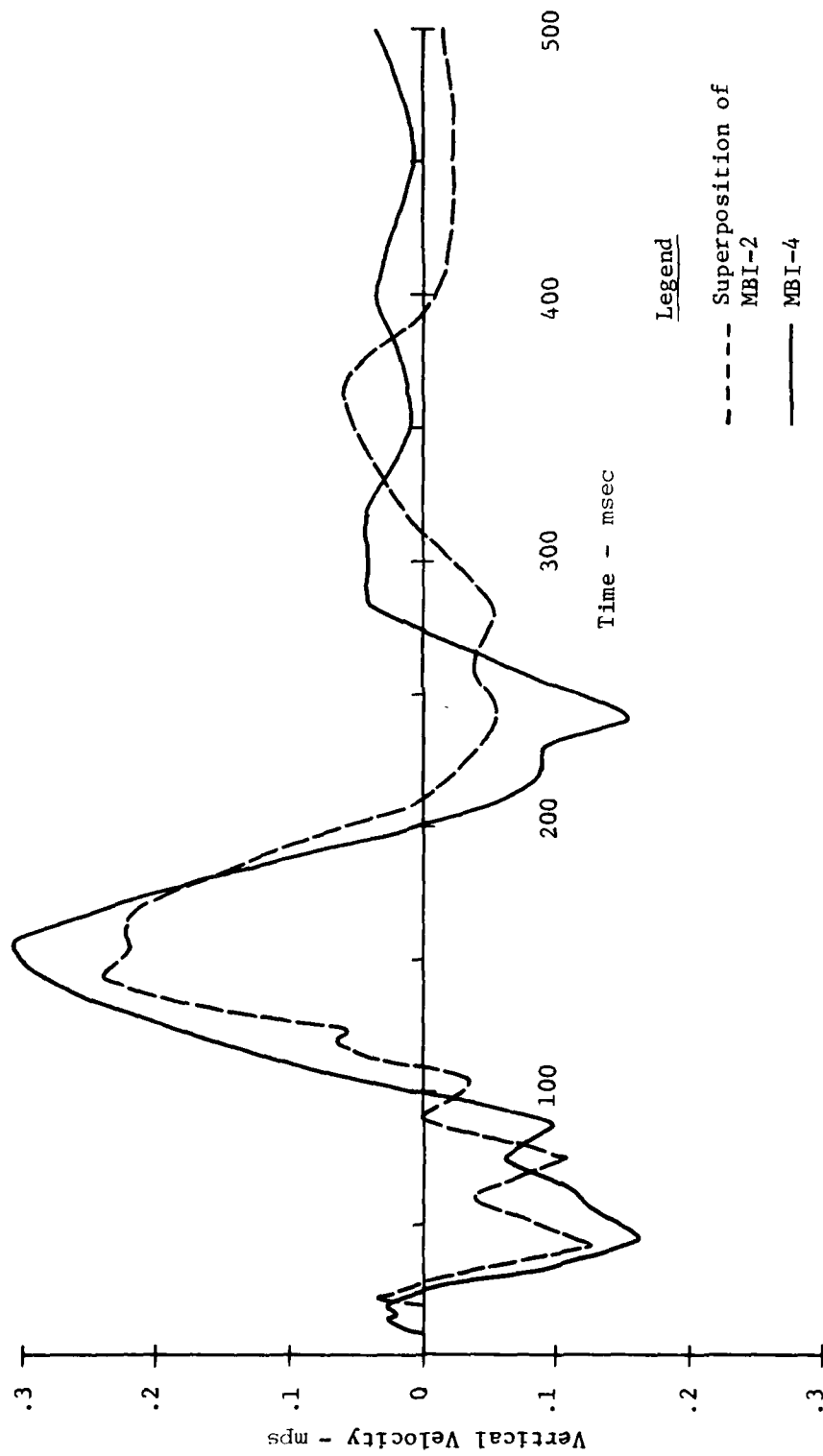


FIGURE A.4: Comparison of MBI-4 Data and Superimposed  
MBI-2 Data  
@ 0/9.15/0 Vertical Velocity

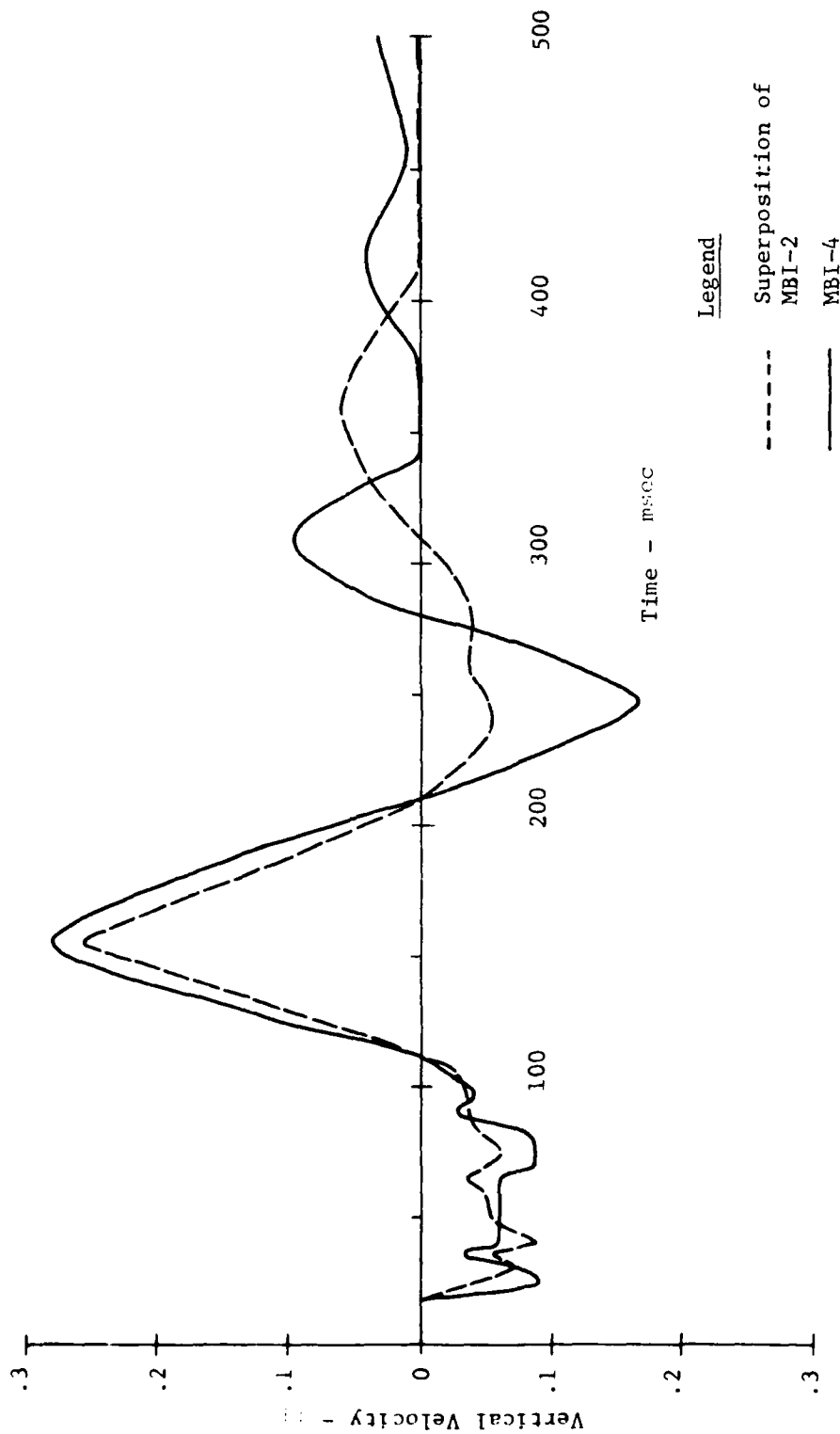


FIGURE A.5: Comparison of MBI-4 Data and Superimposed  
MBI-2 Data  
@ 0/12.20/0 Vertical Velocity

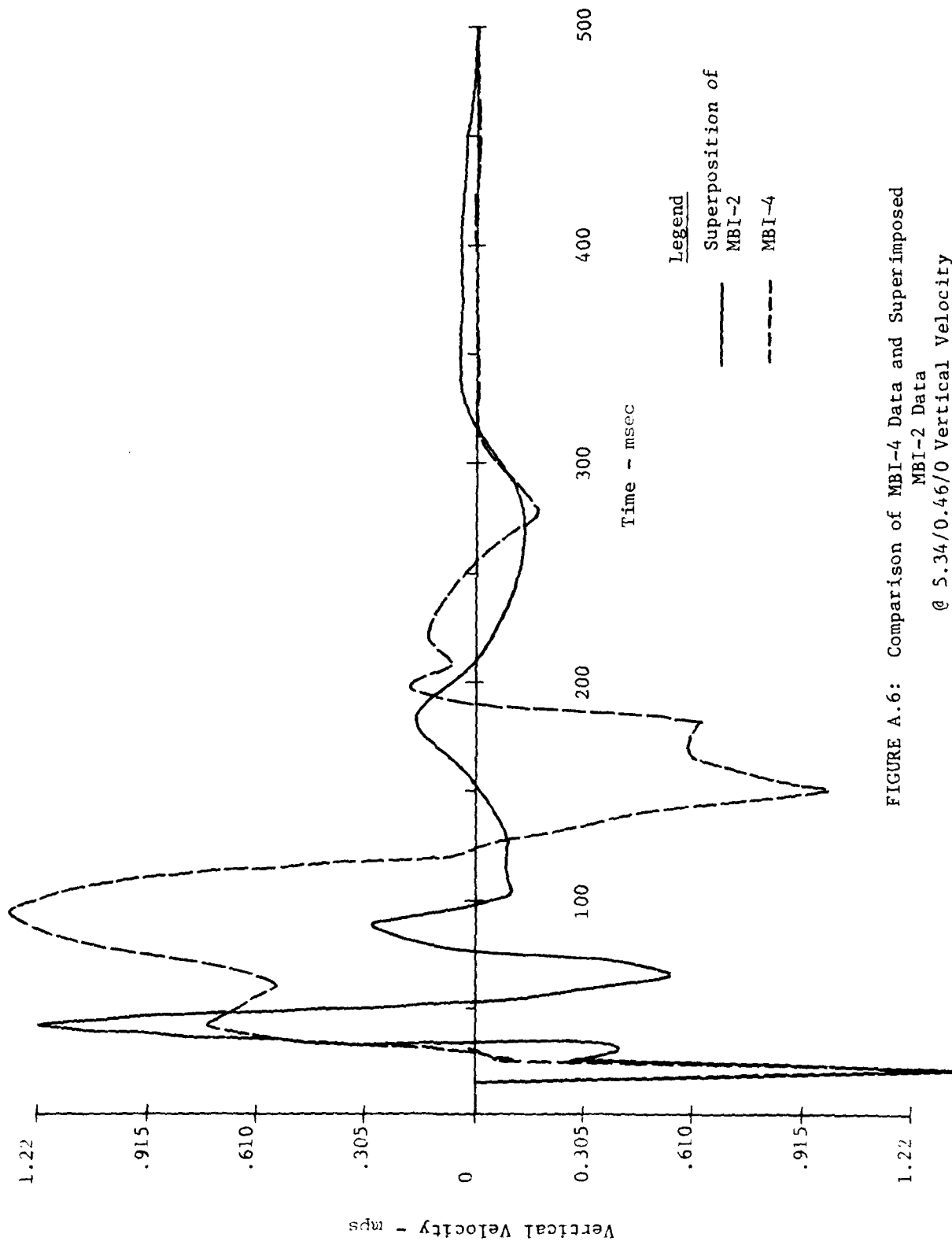


FIGURE A.6: Comparison of MBI-4 Data and Superimposed MBI-2 Data @ 5.34/0.46/0 Vertical Velocity

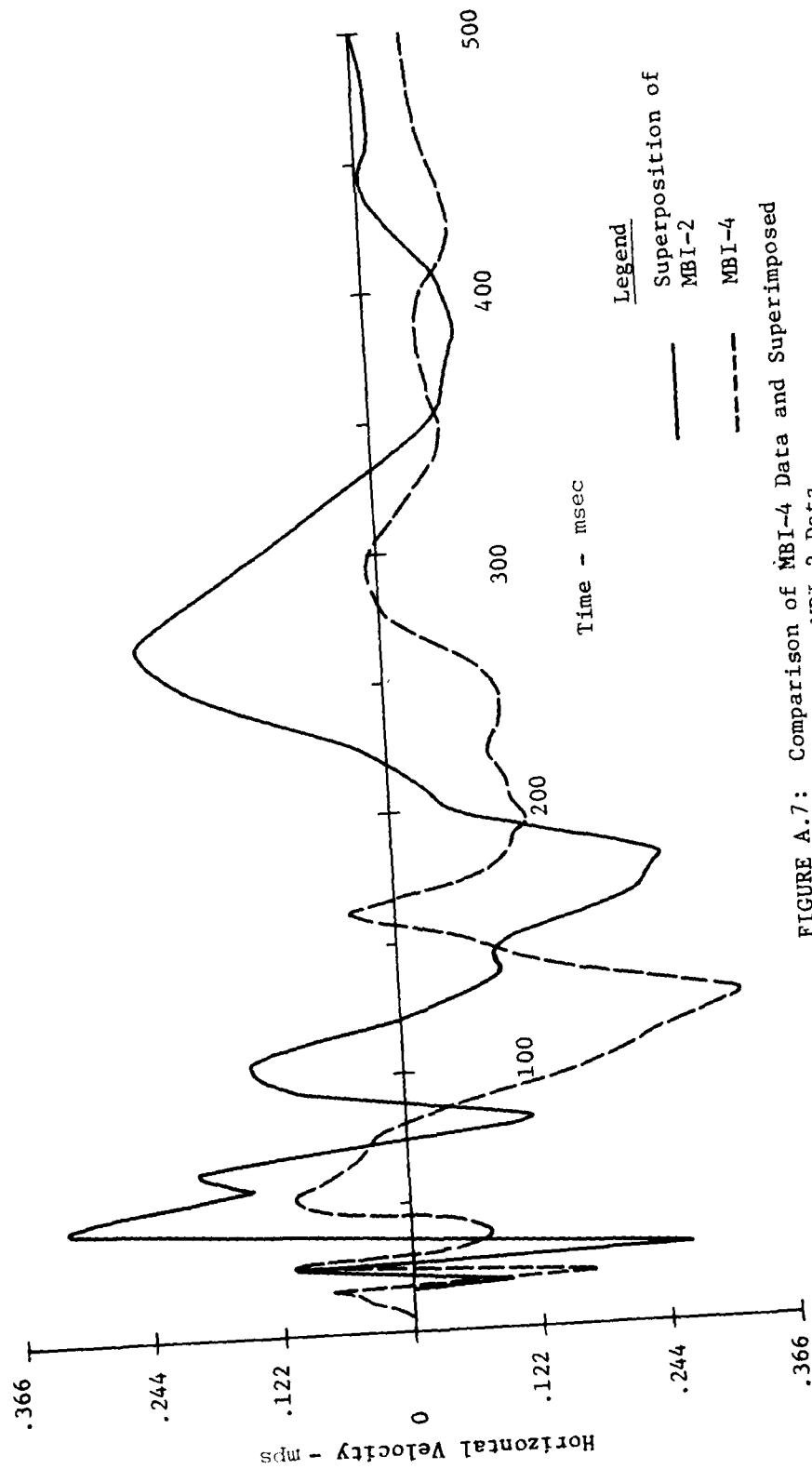


FIGURE A.7: Comparison of MBI-4 Data and Superimposed  
MBI-2 Data  
@ 5.34/0.46/0 Horizontal Velocity

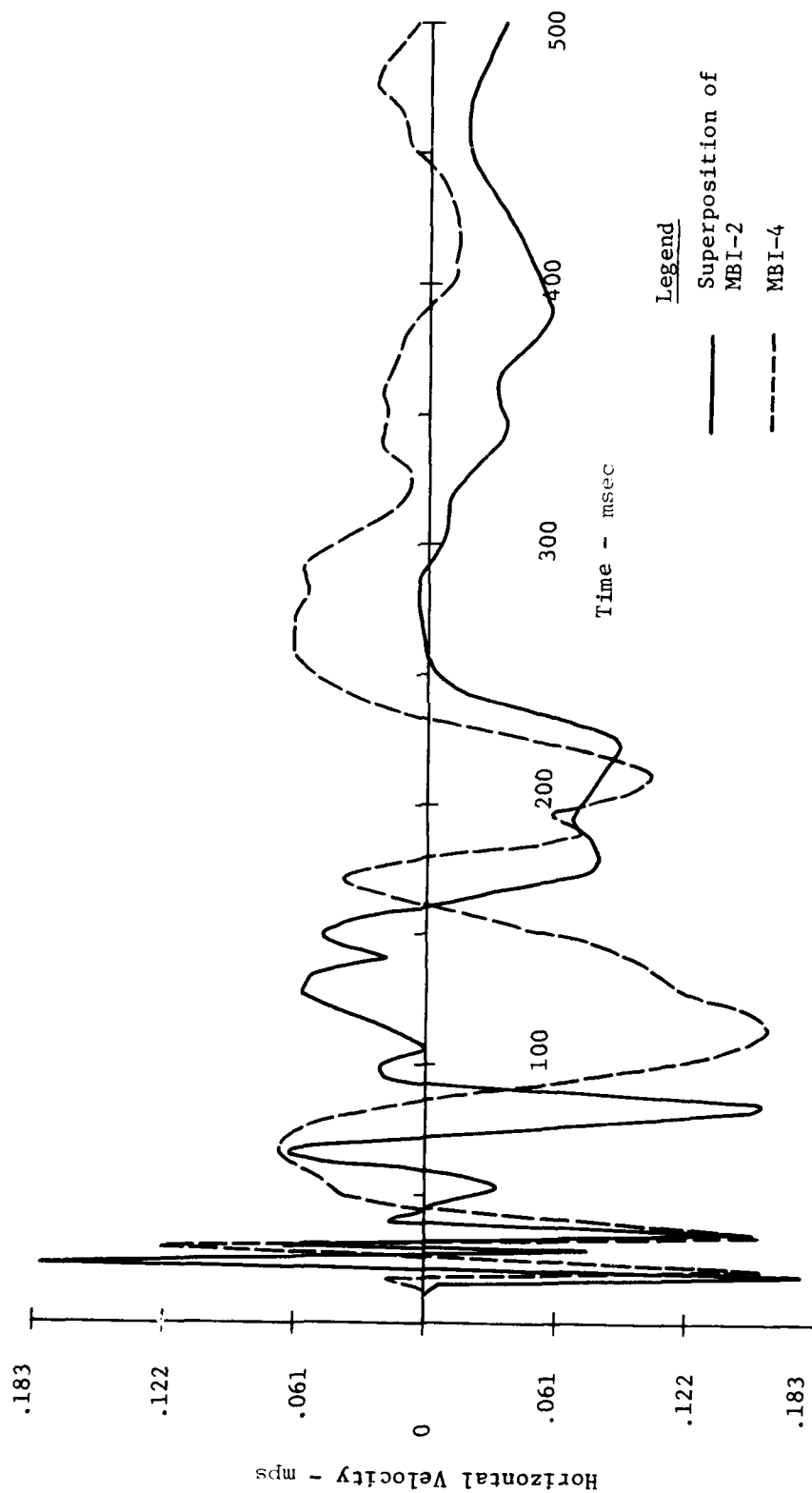


FIGURE A.8: Comparison of MBI-4 Data and Superimposed MBI-2 Data  
@ 5.34/0.46/270 Horizontal Velocity

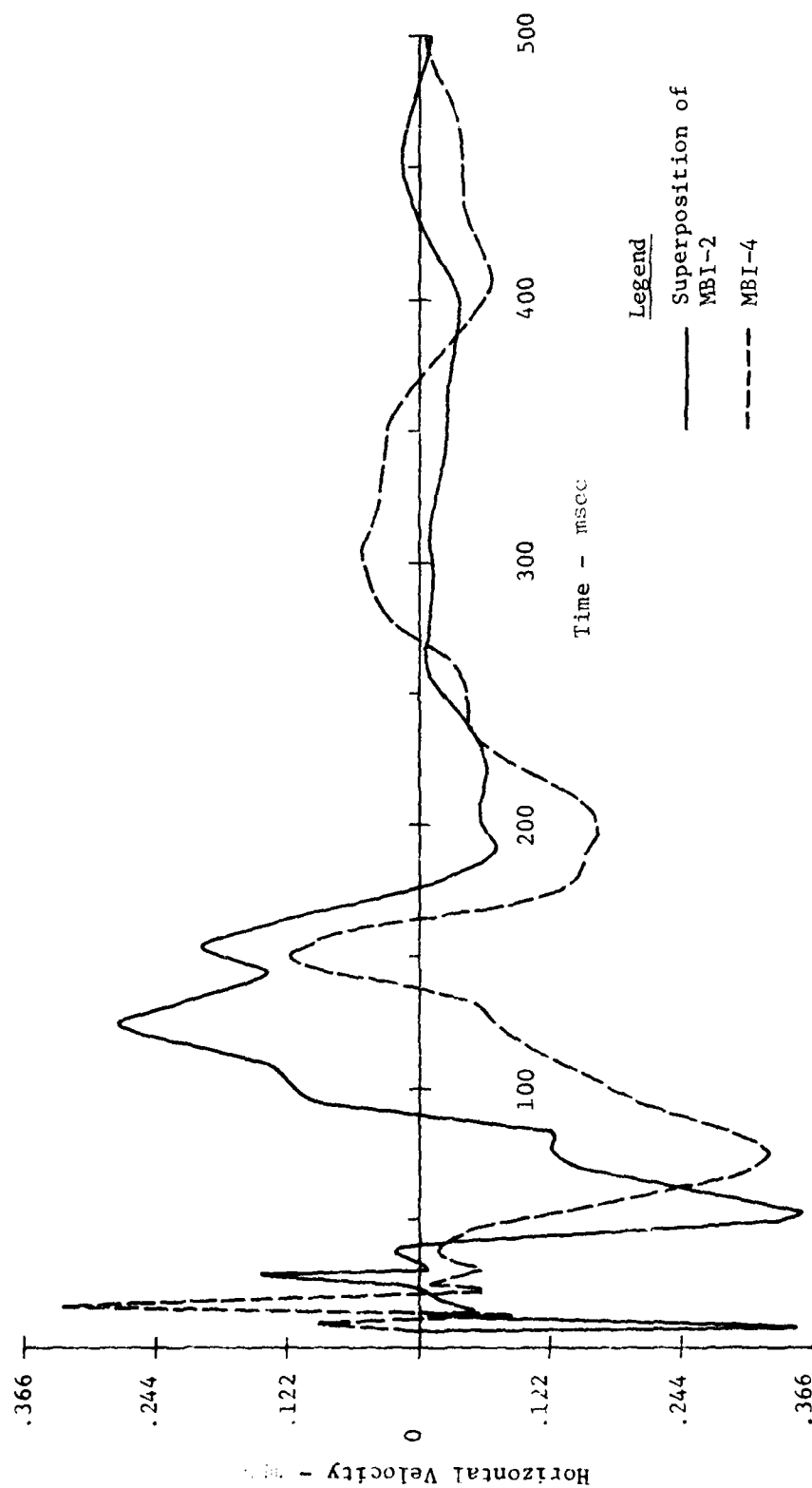


FIGURE A.9: Comparison of MBI-4 Data and Superimposed MBI-2 Data @ 10.68/0.46/270 Horizontal Velocity

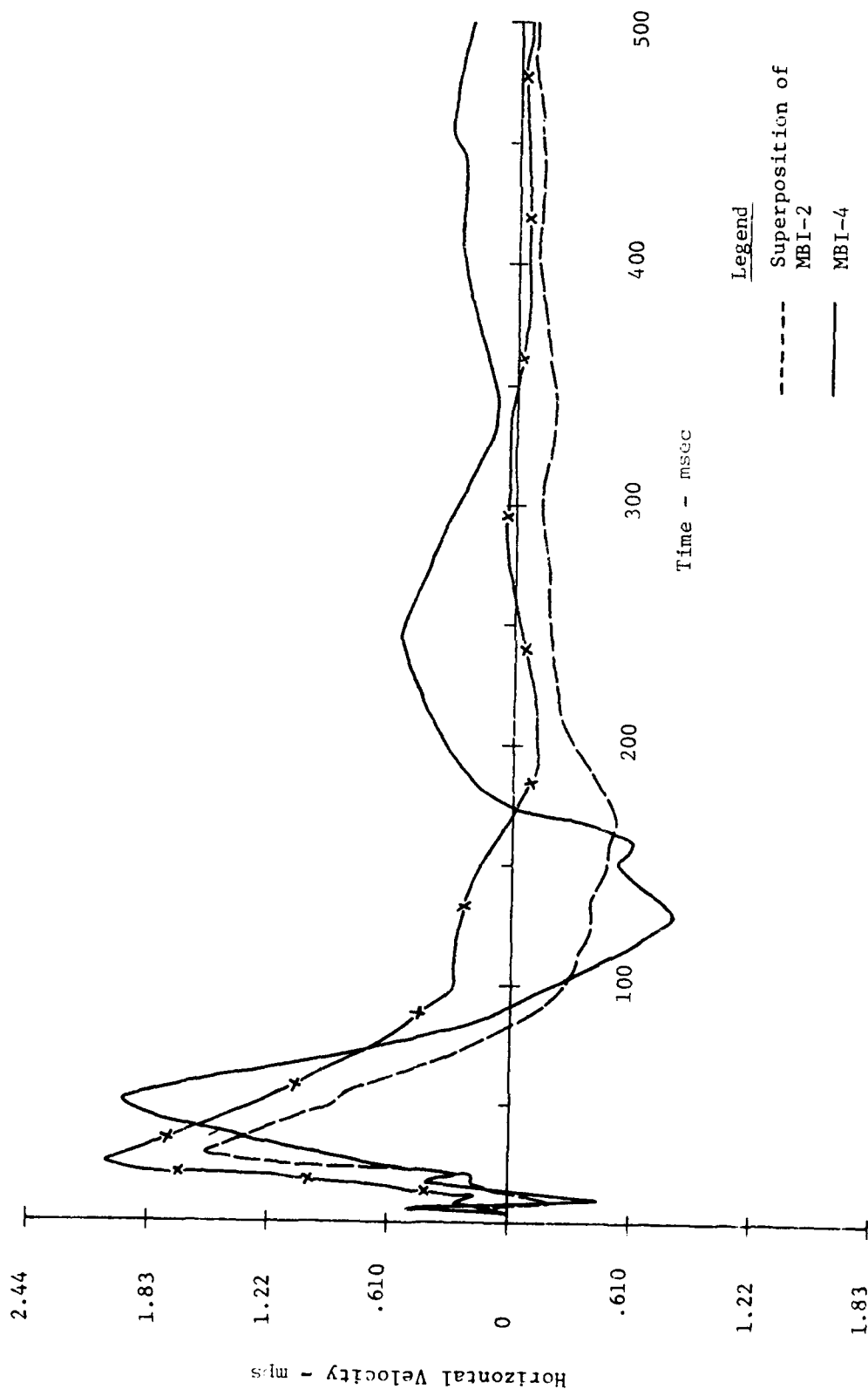


FIGURE A.10: Comparison of MBI-4 Data and Superimposed MBI-2 Data @ 19.22/0.46/254 Horizontal Velocity

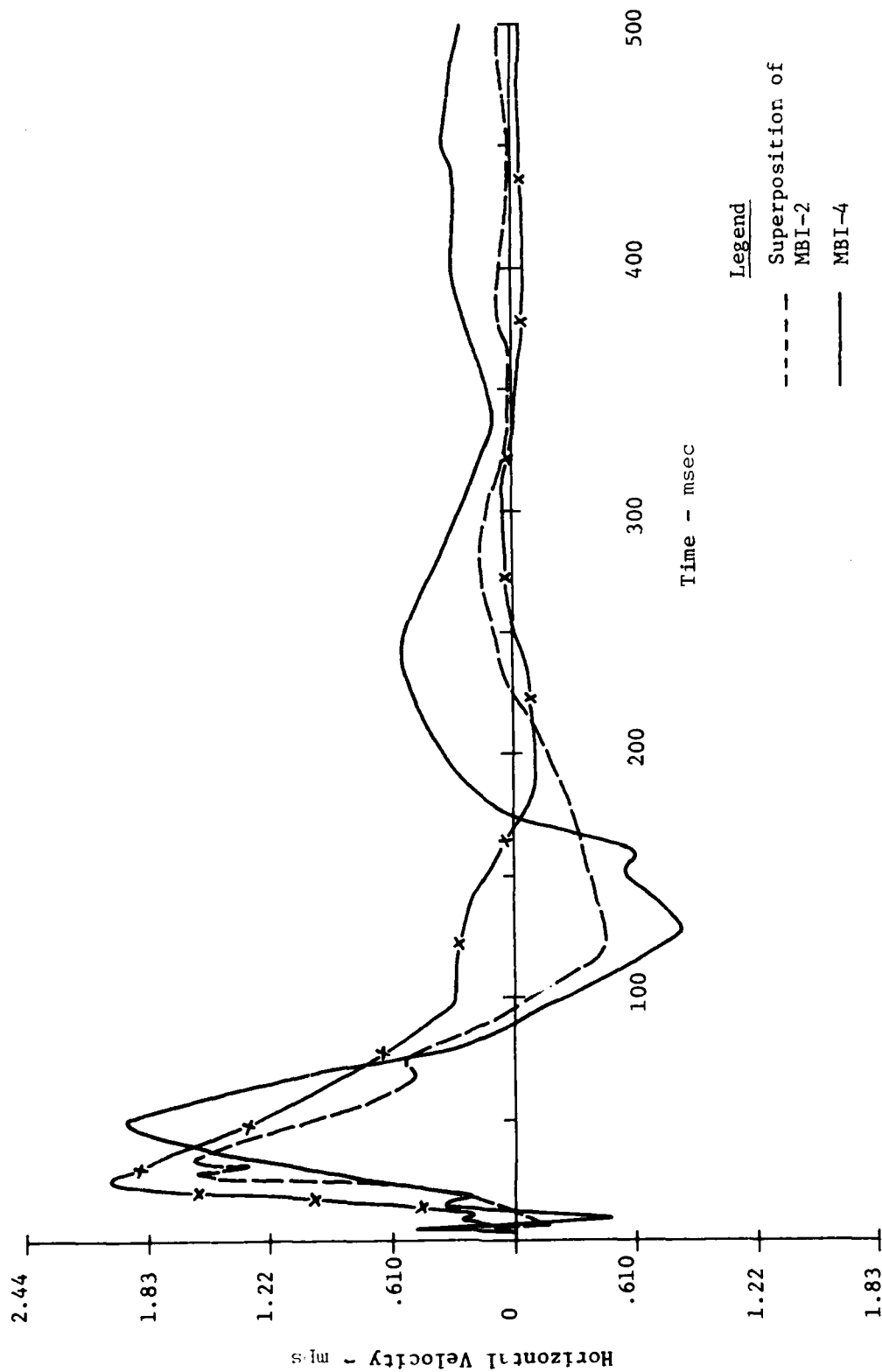


FIGURE A.11: Comparison of MBI-4 Data and Superimposed MBI-2 Data  
@ 26.69/0.46/0 Horizontal Velocity

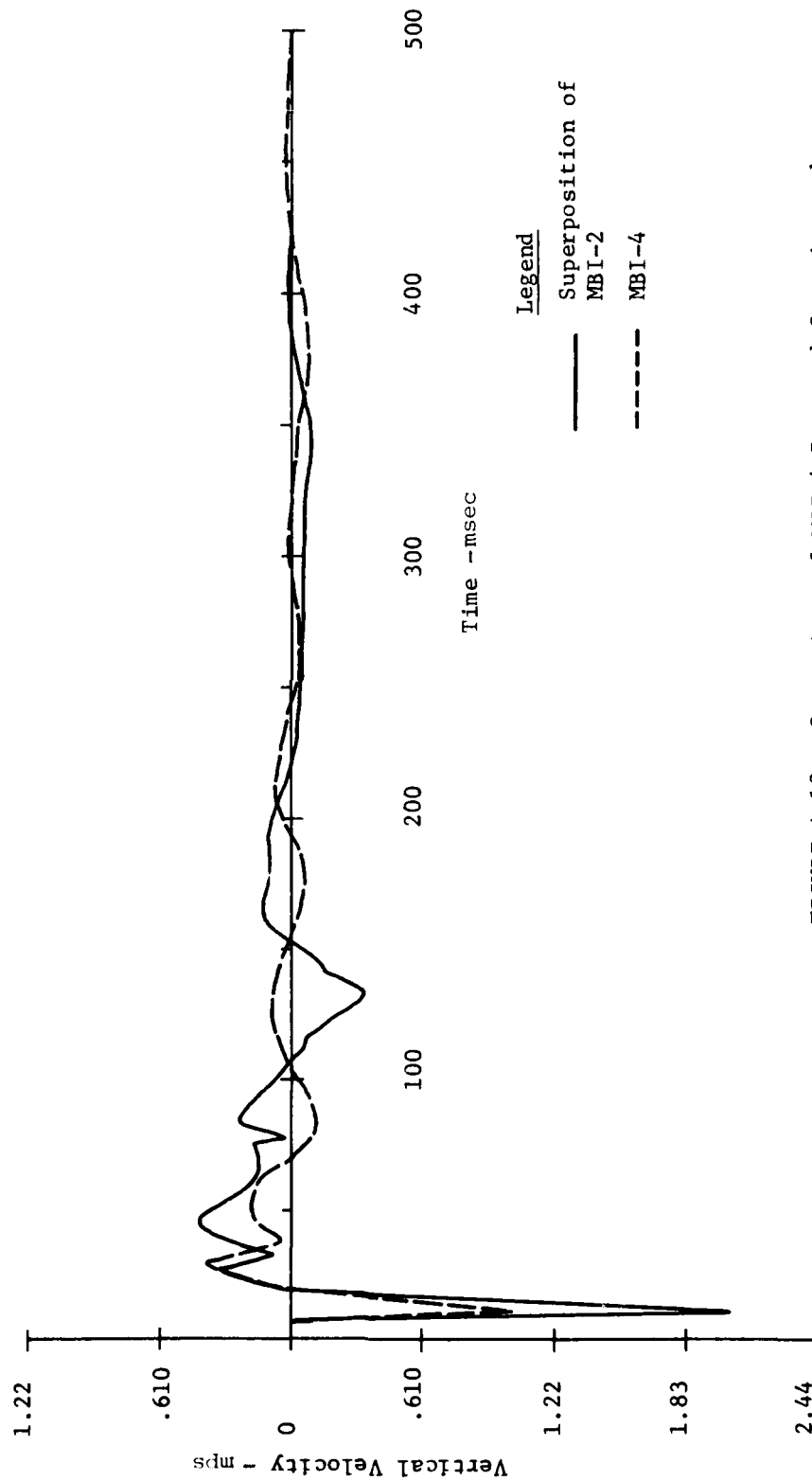


FIGURE A.12: Comparison of MBI-4 Data and Superimposed MBI-2 Data  
@ 32.03/0.46/0 Vertical Velocity

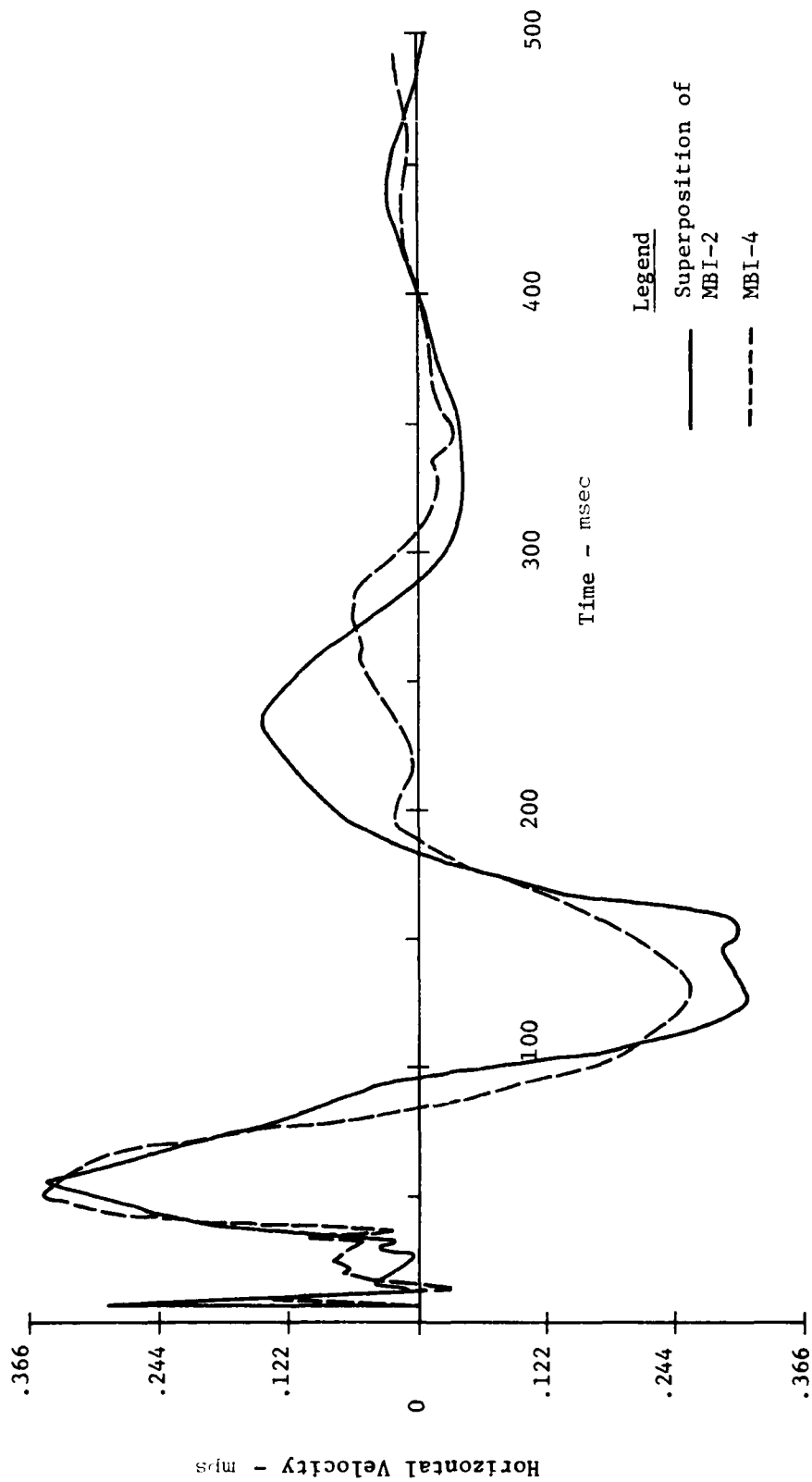


FIGURE A.13: Comparison of MBI-4 Data and Superimposed MBI-2 Data  
@ 32.03/0.46/0 Horizontal Velocity

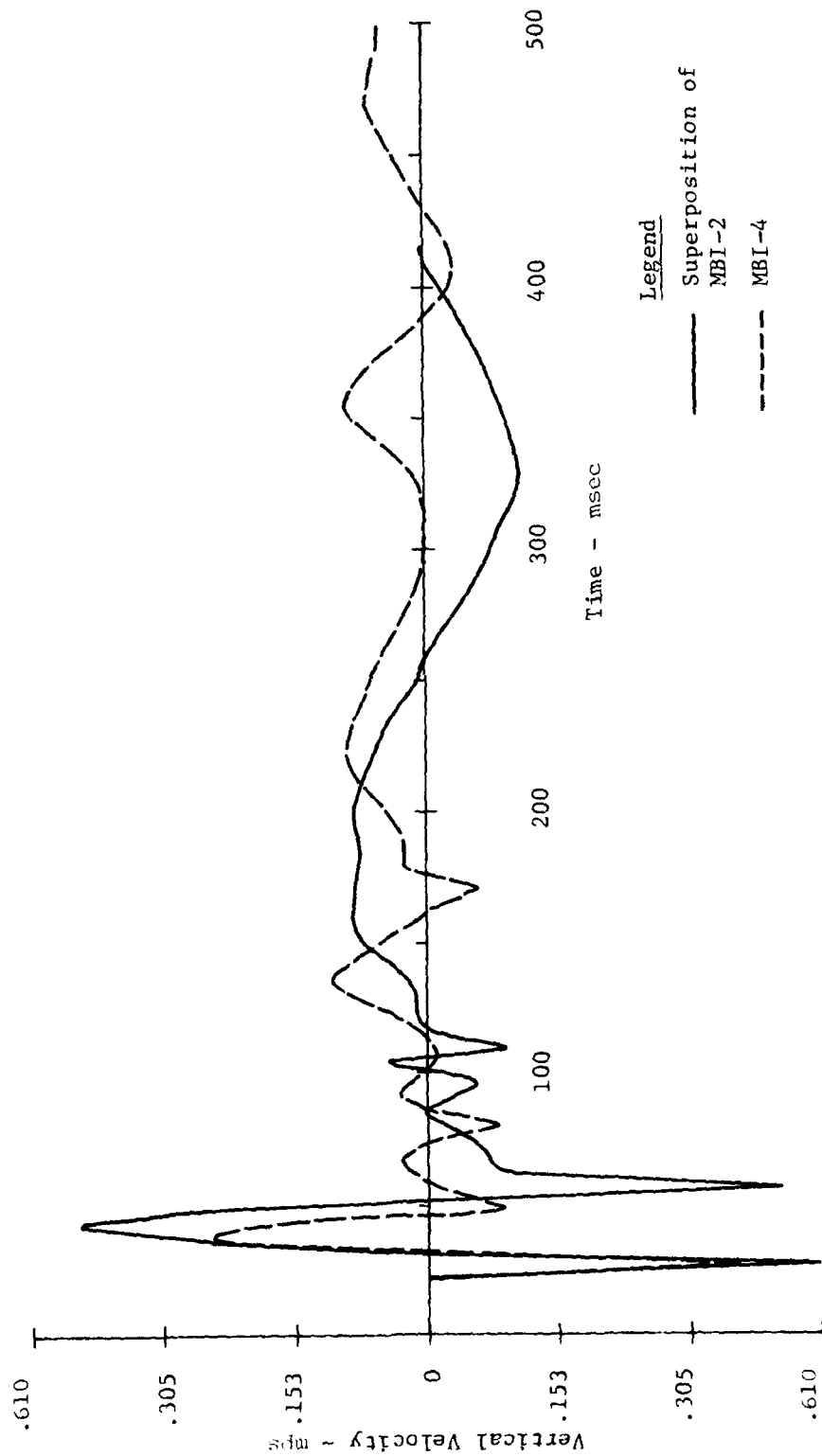


FIGURE A.14: Comparison of MBI-4 Data and Superimposed MBI-2 Data  
@ 42.70/0.46/0 Vertical Velocity

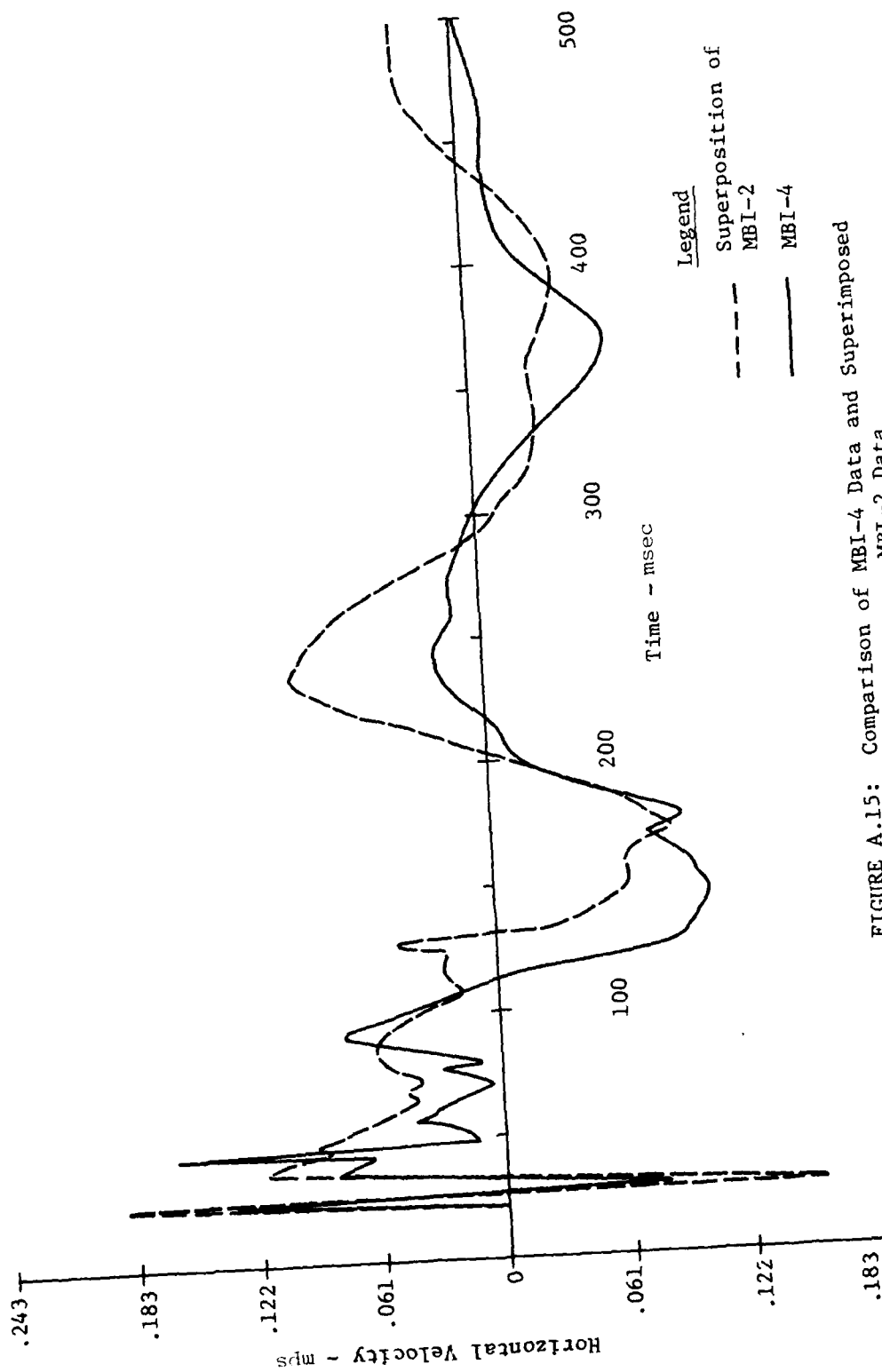


FIGURE A.15: Comparison of MBI-4 Data and Superimposed  
MBI-2 Data  
@ 42.70/0.46/0 Horizontal Velocity

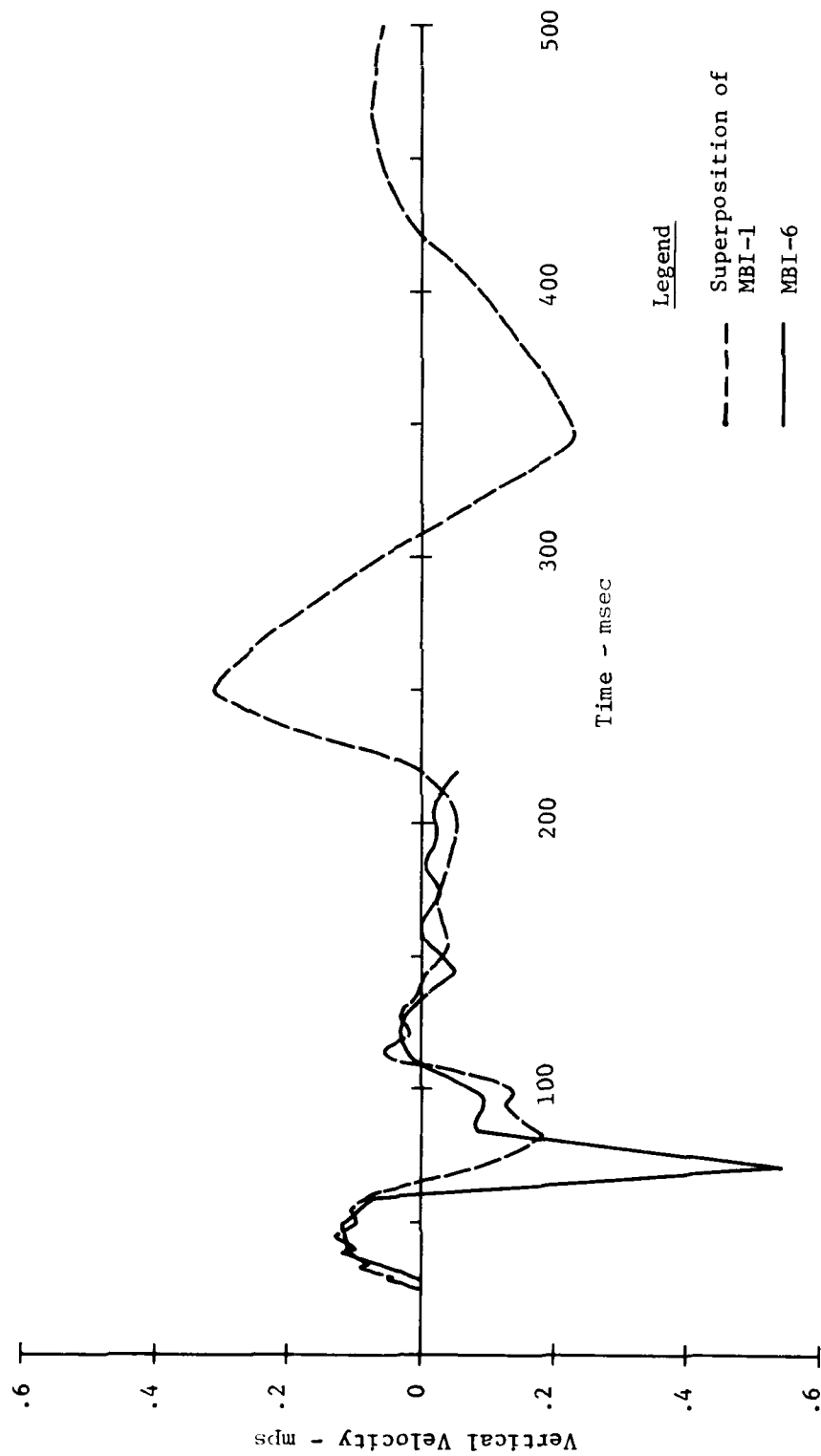


FIGURE A.16: Comparison of MBI-6 Data and Superimposed  
MBI-1 Data  
@ 0/1.52/0 Vertical Velocity

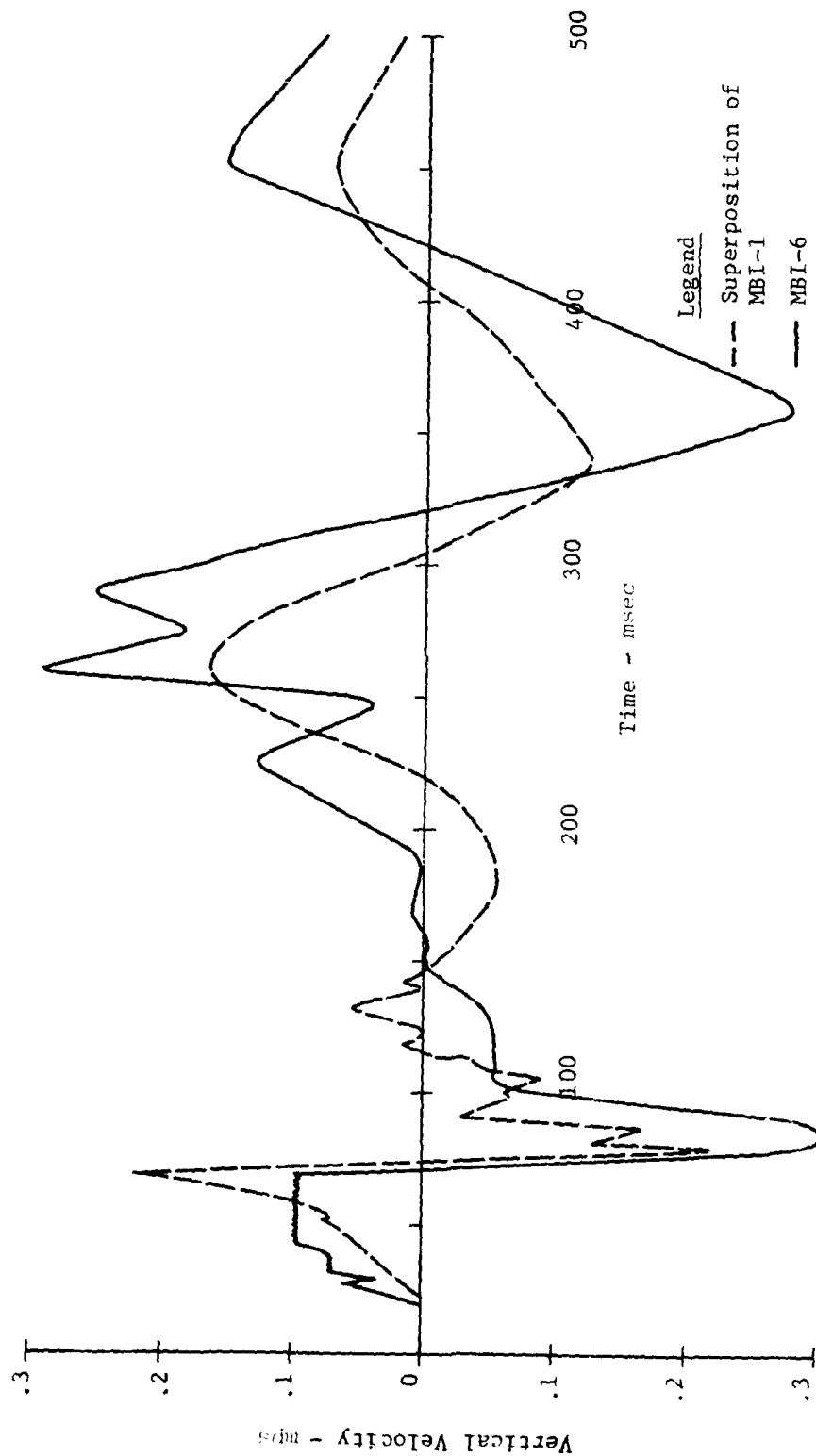


FIGURE A.17: Comparison of MBI-6 Data and Superimposed MBI-1 Data  
@ 0/3.05/0 Vertical Velocity

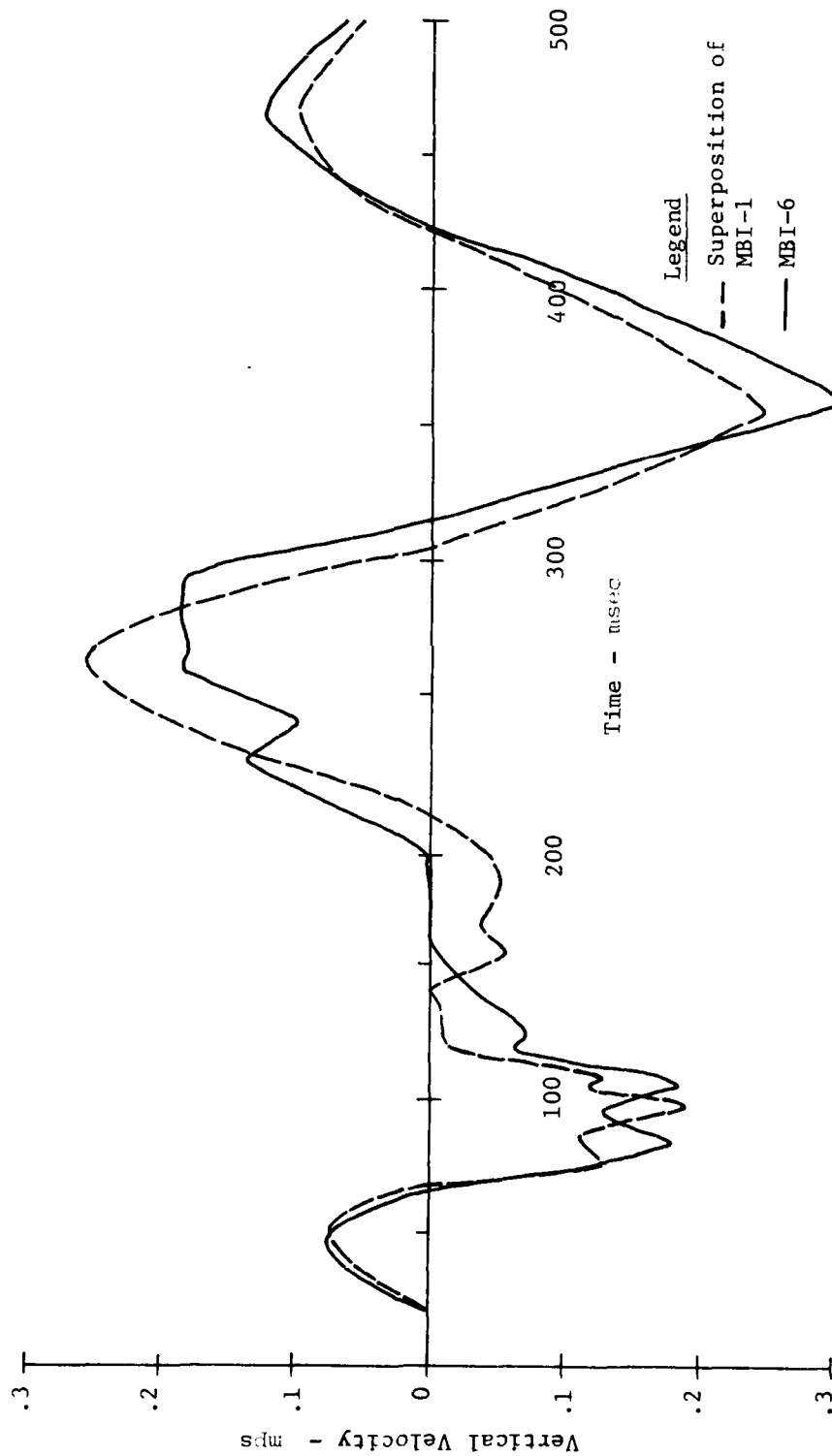


FIGURE A.18: Comparison of MBI-6 Data and Superimposed MBI-1 Data @ 0/6.10/0 Vertical Velocity

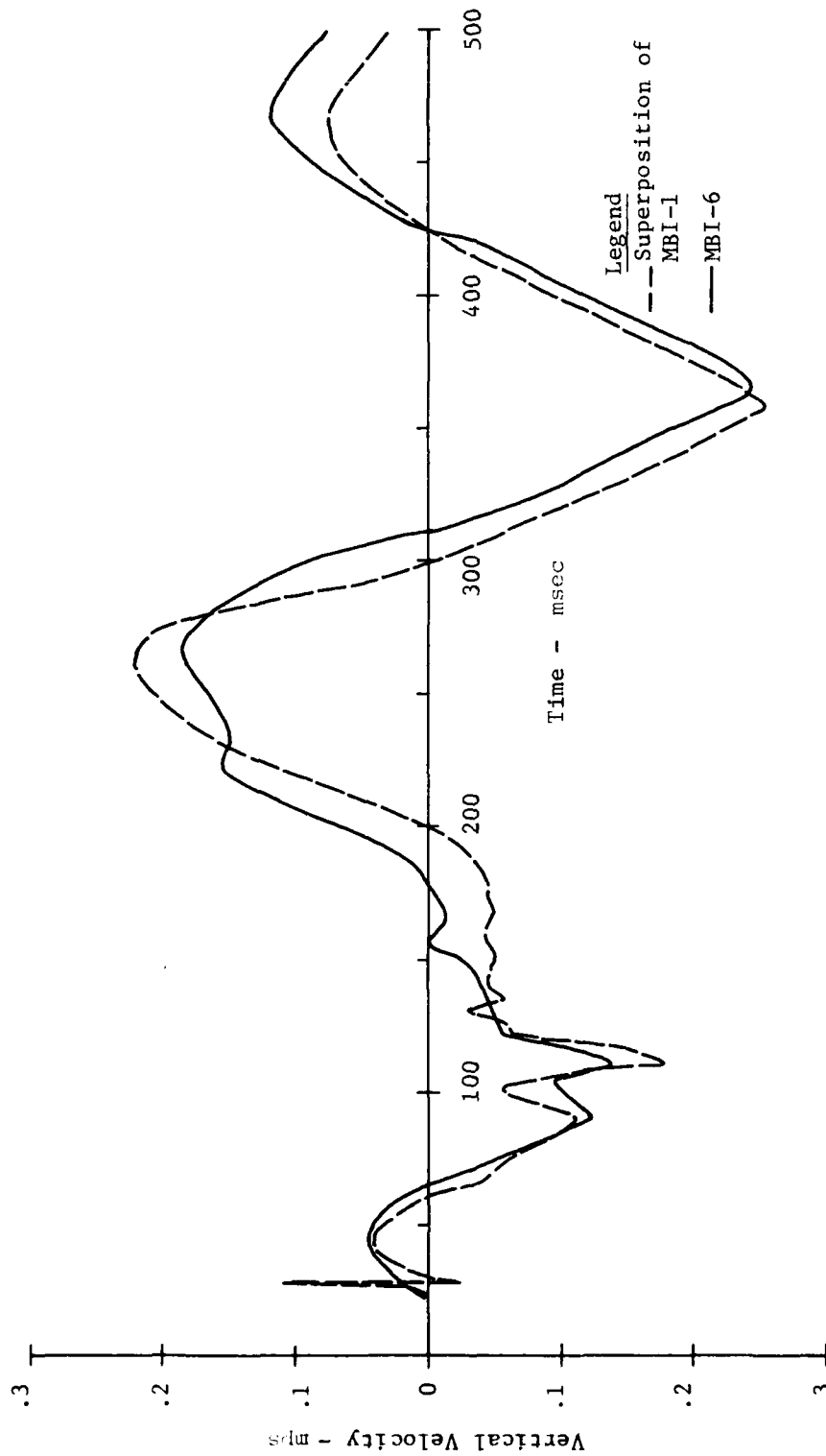


FIGURE A.19: Comparison of MBI-6 Data and Superimposed  
 MBI-1 Data  
 @ 0/9.15/0 Vertical Velocity

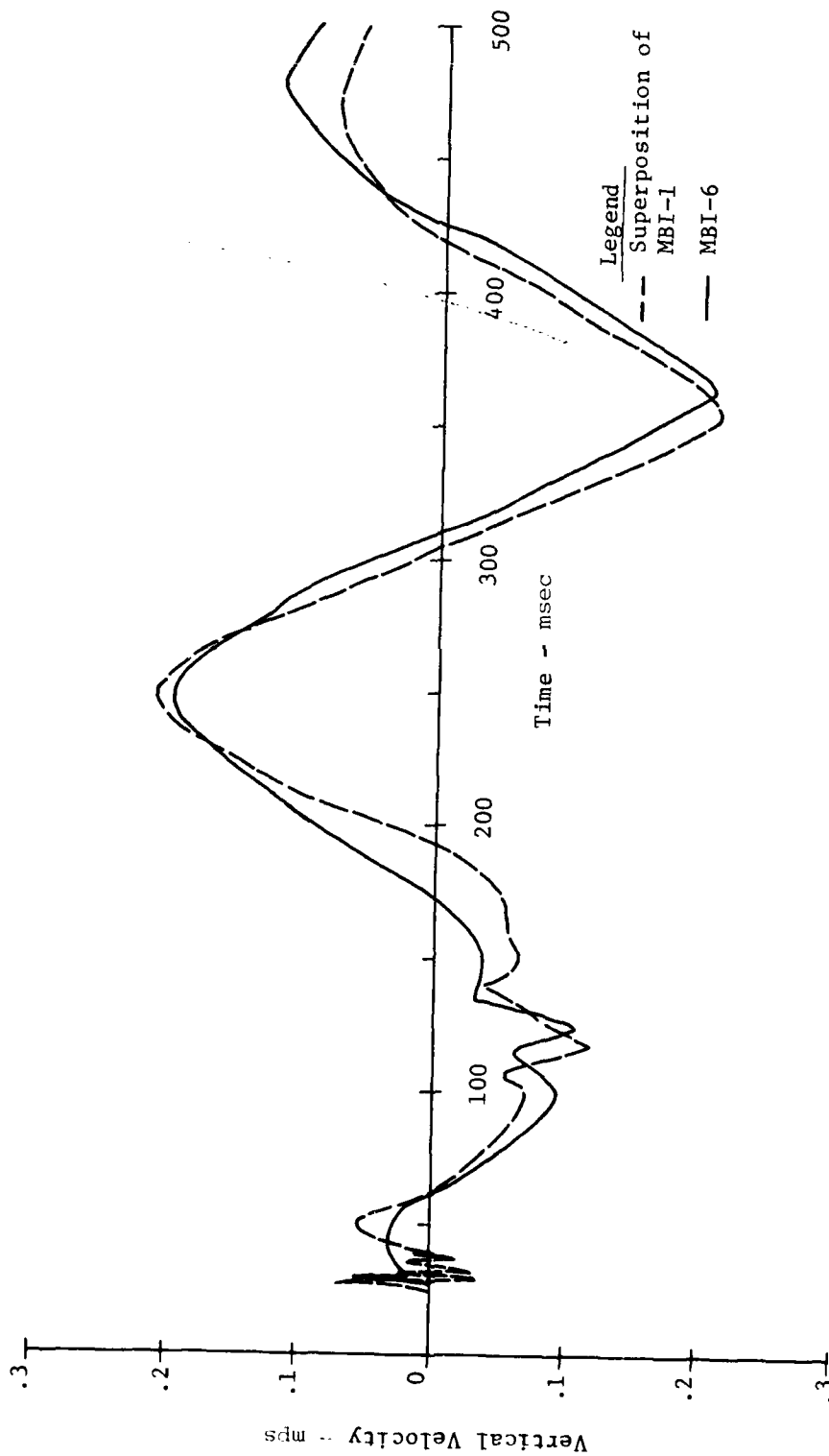


FIGURE A.20: Comparison of MBI-6 Data and Superimposed  
 MBI-1 Data  
 @ 0/12.2/0 Vertical Velocity

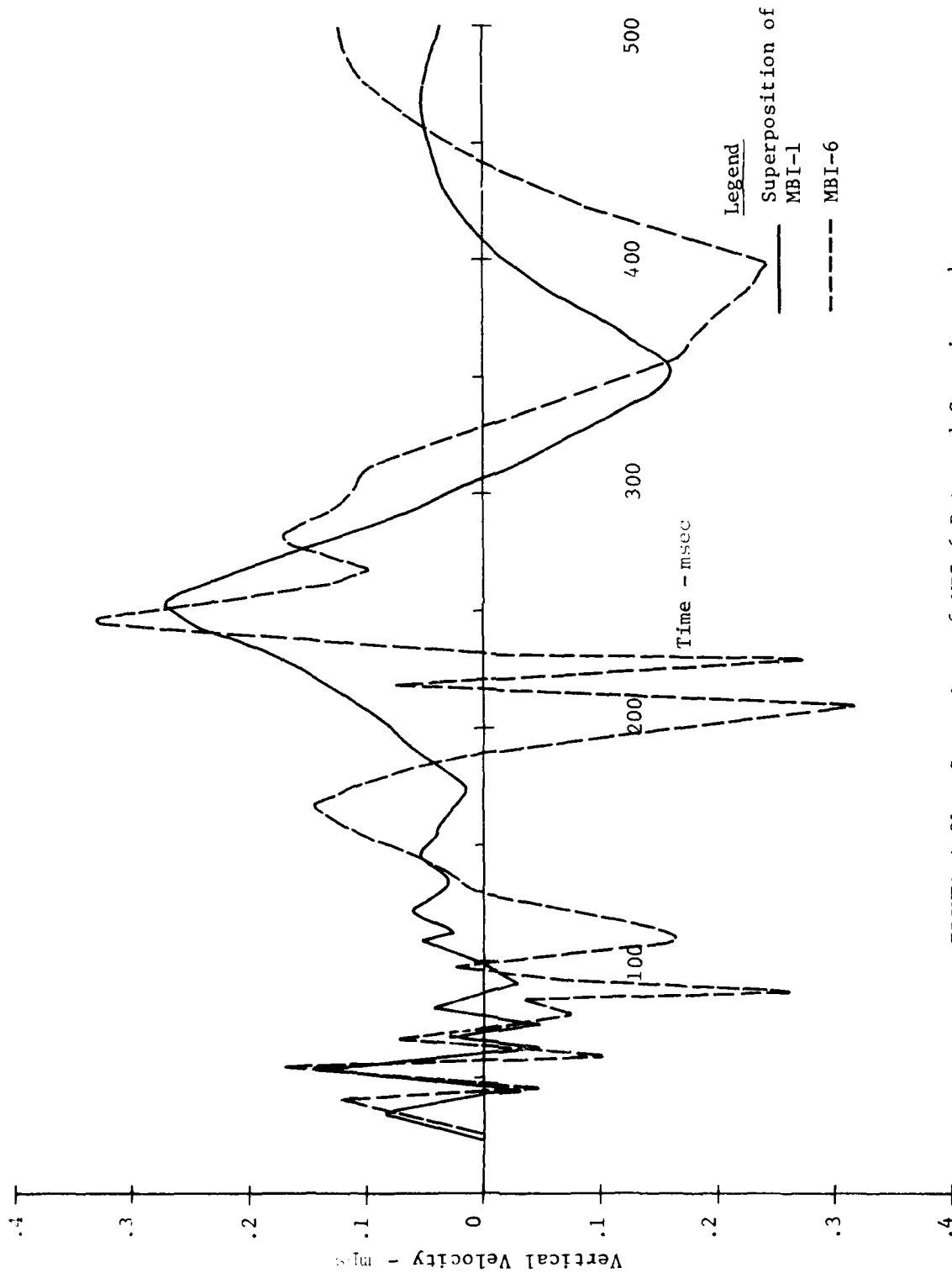


FIGURE A.21: Comparison of MBI-6 Data and Superimposed  
MBI-1 Data  
@ 9.15/0.46/0 Vertical Velocity

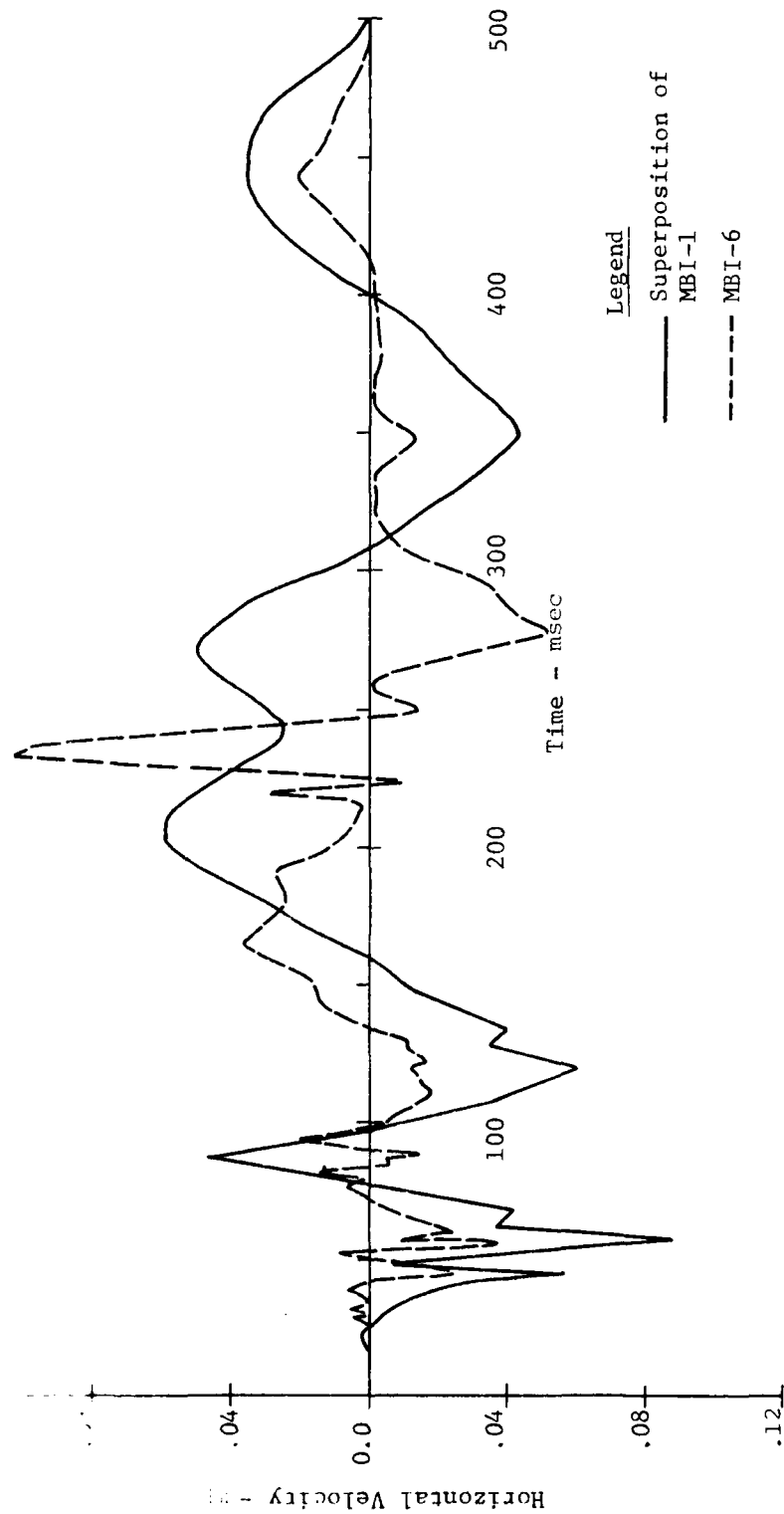


FIGURE A.22: Comparison of MBI-6 Data and Superimposed  
MBI-1 Data  
@ 9.15/0.46/0 Horizontal Velocity

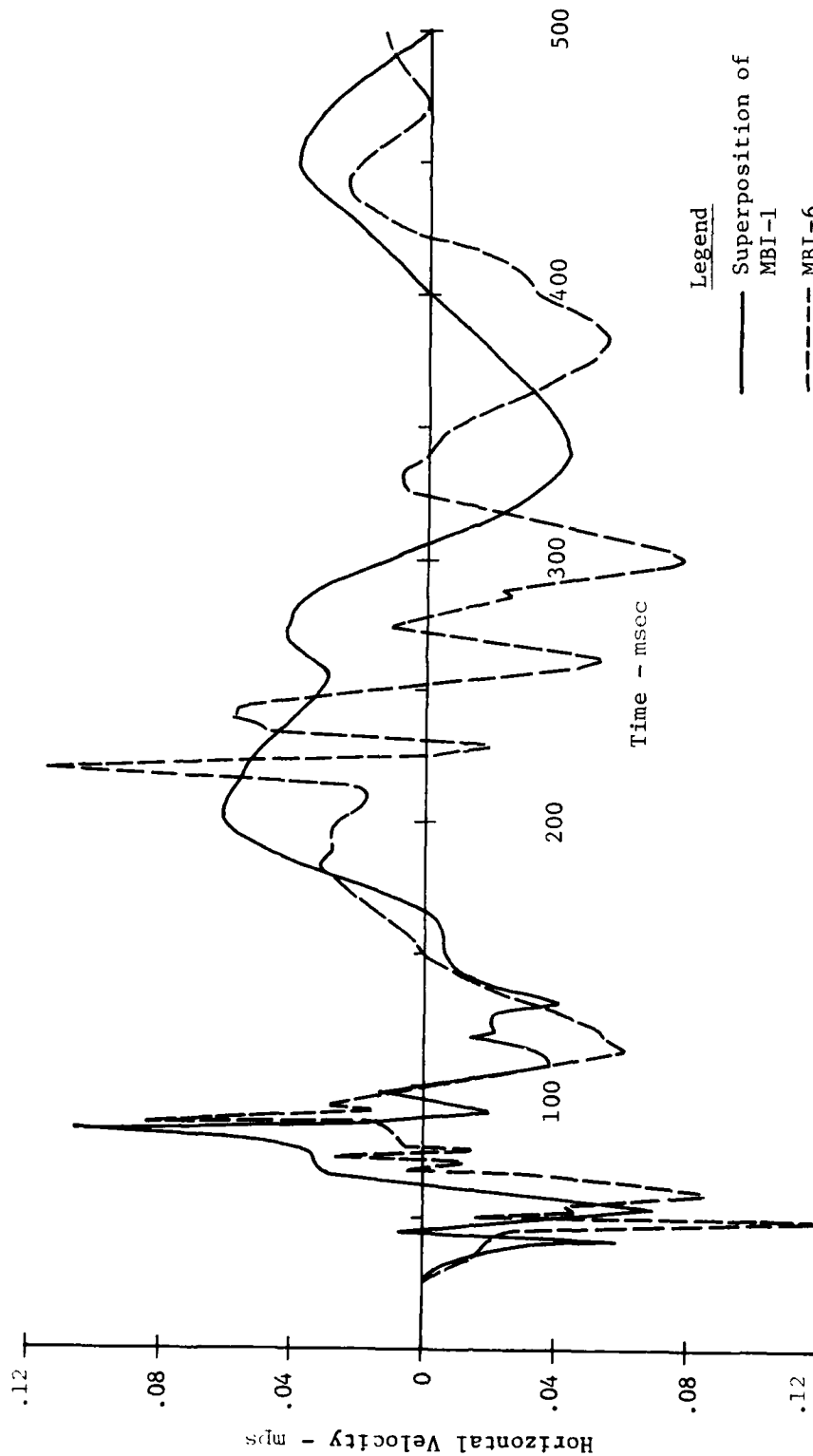


FIGURE A.23: Comparison of MBI-6 Data and Superimposed  
MBI-1 Data  
@ 9.15/0.46/270 Horizontal Velocity

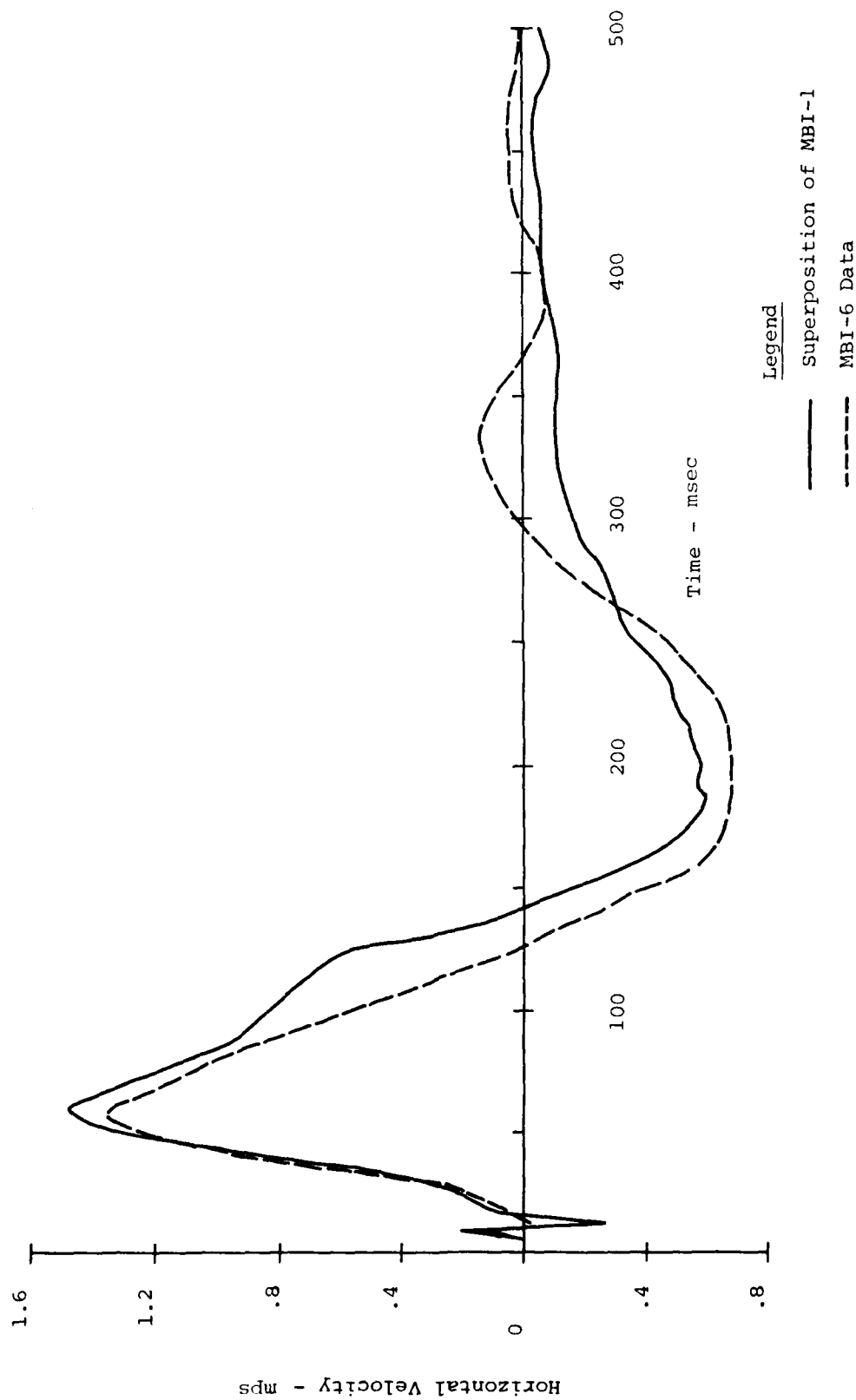


FIGURE A.24: Comparison of MBI-6 with superposition of MBI-1 @ 32.94/0.46/0 Horizontal Velocity

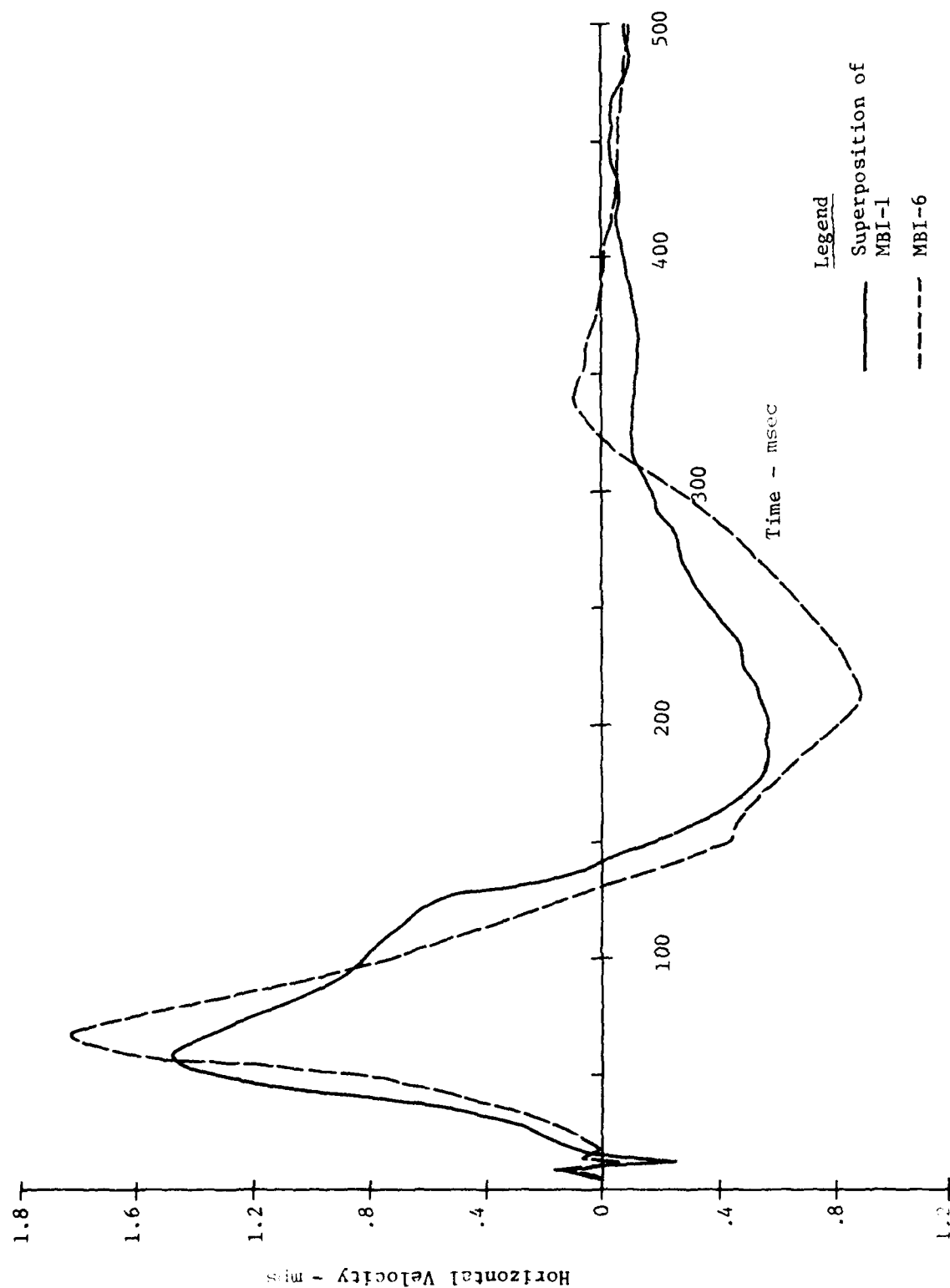


FIGURE A.25: Comparison of MBI-6 Data and Superimposed MBI-1 Data  
@ 45.75/0.46/0 Horizontal Velocity

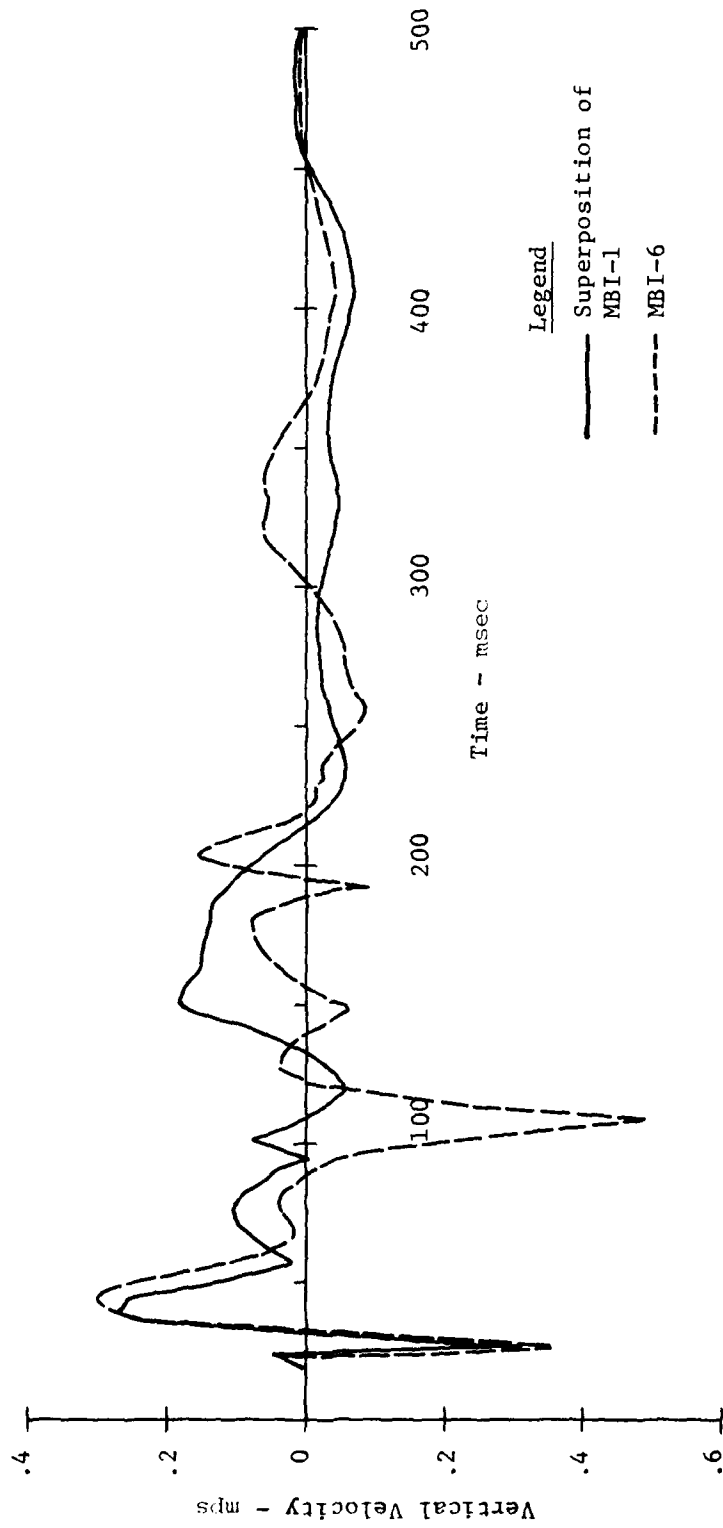


FIGURE A.26: Comparison of MBI-6 Data and Superimposed  
MBI-1 Data  
@ 54.90/0.46/0 Vertical Velocity

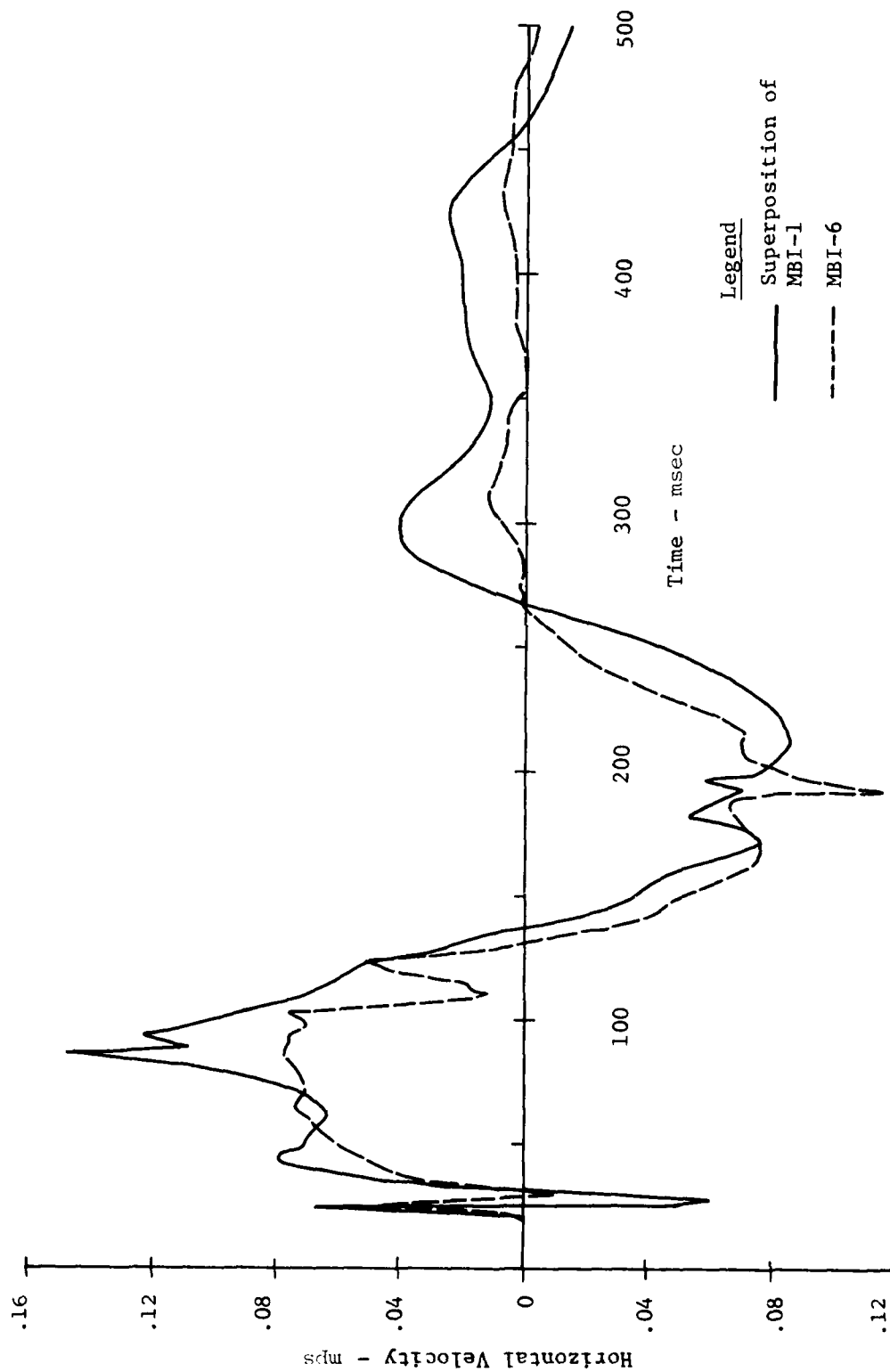


FIGURE A.27: Comparison of MBI-6 Data and Superimposed MBI-1 Data  
@ 54.90/0.46/0 Horizontal Velocity

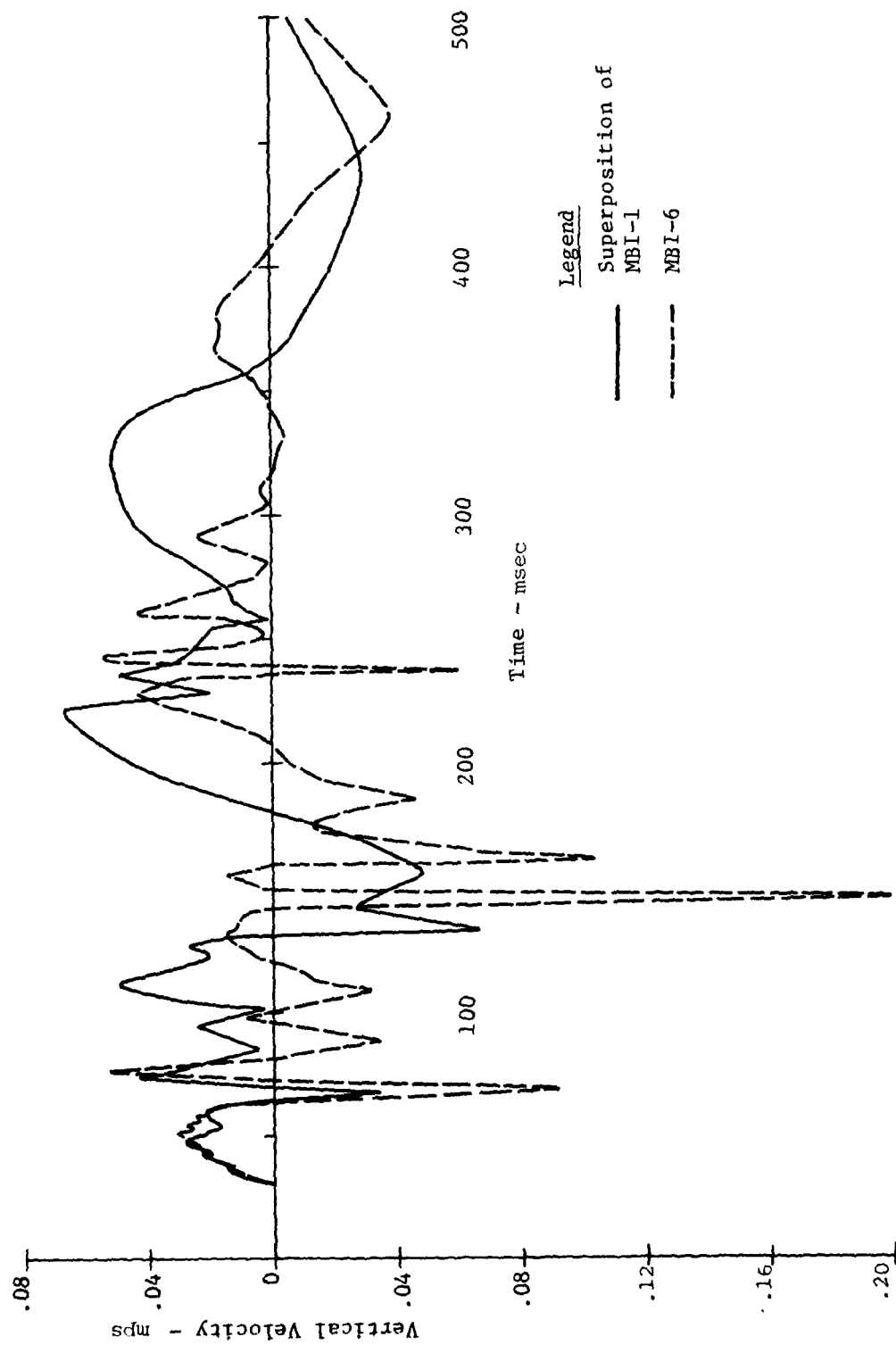


FIGURE A.28: Comparison of MBI-6 Data and Superimposed  
MBI-1 Data  
@ 73.2/0.46/0 Vertical Velocity

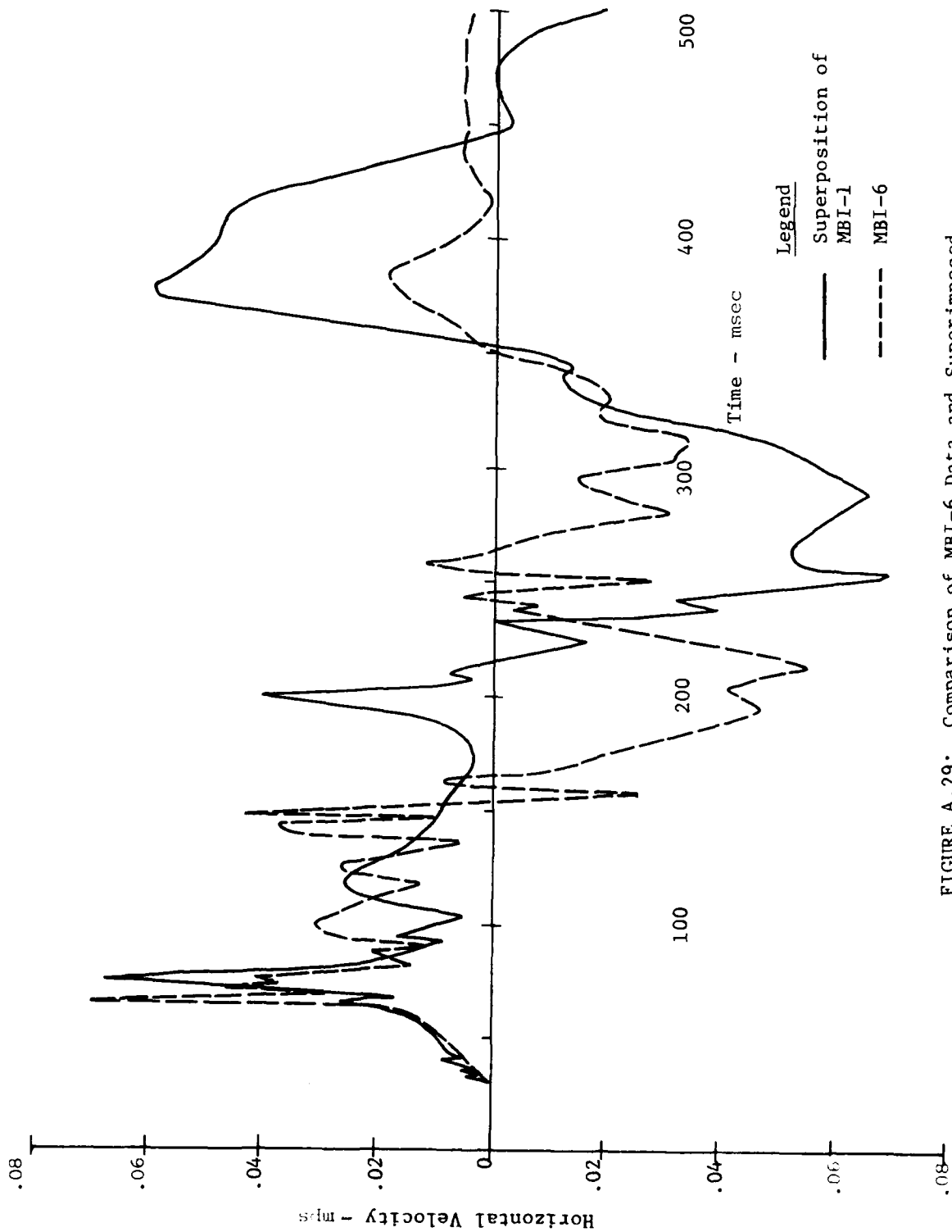


FIGURE A.29: Comparison of MBI-6 Data and Superimposed  
MBI-1 Data  
@ 73.2/0.46/0 Horizontal Velocity

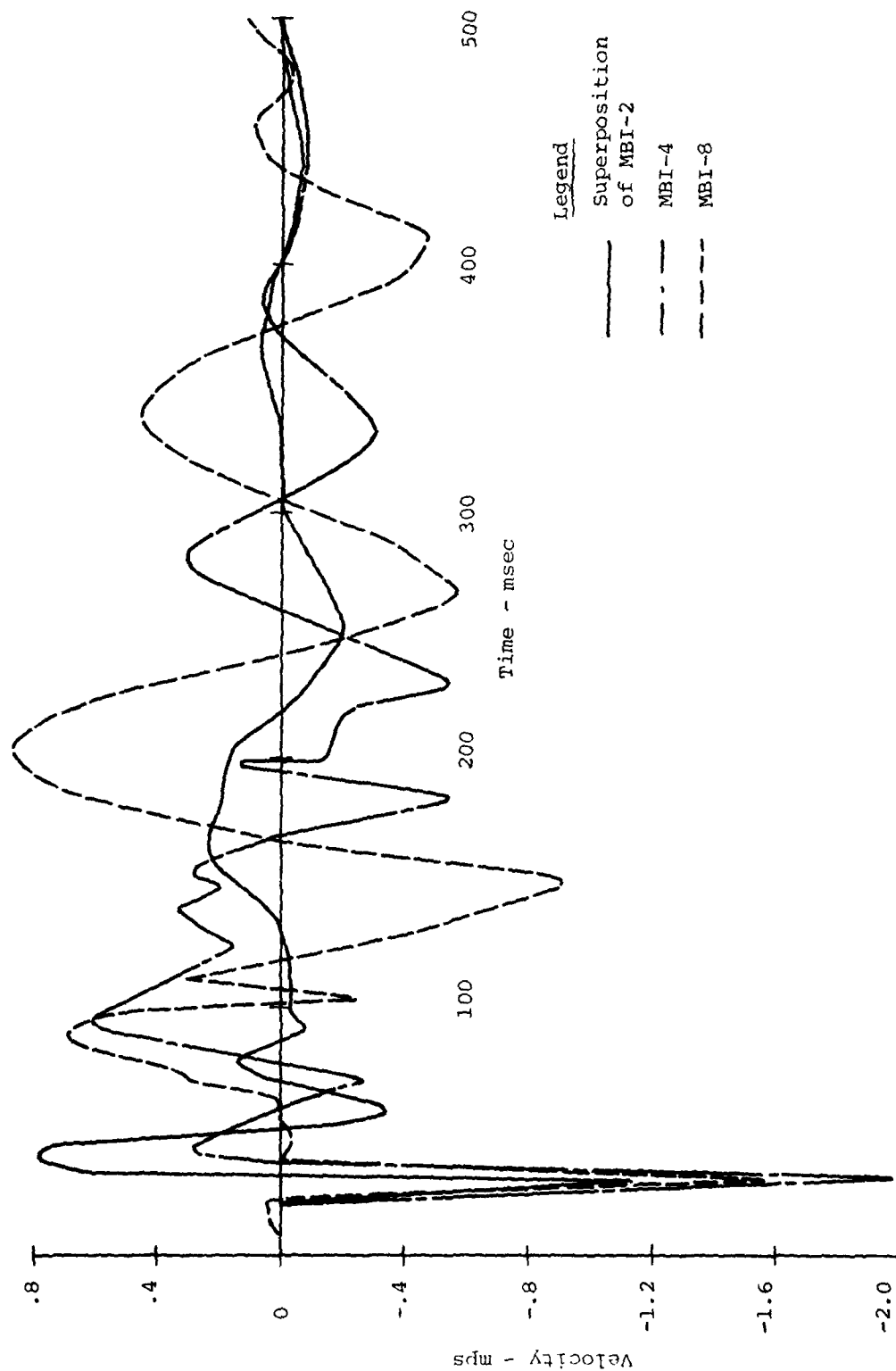


FIGURE A.30: Comparison of MBI-8 Data with MBI-4 Data and Superimposed MBI-2 Data @ 0/1.52/0 Vertical Velocity

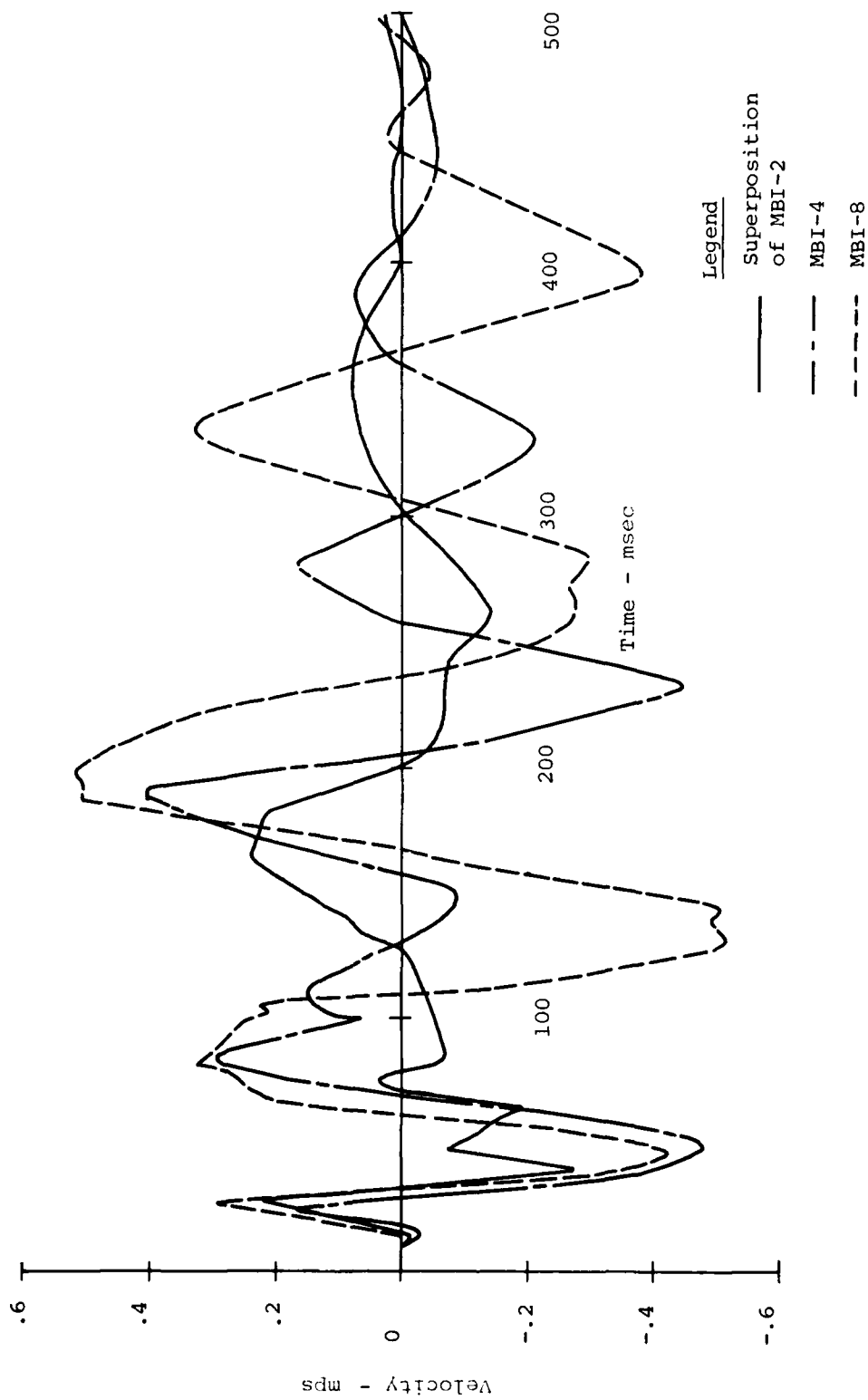


FIGURE A.31: Comparison of MBI-8 Data with MBI-4 Data and Superimposed MBI-2 Data @ 0/3.05/0 Vertical Velocity

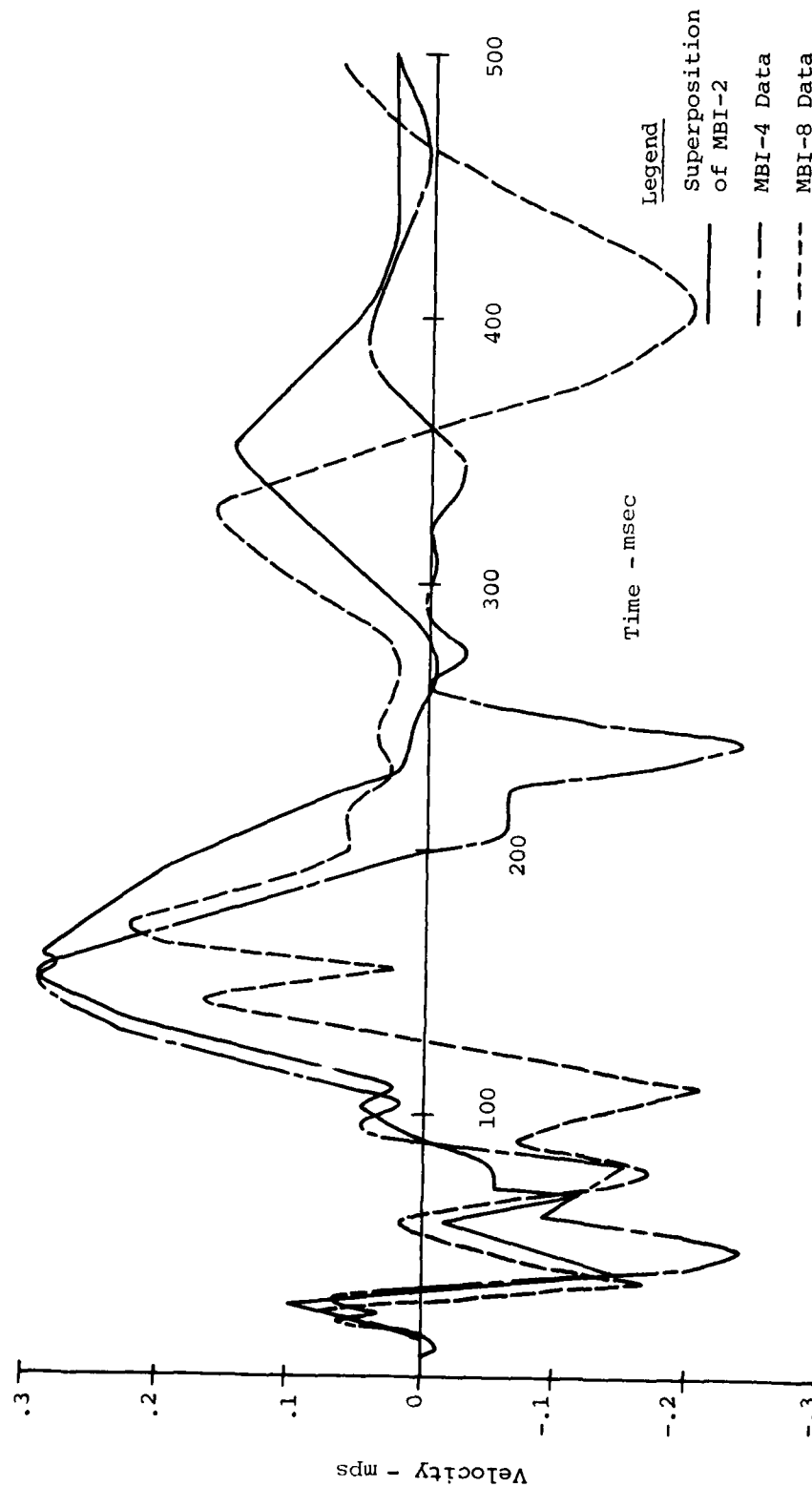


FIGURE A.32: Comparison of MBI-8 Data with MBI-4 Data and Superimposed MBI-2 Data @ 0/6.10/0 Vertical Velocity

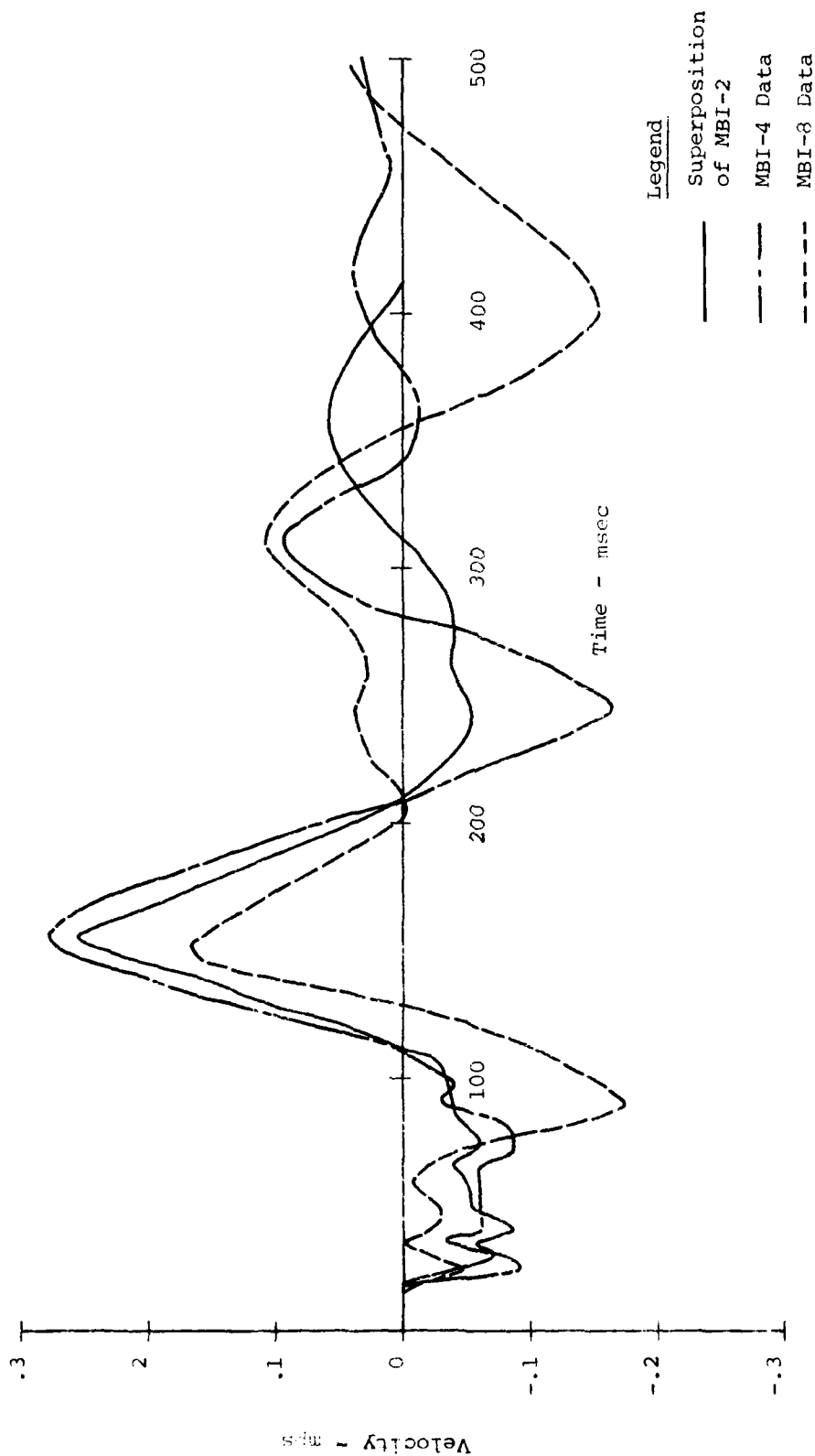


FIGURE A.33: Comparison of MBI-8 Data with MBI-4 Data and Superimposed MBI-2 Data @ 0/12.20/0 Vertical Velocity

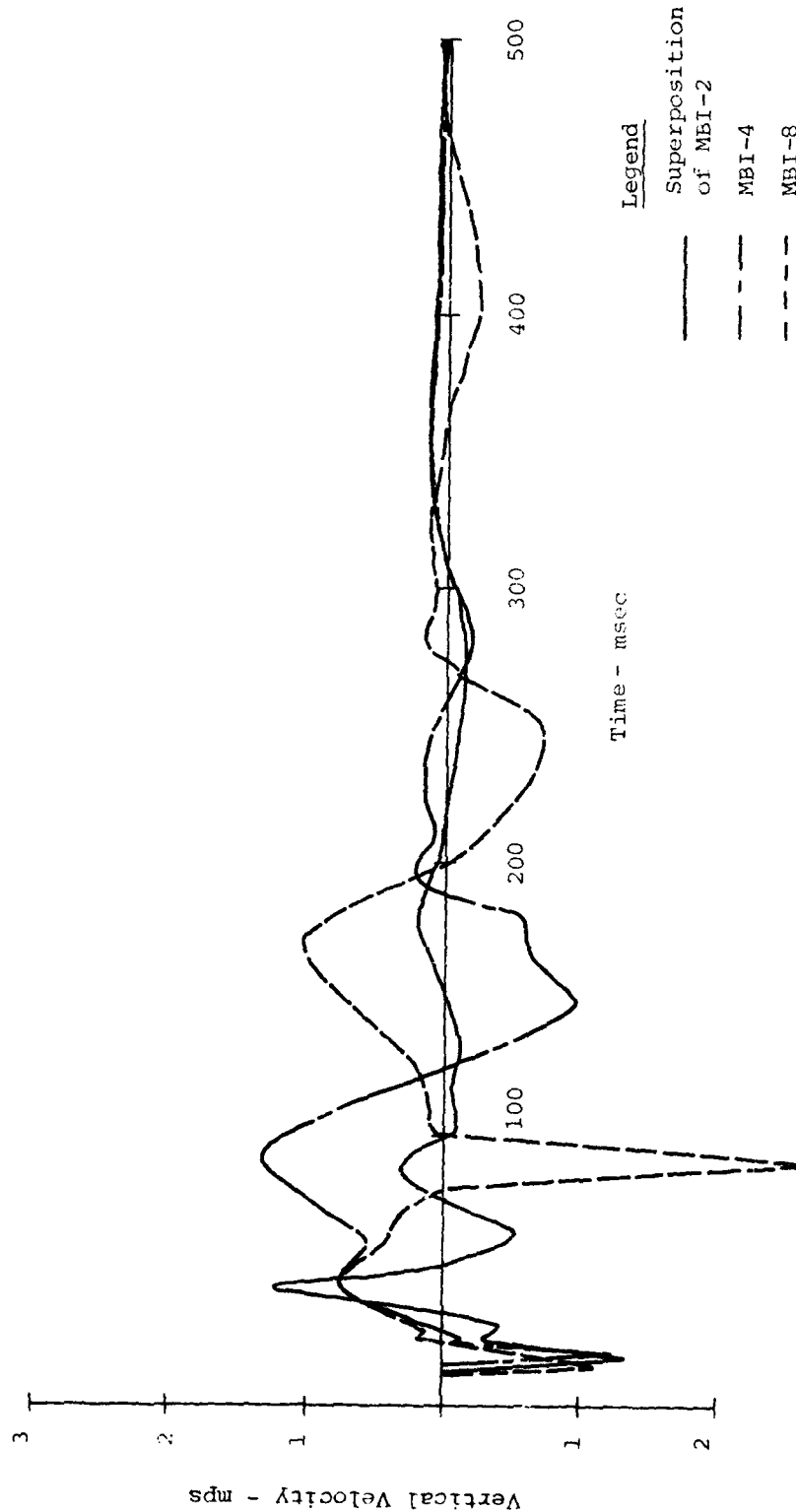
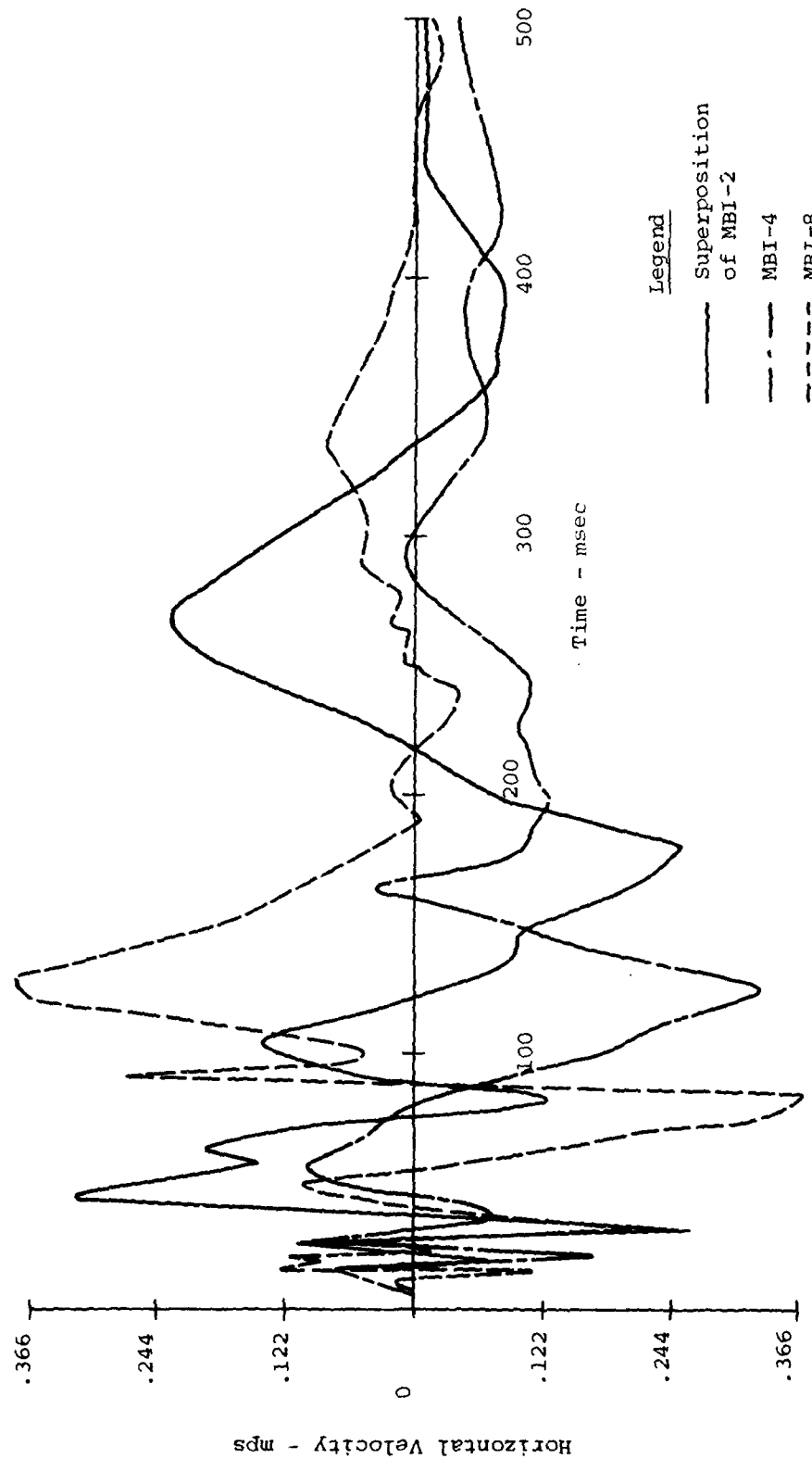


FIGURE A.34: Comparison of MBI-8 Data with MBI-4 Data and Superimposed MBI-2 Data @ 5.34/0.46/0 Vertical Velocity



A. 36

FIGURE A.35: Comparison of MBI-8 Data with MBI-4 Data and Superimposed MBI-2 Data @ 5.34/0.46/0 Horizontal Velocity

AD-A088 510

CIVIL SYSTEMS INC ALBUQUERQUE NM  
MISERS BLUFF PHASE I GROUND SHOCK ANALYSIS OF THE MULTIPLE BURS-ETC(U)  
AUG 78 J S PHILLIPS, J L BRATTON

F/6 18/3

DNA001-77-C-0301

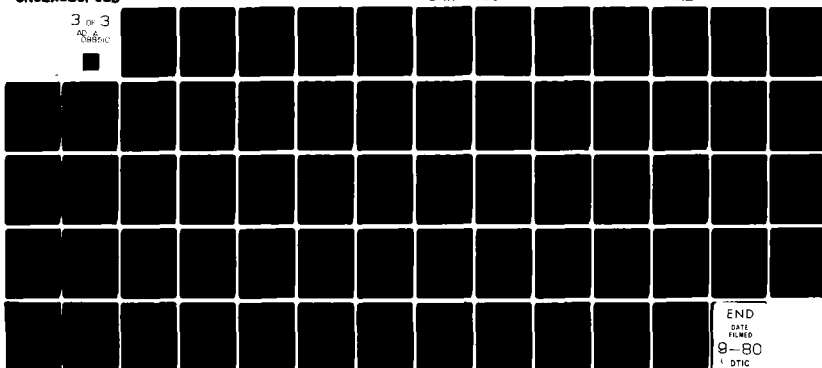
UNCLASSIFIED

DNA-5089Z

NL

3 of 3

AD-A  
088510



END

DATE

FILED

8-80

DTIC

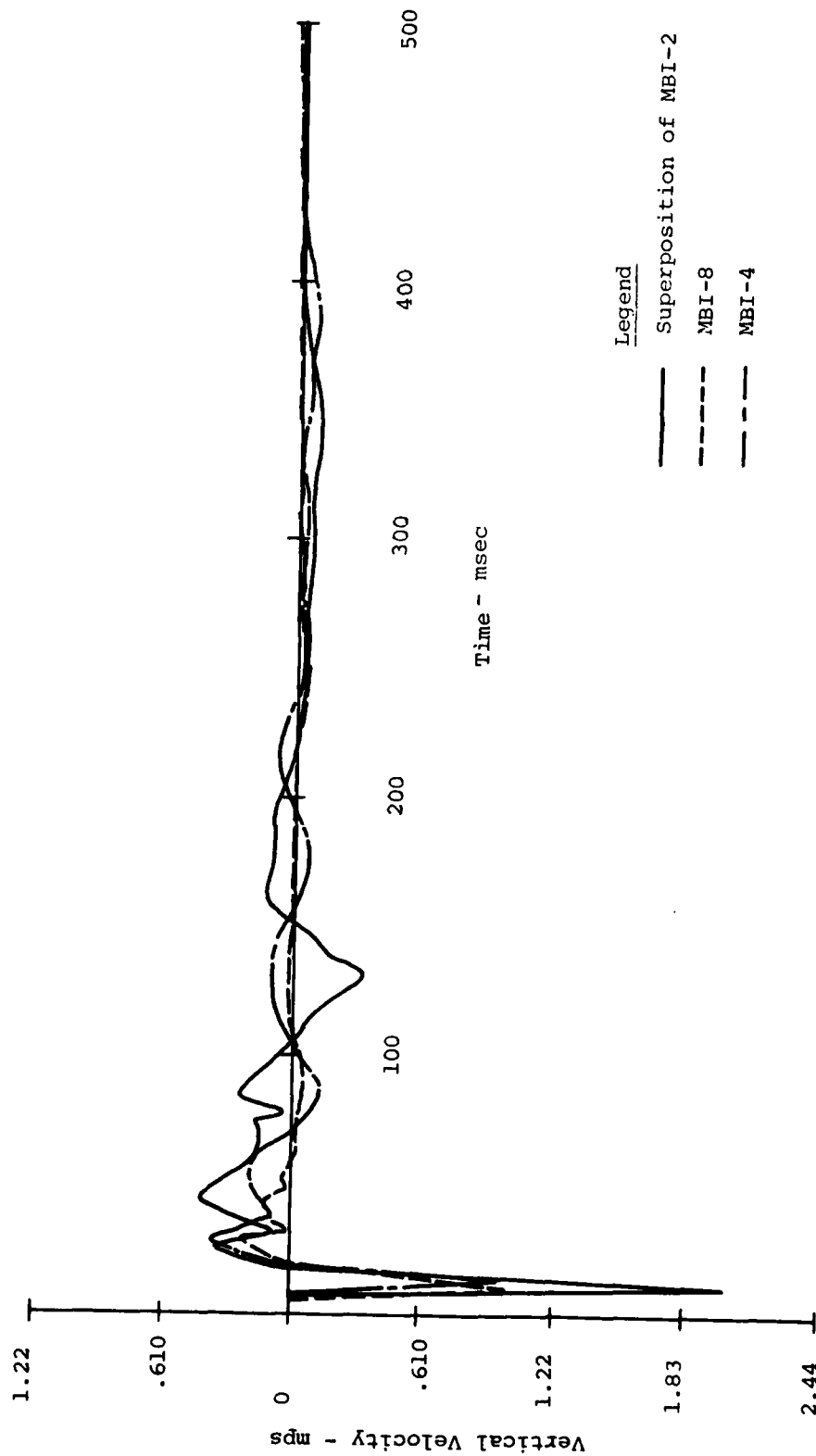


FIGURE A.36: Comparison of MBI-8 Data with MBI-4 Data and Superimposed MBI-2 Data @ 32.03/0.46/0 Vertical Velocity

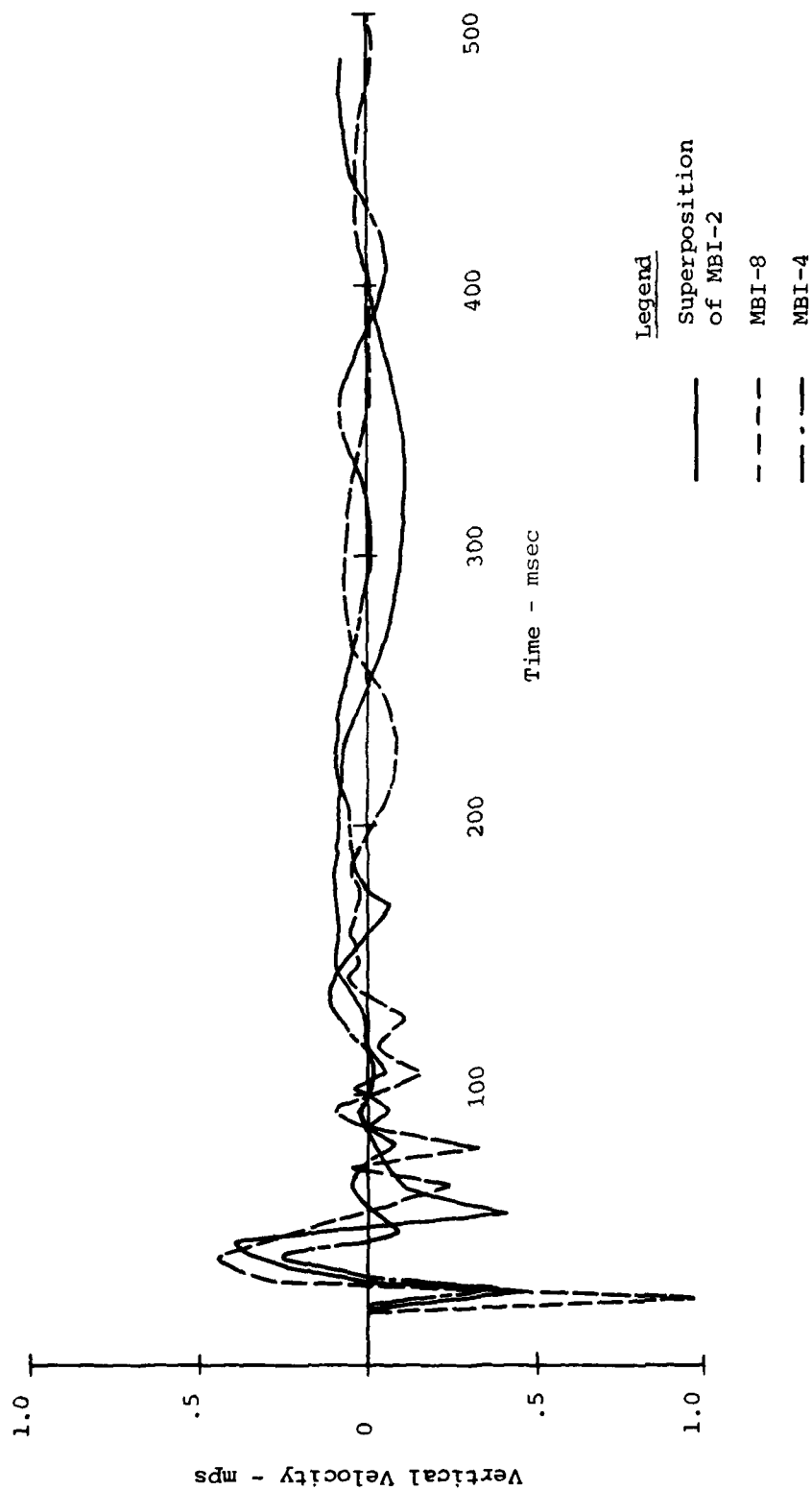


FIGURE A.37: Comparison of MBI-8 Data with MBI-4 Data and Superimposed MBI-2 Data @ 73.93/0.46/0 Vertical Velocity

## APPENDIX B

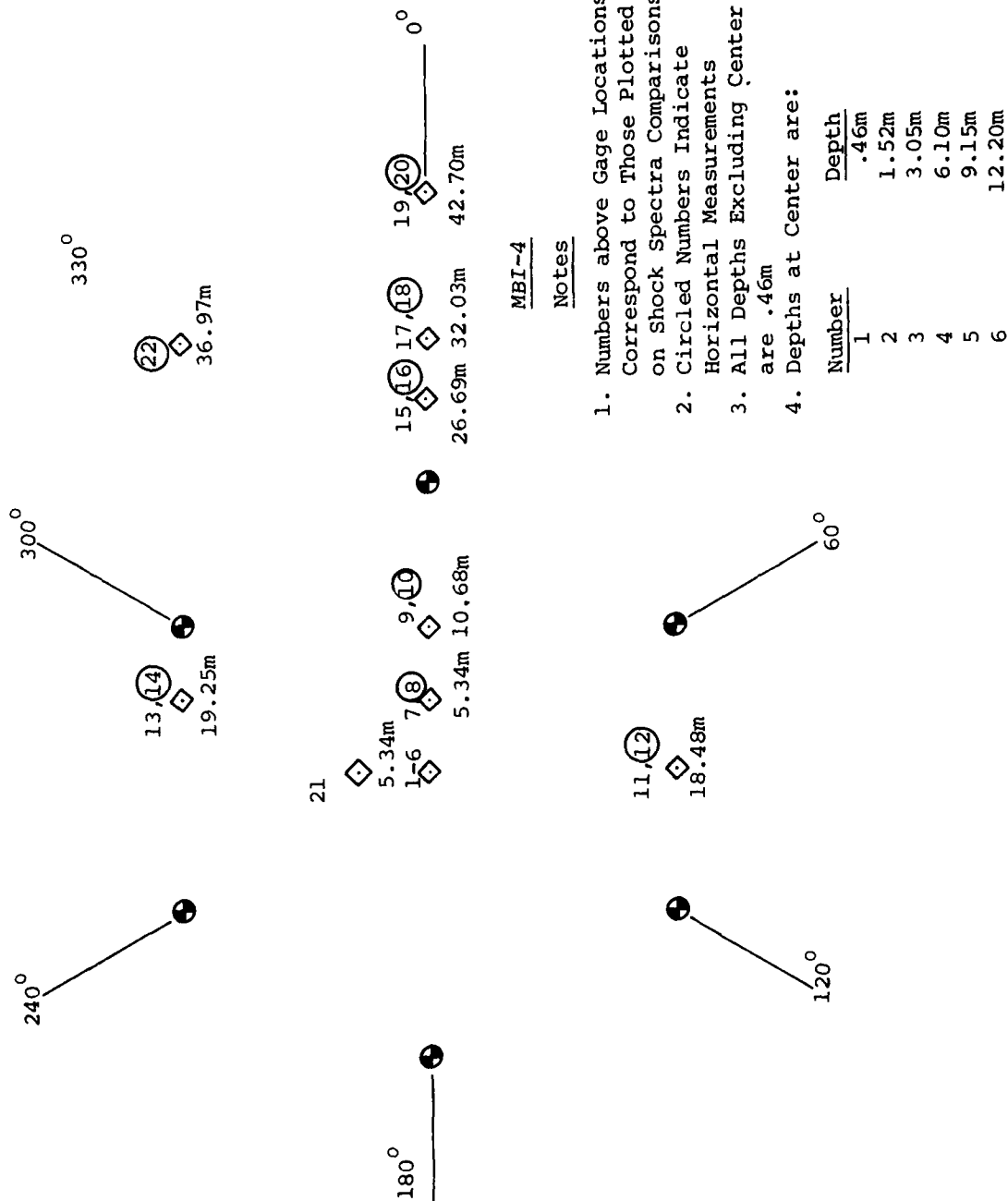
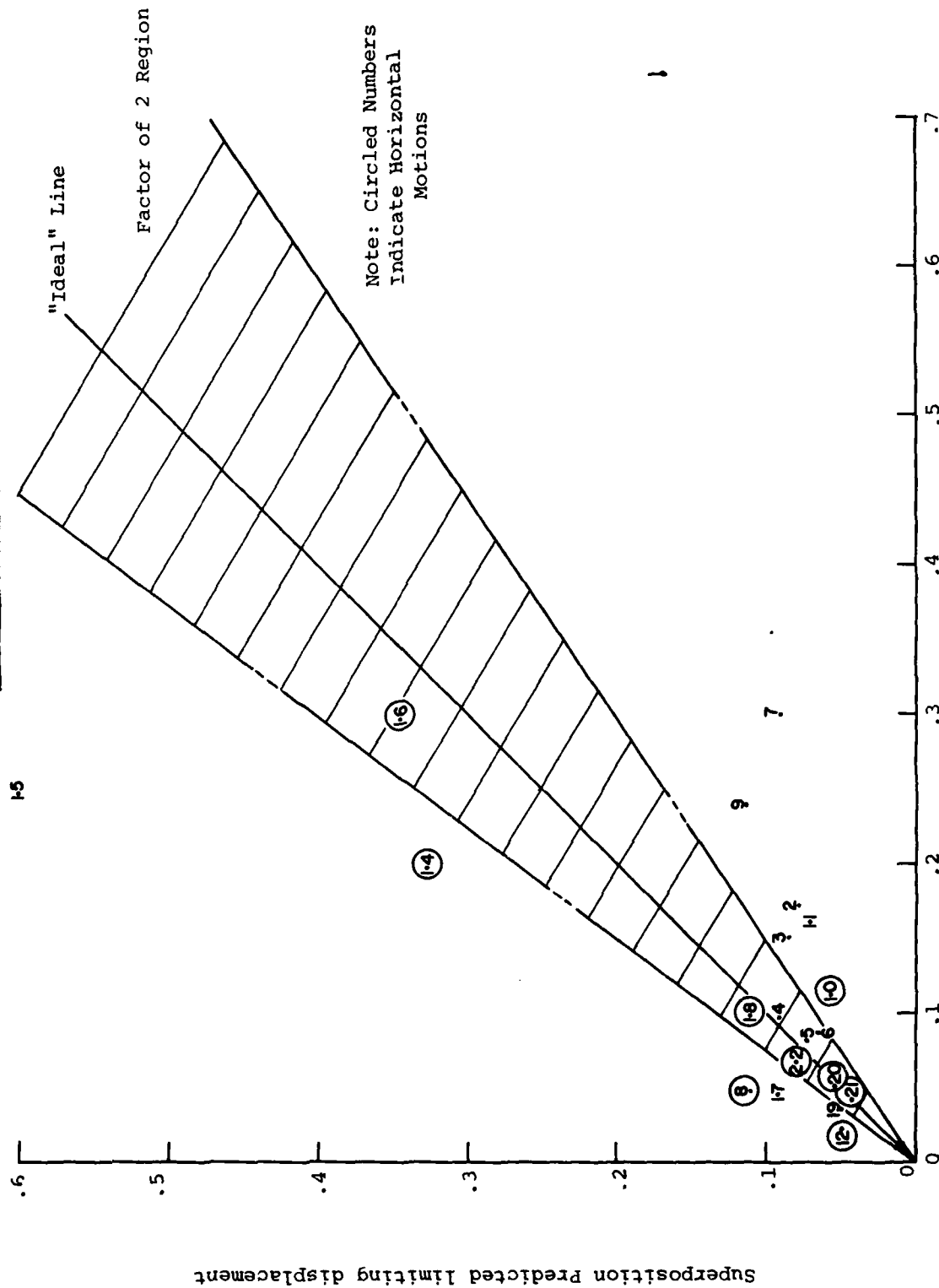


FIGURE B.1: Location of Shock Spectra Comparisons for MBI-4

1-3

MBI-4

Shock Spectra Comparisons



Note: Circled Numbers  
Indicate Horizontal  
Motions

FIGURE B.2: Evaluation Plot of Limiting Displacements - MBI-4

# MBI-4

## Shock Spectra Comparisons

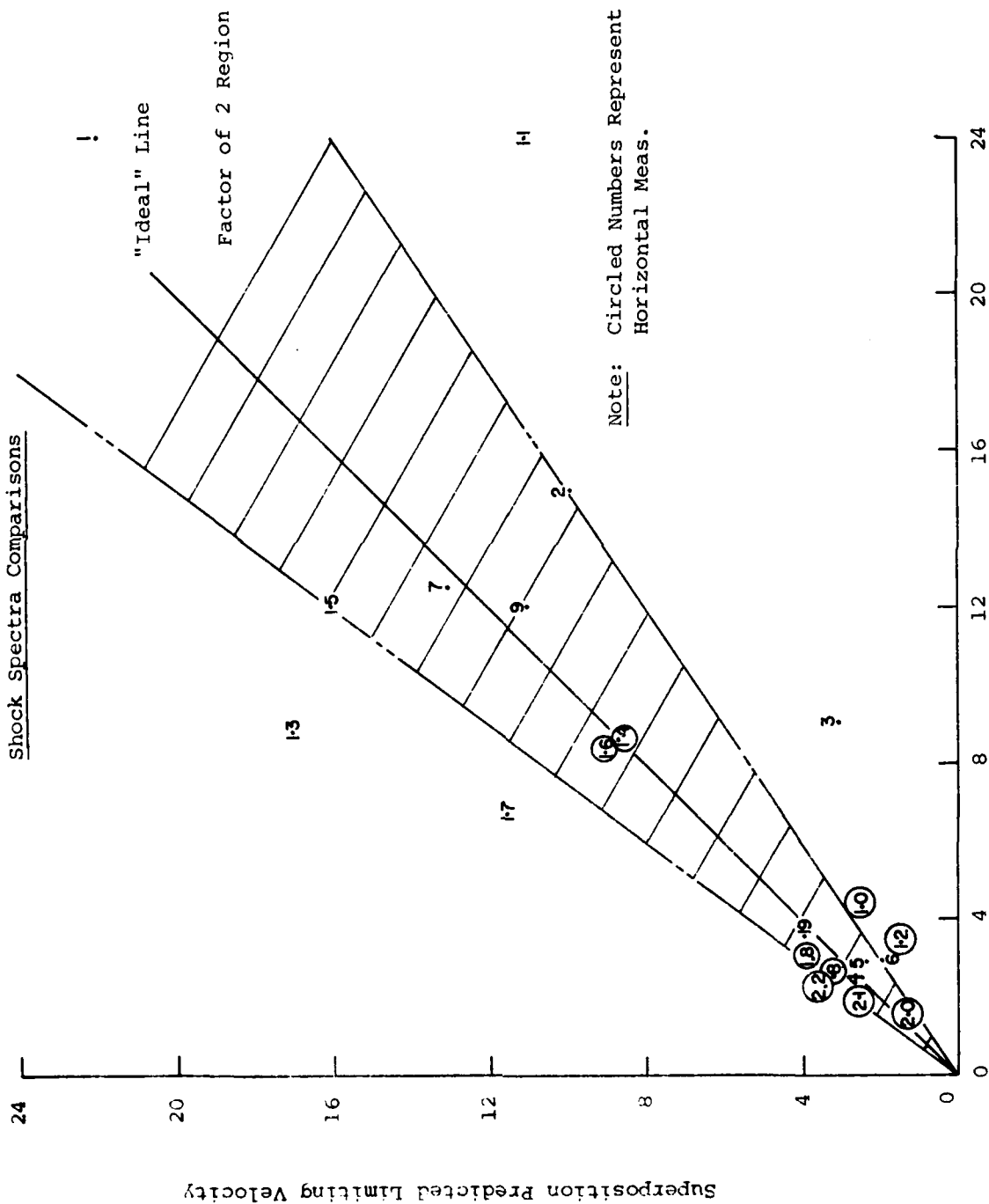


FIGURE B.3: Evaluation Plot of Limiting Velocities - MBI-4

MBI-4

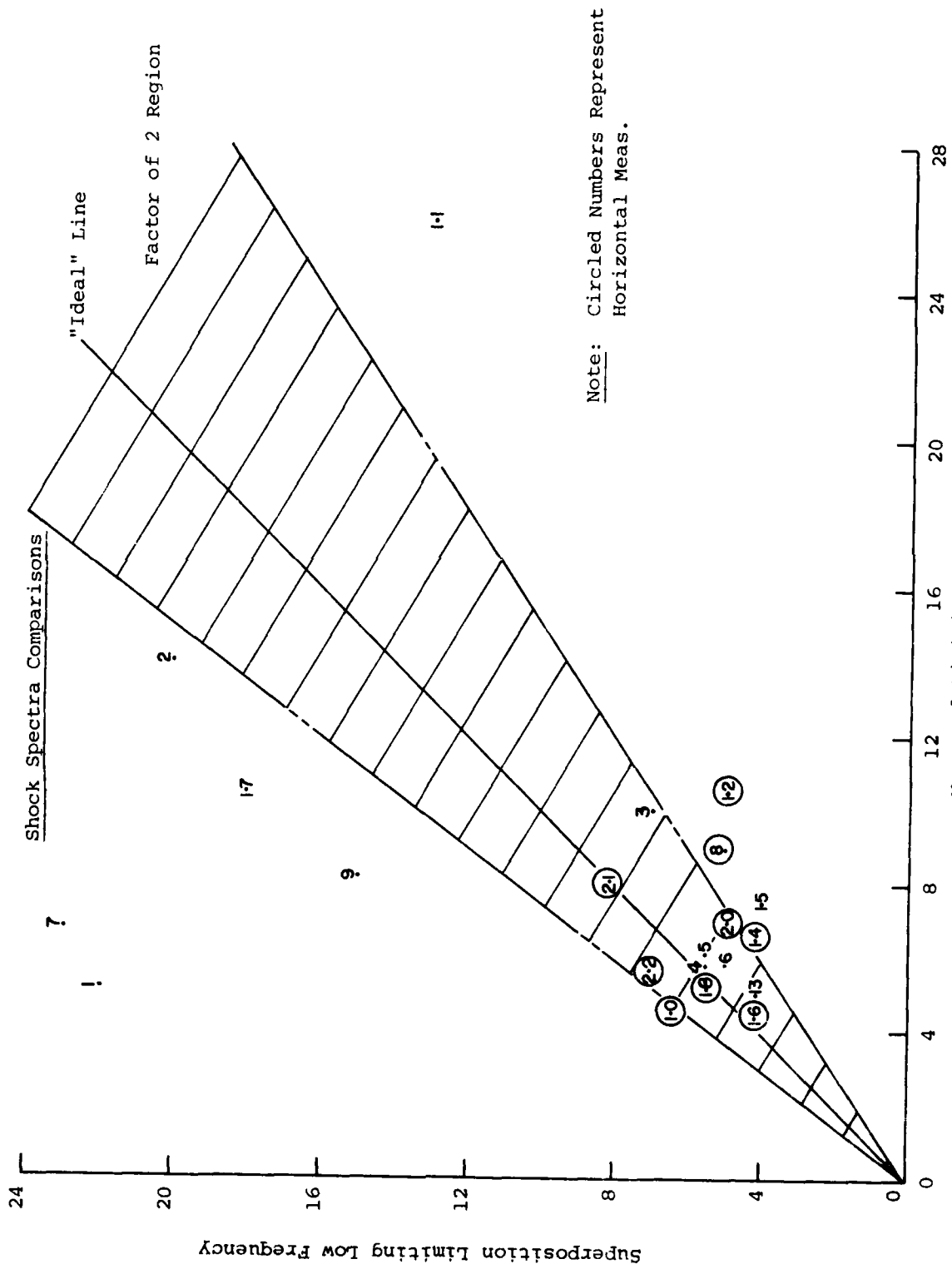


FIGURE B.4: Evaluation Plot of Limiting Low Frequencies - MBI-4

# MBI-4

## Shock Spectra Comparisons

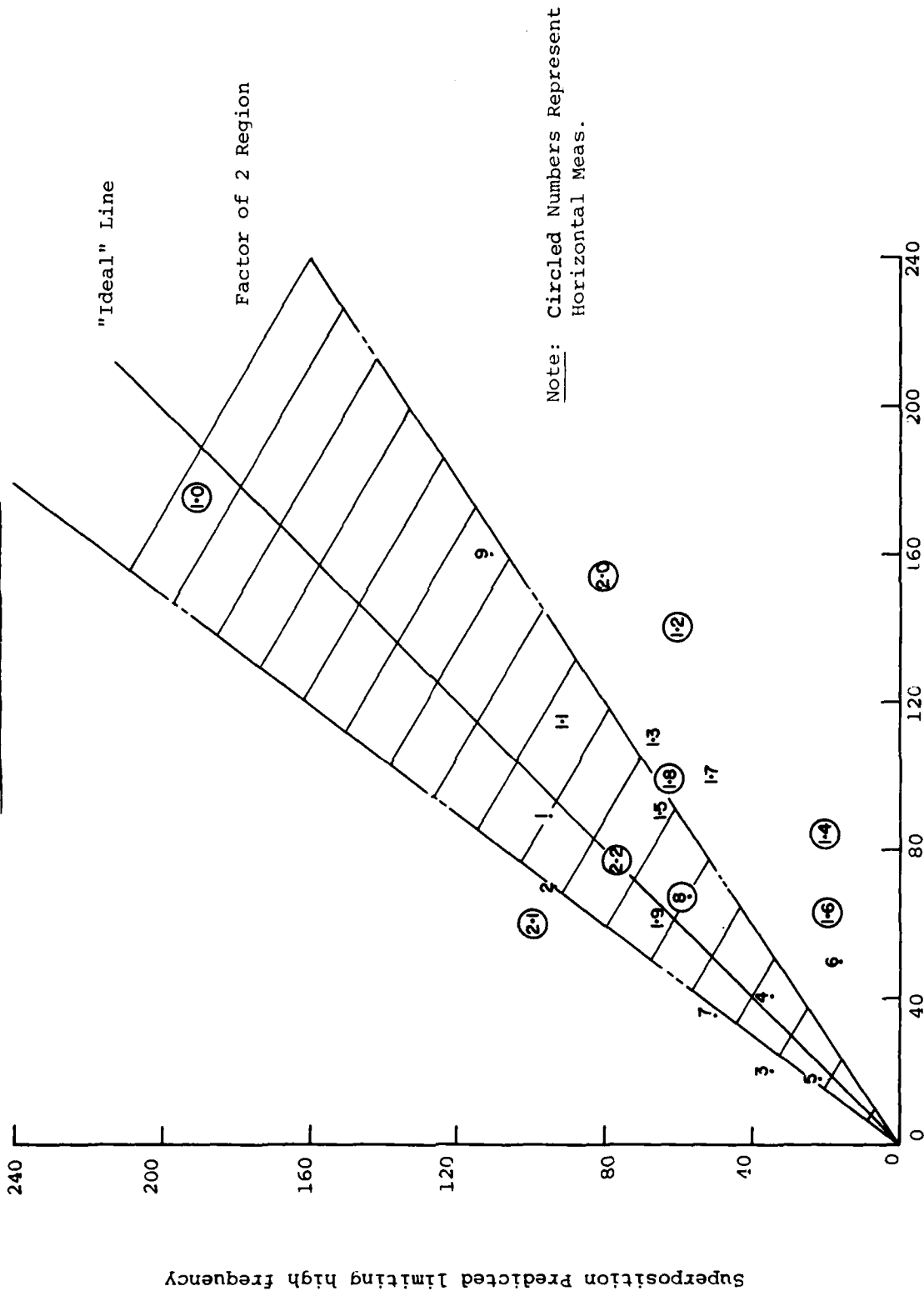


FIGURE B.5: Evaluation Plot of Limiting High Frequencies - MBI-4

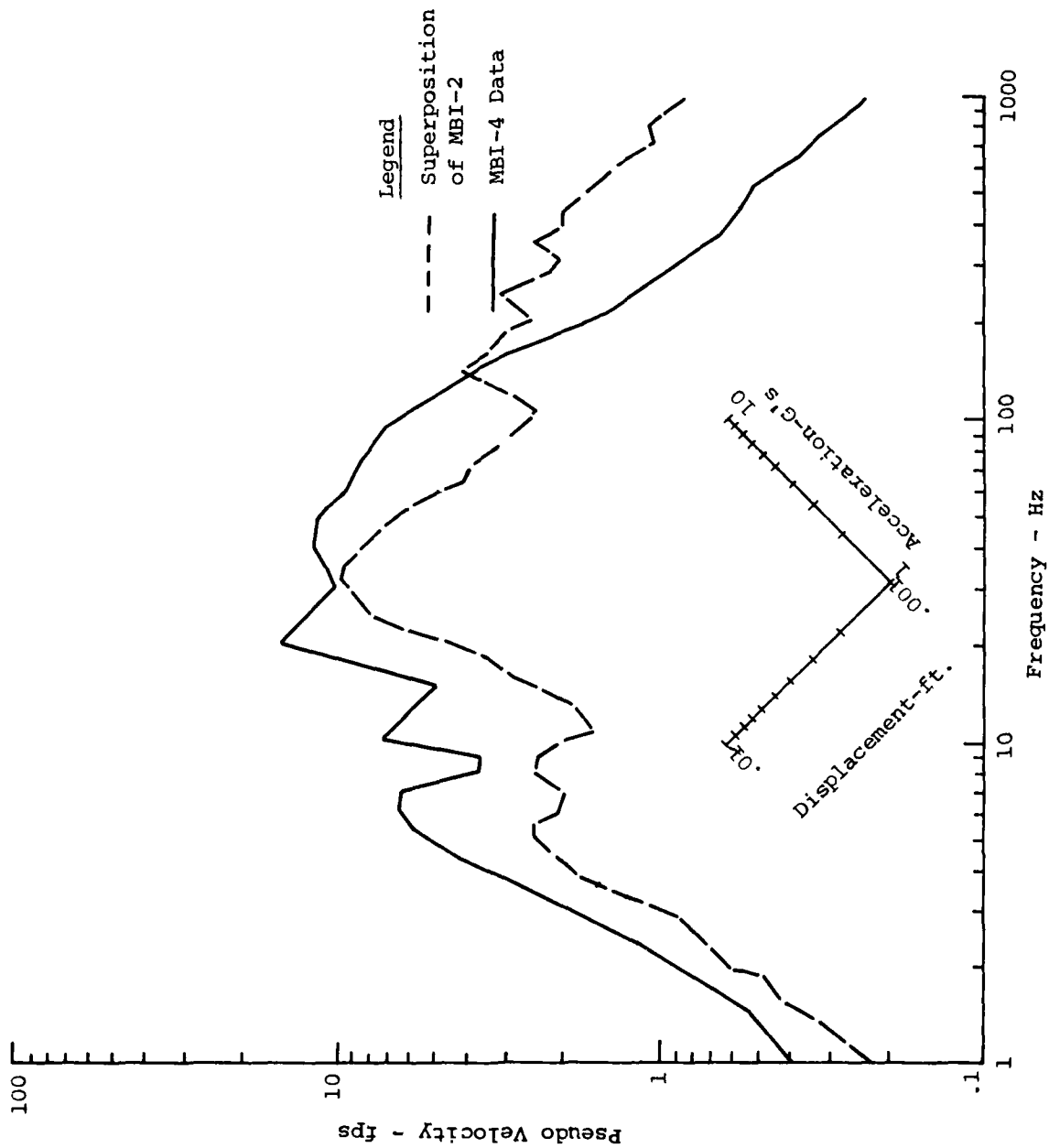


FIGURE B.6: Shock Spectra Comparison of MBI-4 and Superposition of MBI-2 @ 0/1.52/0 Vertical Velocity

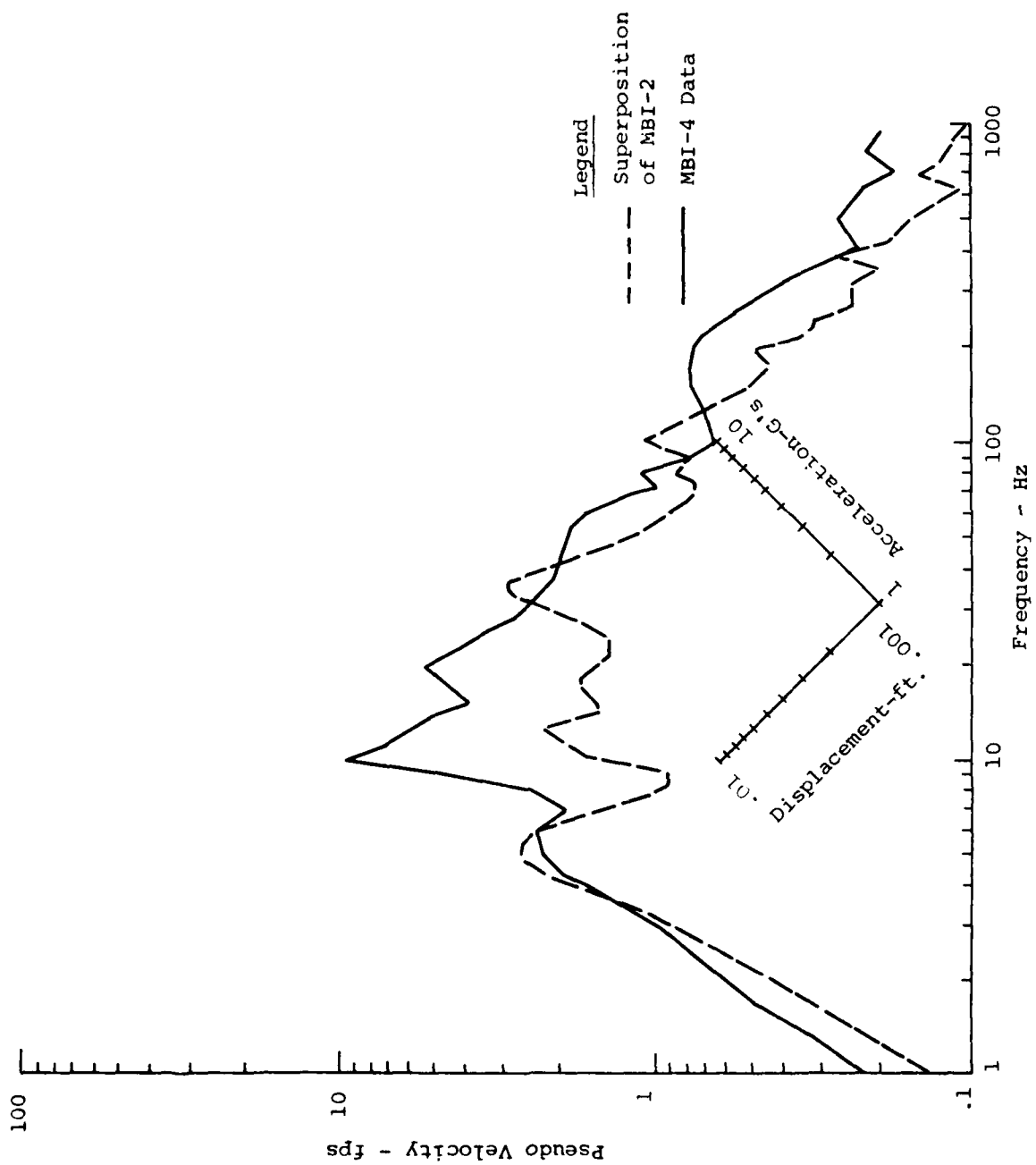


FIGURE B.7: Shock Spectra Comparison of MBI-4 and Superposition of MBI-2 @ 0/3.05/0 Vertical Velocity

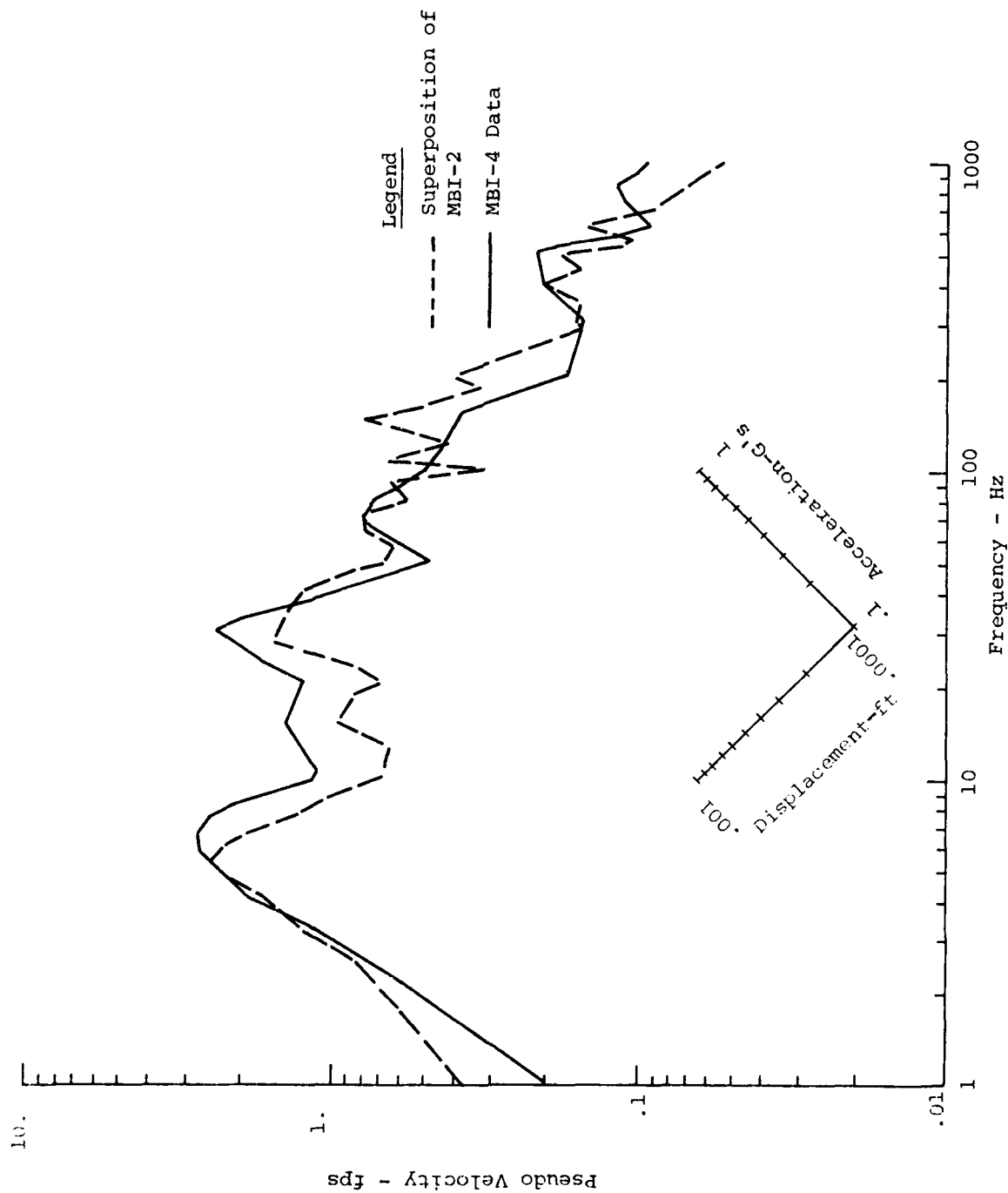


FIGURE B.8: Shock Spectra Comparison of MBI-4 and Superposition of MBI-2 @ 0/6.10/0 Vertical Velocity

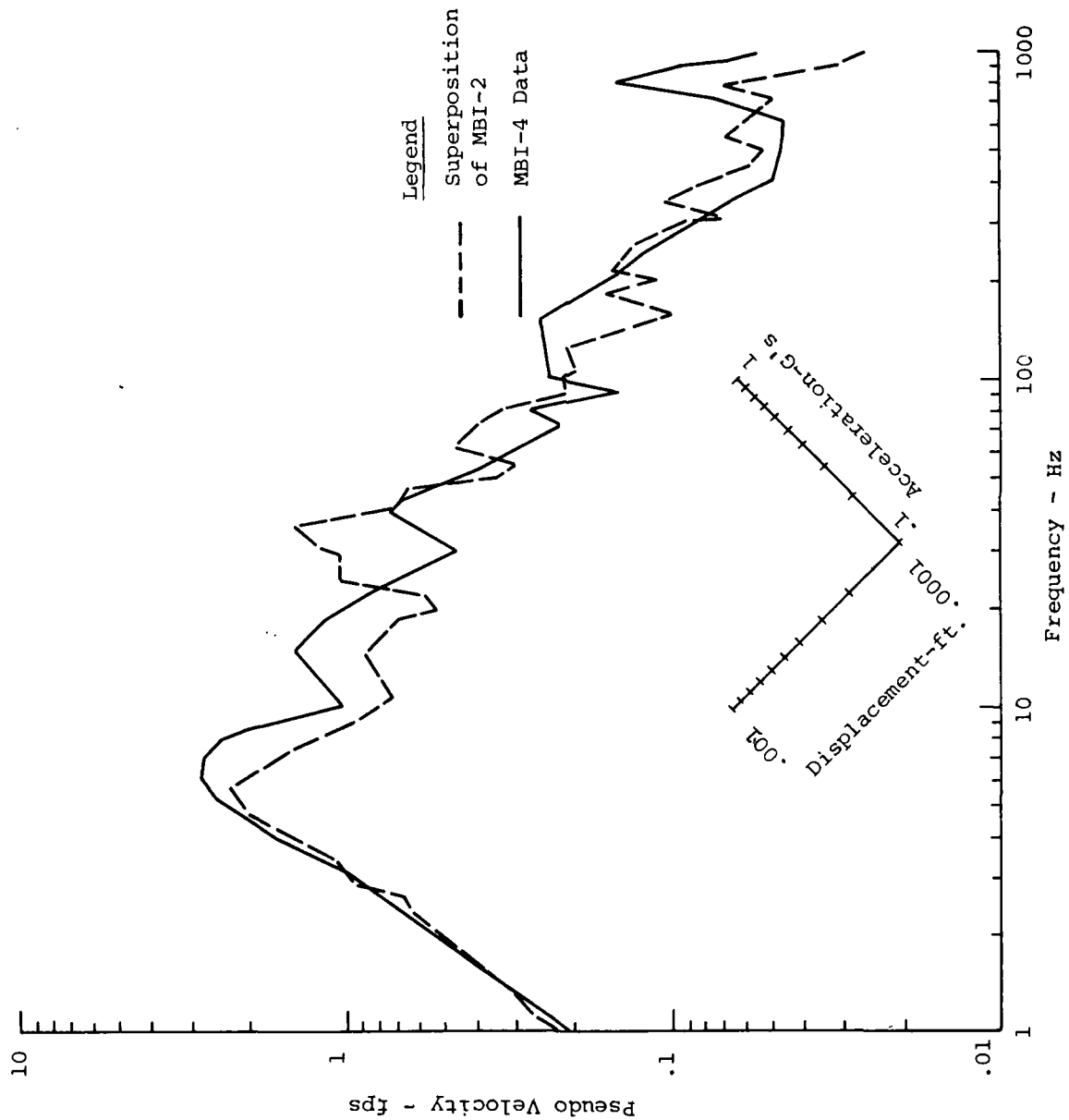


FIGURE B.9: Shock Spectra Comparison of MBI-4 and Superposition of MBI-2 @ 0/9.15/0 Vertical Velocity

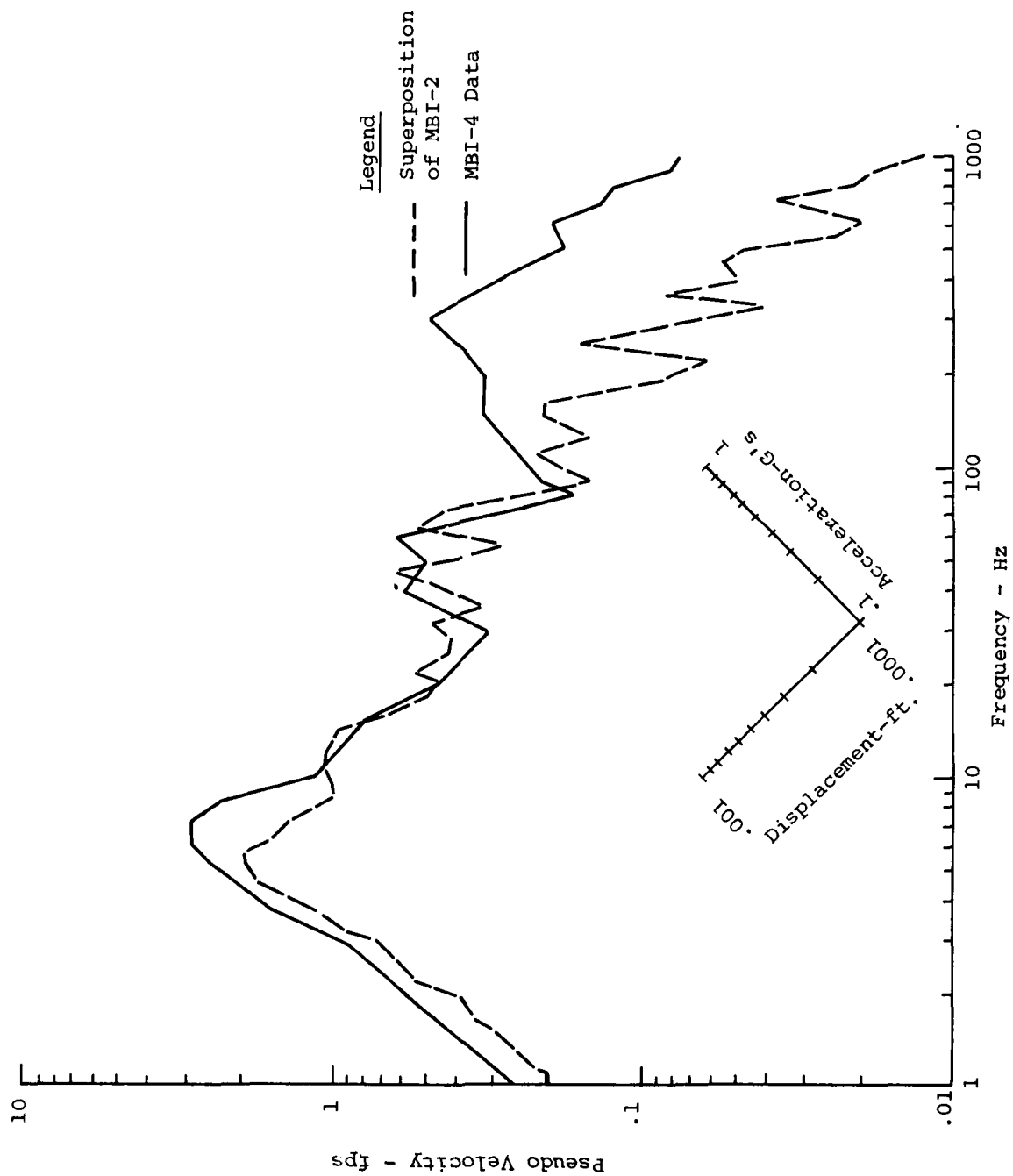


FIGURE B.10: Shock Spectra Comparison of MBI-4 and Superposition of MBI-2 @ 0/12.20/0 Vertical Velocity

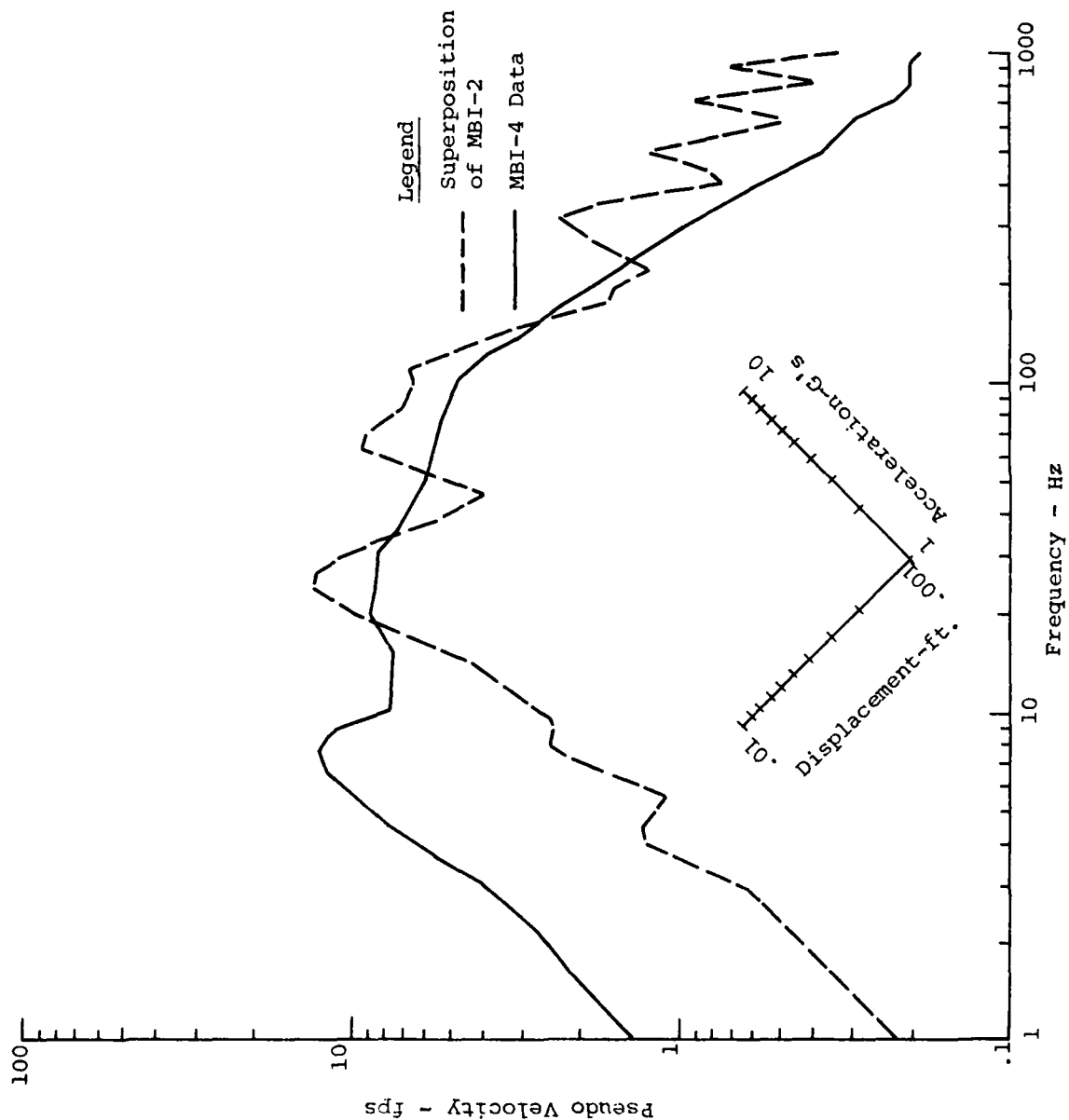


FIGURE B.11: Shock Spectra Comparison of MBI-4 and Superposition of MBI-2 @ 5.34/0.46/0 Vertical Velocity

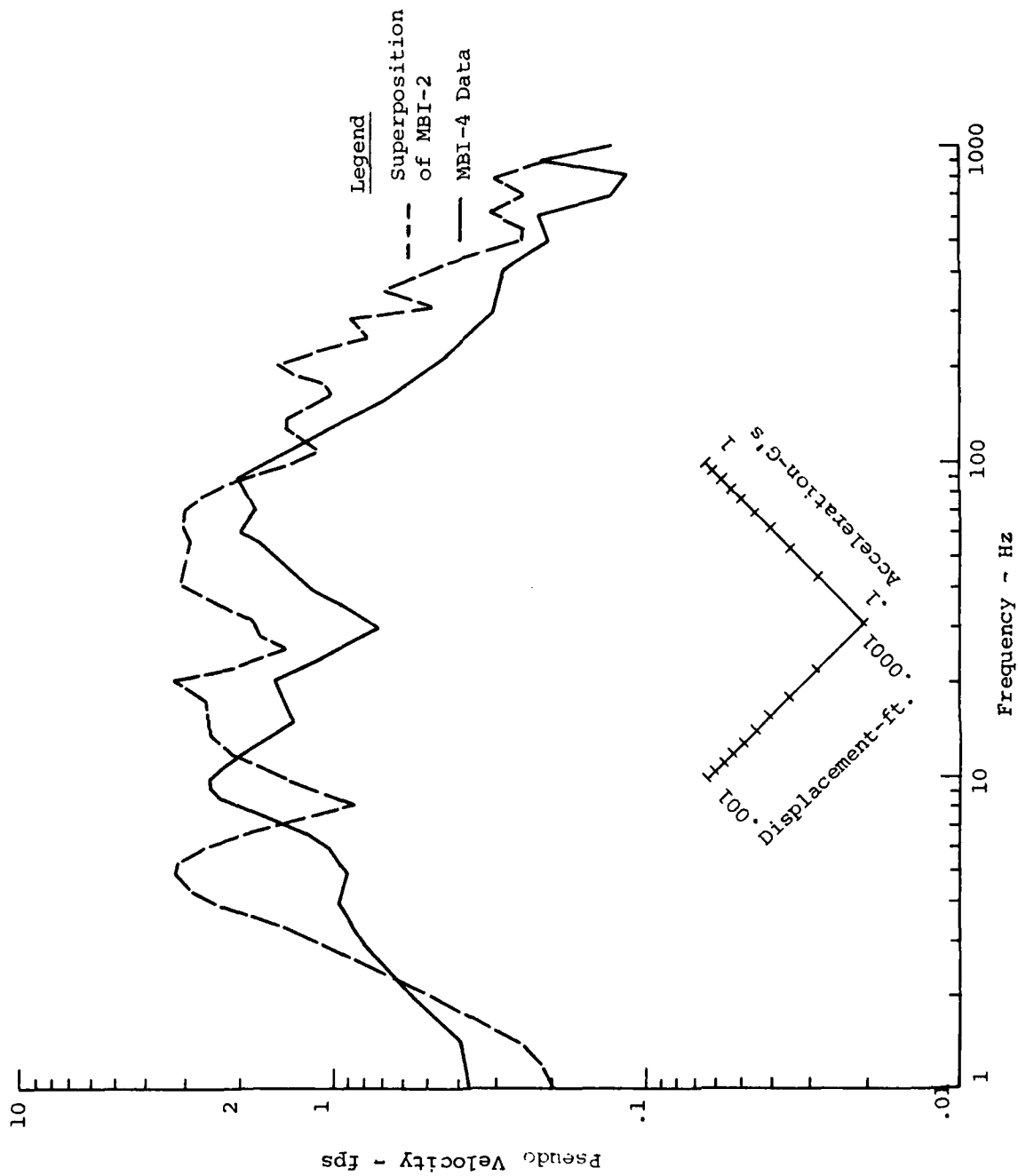


FIGURE B.12: Shock Spectra Comparison of MBI-4 and Superposition of MBI-2 @ 5.34/0.46/0 Horizontal Velocity

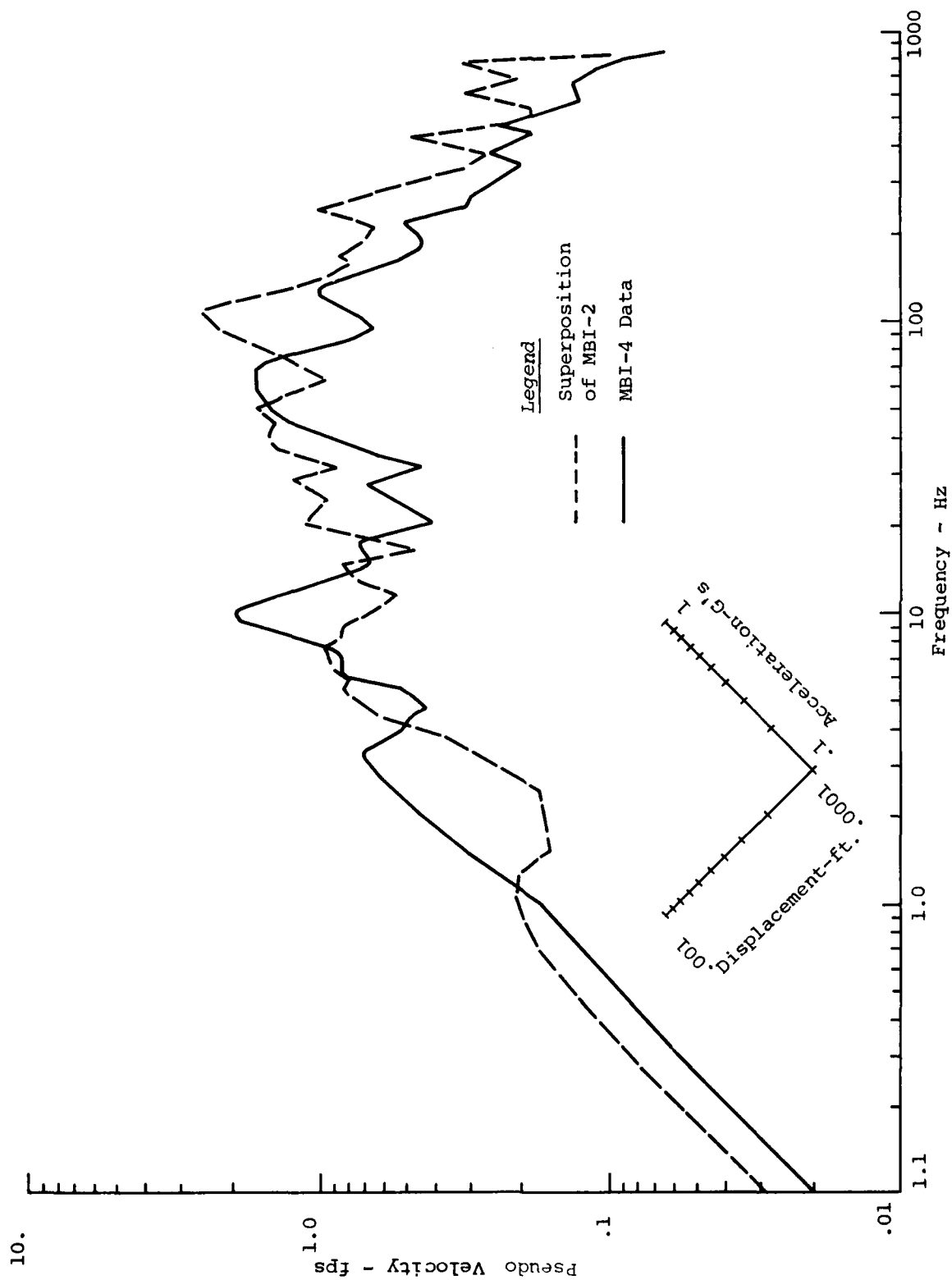


FIGURE B.13: Shock Spectra Comparison of MBI-4 and Superposition of MBI-2 @ 5.34/0.46/270 Horizontal Velocity

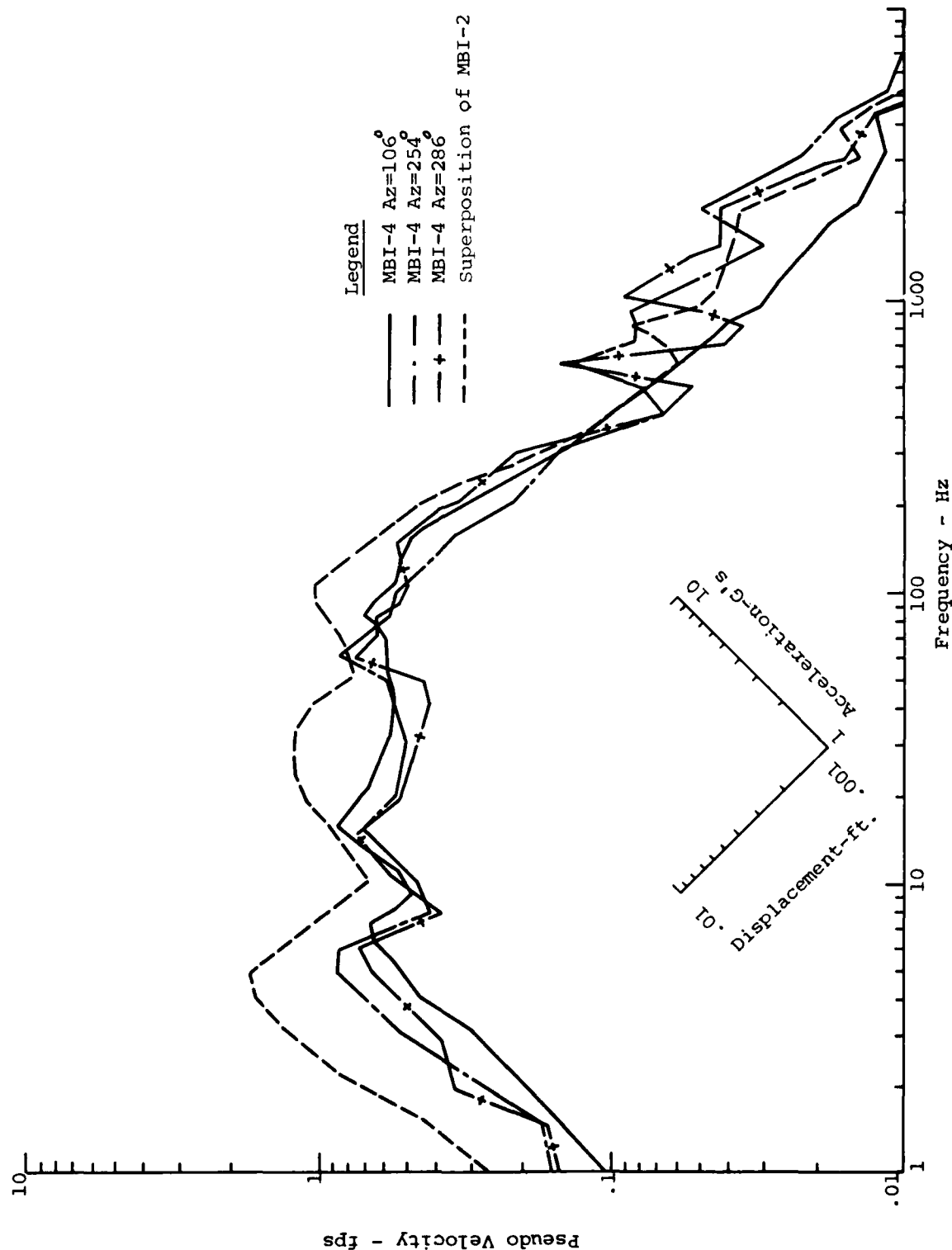


FIGURE B.14: Shock Spectra Comparison of MBI-4 and Superposition of MBI-2 @ 19.25/0.46/ Vertical Velocity

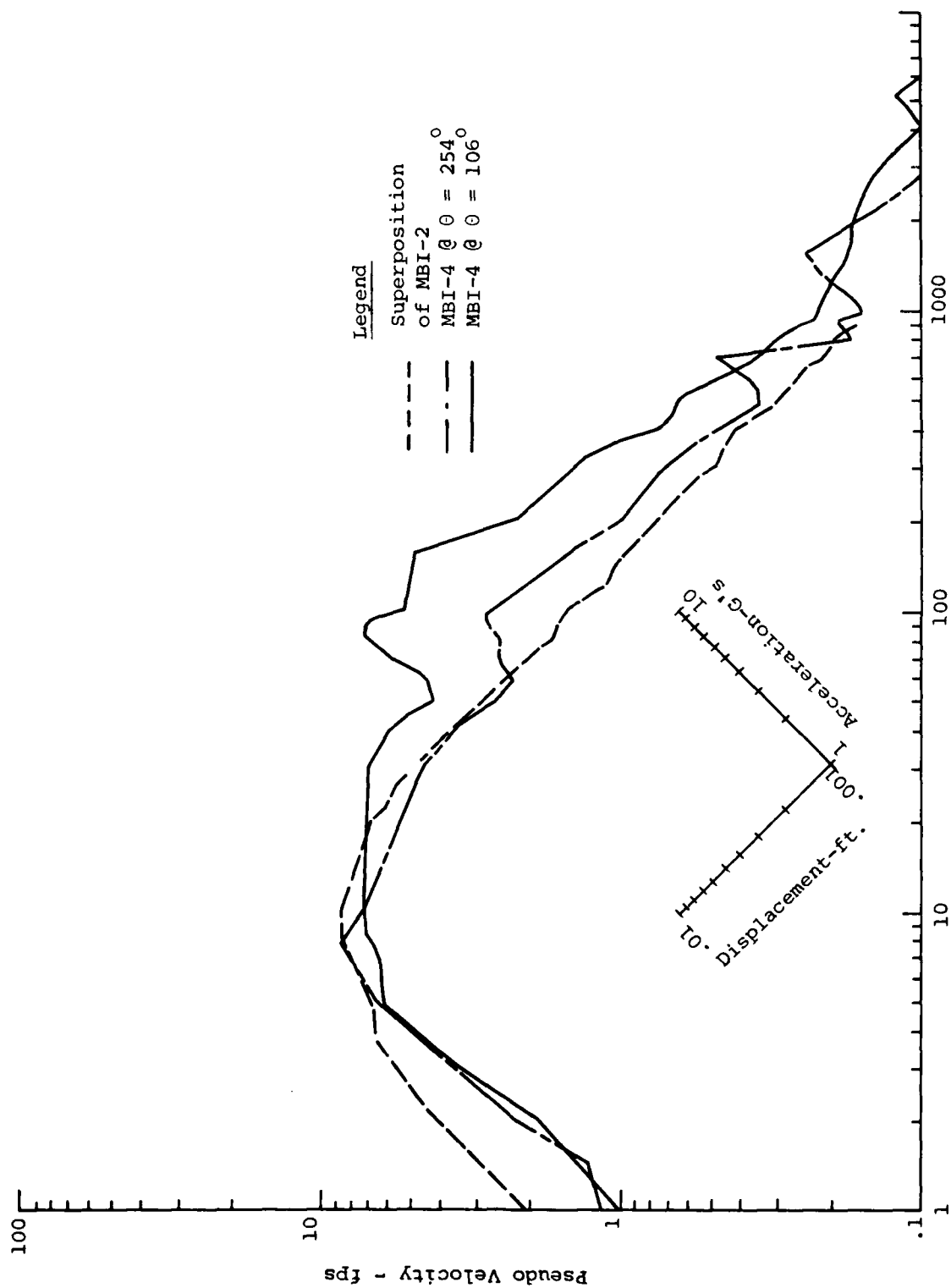


FIGURE B.15: Shock Spectra Comparison of MBI-4 and Superposition of MBI-2 @ 19.25/0.46/ Horizontal Velocity

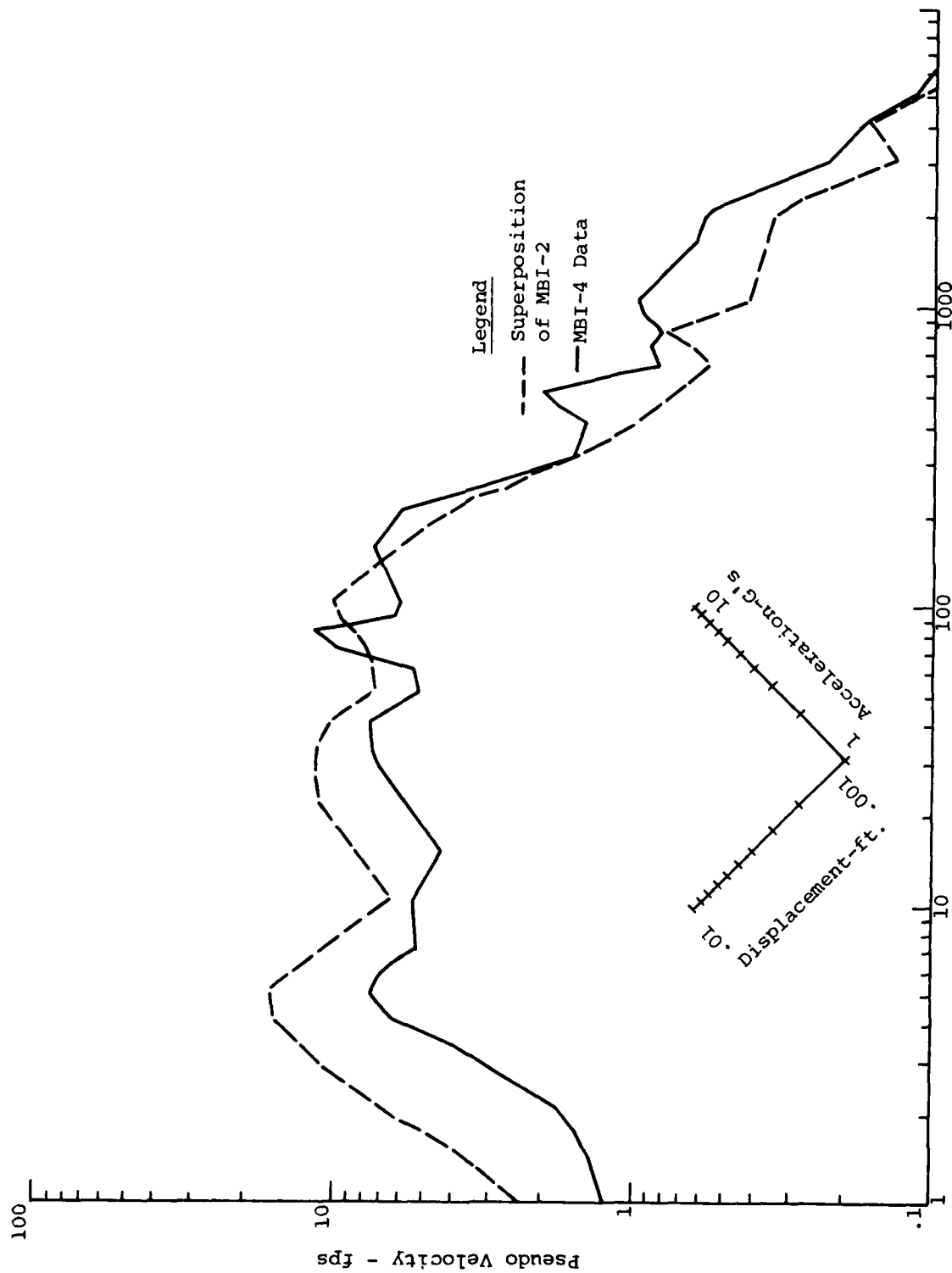


FIGURE B.16: Shock Spectra Comparison of MBI-4 and Superposition of MBI-2 @ 26.69/0.46/0 Vertical Velocity

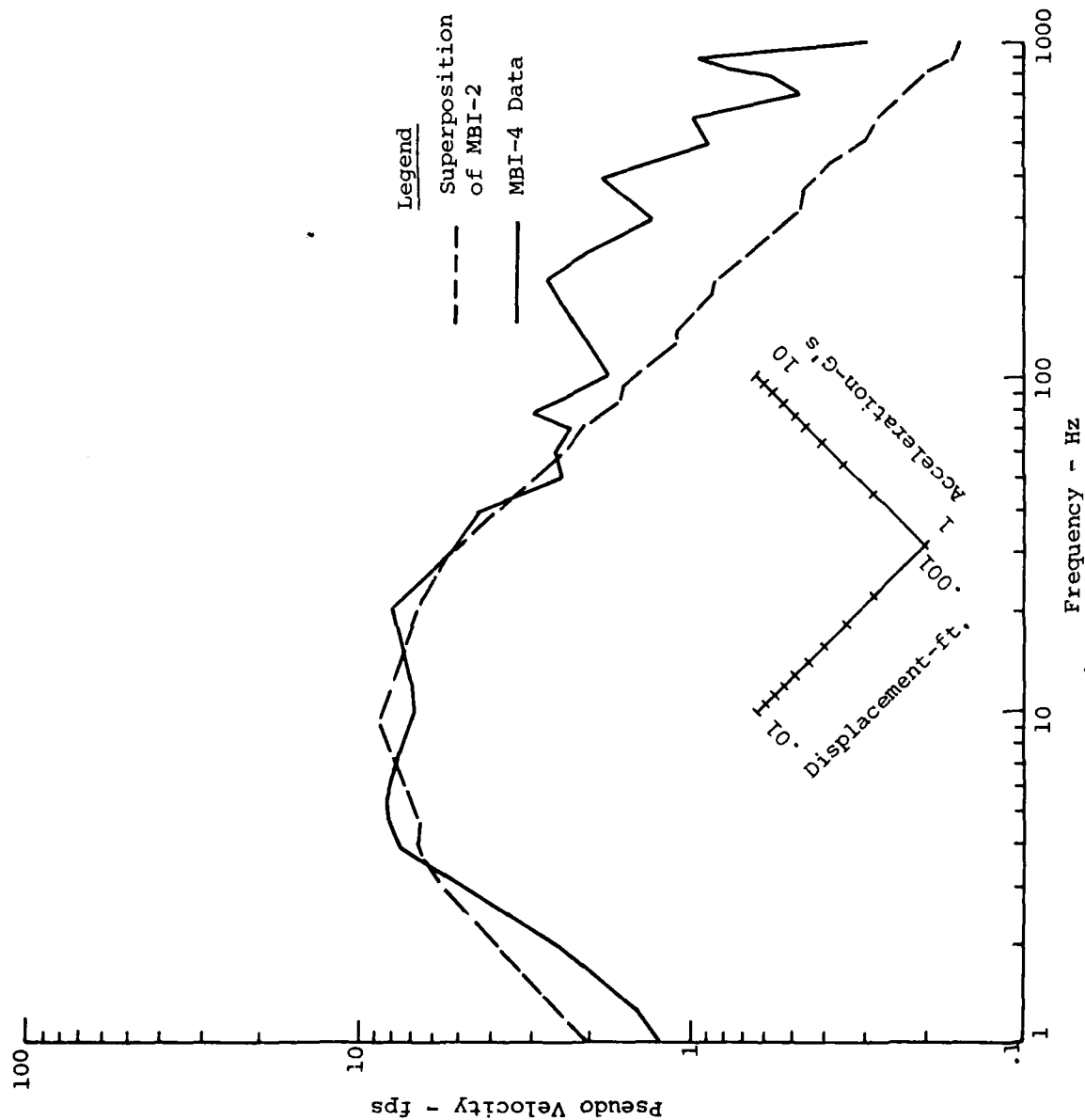


FIGURE B.17: Shock Spectra Comparison of MBI-4 and Superposition of MBI-2 @ 26.69/0.46/0 Horizontal Velocity

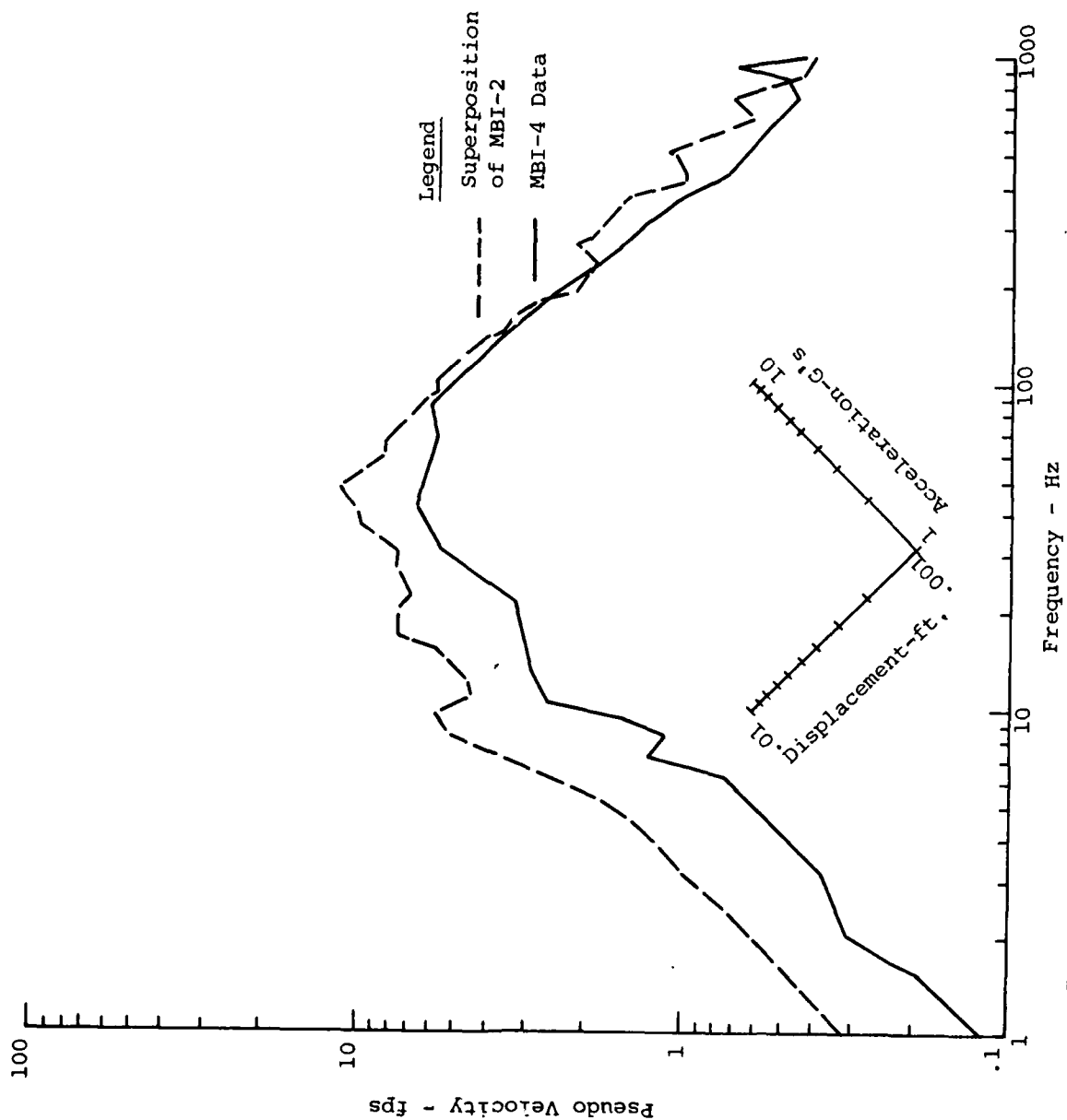


FIGURE B.18: Shock Spectra Comparison of MBI-4 and Superposition of MBI-2 @ 32.03/0.46/0 Vertical Velocity

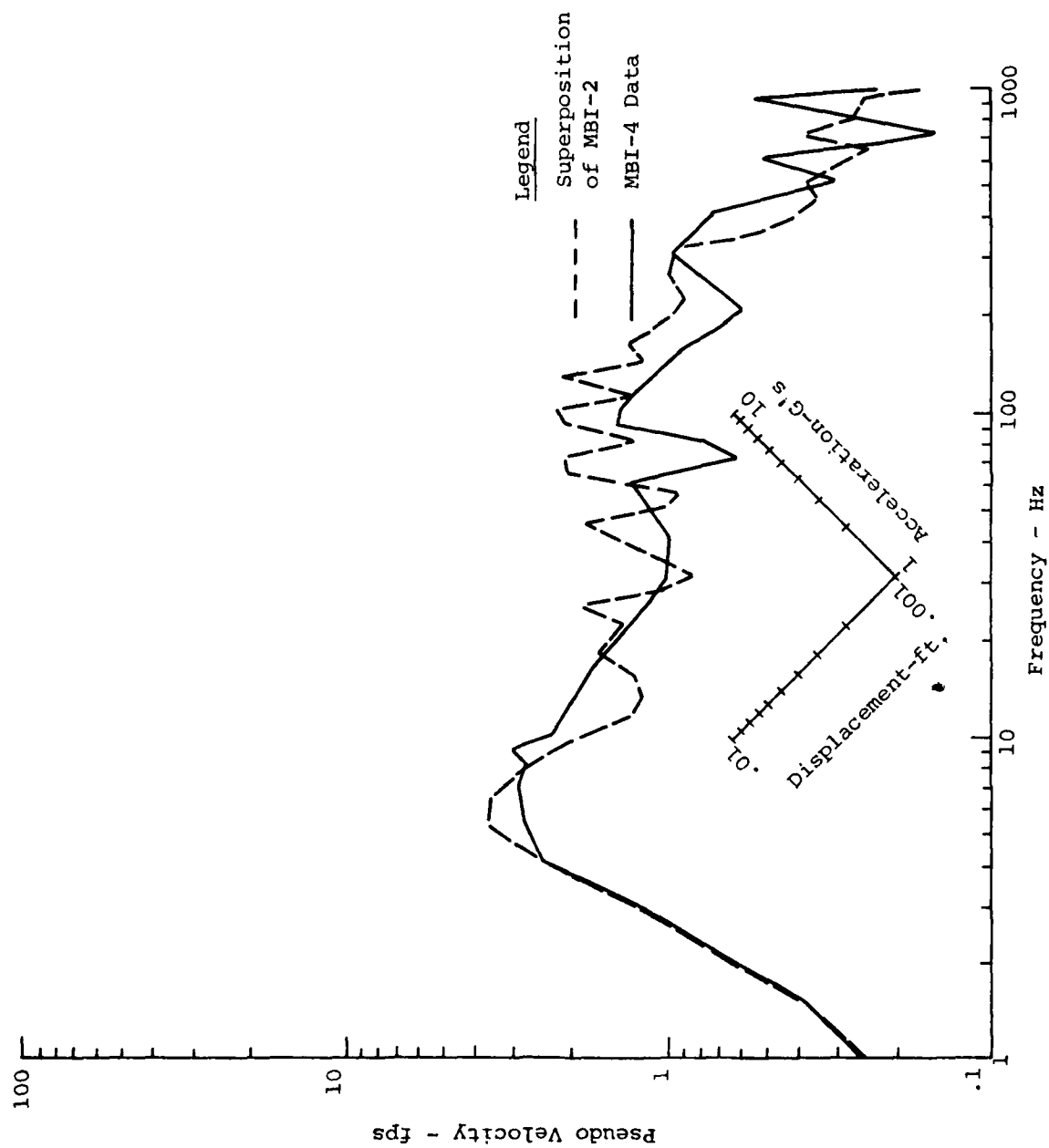


FIGURE B.19: Shock Spectra Comparison of MBI-4 and Superposition of MBI-2 @ 32.03/0.46/0 Horizontal Velocity

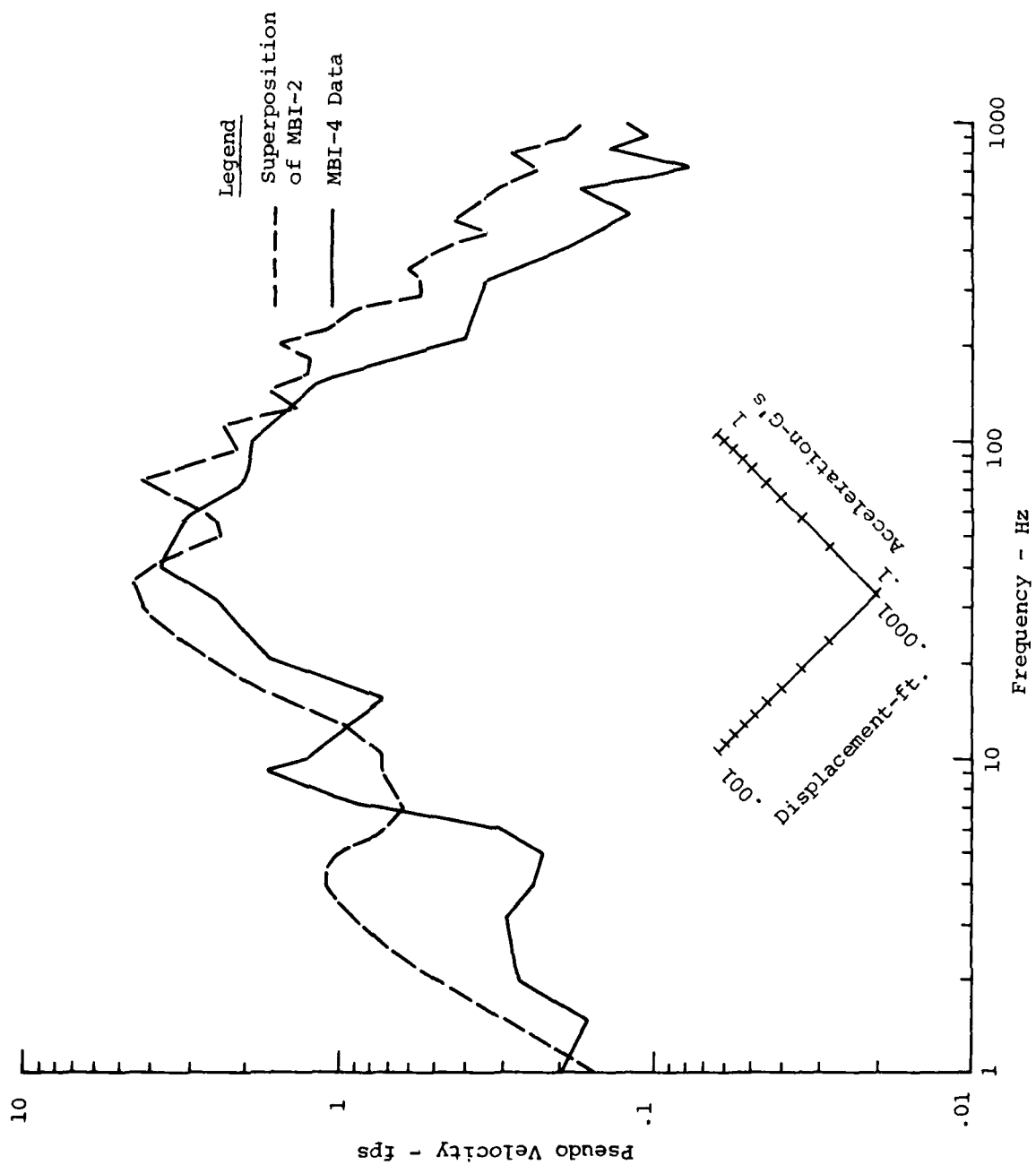
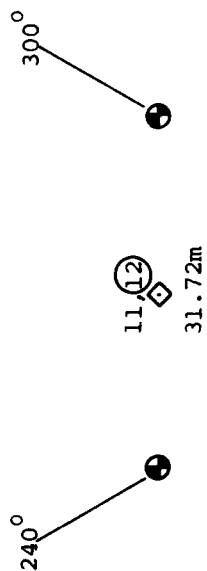


FIGURE B.20: Shock Spectra Comparison of MBI-4 and Superposition of MBI-2 @ 42.70/0.46/0 Vertical Velocity



MBI-6

NOTES

1. Numbers above gage locations correspond to those plotted on shock spectra comparisons
2. Circled numbers indicate horizontal measurements
3. All depths excluding center are .46m depth
4. Depths at center are:

Number	Depth
1	.46m
2	1.52m
3	3.05m
4	6.10m
5	9.15m
6	12.20m

FIGURE B.21: Location of Shock Spectra Comparisons for MBI-6

MBI-6  
Shock Spectra Comparisons

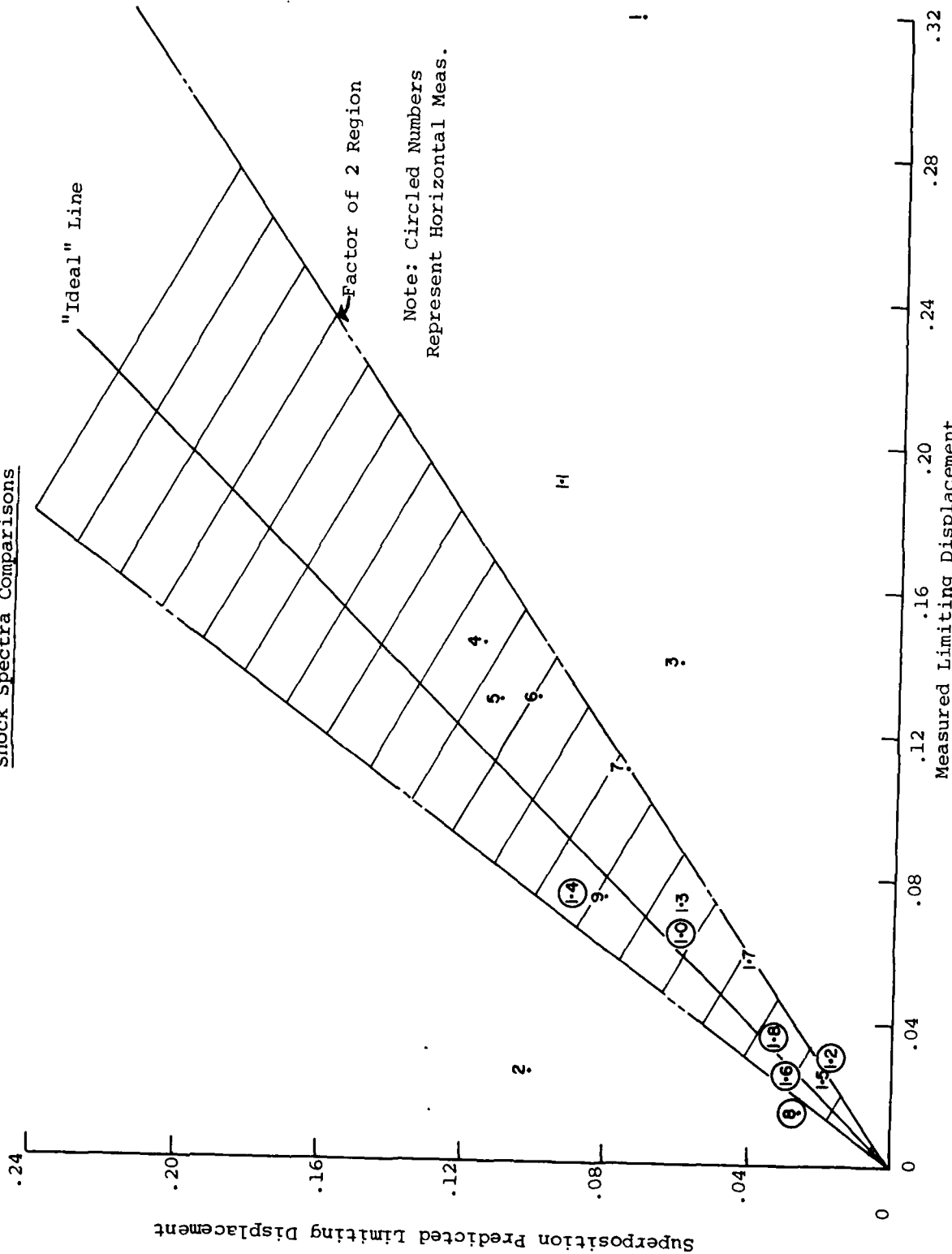


FIGURE B.22: Evaluation Plot of Limiting Displacements - MBI-6

# MBI-6

## Shock Spectra Comparisons

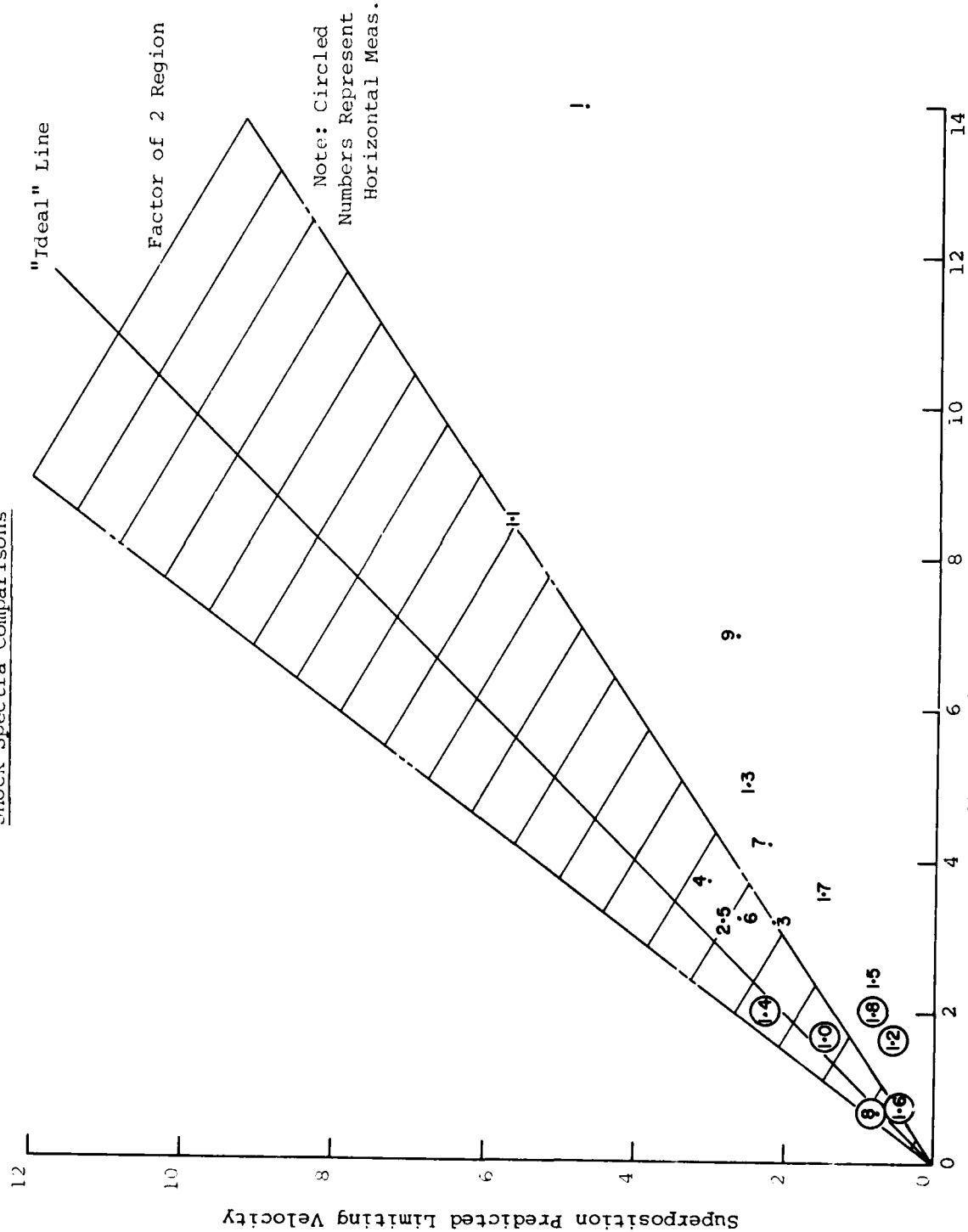


FIGURE B.23: Evaluation Plot of Limiting Velocities - MBI-6

MBI-6  
Shock Spectra Comparisons

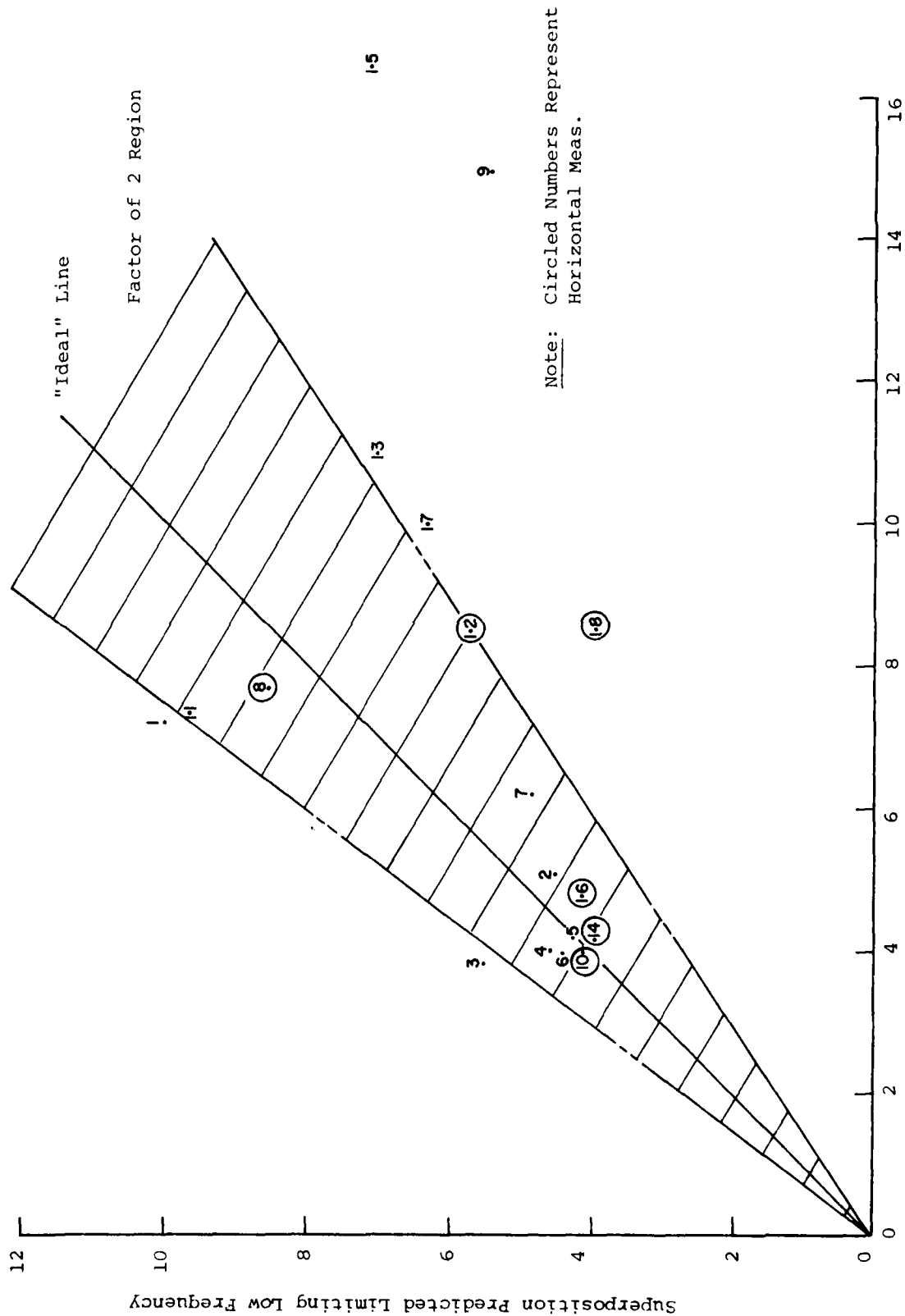


FIGURE B.24: Evaluation Plot of Limiting Low Frequencies - MBI-6

MBI-6

Shock Spectra Comparisons

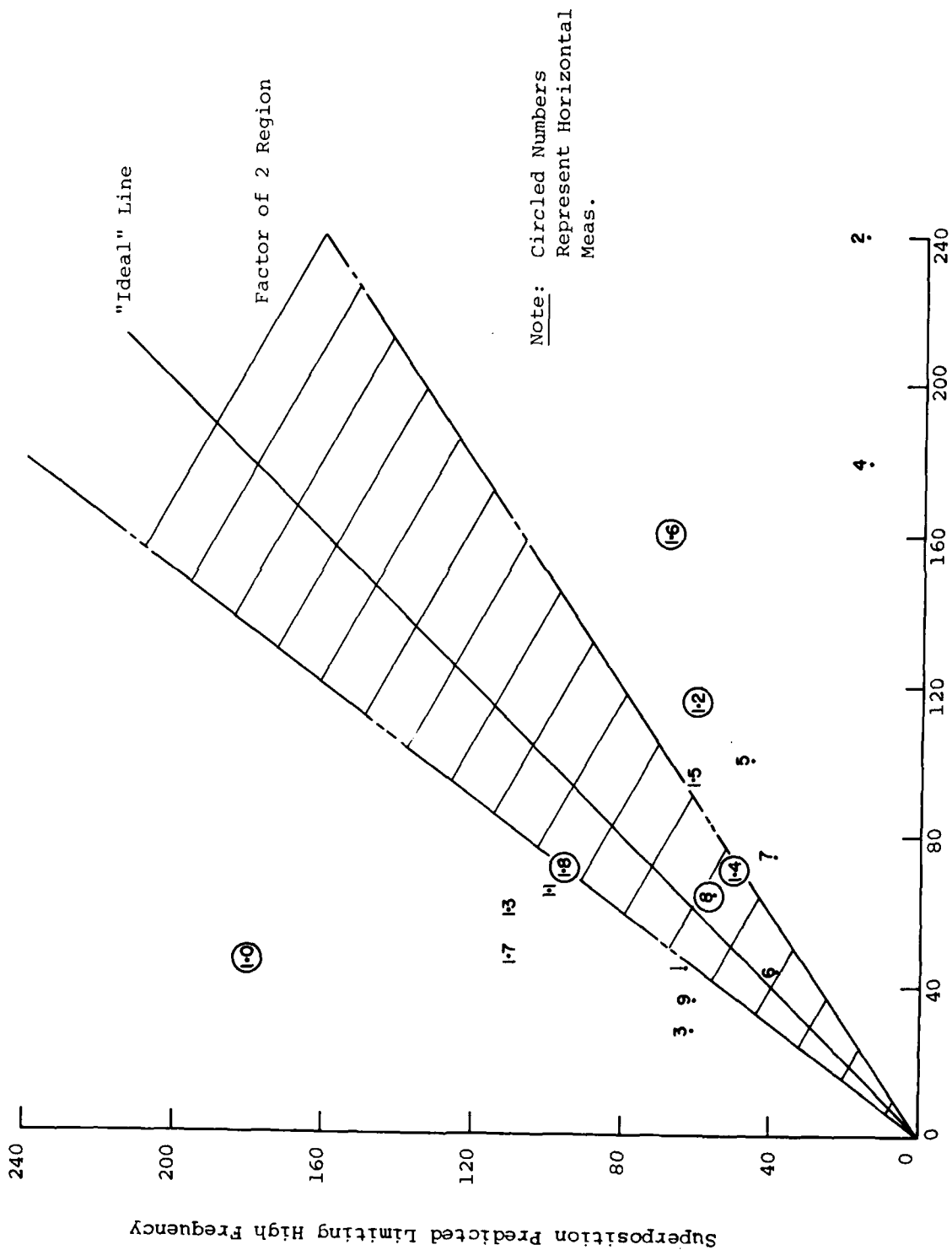


FIGURE B.25: Evaluation Plot of Limiting High Frequencies - MBI-6

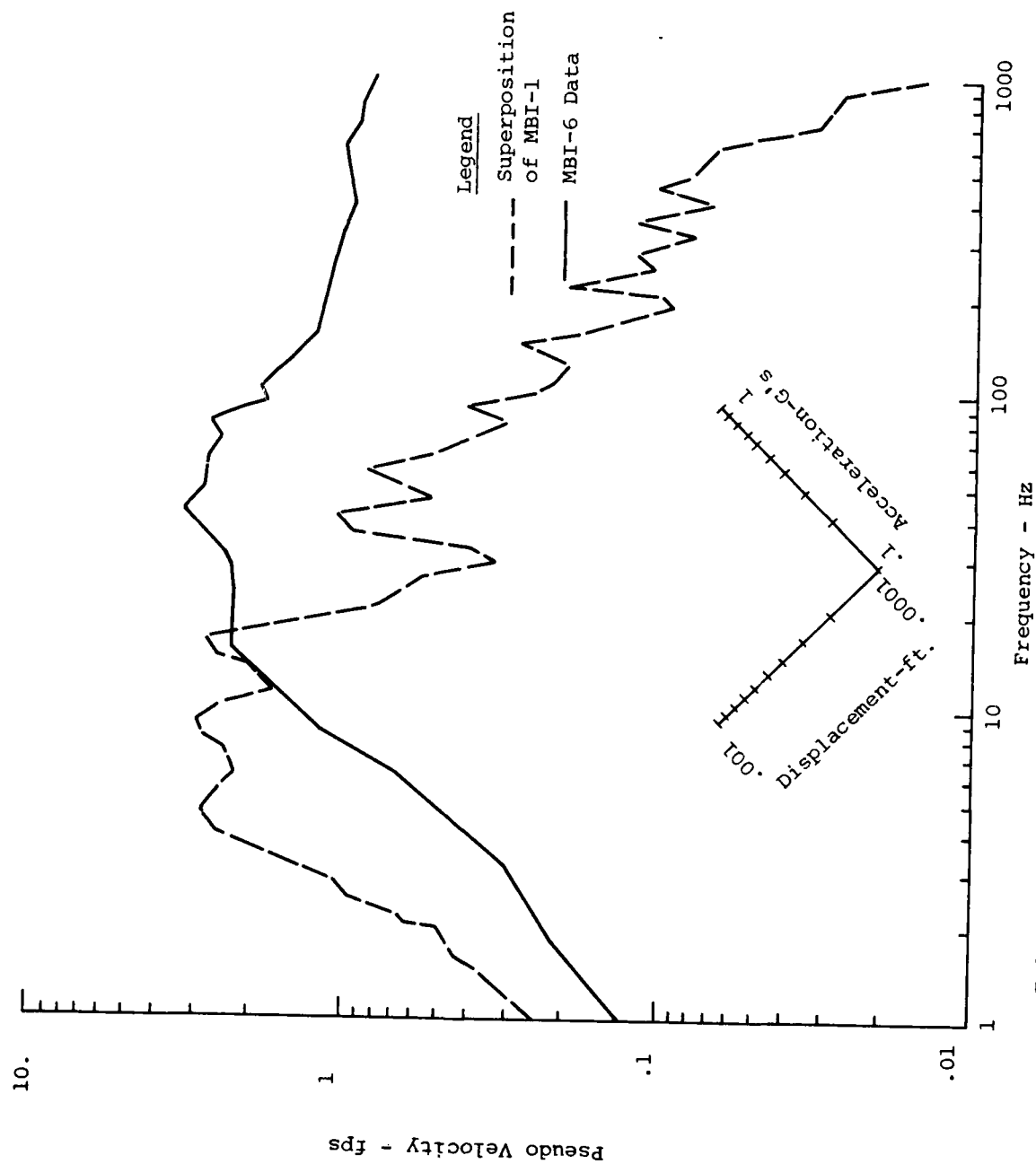


FIGURE B.26: Shock Spectra Comparison of MBI-6 and Superposition of MBI-1 @ 0/1.52/0 Vertical Velocity

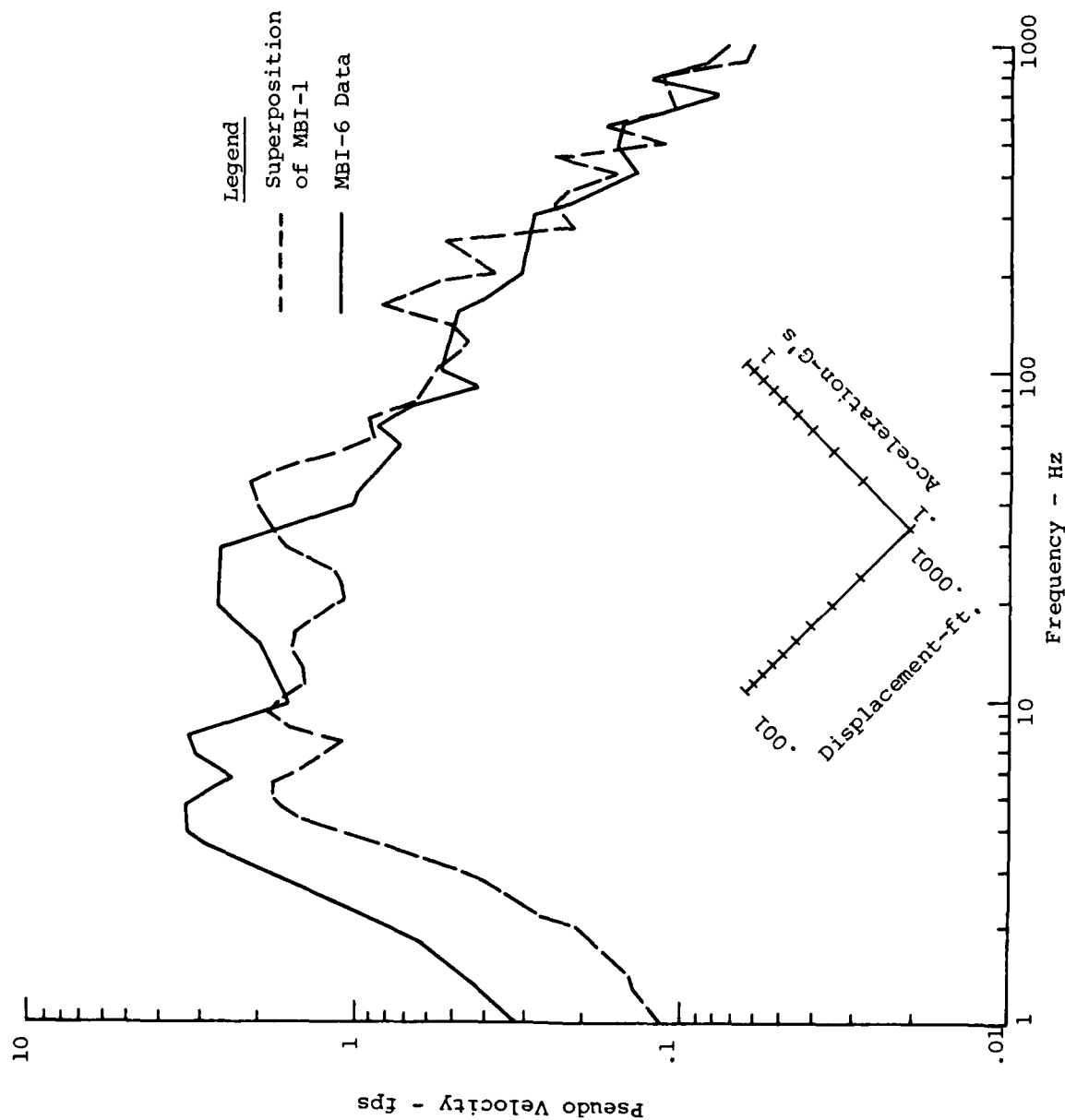


FIGURE B.27: Shock Spectra Comparison of MBI-6 and Superposition of MBI-1 @ 0/3.05/0 Vertical Velocity

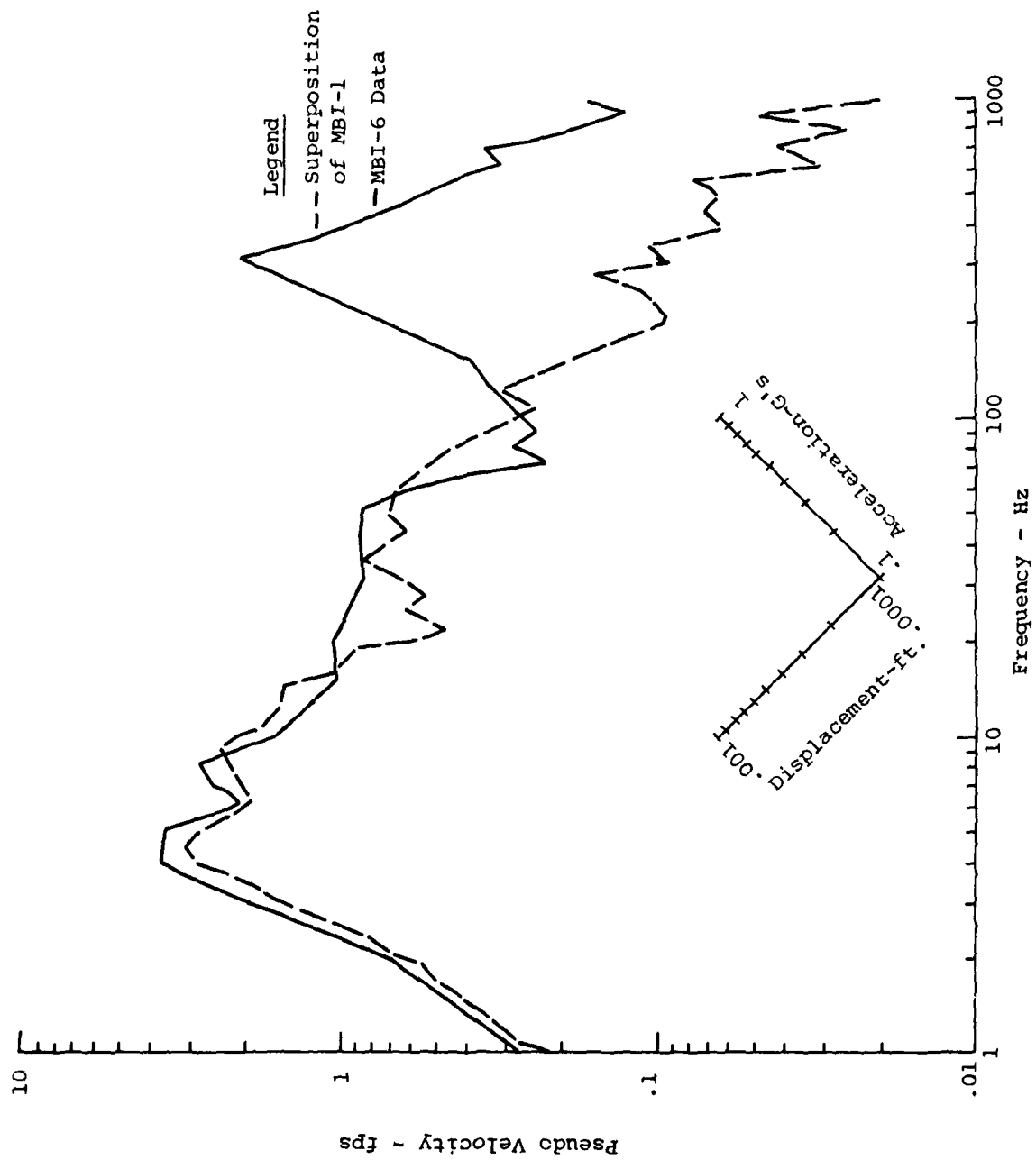


FIGURE B.28 Shock Spectra Comparison of MBI-6 and Superposition of MBI-1 @ 0/6.10/0 Vertical Velocity

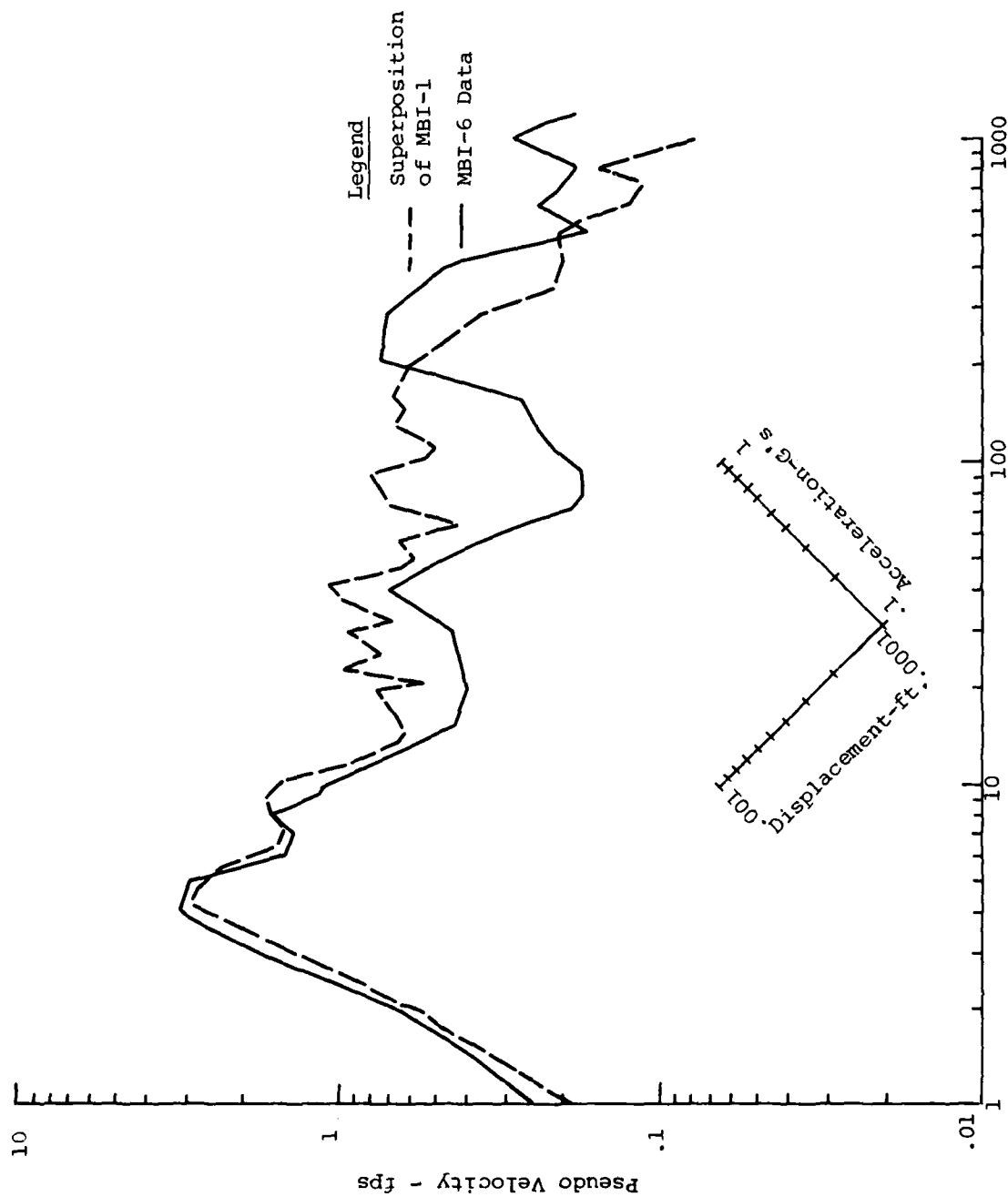


FIGURE B.29: Shock Spectra Comparison of MBI-6 and Superposition of MBI-1 @ 0/9.15/0 Vertical Velocity

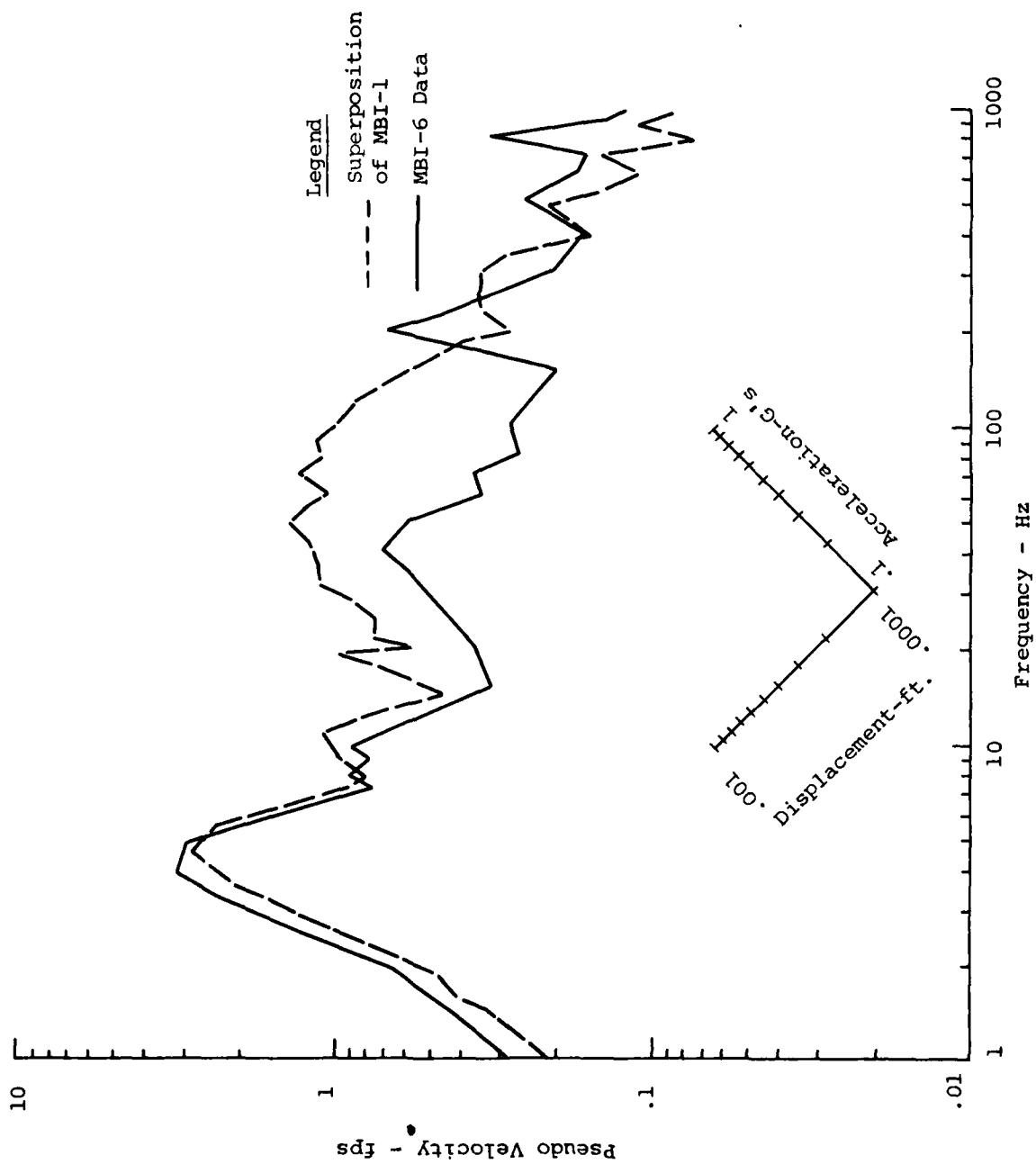


FIGURE B.30 Shock Spectra Comparison of MBI-6 and Superposition of MBI-1 @ 0/12.20/0 Vertical Velocity

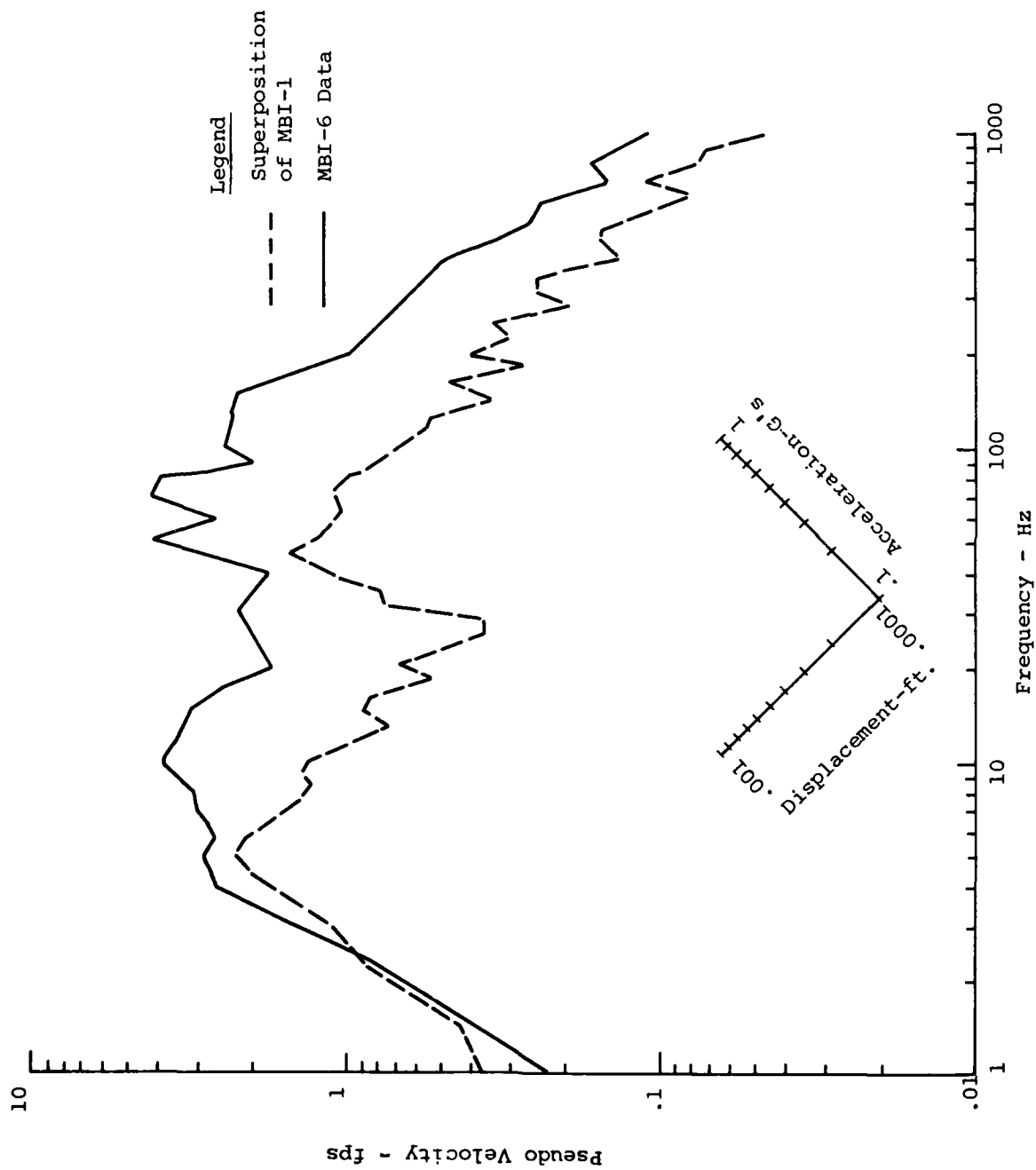


FIGURE B.31: Shock Spectra Comparison of MBI-6 and Superposition of MBI-1 @ 9.15/0.46/0 Vertical Velocity

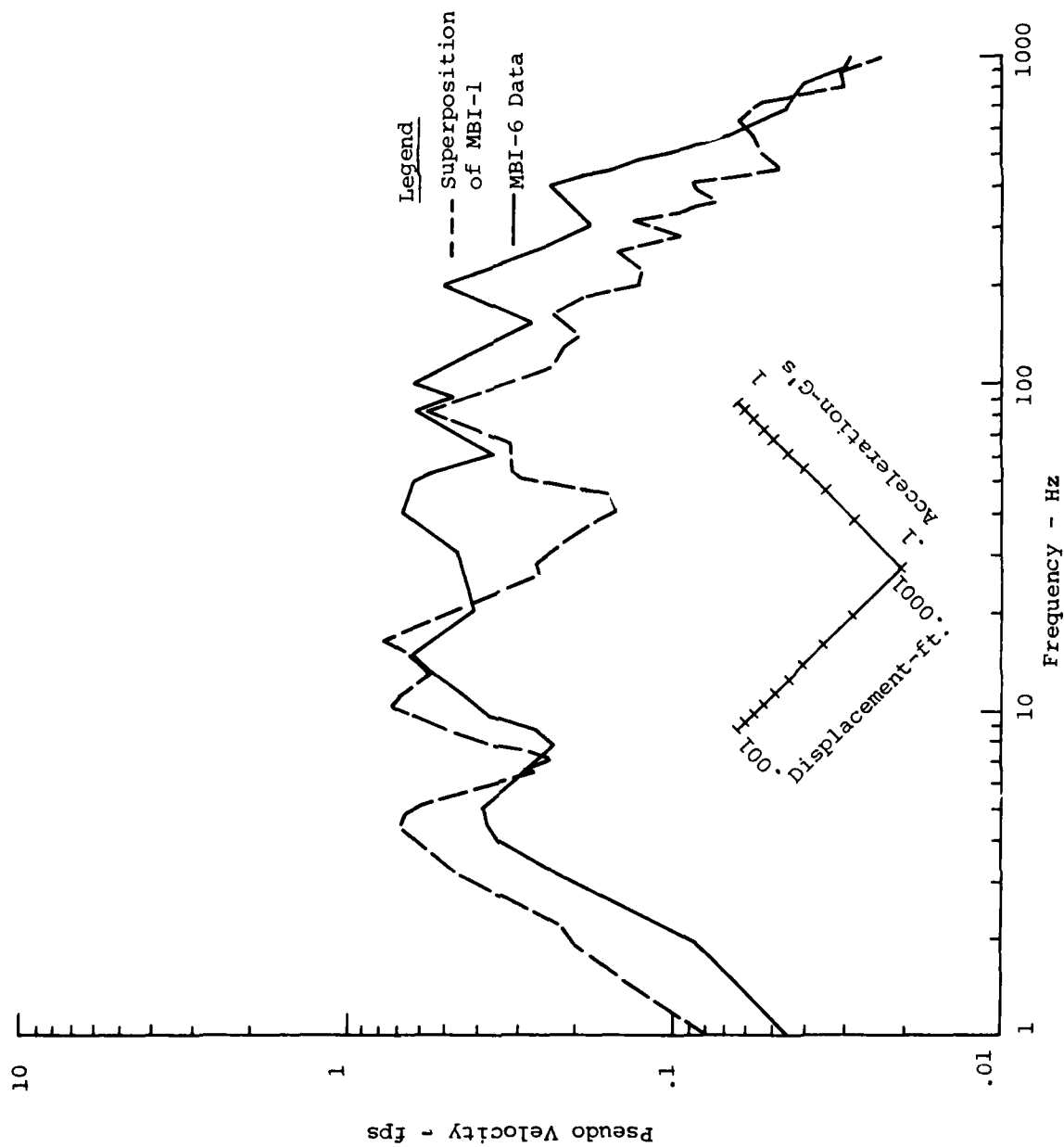


FIGURE B.32: Shock Spectra Comparison of MBI-6 and Superposition of MBI-1 @ 9.15/0.46/0 Vertical Velocity

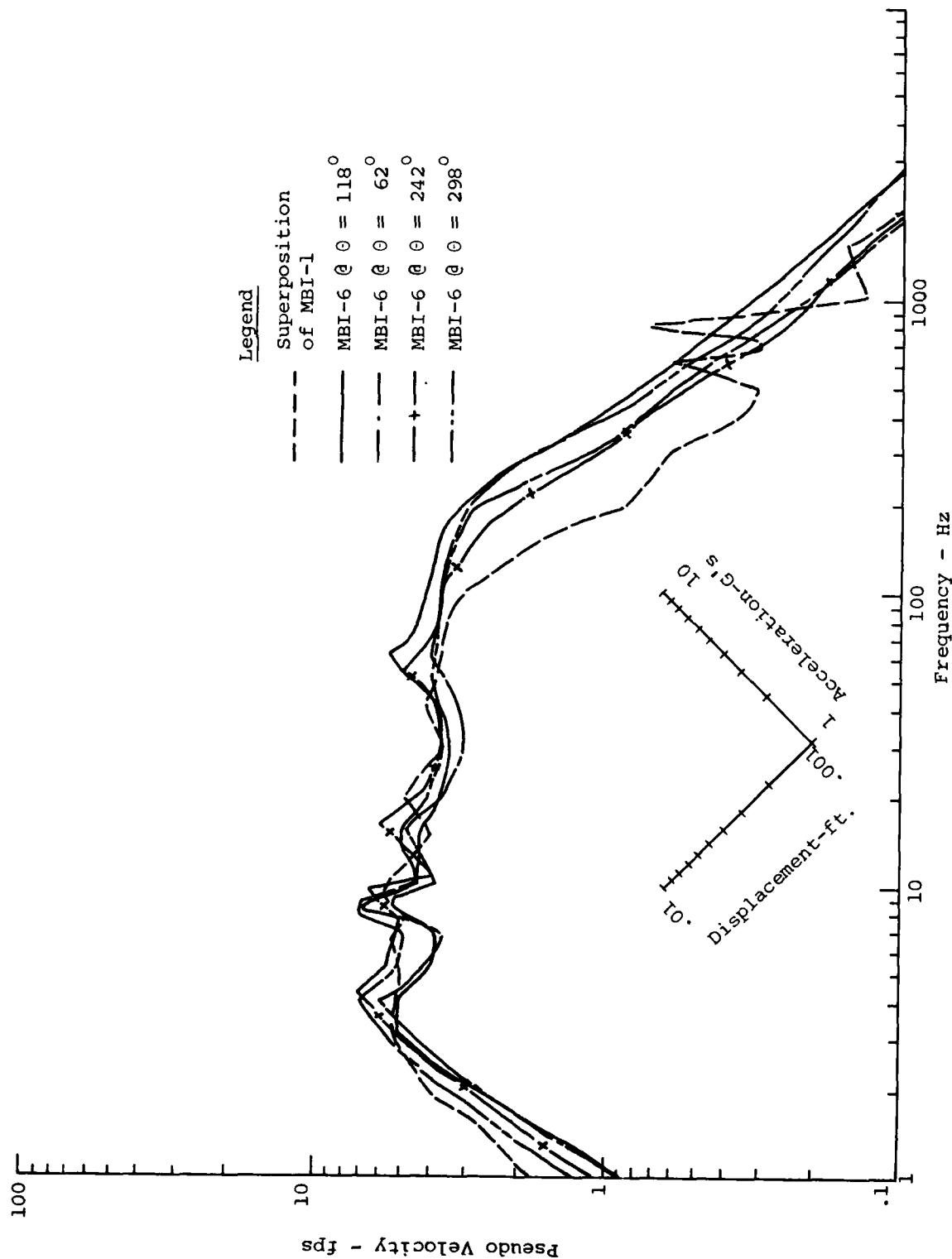


FIGURE B.33: Shock Spectra Comparison of MBI-6 and Superposition of MBI-1 @ 32.94/0.46/ Vertical Velocity

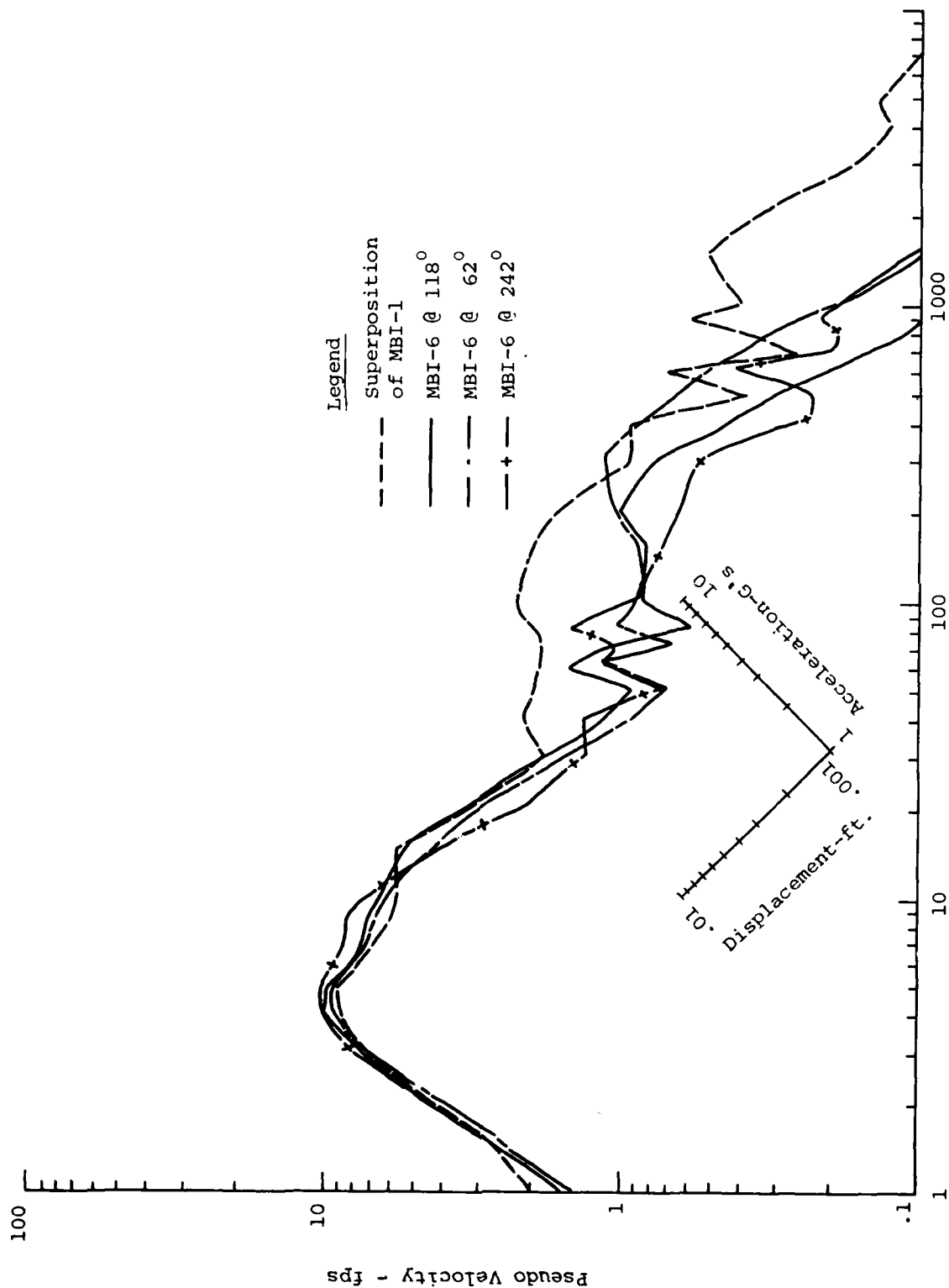


FIGURE B.34: Shock Spectra Comparison of MBI-6 and Superposition of MBI-1 @ 32.94/0.46/ Horizontal Velocity

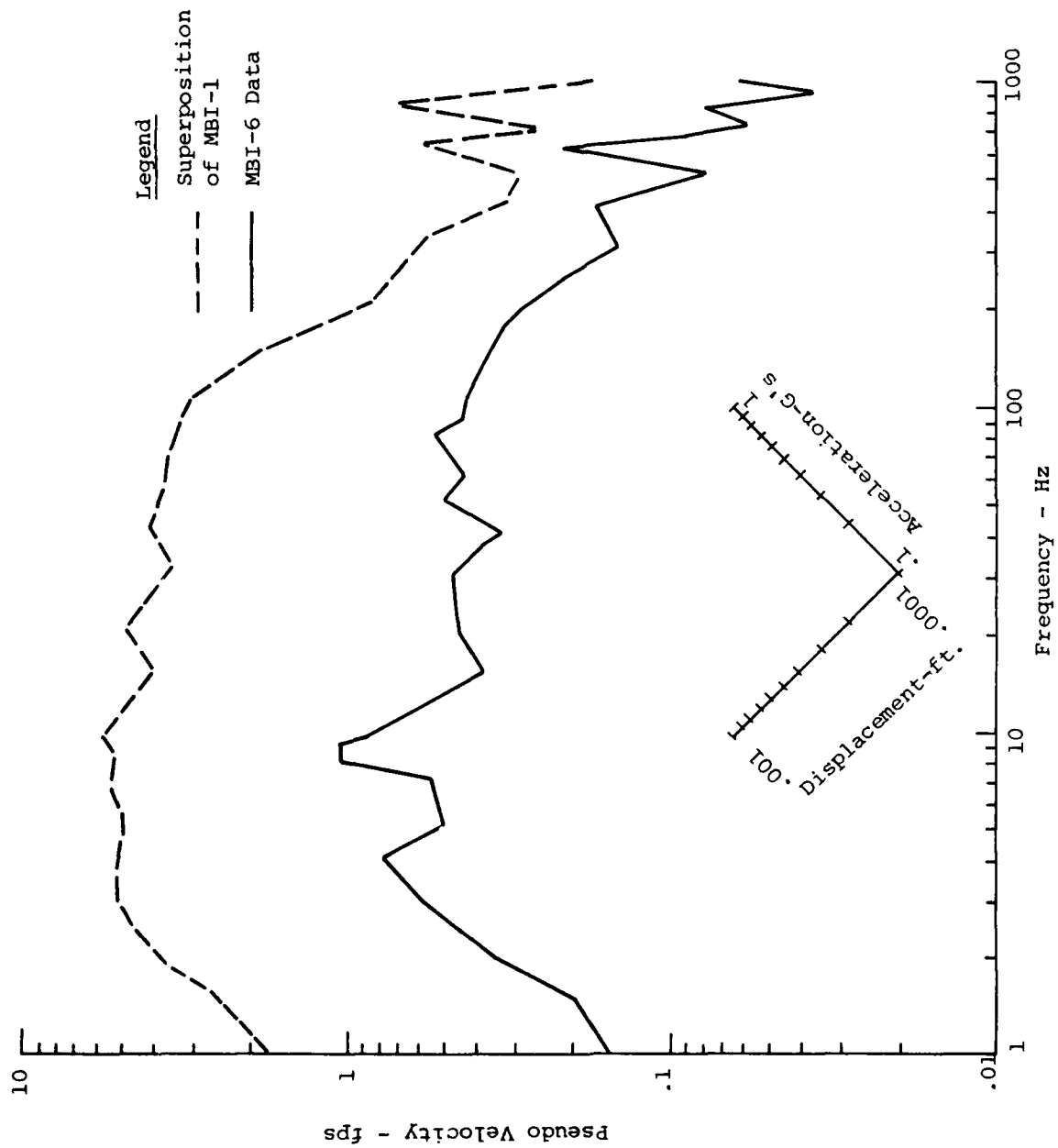


FIGURE B.35: Shock Spectra Comparison of MBI-6 and Superposition of MBI-1 @ 45.75/0.46/0 Vertical Velocity

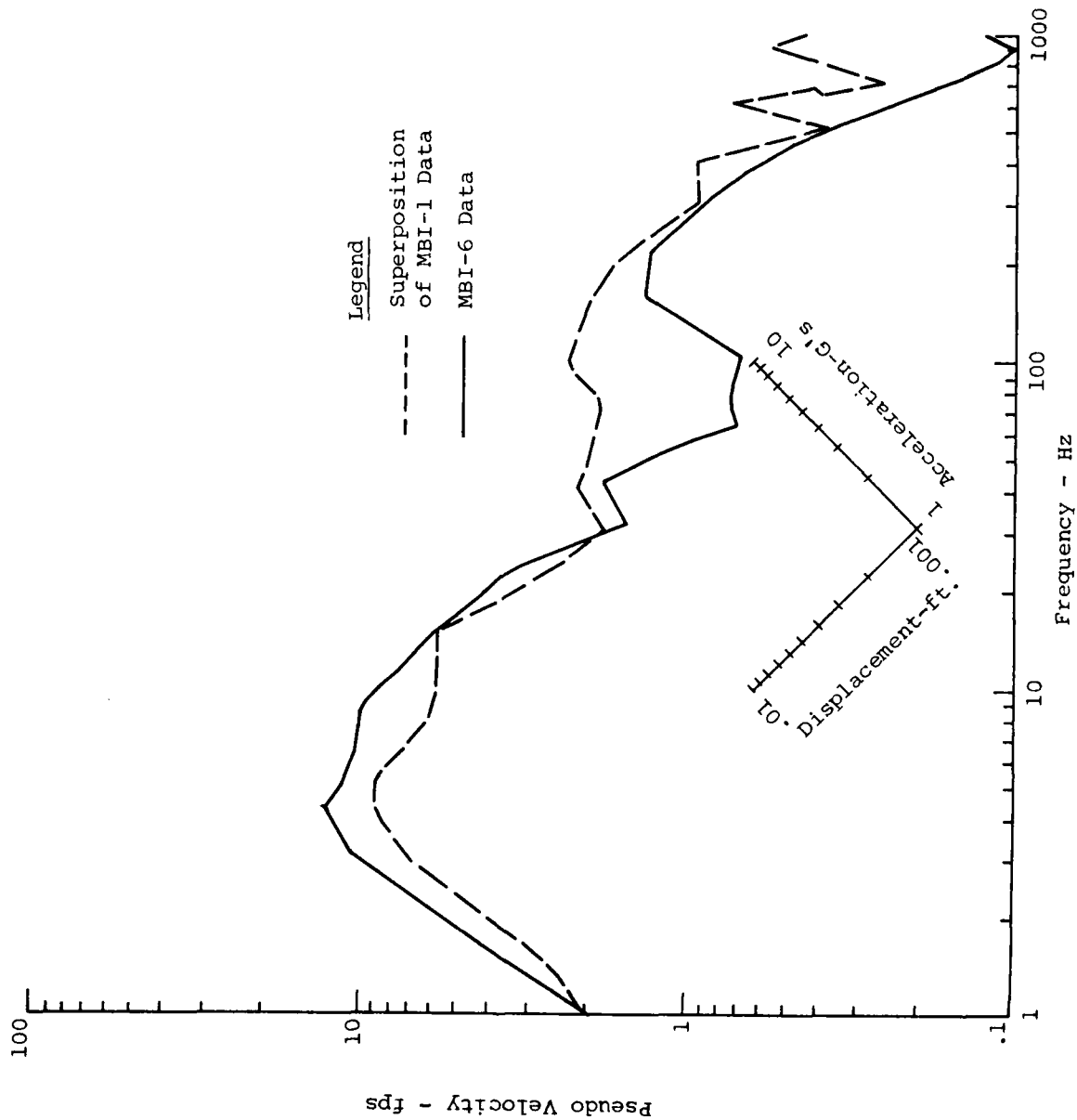


FIGURE B.36 Shock Spectra Comparison of MBI-6 and Superposition of MBI-1 @ 45.75/0.46/0 Horizontal Velocity

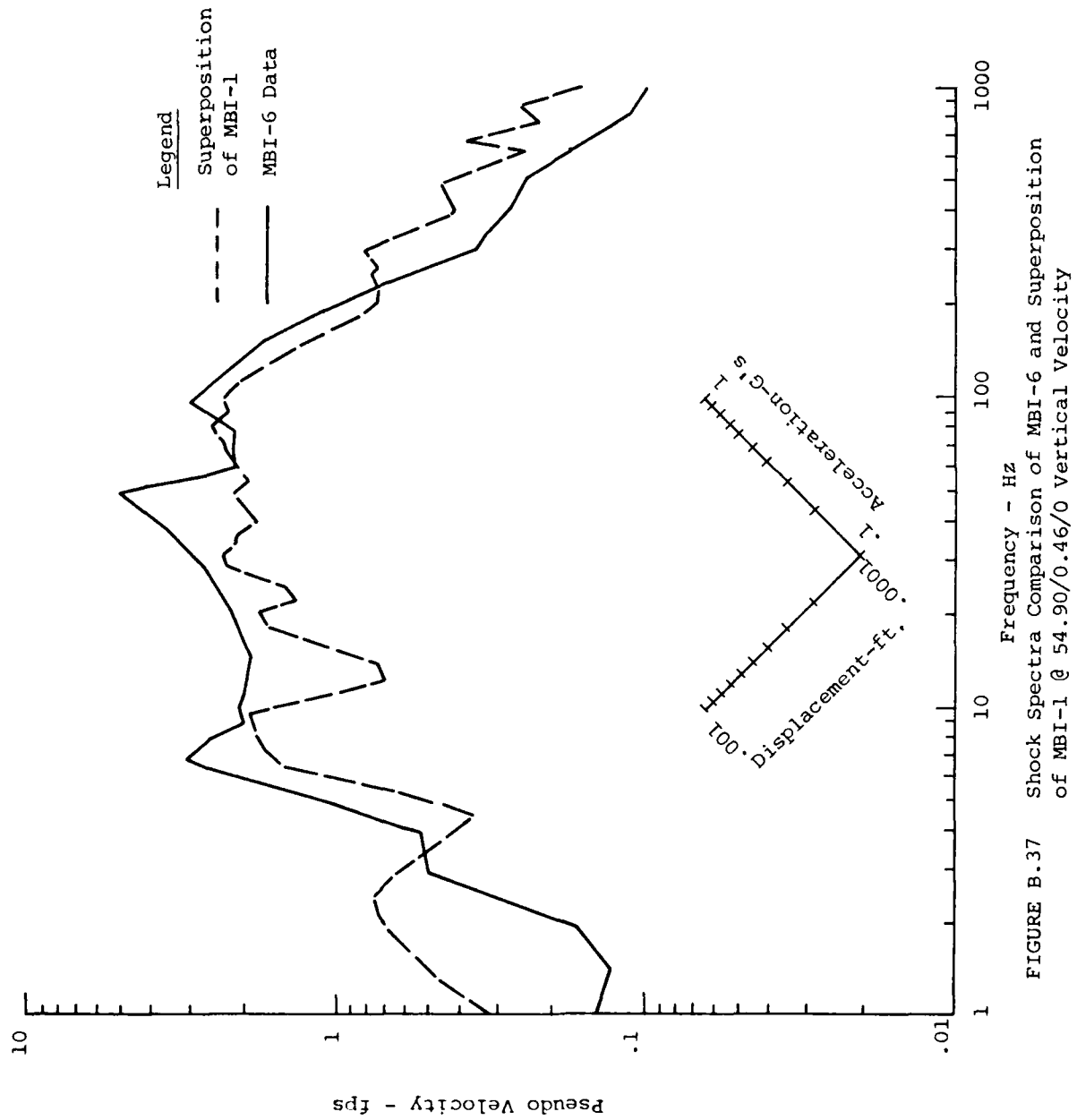


FIGURE B.37 Shock Spectra Comparison of MBI-6 and Superposition of MBI-1 @ 54.90/0.46/0 Vertical Velocity

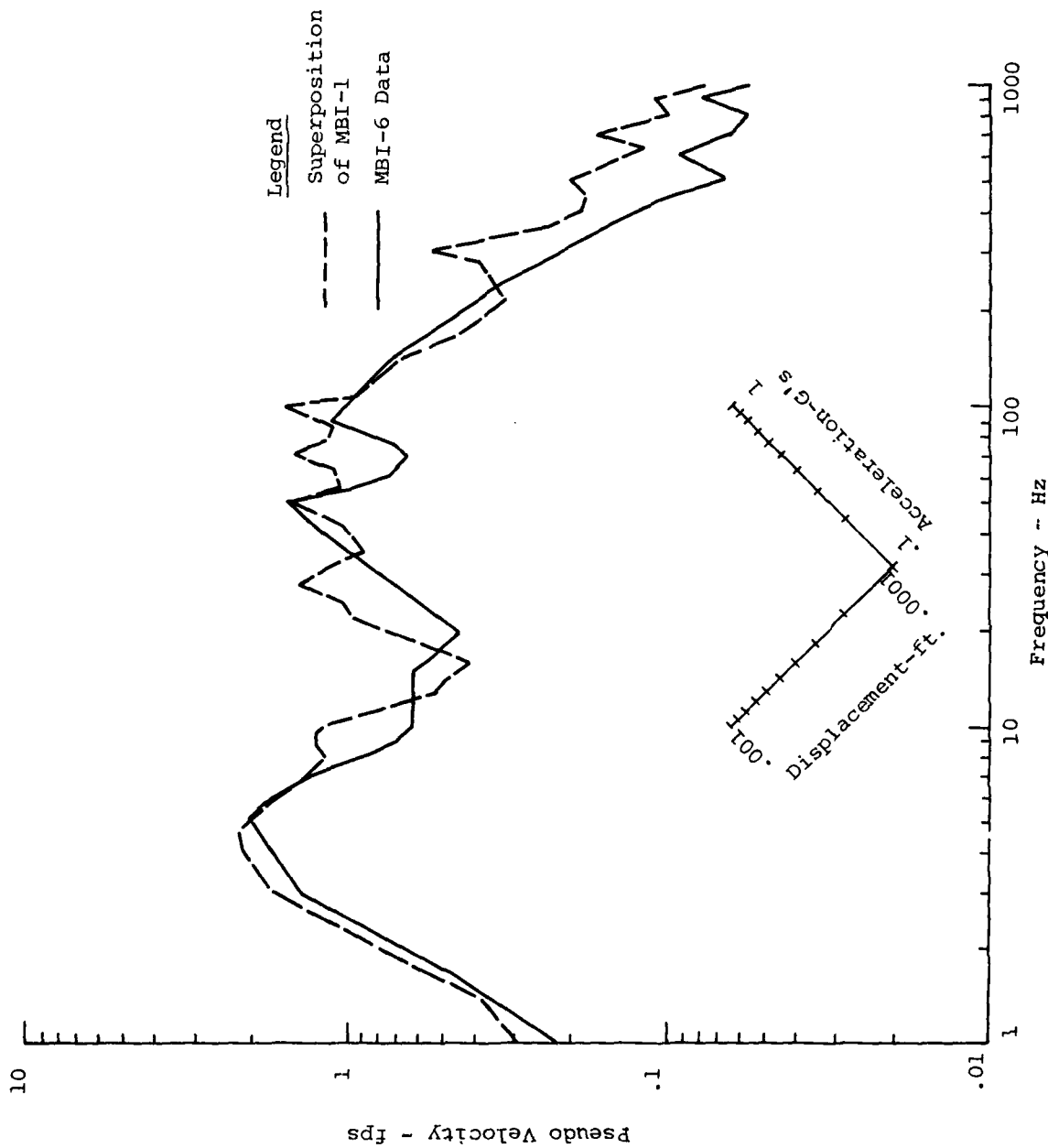


FIGURE B.38: Shock Spectra Comparison of MBI-6 and Superposition of MBI-1 @ 54.90/0.46/0 Horizontal Velocity

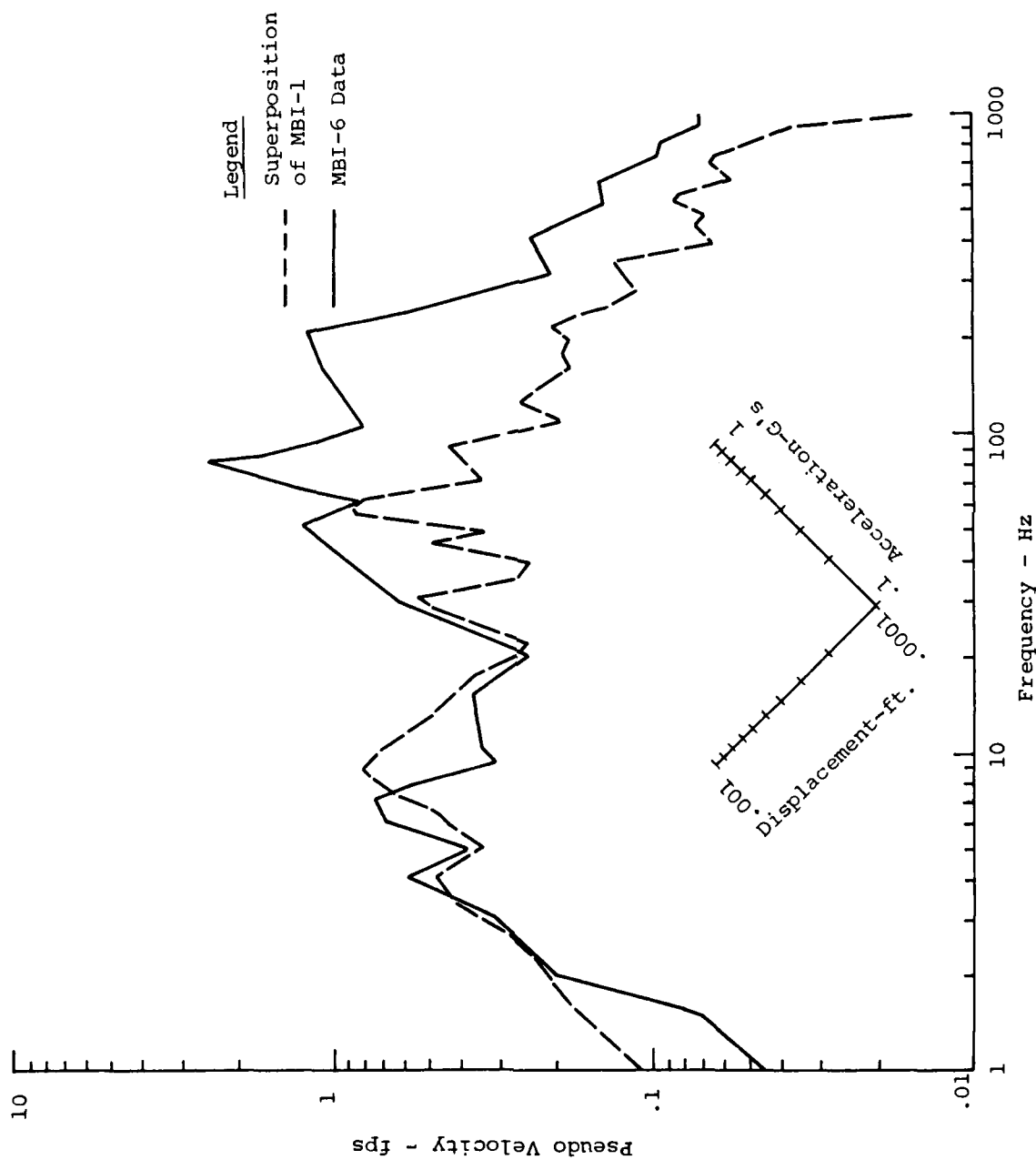


FIGURE B.39: Shock Spectra Comparison of MBI-6 and Superposition of MBI-1 @ 73.20/0.46/0 Vertical Velocity

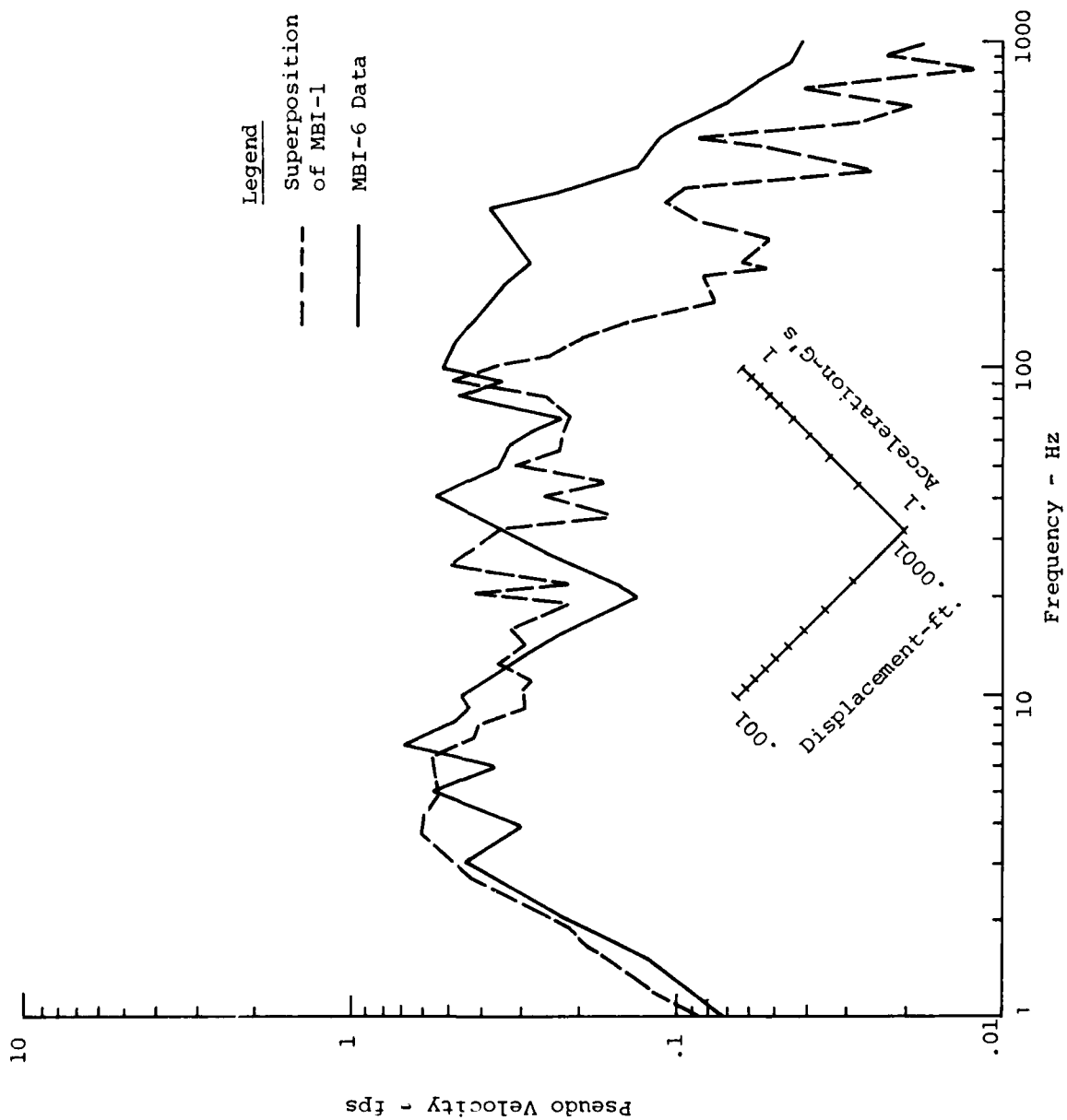


FIGURE B.40: Shock Spectra Comparison of MBI-6 and Superposition of MBI-1 @ 73.20/0.46/0 Horizontal Velocity

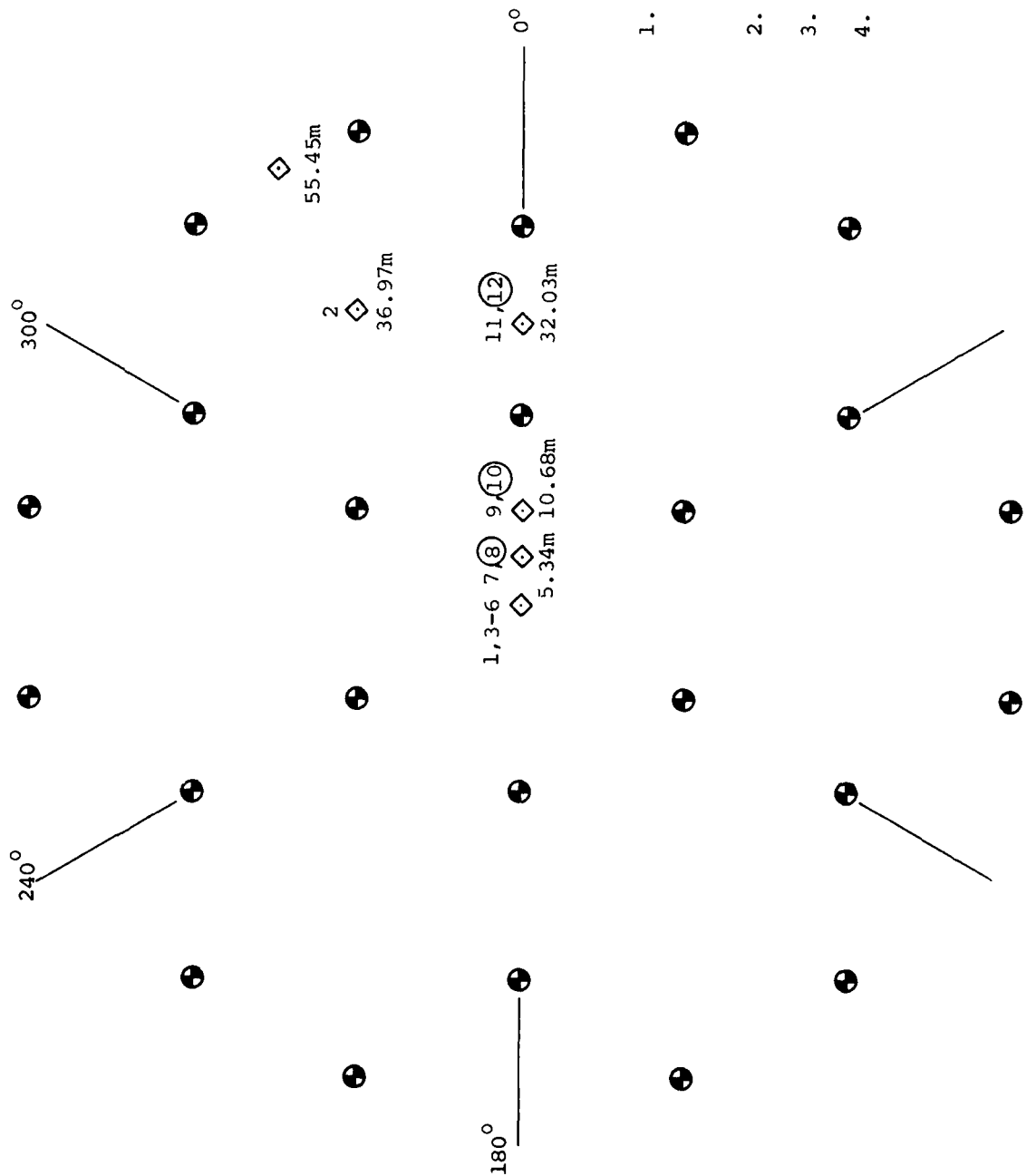


FIGURE B.41: Location of Shock Spectra Comparisons for MBI-8

MBI-8

Shock Spectra Comparisons

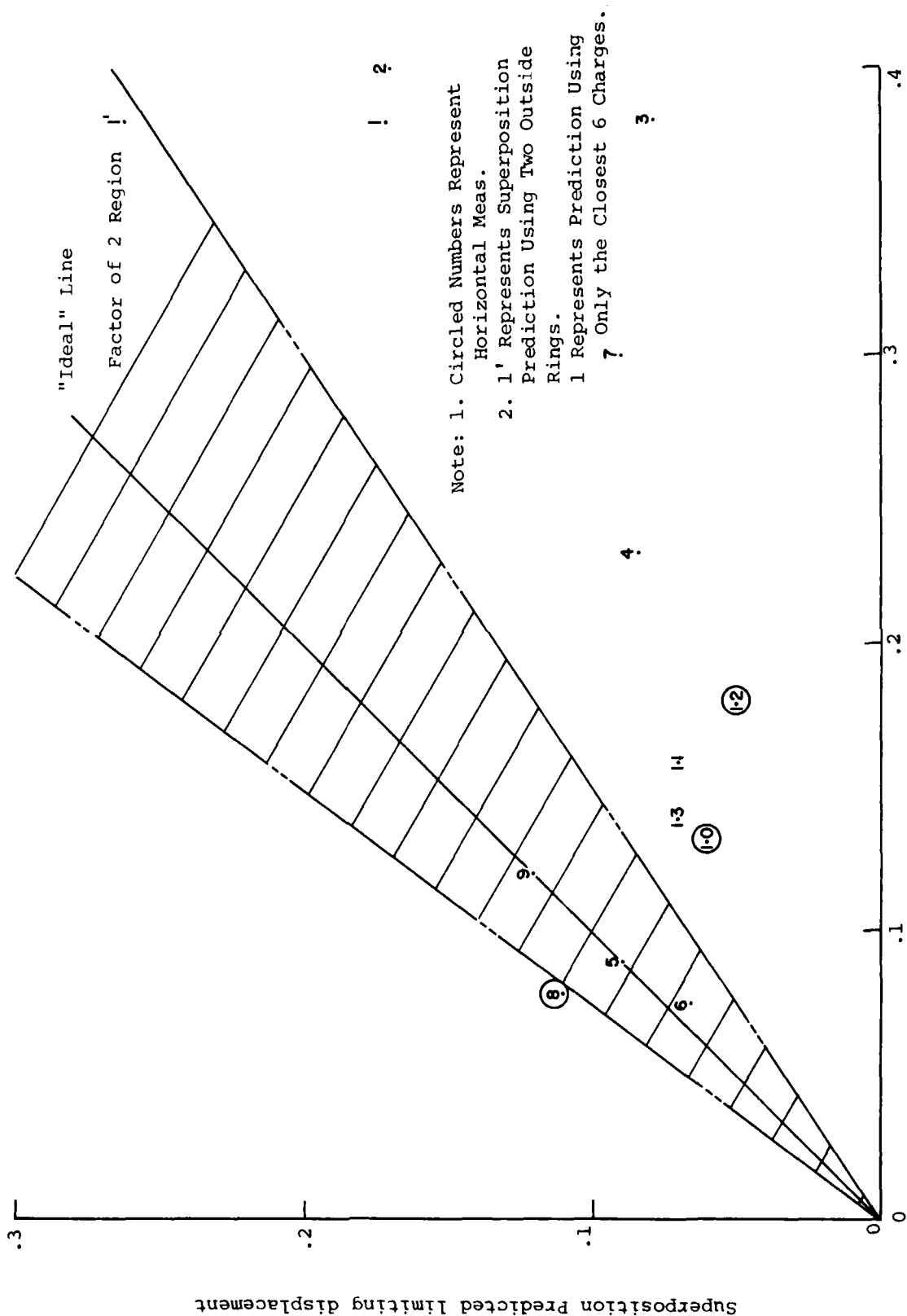


FIGURE B.42: Evaluation Plot of Limiting Displacements - MBI-8

MBI-8

Shock Spectra Comparison

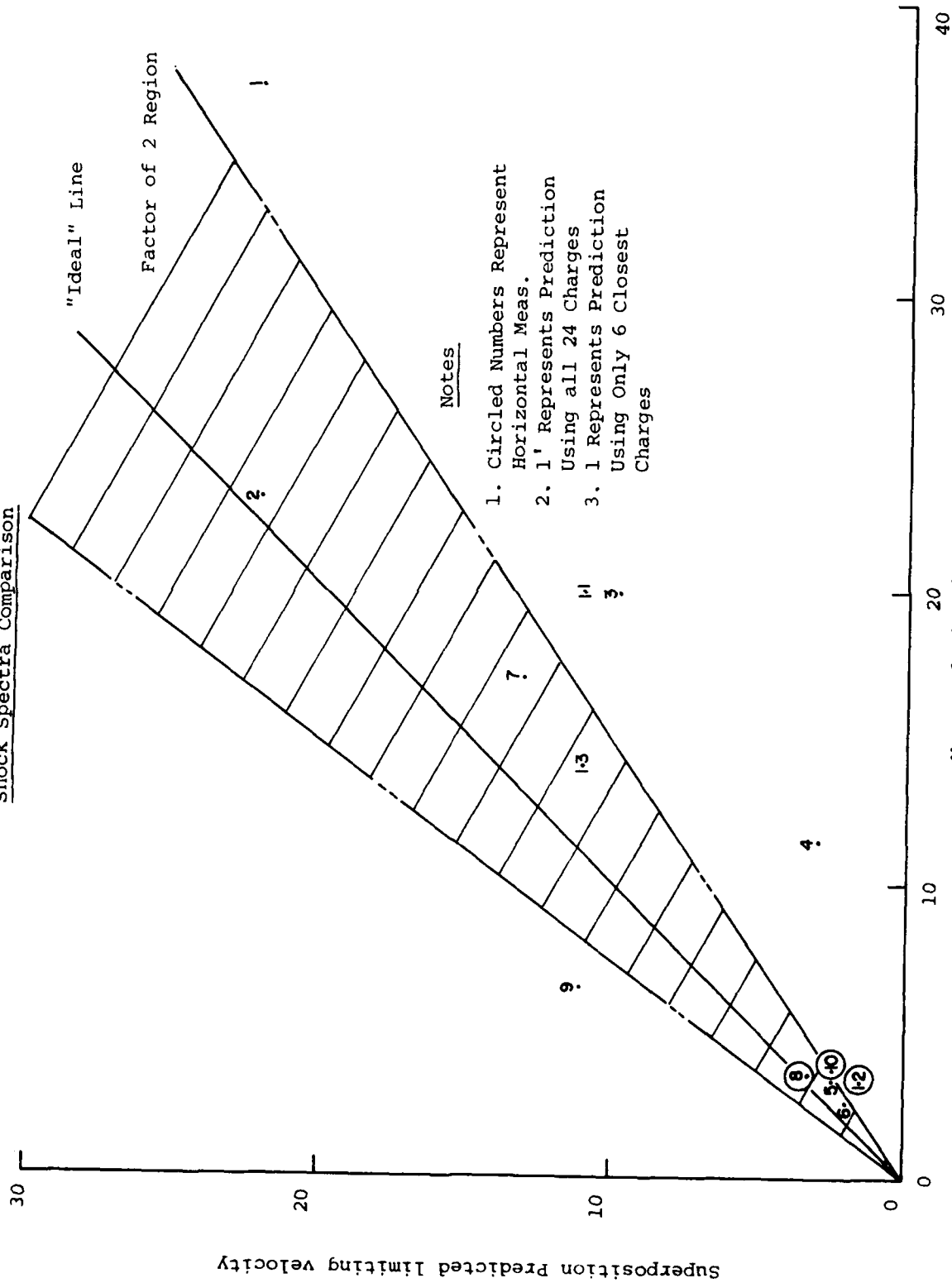


FIGURE B.43: Evaluation Plot of Limiting Velocities - MBI-8

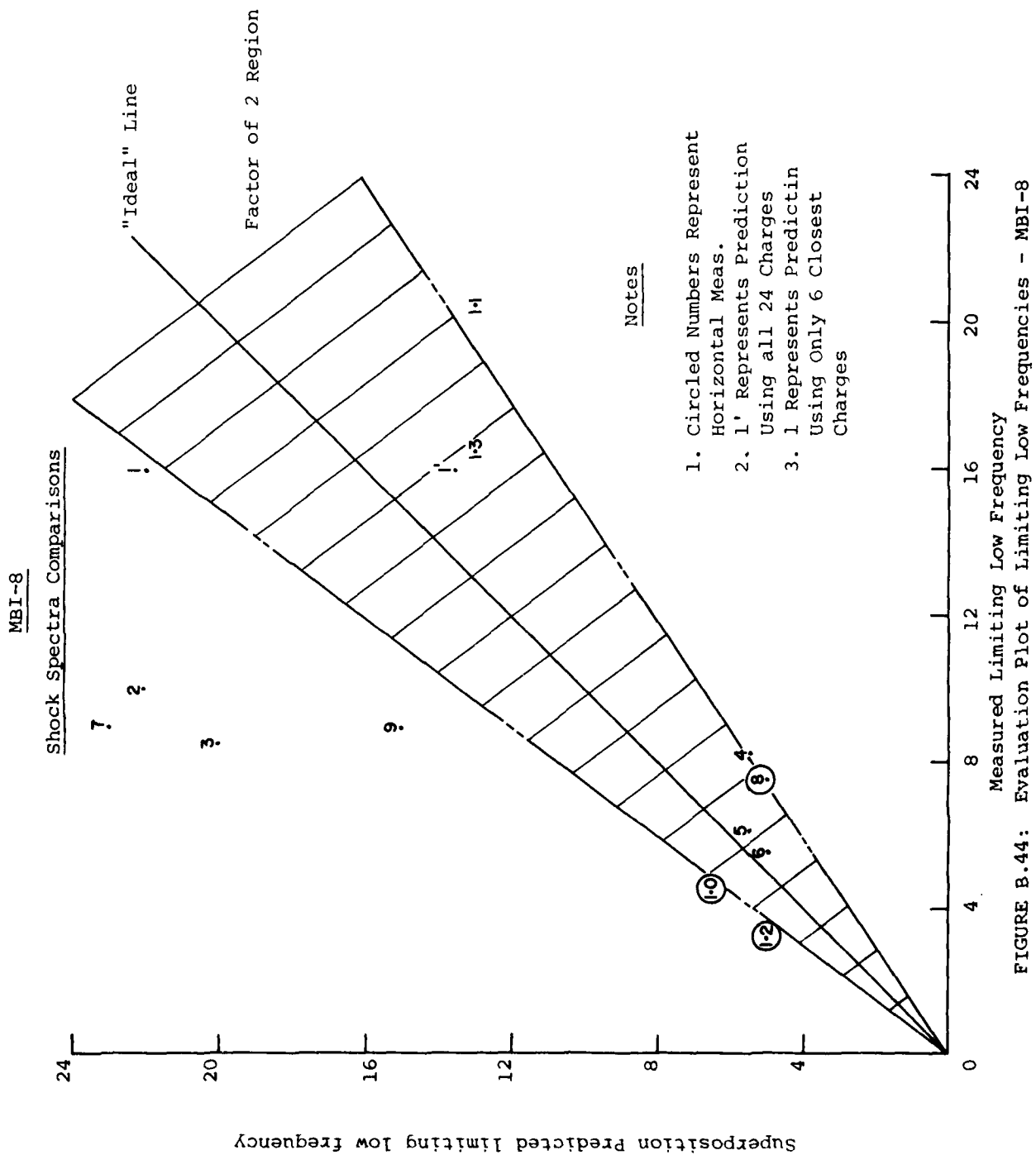


FIGURE B.44: Evaluation Plot of Limiting Low Frequencies - MBI-8

MBI-8

# Shock Spectra Comparisons

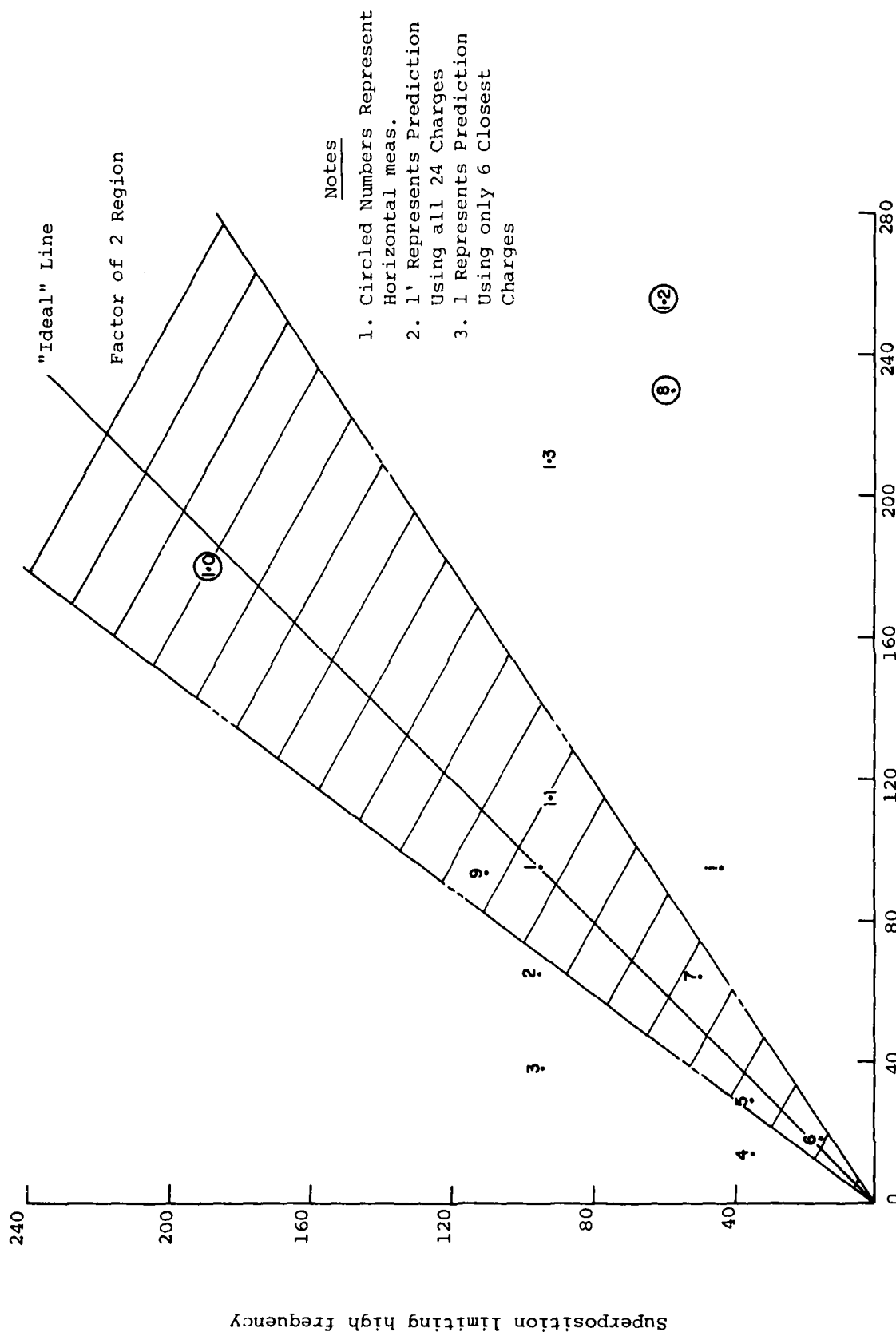


FIGURE B.45: Evaluation Plot of Limiting High Frequencies - MBI-8

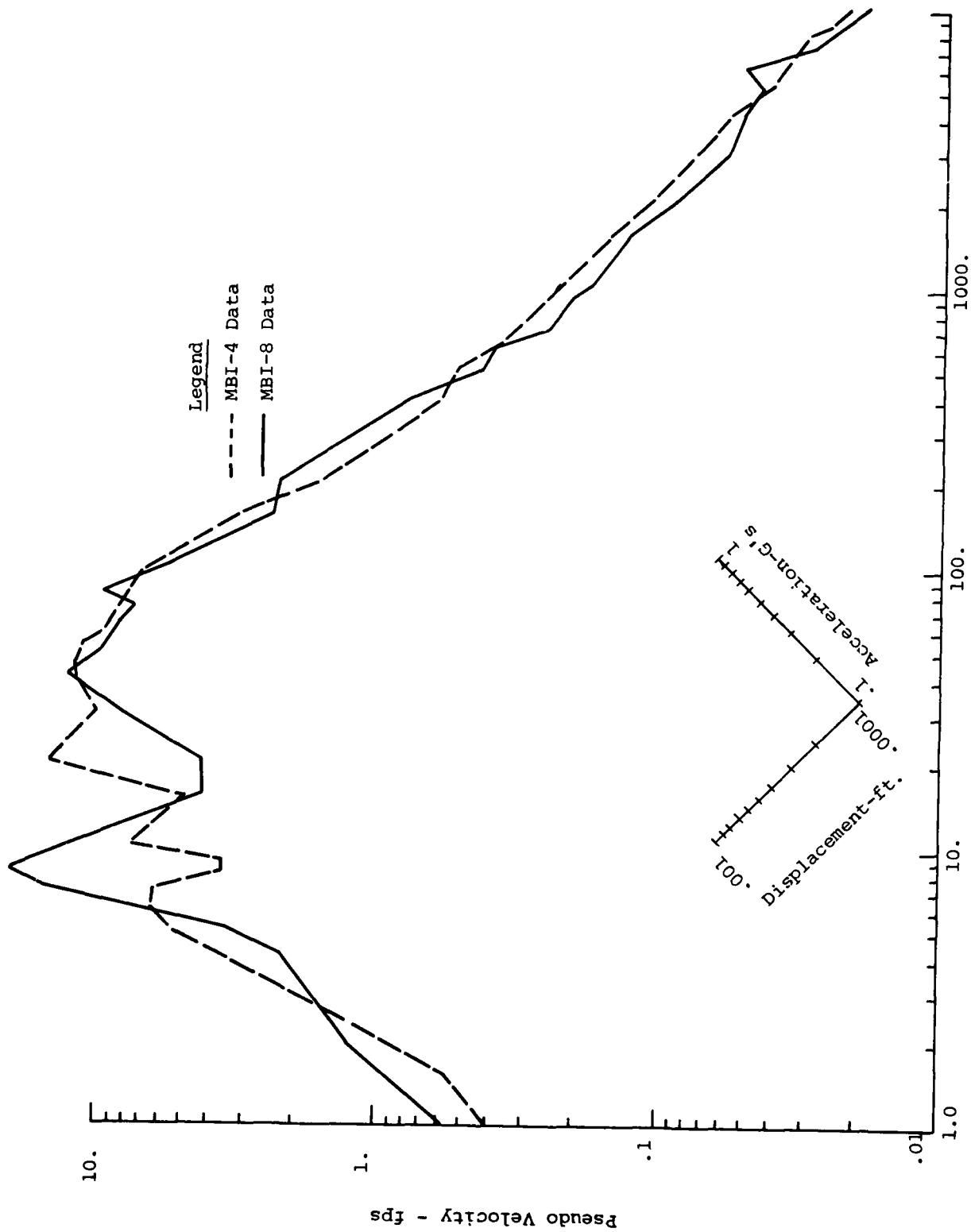


FIGURE B.46: Shock Spectra Comparison of MBI-8 and MBI-4 @ 0/1.52/0 Vertical Velocity

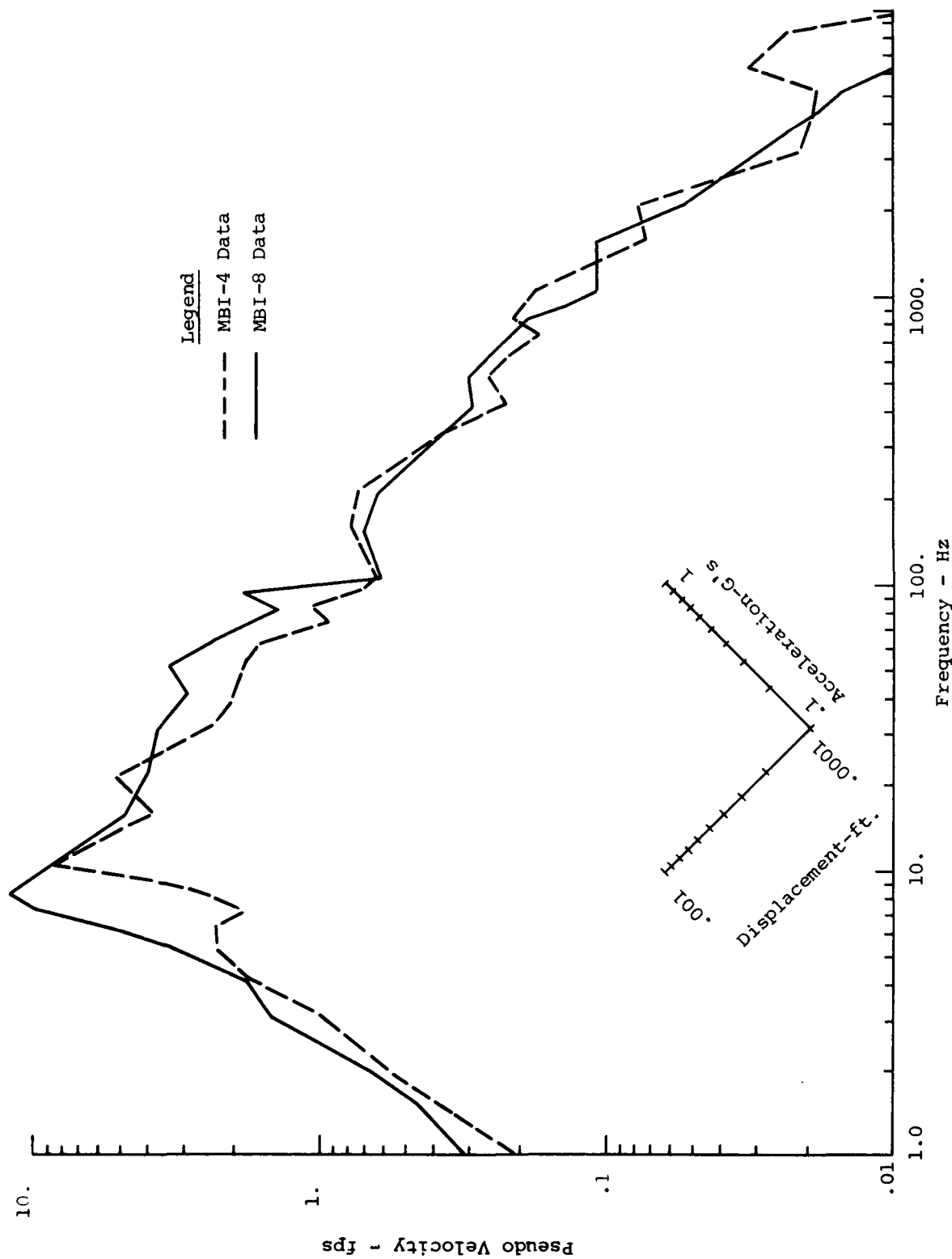


FIGURE B.47: Shock Spectra Comparison of MBI-8 and MBI-4 at 0/3.05/0 Vertical Velocity

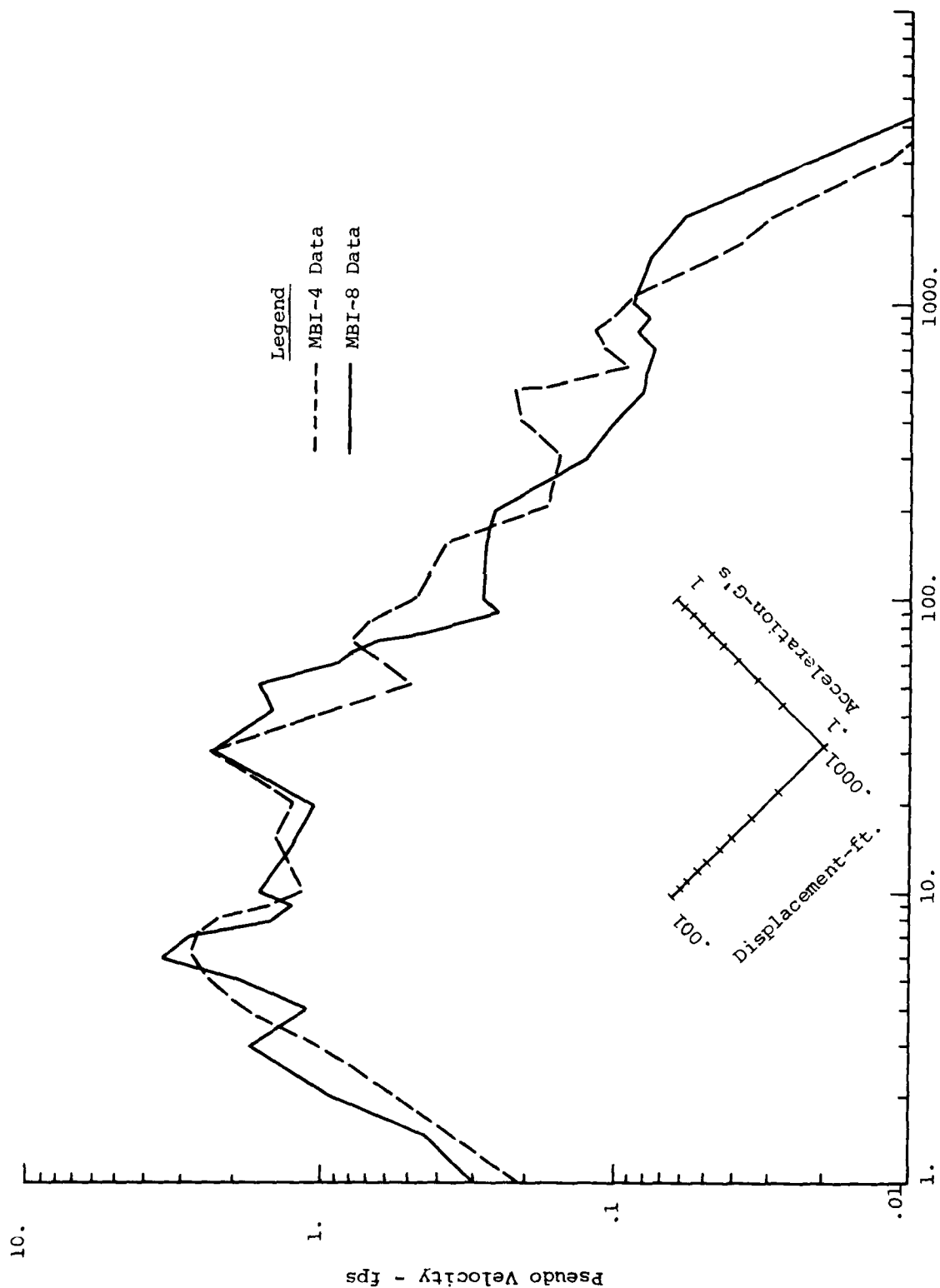


FIGURE B.48: Shock Spectra Comparison of MBI-8 and MBI-4 @ 0/6.10/0 Vertical Velocity

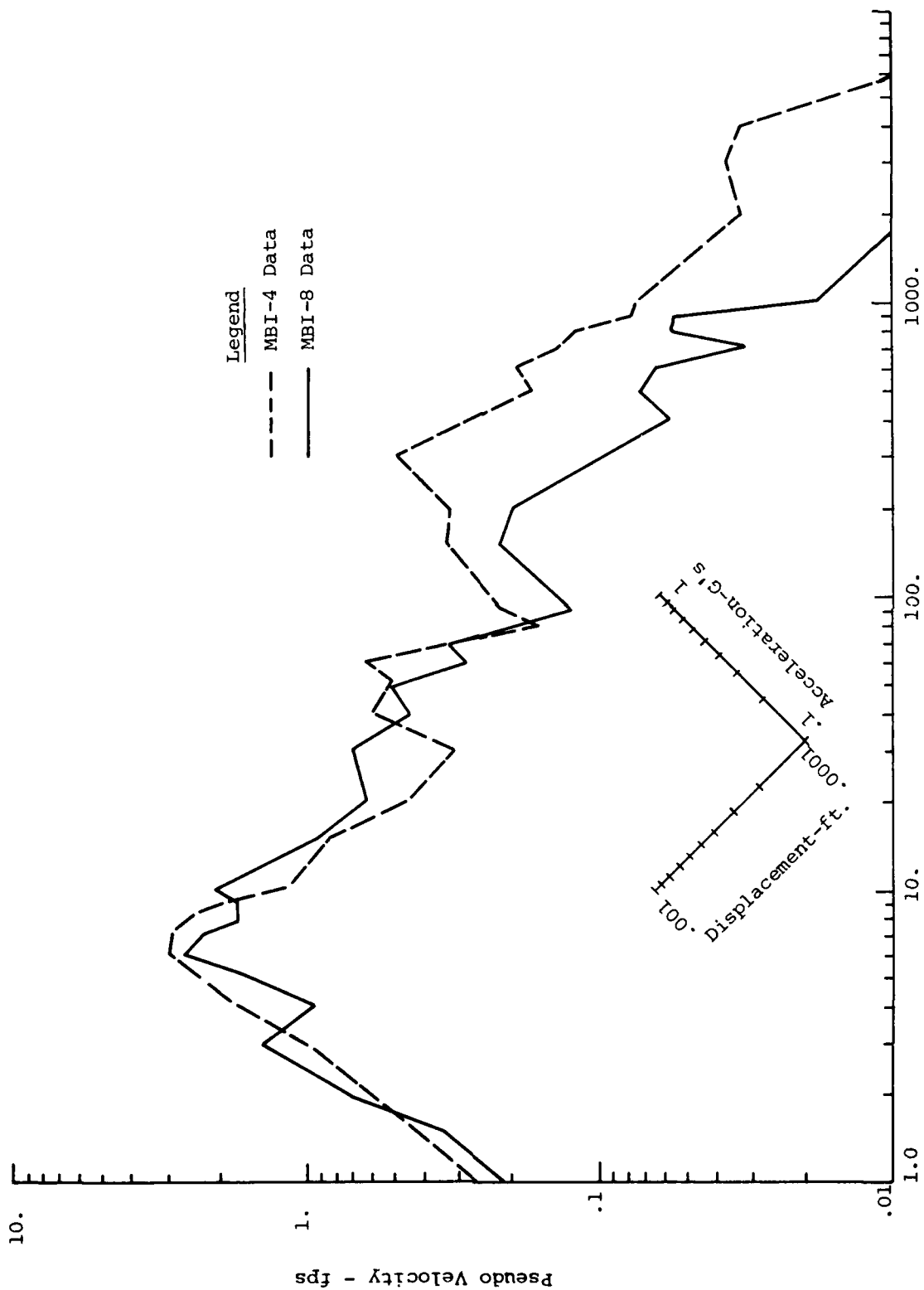


FIGURE B.49: Shock Spectra Comparison of MBI-8 and MBI-4 @ 0/12.20/0 Vertical Velocity

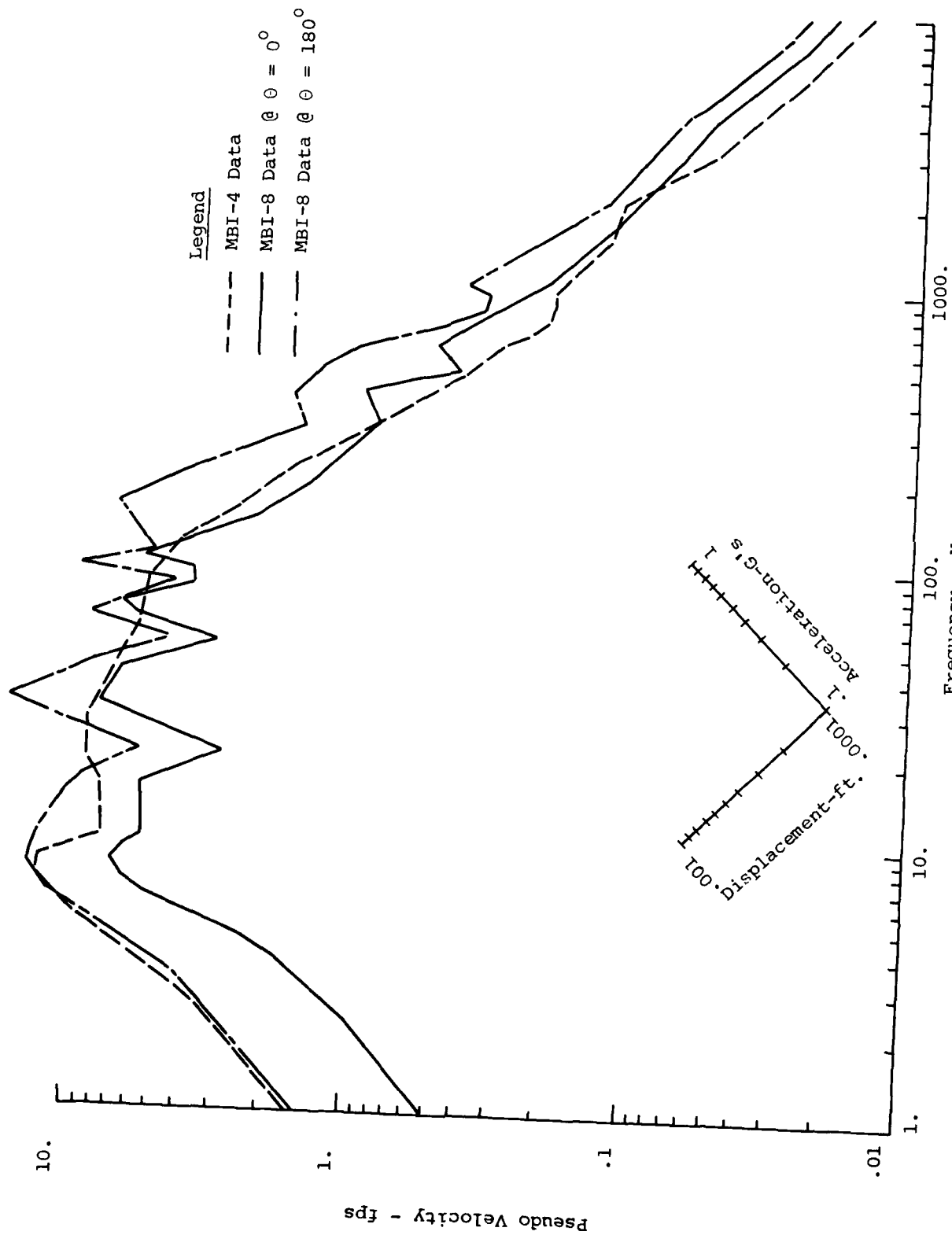


FIGURE B.50: Shock Spectra Comparison of MBI-8 and MBI-4 @ 5.34/0.46/ Vertical Velocity

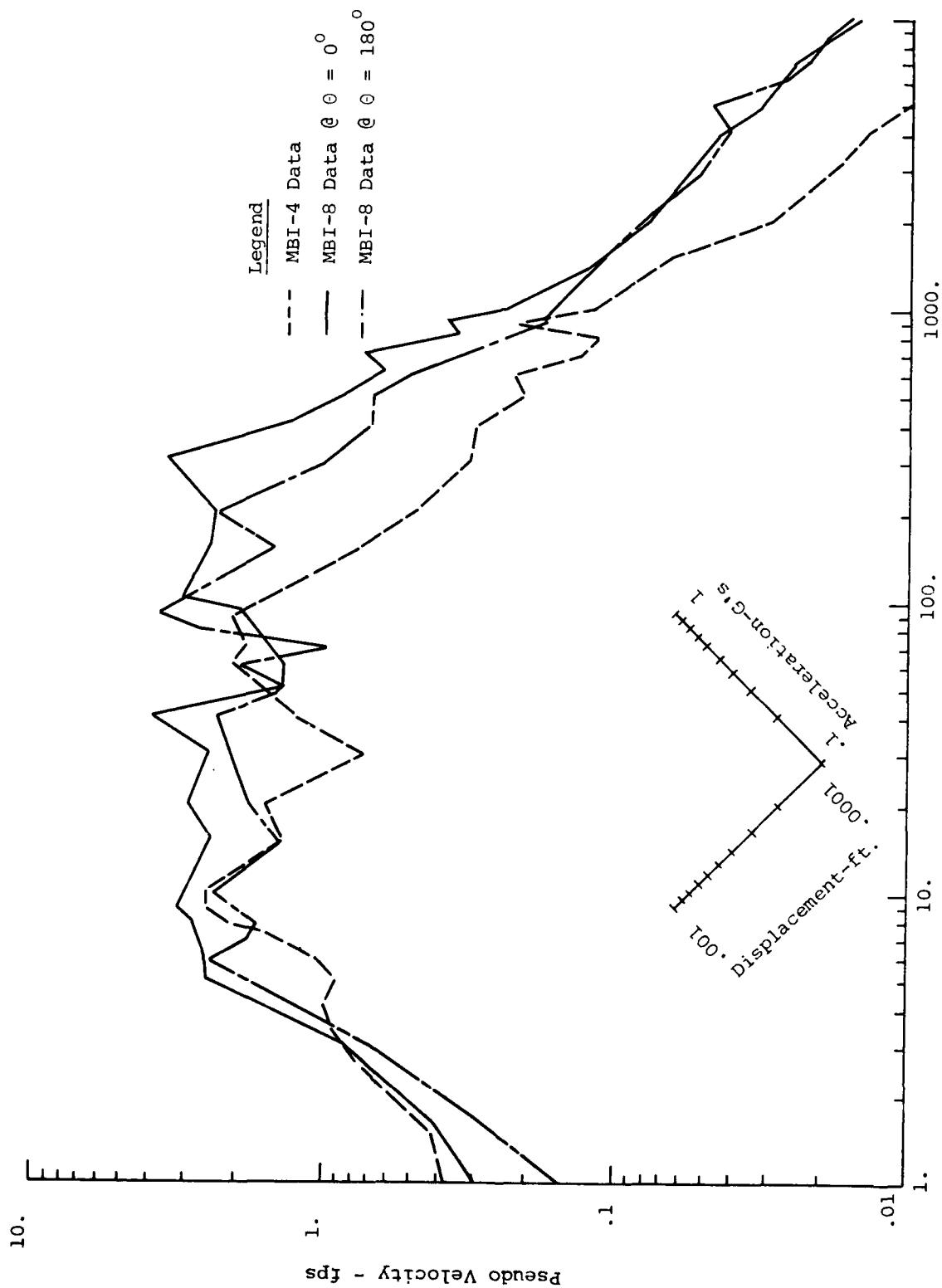


FIGURE B.51: Shock Spectra Comparison of MBI-8 and MBI-4 @ 5.34/0.46/ Horizontal Velocity

APPENDIX C

C.1

Table C1: Peak Airblast Parameters  
Measured in MBI-4

Gage Location (R-m, $\theta$ )	Peak Overpressure MPa	Peak Impulse MPa-sec	Peak Underpressure MPa
0.915 - 150	1.60	$7.34 \times 10^{-3}$	0.059
5.34 - 150	0.483	$3.25 \times 10^{-3}$	0.048
5.34 - 180	0.793	$3.14 \times 10^{-3}$	0.050
10.68 - 150	1.10	$3.45 \times 10^{-3}$	0.030
10.68 - 180	0.897	$3.12 \times 10^{-3}$	0.028
19.25 - 166	3.03	$1.96 \times 10^{-3}$	0.069
18.48 - 150	5.31	$6.28 \times 10^{-3}$	-
18.67 - 142	1.55	$3.24 \times 10^{-3}$	0.034
19.24 - 134	3.45	$1.38 \times 10^{-3}$	0.083
39.96 - 90	0.231	$1.21 \times 10^{-3}$	0.017
39.96 - 30	0.241	$1.19 \times 10^{-3}$	0.027
39.96 - 330	0.221	$1.19 \times 10^{-3}$	0.026
39.96 - 270	0.207	$1.21 \times 10^{-3}$	0.027
39.96 - 210	0.214	$1.12 \times 10^{-3}$	0.026

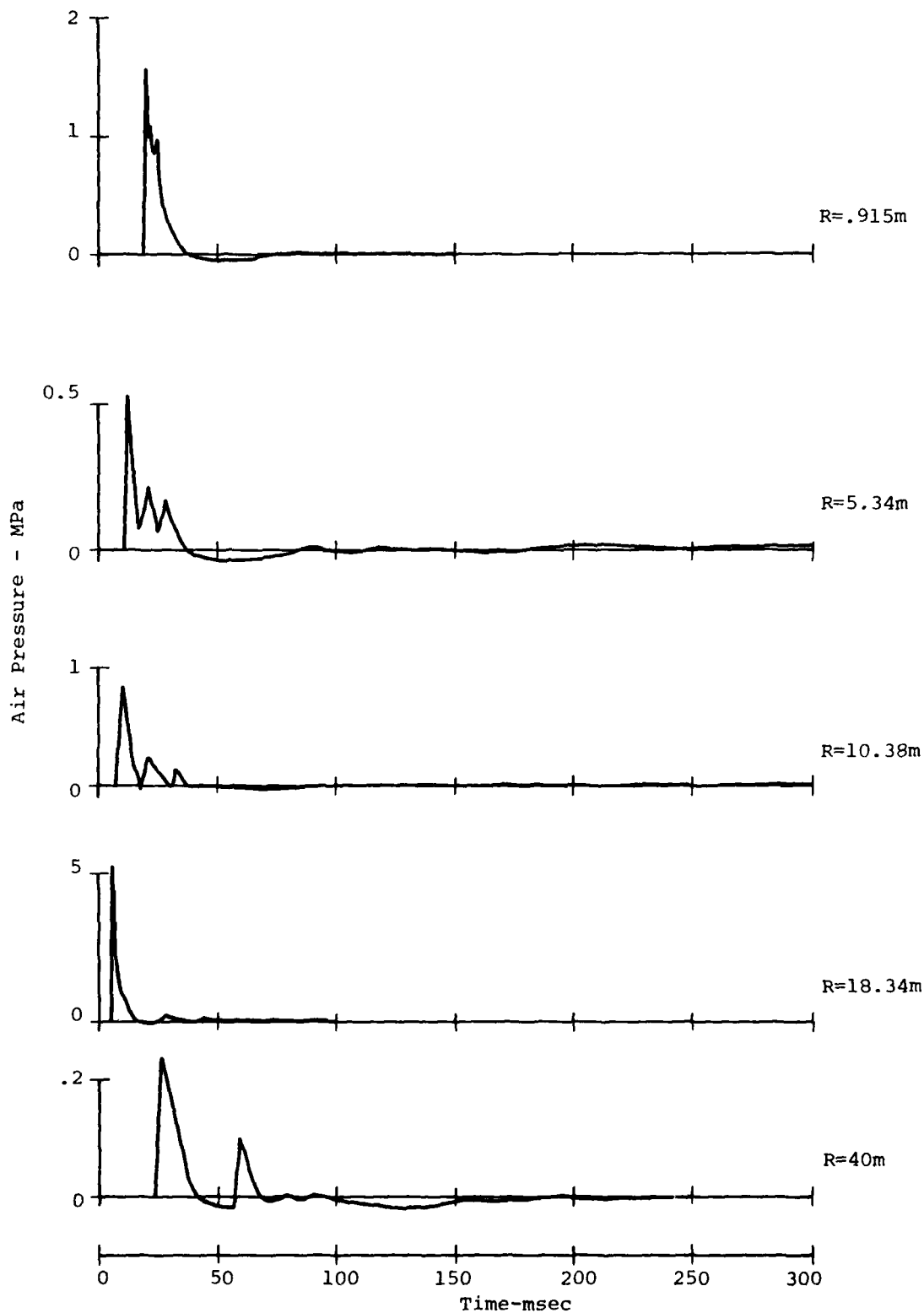


Figure C.1: Overpressure Waveforms Measured on Bisector, MBI-4

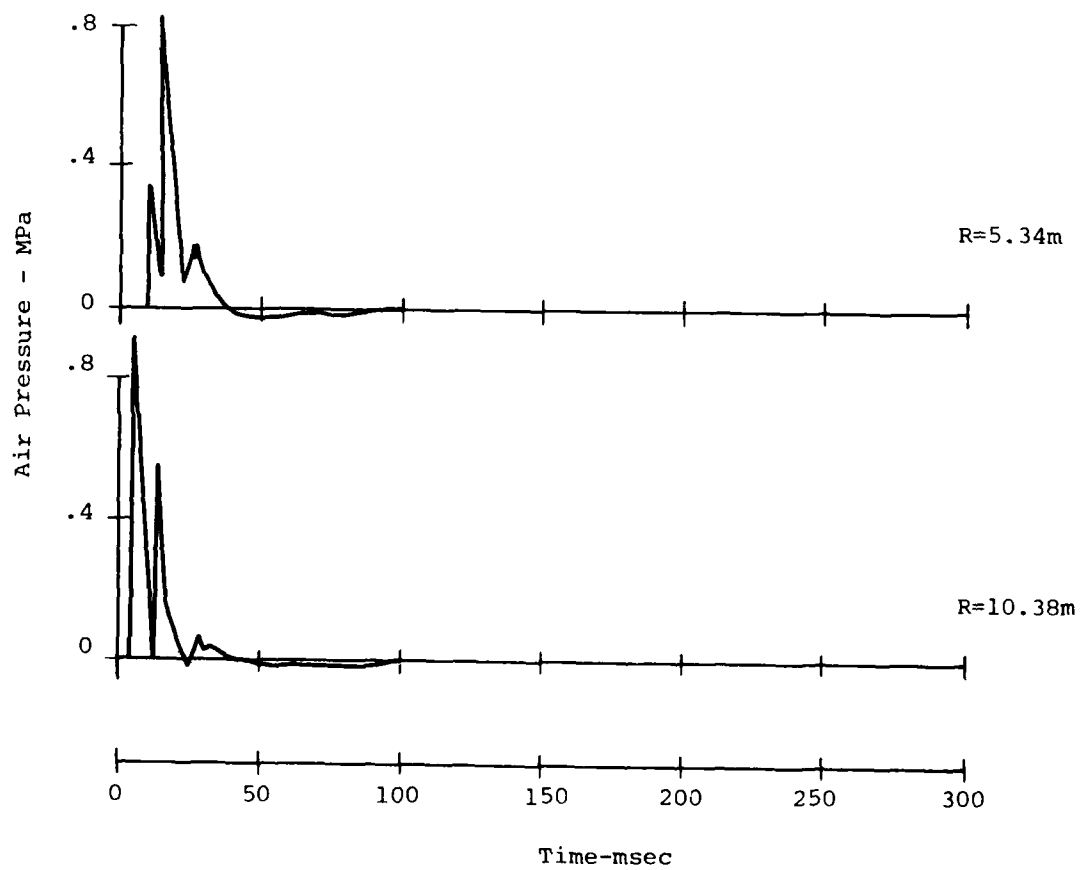


Figure C.2: Overpressure Waveforms Measured on Charge Line, MBI-4

Table C2: Peak Airblast Parameters  
Measured in MBI-6

Gage Location (R-m, $\theta$ )	Peak Overpressure MPa	Peak Impulse MPa-sec	Peak Underpressure MPa
0.915 - 150	0.421	$2.83 \times 10^{-3}$	0.038
3.05 - 150	0.214	$2.83 \times 10^{-3}$	0.038
4.58 - 150	0.152	$2.38 \times 10^{-3}$	0.038
9.15 - 150	0.171	$1.97 \times 10^{-3}$	0.031
9.64 - 168.4	0.069	$1.72 \times 10^{-3}$	0.028
18.3 - 150	0.234	$1.37 \times 10^{-3}$	0.024
18.55 - 159	0.103	$1.03 \times 10^{-3}$	0.021
31.72 - 150	0.455	$2.07 \times 10^{-3}$	0.041
31.82 - 155	0.207	$1.24 \times 10^{-3}$	0.034
32.30 - 161	0.531	$9.03 \times 10^{-4}$	-
54.29 - 150	0.176	$1.07 \times 10^{-3}$	0.021
54.38 - 153	0.085	$1.1 \times 10^{-3}$	0.021
66.19 - 217	0.097	$7.86 \times 10^{-4}$	0.022
66.26 - 152.6	0.073	$7.93 \times 10^{-4}$	0.014
73.2 - 150	0.090	$8.0 \times 10^{-4}$	0.014
73.26 - 152.4	0.057	$5.66 \times 10^{-4}$	0.010
91.50 - 150	0.038	$4.28 \times 10^{-4}$	0.007
4.58 - 180	0.145	$2.0 \times 10^{-3}$	0.034
9.15 - 180	0.112	$1.93 \times 10^{-3}$	0.034
18.30 - 180	0.138	$1.24 \times 10^{-3}$	0.028
45.75 - 180	0.490	$8.97 \times 10^{-4}$	-
54.90 - 180	0.145	$6.69 \times 10^{-4}$	0.015
66.19 - 30	0.081	$6.21 \times 10^{-4}$	0.014
73.20 - 180	0.043	$2.9 \times 10^{-4}$	0.009
66.19 - 270	0.097	$8.28 \times 10^{-4}$	0.014

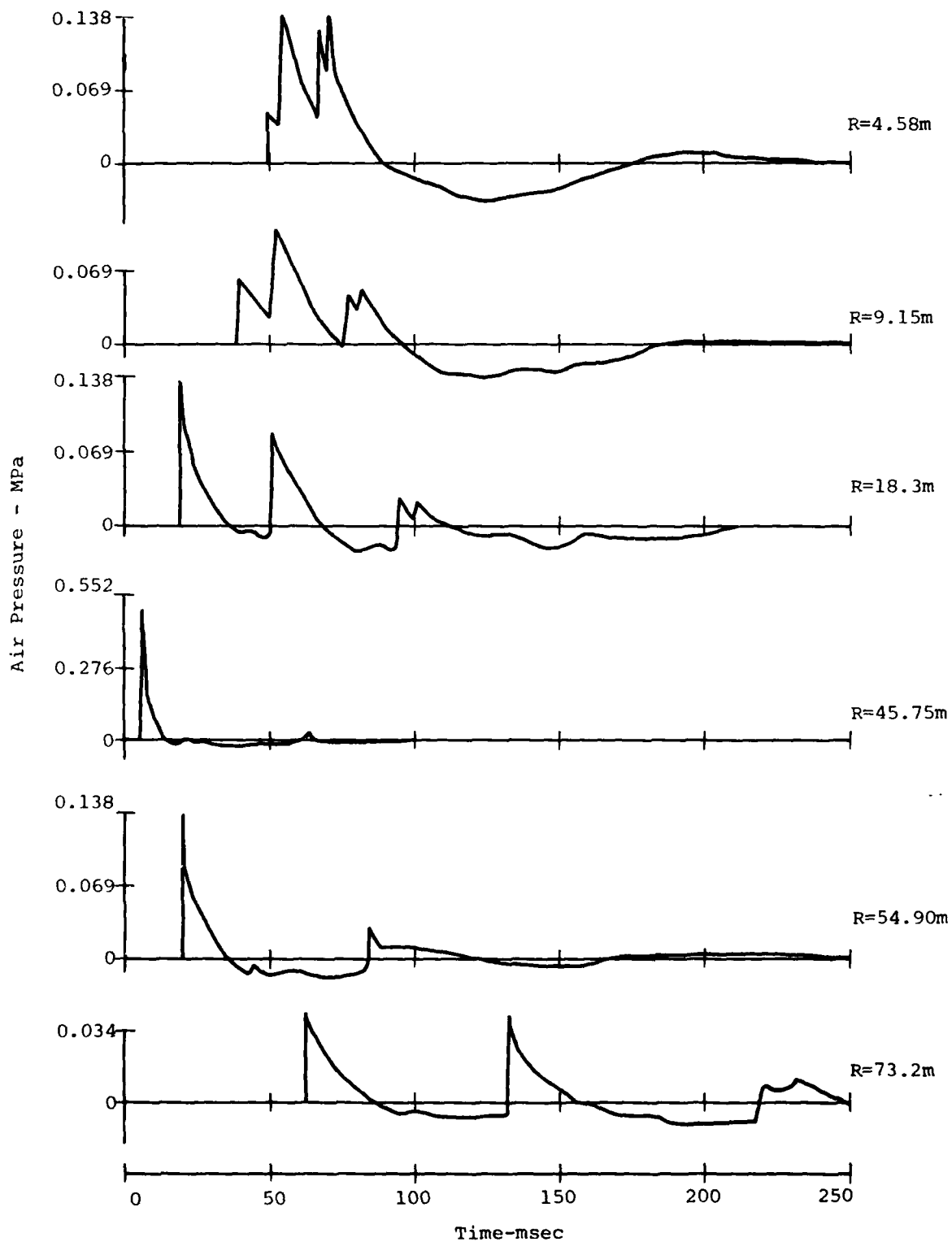


Figure C.3: Overpressure Waveforms Measured on Charge Line MBI-6

Table C3: Peak Airblast Parameters  
Measured in MBI-8

Gage Location (R-m, $\theta$ )	Peak Overpressure MPa	Peak Impulse MPa-sec	Peak Underpressure MPa
2.44 - 60	0.690	$5.38 \times 10^{-3}$	0.062
5.34 - 30	0.828	$3.19 \times 10^{-3}$	0.055
5.34 - 60	0.483	$4.32 \times 10^{-3}$	0.028
10.68 - 30	0.807	$4.53 \times 10^{-3}$	0.028
10.68 - 60	0.552	$4.74 \times 10^{-3}$	0.033
18.48 - 30	1.47	$5.79 \times 10^{-3}$	0.052
18.79 - 38	1.24	$5.17 \times 10^{-3}$	-
19.25 - 46	2.50	$3.59 \times 10^{-3}$	0.086
26.29 - 30	1.03	$4.09 \times 10^{-3}$	0.019
26.69 - 60	2.93	-	-
28.12 - 39	0.621	$4.34 \times 10^{-3}$	0.022
31.63 - 30	0.499	$3.43 \times 10^{-3}$	0.014
32.03 - 60	2.72	$7.86 \times 10^{-3}$	0.052
34.53 - 30	0.603	$4.34 \times 10^{-3}$	0.086
35.44 - 35	0.234	$3.97 \times 10^{-3}$	0.028
37.36 - 60	2.31	$2.76 \times 10^{-3}$	-
36.97 - 30	1.41	$7.59 \times 10^{-3}$	-
36.97 - 90	2.24	$8.0 \times 10^{-3}$	0.055
36.97 - 150	3.71	$8.53 \times 10^{-3}$	0.052
36.97 - 210	4.48	$8.14 \times 10^{-3}$	0.069
36.97 - 270	2.76	$9.31 \times 10^{-3}$	0.041
36.97 - 330	2.76	$9.48 \times 10^{-3}$	0.041
42.30 - 30	0.414	$3.14 \times 10^{-3}$	0.041
47.64 - 30	1.90	$4.53 \times 10^{-3}$	-
55.45 - 0	0.503	$2.62 \times 10^{-3}$	0.034
55.45 - 30	2.07	$5.31 \times 10^{-3}$	0.055
73.93 - 0	0.117	$1.81 \times 10^{-3}$	0.007
74.12 - 30	0.241	$1.59 \times 10^{-3}$	0.017

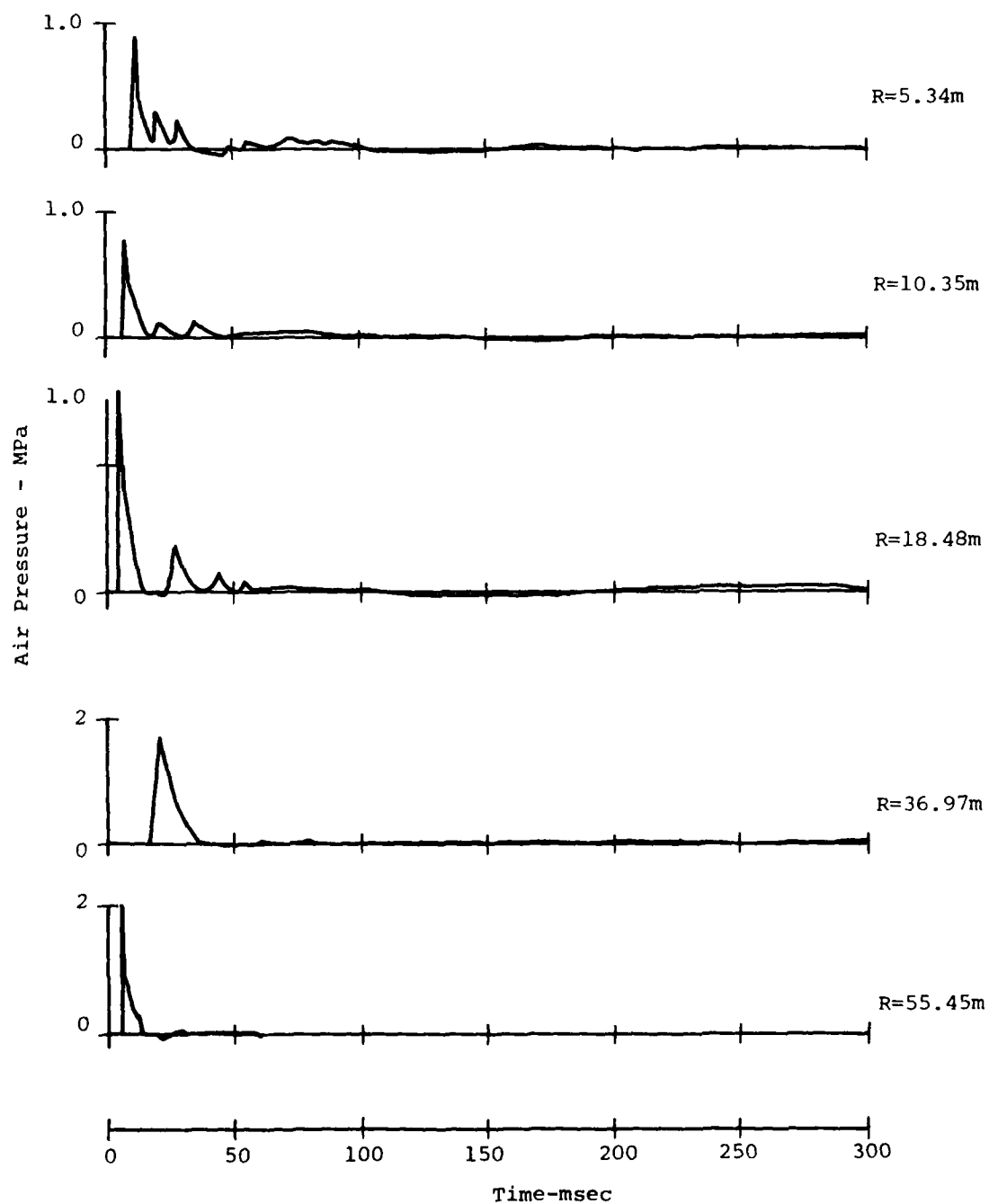


Figure C.4: Overpressure Waveforms Measured on Charge Line, MBI-8

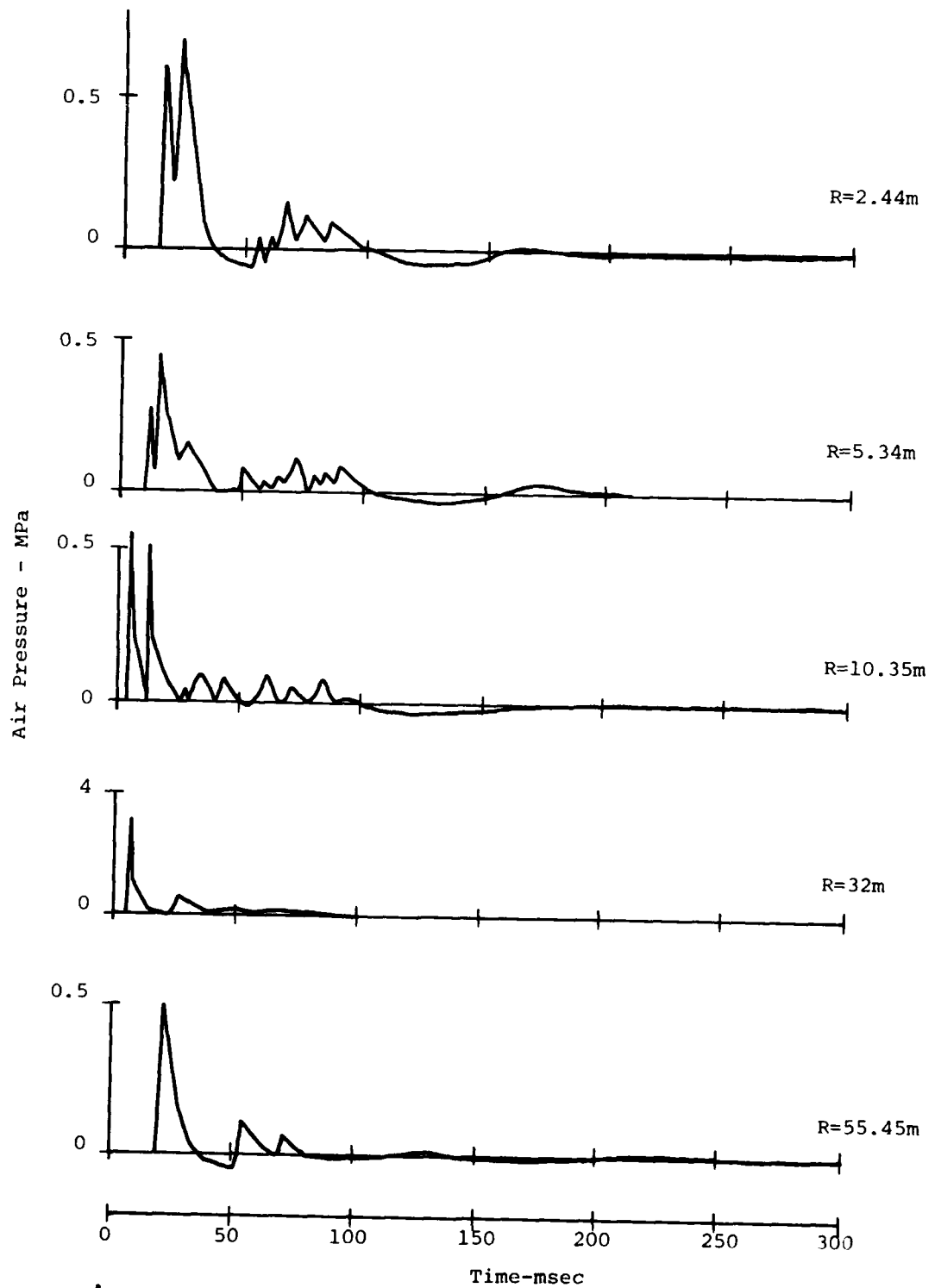


Figure C.5: Overpressure Waveforms Measured on Bisector, MBI-8

## DISTRIBUTION LIST

### DEPARTMENT OF DEFENSE

Assistant to the Secretary of Defense  
Atomic Energy  
ATTN: Executive Assistant

Defense Advanced Rsch. Proj. Agency  
ATTN: TIO

Defense Intelligence Agency  
ATTN: RDS-3A

Defense Nuclear Agency  
ATTN: SPSS, G. Ullrich  
3 cy ATTN: SPSS, J. Galloway  
4 cy ATTN: TITL

Defense Technical Information Center  
12 cy ATTN: DD

Field Command  
Defense Nuclear Agency  
ATTN: FCTMD  
ATTN: FCPR

Field Command  
Defense Nuclear Agency  
Livermore Division  
ATTN: FCPR

Joint Strat. Tgt. Planning Staff  
ATTN: XPFS  
ATTN: NRI-STINFO Library

Undersecretary of Defense for Rsch. & Engrg.  
ATTN: Strategic & Space Systems (OS)

### DEPARTMENT OF THE ARMY

BMD Advanced Technology Center  
Department of the Army  
ATTN: ATC-T

Chief of Engineers  
Department of the Army  
ATTN: DAEN-ADI-L  
ATTN: DAEN-MPE-I, D. Reynolds  
ATTN: DAEN-RDM  
ATTN: DAEN-RDL

Harry Diamond Laboratories  
Department of the Army  
ATTN: DELHD-I-TL  
ATTN: DELHD-N-P

U.S. Army Ballistic Research Labs.  
ATTN: DRDAR-BLE, J. Keefer  
ATTN: DRDAR-TSB-S

U.S. Army Cold Region Res. Engr. Lab.  
ATTN: Library

U.S. Army Construction Engr. Res. Lab.  
ATTN: Library

U.S. Army Engineer Center  
ATTN: Technical Library

### DEPARTMENT OF THE ARMY (Continued)

U.S. Army Engr. Waterways Exper. Station  
ATTN: Library  
ATTN: WESSD, G. Jackson  
ATTN: WESSA, W. Flathau

U.S. Army Material & Mechanics Rsch. Ctr.  
ATTN: Technical Library

U.S. Army Materiel Dev. & Readiness Cmd.  
ATTN: DRXAM-TL

U.S. Army Nuclear & Chemical Agency  
ATTN: Library

### DEPARTMENT OF THE NAVY

Naval Construction Battalion Center  
ATTN: Code L53, J. Forrest  
ATTN: Code L51, J. Crawford  
ATTN: Code LOBA

Naval Facilities Engineering Command  
ATTN: Code 09M22C

Naval Postgraduate School  
ATTN: G. Lindsay  
ATTN: Code 0142, Library

Naval Research Laboratory  
ATTN: Code 2627

Naval Surface Weapons Center  
ATTN: Code X211  
ATTN: Code F31

Naval Surface Weapons Center  
ATTN: Tech. Library & Info. Services Branch

Office of Naval Research  
ATTN: Code 715

### DEPARTMENT OF THE AIR FORCE

Air Force Institute of Technology  
ATTN: Library

Air Force Systems Command  
ATTN: DLWM

Air Force Weapons Laboratory  
Air Force Systems Command  
ATTN: DEY  
ATTN: SUL  
ATTN: NTES-S  
ATTN: NTEO  
ATTN: NTES-G  
ATTN: NTE, M. Plamondon  
ATTN: NT, D. Payton  
ATTN: NTED-I  
ATTN: NTED-A

Assistant Chief of Staff  
Intelligence  
Department of the Air Force  
ATTN: IN

DEPARTMENT OF THE AIR FORCE (Continued)

Assistant Secretary of the Air Force  
Research, Development & Logistics  
Department of the Air Force  
ATTN: SAFALR/Dep. for Strat. & Space Sys.

Ballistic Missile Office  
Air Force Systems Command  
ATTN: MNNX, W. Crabtree  
ATTN: MNNXH, D. Gage

Deputy Chief of Staff  
Research, Development, & Acq.  
Department of the Air Force  
ATTN: AFRDQA  
ATTN: AFRDPN  
ATTN: AFRD-M, L. Montulli  
ATTN: AFRDQSM

Strategic Air Command  
Department of the Air Force  
ATTN: XPFS  
ATTN: NRI-STINFO Library

Vela Seismology Center  
Department of the Air Force  
ATTN: G. Ullrich

DEPARTMENT OF ENERGY CONTRACTORS

Lawrence Livermore Laboratory  
ATTN: D. Glenn

Los Alamos Scientific Laboratory  
ATTN: C. Keller  
ATTN: R. Sanford

Sandia Laboratories  
ATTN: A. Chabai  
ATTN: Org. 1250, W. Brown

OTHER GOVERNMENT AGENCY

Federal Emergency Management Agency  
ATTN: Hazard Eval. & Vul. Red. Div.

DEPARTMENT OF DEFENSE CONTRACTORS

Acurex Corp.  
ATTN: K. Triebes  
ATTN: J. Stockton  
ATTN: C. Wolf

Aerospace Corp.  
ATTN: H. Mirels  
ATTN: Technical Information Services

Agbabian Associates  
ATTN: M. Agbabian

Applied Theory, Inc.  
ATTN: J. Trulio

Boeing Co.  
ATTN: Aerospace Library  
ATTN: S. Strack

California Research & Technology, Inc.  
ATTN: Library  
ATTN: M. Rosenblatt

DEPARTMENT OF DEFENSE CONTRACTORS (Continued)

Civil Systems, Inc.  
ATTN: J. Bratton

Civil Systems, Inc.  
ATTN: S. Melzer

Eric H. Wang  
Civil Engineering Rsch. Fac.  
ATTN: J. Kovarna  
ATTN: P. Lodde

General Electric Company—TEMPO  
ATTN: DASIAC

H-Tech Labs., Inc.  
ATTN: B. Hartenbaum

Higgins, Auld & Associates  
ATTN: N. Higgins  
ATTN: H. Auld

IIT Research Institute  
ATTN: Documents Library

J. H. Wiggins Co., Inc.  
ATTN: J. Collins

Merritt CASES, Inc.  
ATTN: Library

Mission Research Corp.  
ATTN: G. McCartor  
ATTN: C. Longmire

Nathan M. Newmark Consult. Eng. Svcs.  
ATTN: W. Hall  
ATTN: N. Newmark

Pacific-Sierra Research Corp.  
ATTN: H. Brode

Pacifica Technology  
ATTN: Library  
ATTN: R. Allen

Physics International Co.  
ATTN: Technical Library  
ATTN: F. Sauer  
ATTN: J. Thomsen

R & D Associates  
ATTN: Technical Information Center  
ATTN: R. Port  
ATTN: J. Carpenter  
ATTN: C. MacDonald  
ATTN: J. Lewis

Science Applications, Inc.  
ATTN: H. Wilson  
ATTN: R. Schlaug  
ATTN: Technical Library

Science Applications, Inc.  
ATTN: D. Houe

Science Applications, Inc.  
ATTN: B. Chambers III

DEPARTMENT OF DEFENSE CONTRACTORS (Continued)

SRI International

ATTN: Library  
ATTN: G. Abrahamson  
ATTN: D. Johnson  
ATTN: J. Colton

Systems, Science & Software, Inc.  
ATTN: C. Needham

Systems, Science & Software, Inc.

ATTN: K. Pyatt  
ATTN: Library  
ATTN: J. Barthel  
ATTN: C. Dismukes

Systems, Science & Software, Inc.  
ATTN: J. Murphy

Systems, Science & Software, Inc.  
ATTN: C. Hastings

DEPARTMENT OF DEFENSE CONTRACTORS (Continued)

Terra Tek, Inc.

ATTN: Library  
ATTN: A. Abou-Sayed

TRW Defense & Space Sys. Group

ATTN: Technical Information Center  
ATTN: N. Lipner

TRW Defense & Space Sys. Group

ATTN: G. Hulcher

Weidlinger Assoc., Consulting Engineers

ATTN: T. Sandler

Weidlinger Assoc., Consulting Engineers

ATTN: J. Isenberg